



© Copyright by Mahadi Masud 2019

All Rights Reserved

NON-CONTACT LAP SPLICES IN GEOMETRICALLY DISSIMILAR BRIDGE COLUMN  
TO DRILLED SHAFT CONNECTIONS

A Dissertation

Presented to

the Faculty of the Department of Civil and Environmental Engineering

University of Houston

In Partial Fulfillment

of the Requirements for the Degree

Doctor of Philosophy

in Civil Engineering

by

Mahadi Masud

May 2019

NON-CONTACT LAP SPLICES IN GEOMETRICALLY DISSIMILAR BRIDGE COLUMN  
TO DRILLED SHAFT CONNECTIONS

---

Mahadi Masud

Approved:

---

Chair of the Committee  
Yi-Lung Mo, Moores Professor,  
Civil and Environmental Engineering

Committee Members:

---

Thomas T. C. Hsu, Moores Professor,  
Civil and Environmental Engineering

---

Yongqian Lin, Director of Bridge Design,  
Texas Department of Transportation - Houston  
District

---

Mohamad Y. Mansour, Adjunct Professor,  
Civil and Environmental Engineering

---

Arghadeep Laskar, Assistant Professor,  
Civil Engineering, Indian Institute of Technology  
Bombay

---

Suresh K. Khator, Associate Dean,  
Cullen College of Engineering

---

Roberto Ballarini, Thomas and Laura Hsu  
Professor and Department Chair,  
Civil and Environmental Engineering

## **Acknowledgments**

I would like to dedicate my dissertation to my family and my advisor, Prof. Y. L. Mo, for their support, caring, belief, and patience. This journey would not have been possible without the support and guidance of my dissertation committee, Prof. Y. L. Mo, Prof. Thomas T. C. Hsu, Dr. Yongqian Lin, Prof. Mohamad Y. Mansour, and Prof. Arghadeep Laskar. I would like to give special thanks to my dissertation committee.

I would like to express my gratitude to the Texas Department of Transportation (TxDOT) (Project 0-6914) for their financial support and collaborative efforts for this project. I would like to especially thank the contributions of the project advisory committee which consists of Joanne Steele, Joe Adams, Patti Dathe, Dr. Yongqian Lin, Wanching Huang, Frank Estrada III, Kathleen Newton, Michael Hyzak, and Steven Austin. Finally, I appreciate the rest of the support staff at the Thomas T. C. Hsu Structural Research Laboratory at the University of Houston. Also, I would like to point out that the opinions, findings, and conclusions presented herein do not reflect the views of the funding institutions or other individuals.

NON-CONTACT LAP SPLICES IN GEOMETRICALLY DISSIMILAR BRIDGE COLUMN  
TO DRILLED SHAFT CONNECTIONS

An Abstract

of a

Dissertation

Presented to

the Faculty of the Department of Civil and Environmental Engineering

University of Houston

In Partial Fulfillment

of the Requirements for the Degree

Doctor of Philosophy

in Civil Engineering

by

Mahadi Masud

May 2019

vi

## Abstract

Contact lap splices are widely used for the construction of reinforced concrete structures. But, it is often required to provide a reinforcing steel splicing arrangement with non-contact lap splices due to the limitation of internal space or geometric irregularity for the connection of non-circular bridge columns interfacing directly with circular drilled shafts. However, there is a concern on the safety and cost-effectiveness of such non-contact lap splices because the guidelines in the current AASHTO LRFD code and studies on this type of connection are limited. This study presents an experimental and analytical investigation of non-contact lap splices in non-circular bridge column to circular drilled shaft connections. Eleven large-scale column-drilled shaft specimens were tested to investigate the effects of the critical parameters affecting the performance of non-contact lap splices: the non-contact distance between the spliced bars, the lap splice length and the amount of transverse reinforcement in the non-contact lap splice zone. The specimens were subjected to flexure action with both monotonic and cyclic loading. The test results showed that the specimens with larger non-contact splice distance generally exhibited lower lateral stiffness and lower capacity. The increase in the non-contact splice distance yielded significant inclined cracks and splitting cracks in the non-contact lap splice zone. The angle of inclined cracks was observed to increase with increasing the non-contact splice distance. Furthermore, a three-dimensional finite element analysis (FEA) was performed on the test specimens, and the finite element simulated results were compared with the test outcomes. Using the validated FEA models, a thorough parametric study was performed to understand the effect of the critical parameters. The results of this study provide a basic understanding of the behavior of non-contact lap splices in non-circular columns to circular drilled shaft connections. Based on the findings from the experimental and analytical investigation, a set of design recommendations is provided for the design of non-contact splices in geometrically dissimilar bridge column to drilled shaft connections. In conclusion, with the consideration of the current AASHTO LRFD code and the proposed guidelines, a safe and efficient non-circular column to circular drilled shaft connection can be constructed.

## Table of Contents

Acknowledgments.....	v
Abstract.....	vii
Table of Contents.....	viii
List of Figures.....	xiii
List of Tables .....	xvi
Chapter 1 Introduction.....	1
1.1    Problem Statement.....	1
1.2    Research Objectives.....	4
1.3    Outline of the Dissertation.....	5
Chapter 2 Background on the Behavior of Non-Contact Lap Splices .....	7
2.1    Overview.....	7
2.2    Behavior of Non-Contact Lap Splices .....	7
2.2.1    Behavior of Non-Contact Lap Splices in Plate Specimens.....	7
2.2.2    Behavior of Non-Contact Lap Splices in Column-Drilled Shaft Specimens.....	14
2.3    Provisions on the Design of Structures with Non-Contact Lap Splices.....	21
2.3.1    AASHTO LRFD Bridge Design Specifications (2014).....	21
2.3.2    ACI Building Code Requirements for Structural Concrete and Commentary (2014)	24
2.3.3    AASHTO LRFD Bridge Design Specifications Interim Revisions (2015) .....	27
2.3.4    TxDOT Bridge Design Manual (2015).....	28
2.3.5    AASHTO LRFD Bridge Design Specifications Interim Revisions (2016) .....	28

2.4	Summary .....	29
Chapter 3 Experimental Program.....		31
3.1	Overview.....	31
3.2	Representative Full-Scale Column-Drilled Shaft Connection .....	31
3.3	Test Variables .....	31
3.3.1	Non-Contact Lap Splice Distance.....	31
3.3.2	Non-Contact Lap Splice Length .....	32
3.3.3	Amount of Transverse Reinforcement in the Non-Contact Lap Splice Zone of Rectangular Columns.....	32
3.4	Design of the Test Specimens .....	33
3.4.1	Design of the Test Specimens in Phase I .....	33
3.4.2	Design of the Test Specimens in Phase II.....	37
3.5	Fabrication of the Test Specimens .....	39
3.6	Laboratory Test Setup.....	44
3.7	Instrumentation .....	46
3.7.1	Linear Variable Differential Transformers (LVDTs) .....	46
3.7.2	Strain Gages on the Reinforcing Bars.....	46
3.7.3	Digital Image Correlation (DIC)-Based Non-contact Measurement System.....	47
3.7.4	Data Acquisition .....	47
3.8	Loading Protocol.....	49
3.8.1	Preliminary Finite Element Analysis of the Bent 17 Column-Drilled Shaft Connection .....	49

3.8.2	Preliminary Test on Specimen 1 .....	54
3.8.3	Test Procedure .....	55
Chapter 4 Experimental Results.....		57
4.1	Overview.....	57
4.2	Material Properties.....	57
4.3	Summary of Experimental Results .....	59
4.3.1	Specimens in Phase I .....	59
4.3.2	Specimens in Phase II .....	70
4.4	Discussion of Experimental Results .....	76
4.4.1	Load vs. Displacement Relationships .....	76
4.4.2	Effect of Cyclic loading .....	80
4.4.3	Strains in the Reinforcing Bars .....	81
4.4.4	Crack Patterns .....	89
4.5	Summary .....	97
Chapter 5 Finite Element Analysis .....		100
5.1	Overview.....	100
5.2	Finite Element Analysis of the Test Specimens.....	100
5.2.1	Three-dimensional Finite Element Modeling of the Specimens.....	100
5.2.2	Constitutive Models of Materials.....	103
5.2.3	Loading .....	104
5.2.4	Finite Element Simulated Results of the Test Specimens.....	106

5.3	Parametric Study on the Test Specimens .....	117
5.3.1	Effect of Lap Splice Length .....	118
5.3.2	Effect of Non-Contact Lap Splice Distance.....	121
5.3.3	Effect of Amount of Transverse Reinforcement in the Non-Contact Lap Splice Zone of Rectangular Columns .....	125
5.4	Finite Element Analysis of a Full-Scale Column-Drilled Shaft Structure .....	129
5.5	Summary .....	137
Chapter 6 Design Recommendations and Modifications to Design Provisions.....		139
6.1	Overview .....	139
6.2	Design Recommendations .....	139
6.2.1	Non-contact Lap Splice Length .....	139
6.2.2	Non-contact Lap Splice Distance.....	139
6.2.3	Amount of Transverse Reinforcement in Non-circular Columns .....	140
6.3	Validation of Modifications to Design Provisions.....	140
6.3.1	Non-contact Lap Splice Length .....	140
6.3.2	Non-contact Lap Splice Distance.....	141
6.3.3	Amount of Transverse Reinforcement in Non-circular Columns .....	141
6.4	Design Examples .....	142
6.4.1	Longitudinal Reinforcement in the Column and the Drilled Shaft .....	142
6.4.2	Non-Contact Lap Splice Length .....	145
6.4.3	Amount of Transverse Reinforcement in the Column .....	150
6.4.4	Amount of Transverse Reinforcement in the Drilled Shaft .....	152

6.4.5	Detailed Drawings .....	154
6.5	Summary .....	157
Chapter 7 Conclusions and Future Work .....		158
7.1	Summary .....	158
7.2	Conclusions.....	160
7.2.1	Conclusions from the Experimental Investigation.....	160
7.2.2	Conclusions from the Finite Element Analysis and Parametric Study .....	162
7.3	Future Work.....	163
References.....		164
Appendix A.....		168
Appendix B .....		179
Appendix C .....		195
Appendix D.....		213

## List of Figures

Fig. 1-1: Typical rectangular column-circular drilled shaft connection in the design-build project- State Highway 99 segments f and g. ....	3
Fig. 1-2: Bent 17 column-circular drilled shaft connection in the design-build project (State Highway 99 segments f and g). ....	4
Fig. 2-1: Contact and non-contact lap splices. ....	7
Fig. 2-2: Non-contact lap spliced flat-plate specimens. ....	8
Fig. 2-3: Effective Lap Length. ....	9
Fig. 2-4: Non-contact lap spliced slab specimens. ....	11
Fig. 2-5: Flat panel specimens. ....	12
Fig. 2-6: Two-dimensional behavioral model for non-contact lap splices. ....	13
Fig. 2-7: Three-dimensional behavioral model for non-contact lap splices in circular column-shaft specimens. ....	15
Fig. 2-8: Column-shaft specimens with non-contact lap splices. ....	17
Fig. 2-9: Behavioral model for non-contact lap splices in rectangular sections. ....	18
Fig. 2-10: Tests on column-oversized drilled shaft assemblies. ....	20
Fig. 3-1: Typical reinforcement details of test specimens in Phase I. ....	36
Fig. 3-2: Typical reinforcement details of test specimens in Phase II. ....	39
Fig. 3-3: Various stages of fabrication of the specimens. ....	43
Fig. 3-4: Test setup. ....	45
Fig. 3-5: Location of LVDTs. ....	46
Fig. 3-6: DIC-based non-contact measurement system (West side). ....	47
Fig. 3-7: HBM Spider 8 data acquisition system. ....	48
Fig. 3-8: Vishay data acquisition system. ....	49
Fig. 3-9: Three-dimensional (3D) finite element model of the Bent 17 column-drilled shaft structure. ....	51

Fig. 3-10: Stress-strain curves of concrete in compression and tension. ....	52
Fig. 3-11: Stress-strain relationship of reinforcing steel using bilinear elastoplastic model. ....	52
Fig. 3-12: Column longitudinal bars on the “tension side” of the FEA model of the Bent 17 column-drilled shaft structure.....	53
Fig. 3-13: Stresses in the column longitudinal bars of Bent 17 column-shaft structure. ....	54
Fig. 3-14: Loading procedure. ....	56
Fig. 4-1: Load vs. displacement relationship of the specimens in Phase I.....	66
Fig. 4-2: Flexural cracks on the column (east face).....	68
Fig. 4-3: Flexural cracks on the drilled shaft (east face).....	69
Fig. 4-4: Splitting and inclined cracks on the column (east face).....	70
Fig. 4-5: Load vs. displacement relationship of the specimens in Phase II. ....	73
Fig. 4-6: Flexural cracks on the column (east face).....	74
Fig. 4-7: Flexural cracks on the drilled shaft (east face).....	75
Fig. 4-8: Splitting and inclined cracks on the column (east face).....	76
Fig. 4-9: Applied load vs. lateral displacement relationships of Specimens 1 to 4. ....	77
Fig. 4-10: Applied load vs. lateral displacement relationships of Specimens 1, 5, 6 and 7.....	78
Fig. 4-11: Location of the dowel bars. ....	78
Fig. 4-12: Applied load vs. lateral displacement relationships of Specimens 8 to 11. ....	80
Fig. 4-13: Strains in the reinforcing bars in Phase I.....	87
Fig. 4-14: Strains in the reinforcing bars in Phase II.....	88
Fig. 4-15: Typical opening at the column-drilled shaft interface (North-east face of Specimen 2). .....	90
Fig. 4-16: Opening at the column-drilled shaft interface.....	90
Fig. 4-17: Major (tensile) principal strain in the non-contact lap splice zone in the rectangular column (West side).....	93
Fig. 4-18: Crack widths of the inclined cracks. ....	94

Fig. 4-19: Splitting crack propagation atop the drilled shaft of Specimen 7. ....	95
Fig. 4-20: Crack widths of the splitting cracks. ....	96
Fig. 5-1: Finite element model of the column-drilled shaft specimens.....	102
Fig. 5-2: Typical bond stress vs. slip relationship.....	103
Fig. 5-3: Comparison of simulated results with test outcomes: load vs. lateral displacement relationship.....	109
Fig. 5-4: Typical opening at the bridge column-to-drilled shaft interface.....	110
Fig. 5-5: Opening at the column-drilled shaft interface.....	111
Fig. 5-6: Cracks patterns and failure modes on the simulated specimens. ....	117
Fig. 5-7: Load vs. lateral displacement relationship. ....	121
Fig. 5-8: Load vs. lateral displacement relationship. ....	123
Fig. 5-9: Location of dowel bars on the south side of the FEA models.....	124
Fig. 5-10: Stresses on the dowel bars located on the south side of the FEA models at the Load Level B (66.75 kips). ....	124
Fig. 5-11: Simulated load vs. lateral displacement relationship. ....	128
Fig. 5-12: Tensile stresses in the ties of non-contact lap splice zone of the column. ....	129
Fig. 5-13: Finite element model of the Bent 17 column-drilled shaft connection. ....	133
Fig. 5-14: Load vs. displacement relationships of Bent 17 column-shaft connection FEA specimens. ....	133
Fig. 5-15: Tensile damage in the non-contact lap splice zone of the drilled shaft.....	136
Fig. 6-1: P-M diagram of the column of Bent 17 column-drilled shaft connection.....	145
Fig. 6-2: Details of reinforcement in the Bent 17 column-drilled shaft connection. ....	156

## List of Tables

Table 2-1: Classes of tension lap splices (Table 5.11.5.3.1-1 [2]).....	23
Table 2-2: Development Length of Deformed Bars or Deformed Wires (Table 25.4.2.2 [16]) ....	26
Table 2-3: Lap Splice Lengths of Deformed Bars and Deformed Wires in Tension (Table 25.5.2.1 [16]) .....	27
Table 3-1: Details of test specimens in Phase I .....	35
Table 3-2: Details of test specimens in Phase II .....	38
Table 3-3: PCC mixture design for Specimens 1 to 4 in Phase I.....	40
Table 3-4: SCC mixture design for the column part of Specimens 5 to 11 .....	41
Table 3-5: PCC mixture design for the drilled shaft and footing part of Specimens 5 to 11 .....	42
Table 4-1: Material properties of concrete.....	58
Table 4-2: Material properties of deformed steel bars .....	59
Table 4-3: Change in lateral displacement of the specimen due to the cyclic loading .....	81
Table 4-4: Summary of yielding of different types of bars and the corresponding applied loads .	89
Table 4-5: Summary of crack patterns and their corresponding applied loads.....	97
Table 5-1: Material parameters for the concrete damaged plasticity model .....	105
Table 5-2: Material parameters for the bilinear elastoplastic steel model .....	106
Table 5-3: Details of FEA models for studying the effects of lap splice length and lap splice distance .....	119
Table 5-4: Details of the FEA models for studying the effect of the amount of transverse reinforcement in the rectangular columns.....	126
Table 5-5: Comparison of tensile stresses in the ties of non-contact lap splice zone of the column .....	128
Table 5-6: Description of FEA models for investigating the effect of splice length on the structural behavior of non-contact lap spliced connections. ....	131

## Chapter 1 Introduction

### 1.1 Problem Statement

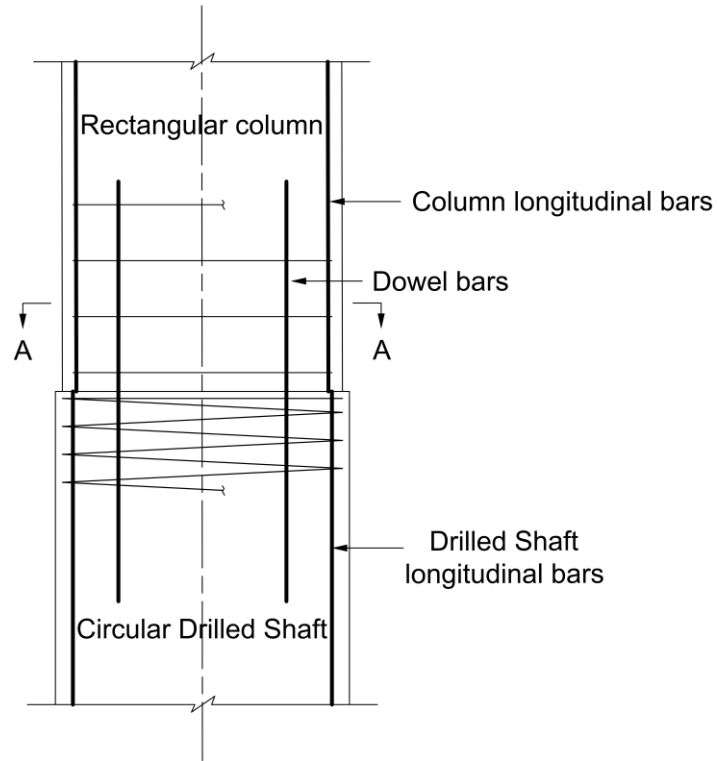
Contact lap splices are widely used for the construction of reinforced concrete structures. However, it is often required to provide a reinforcing steel splicing arrangement with non-contact lap splices for the connection of non-circular bridge columns interfacing directly with circular drilled shafts [1]. However, there is a concern on the safety and cost-effectiveness of such non-contact lap splices in bridge column to drilled shaft connections because the guidance in the current AASHTO LRFD Bridge Design Specifications [2] and studies on this type of connection are limited [3]. Especially if the column to drilled shaft connection involves a non-circular column framed directly with a circular drilled shaft as shown in Fig. 1-1, there are several issues where design guidance is not clear and may require advanced modeling validated by experiments to ensure a desired structural behavior.

The guidelines provided by Article 5.11.5.2.1 of AASHTO LRFD Bridge Design Specifications (BDS) [2] for designing non-contact lap splices are based on limited scope tests published in WSDOT-TRAC Report WA-RD 417.1 [4]. This WSDOT-TRAC report only examined the case of round columns with a diameter smaller than the supporting drilled shafts. For that particular case, the column reinforcement was extended into the supporting drilled shaft to make the construction joint, and the extended column reinforcement formed a non-contact lap splice with the drilled shaft reinforcement. However, in the case of a non-circular column framing with a circular drilled shaft, if the circular drilled shaft has a diameter equal to or smaller than the larger cross-sectional dimension of the non-circular column, then the column longitudinal reinforcement cannot be extended into the supporting drilled shaft due to the limitation of internal space or geometric irregularity as shown in Fig. 1-1. Instead, non-contact (offset) dowel bars have been typically used to connect the column and the supporting drilled shaft as shown in Fig. 1-1 and Fig. 1-2. These dowel bars would form non-contact lap splices with the column reinforcement, and the drilled shaft

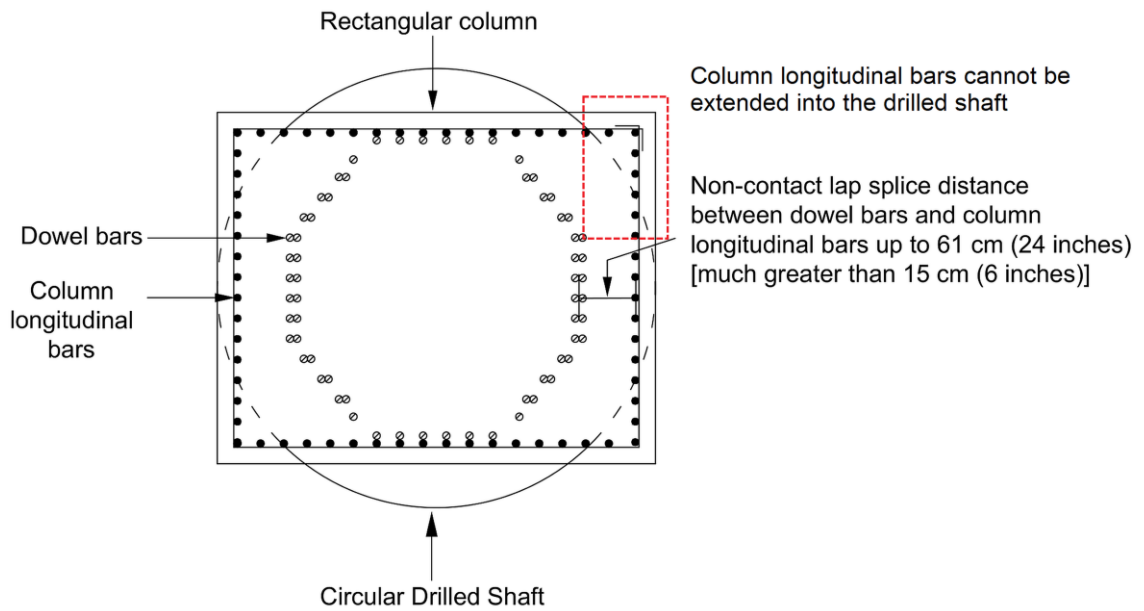
reinforcement and no experimental data are available on the behavior of non-contact lap splices in non-circular columns of such connections.

Furthermore, Article 5.11.5.2.1 of the current AASHTO LRFD code [2] specifies that the non-contact lap splices in flexural members shall not be spaced farther apart transversely than one-fifth of the required lap splice length or 6 inches. However, very large spacing of up to 24 inches for non-contact lap splices has been provided in practice which is much greater than 6 inches. The effect of such large spacing on the performance of non-contact lap splices has not been investigated.

Several researchers previously studied the behavior of non-contact lap splices [4-10] in plate and column-drilled shaft specimens. They [4-7] observed that the performance of a non-contact lap splice is primarily affected by the lap splice length of the spliced bars, the non-contact splice distance between the spliced bars and the amount of transverse reinforcement in the non-contact lap splice zone. In the case of geometrically dissimilar column-drilled shaft connections, whether the existing design guidelines [2, 11, and 12] are sufficient to design the lap splice length of such non-contact lap splices remains to be investigated. Furthermore, how the amount of transverse reinforcement affects the performance of the non-contact lap splice in non-circular columns is not clearly understood. It is also important to know how these critical parameters would interact with each other to influence the performance of a non-contact lap splice in non-circular columns. By addressing all these issues, this research aims to provide guidelines for the design of non-contact lap splices in the non-circular column to circular drilled shaft connections to ensure the structural safety, construction economy, and applicability of this kind of bridge substructures [13].



(a) Elevation

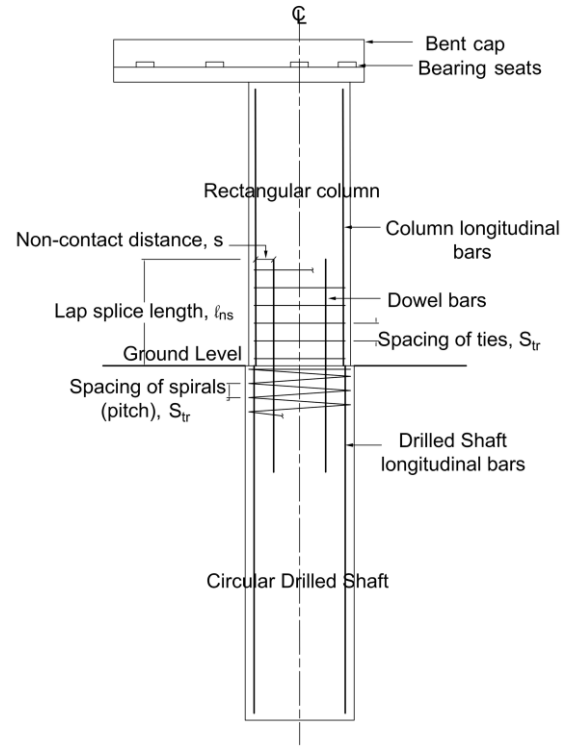


(b) Cross-section A-A

**Fig. 1-1: Typical rectangular column-circular drilled shaft connection in the design-build project- State Highway 99 segments f and g.**



(a) Bent 17 column-drilled shaft connection



(b) Non-contact splices in Bent 17 column-drilled shaft connection

**Fig. 1-2: Bent 17 column-circular drilled shaft connection in the design-build project (State Highway 99 segments f and g).**

## 1.2 Research Objectives

This research focuses on expanding the design criteria of non-contact lap splices at the interface between geometrically dissimilar bridge columns and drilled shaft foundations. In the course of this research, several important aspects were considered:

- a) Investigate the influence of non-contact lap splice distance that may vary between the non-contact lap spliced bars on the required lap splice length and the amount of transverse reinforcement, considering geometrically dissimilar bridge column and drilled shaft interface.
- b) Focusing on the most representative column to drilled shaft connections and the most important variables, such as non-contact lap splice distance, splice length of the spliced bars, amount of transverse reinforcement, etc., this research would evaluate the current AASHTO LRFD code

- provisions [2, 11 and 12] and improve them if necessary, especially for bridge substructures with columns that experience significant flexural or tensile demand.
- c) The current AASHTO LRFD code provisions [2] for designing non-contact lap splices are vague and can lead to the conclusion that very large spacing for non-contact lap splices is allowed in bridge column-drilled shaft connections even though the flexural demand-to-capacity ratio can be higher at the column-drilled shaft interface than the rest of the structure. This research would address this issue by providing a clear guideline on the limit of the distance between the non-contact lap spliced bars.
  - d) Develop a three-dimensional finite element analysis model of the test specimens and validate the FEA model by the experimental results.
  - e) Utilize the validated FEA model to perform a parametric study to investigate further the influence of the critical parameters affecting the performance of non-contact lap splices.

### **1.3 Outline of the Dissertation**

A thorough background on the design and behavior of non-contact lap splices in column-drilled shaft specimens and plate specimens is presented in Chapter 2. Also, an overview of the relevant code provisions on the design of structures with non-contact lap splices is presented.

In Chapter 3, the experimental program is described in detail. An overview of the test variables, the design of the test specimens, and the fabrication of the specimens is presented. The test setup and instrumentation are described, and the overall loading procedure is outlined.

Experimental results are presented in Chapter 4. A detailed comparison of load vs. displacement relationships, strains in the reinforcing bars, crack patterns, and failure modes are presented in provided in this chapter.

Thorough finite element analyses of the test specimens and the outcomes of the finite element analyses are presented in Chapter 5. An in-depth parametric study of the test specimens is also

presented in this chapter. Also, finite element analyses of the representative full-scale column-drilled shaft connections are provided in Chapter 5.

The design recommendations are presented in Chapter 6 including the modifications to design provisions. Conclusions of the research program are summarized in Chapter 7.

## Chapter 2 Background on the Behavior of Non-Contact Lap Splices

### 2.1 Overview

Spliced bars of non-contact lap splices do not touch, and such splices are permitted in practice provided the distance between the spliced bars meets the AASHTO code requirements [2] as shown in Fig. 2-1 [14]. Several researchers have previously studied the behavior of non-contact lap splices [4-10]. This chapter discusses the findings from those researchers. Also, an overview of the current code provisions on the design of structures with non-contact lap splices is also presented.

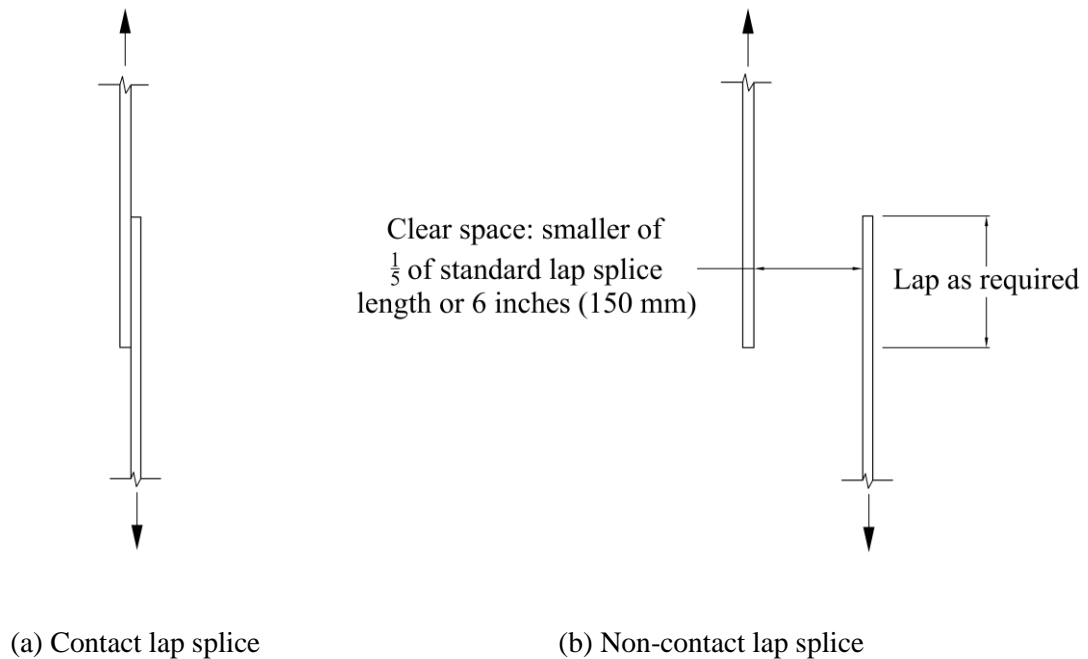


**Fig. 2-1: Contact and non-contact lap splices.**

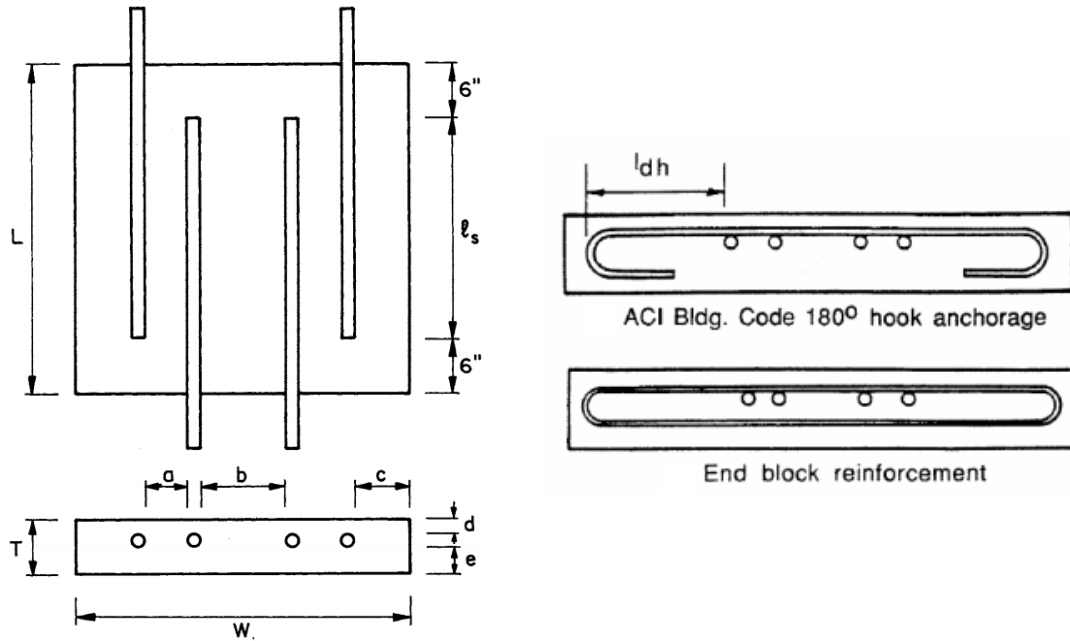
### 2.2 Behavior of Non-Contact Lap Splices

#### 2.2.1 Behavior of Non-Contact Lap Splices in Plate Specimens

##### 2.2.1.1 Sagan et al. (1991)

Sagan et al. [7] investigated the behavior of non-contact lap splices subjected to repeated inelastic tensile loading and monotonic loading up to the yield strength of the spliced bars where investigated variables included non-contact lap splice distance, splice bar size, the amount and

distribution of transverse reinforcement and lap splice length. They tested forty-seven full-scale flat-plate specimens with non-contact lap splices as shown in Fig. 2-2 [7].



(a) Typical spaced lap splice specimen

(b) Transverse reinforcement details

**Fig. 2-2: Non-contact lap spliced flat-plate specimens.**

They concluded that the ultimate load capacity of a splice was independent of the non-contact lap splice distance up to at least six bar diameters for monotonic loading and under repeated loading up to the yield strength of the splice bars. They also observed that with increasing non-contact lap splice distance, cracking along a lap splice and diagonal surface cracking of the concrete between the spliced bars increased. They also proved that the spacing or distribution of transverse reinforcement is approximately as important as the area of reinforcement provided to withstand cyclic loading. This was because despite providing widely spaced but uniformly distributed transverse reinforcement, the non-contact lap spliced specimens failed in sustaining a significant number of inelastic load cycles.

Based on the test results, Sagan et al. [7] proposed a behavioral model to explain the transfer of forces in the non-contact lap spliced bars. According to the behavioral model, the transfer of forces in the non-contact lap splice was idealized as in a truss in which the forces would transfer from one bar to the other through the concrete between the spliced bars by forming compressive struts in the concrete. The compression field theory was adopted to calculate the capacity of the compressive struts which takes into account the “softening” of the ultimate compressive strength of struts. As the forces are transferred between the spliced bars through the inclined compressive struts (having an inclination angle of 50 degrees as per Sagan et al. [7]), the strut action cannot be formed over the entire length of the lap splice. This means that the transfer length would be reduced and this reduced transfer length was called effective lap length,  $l_{eff}$  as shown in Fig. 2-3 [7].

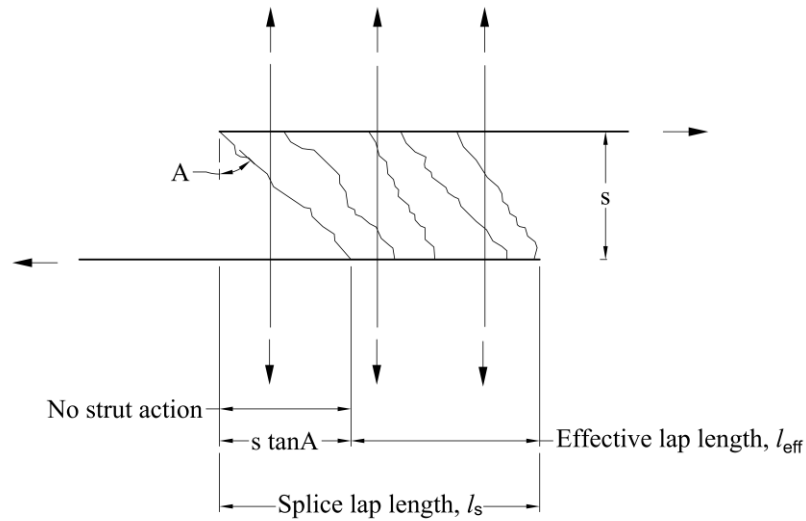


**Fig. 2-3: Effective Lap Length.**

Sagan et al. [7] also suggested that the total non-contact lap splice length,  $l_s$  to be provided when designing a non-contact lap splice should be effective splice length plus 1.2 times the bar offset distance ( $s_p$ ) considering 50 degrees inclination of compression struts as given by

$$l_s = l_{eff} + 1.2s_p. \quad (1)$$

The researchers also proposed design recommendations for minimum transverse reinforcement around non-contact lap splices based on the equilibrium strut-and-tie model as given by

$$s = \frac{1.7A_{tr}l_s}{d_b^2} \leq 6 \text{ inches}, \quad (2)$$

where,

$A_{tr}$  = transverse bar area (in.<sup>2</sup>);

$d_b$  = spliced bar diameter (in.).

#### **2.2.1.2 Hamad and Mansour (1996)**

Hamad and Mansour [5] studied the effect of non-contact lap splice distance in a tension lap splice failing in a splitting mode of failure rather than yielding of spliced bars. The clear non-contact distance between lap spliced bars in eight out of the seventeen tested slab specimens was greater than the 20 percent of the splice length or 6 inches specified by ACI 318-89 [15]. The slabs were tested in positive bending as shown in Fig. 2-4 [5], and the loading was designed to produce a constant moment region in the middle of the slab specimen. In order to allow the random formation of cracks, no transverse reinforcement was provided in the splice region.

The researchers concluded that slabs with non-contact splices of 1.2 inches (10% of splice length), 2.4 inches (20% of splice length), and 3.6 inches (30% of splice length) of non-contact distance showed greater stiffness than the slab with contact splices. However, slabs with non-contact splices of 4.75 inches (40% of splice length) and 6 inches (50% of splice length) of non-contact distance showed decreased stiffness than the slab with contact splices. For slab specimens with non-contact splices of 1.2 inches, 2.4 inches and 3.6 inches of non-contact splice distances, ultimate steel stress was higher than the slab with contact splices. However, in the case of 4.75 inches and 6 inches of non-contact splice distances, the ultimate steel stresses were lower than the steel stresses in the contact splices. Bond strength of the non-contact lap splices decreased for the

spacing of 40 and 50 percent of splice length, but the decrease of bond strength was within 10% of the bond strength of the slab with contact splices. The ACI Building Code [16] limits the non-contact distance of non-contact lap splices to 20 percent of splice length or 6 inches, whichever is smaller. Hamad and Mansour [5] reported that the limit of 20% of splice length for splice spacing was conservative, and optimum spacing for non-contact lap splices should be 30% of splice length.

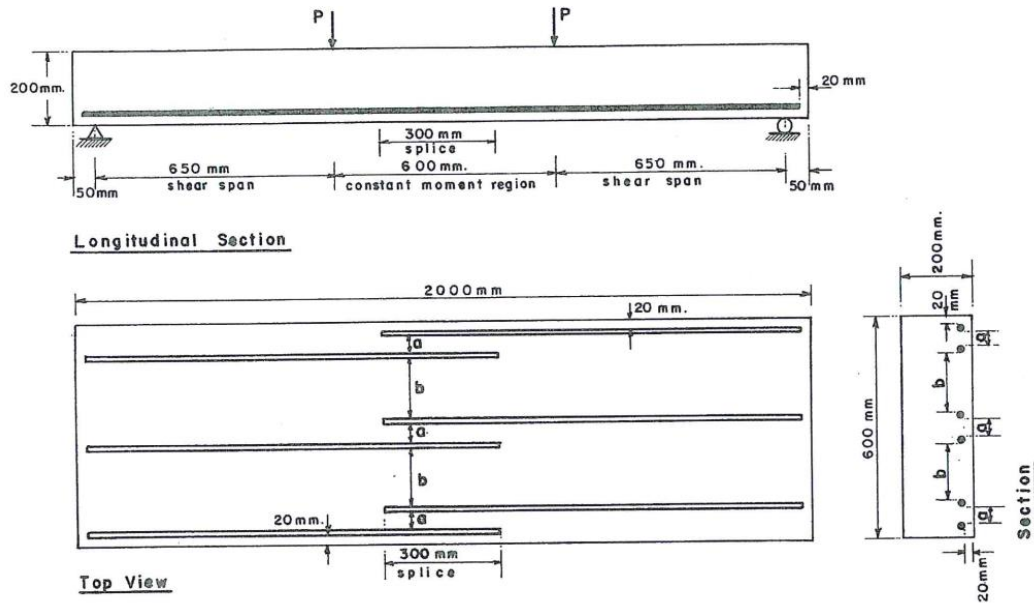


**Fig. 2-4: Non-contact lap spliced slab specimens.**

**2.2.1.3 McLean and Smith (1997)**

McLean and Smith [4] investigated the performance of non-contact lap splices by performing tests similar to Sagan et al. [7] on fifteen flat panel specimens as shown in Fig. 2-5. These panel specimens were subjected to tensile loading to failure. One of the objectives of these tests was to find out whether full capacity in a non-contact lap splice connection can be developed without providing transverse reinforcement around the spliced bars. However, results showed that the test specimens without any transverse reinforcement failed due to tension cracking of the concrete perpendicular to the spliced bars. The researchers reasoned that the cracks occurred due to the in-plane flexural bending of the panels caused by the non-contact lap splice distance. The researchers

also observed that with increasing the non-contact lap splice distance, the transverse reinforcement was heavily loaded proving that the larger the non-contact distance, the greater the contribution of the transverse reinforcement.

Based on the tests of flat panel specimens, the researchers proposed a two-dimensional (2D) behavioral model of non-contact lap splices in tension. Fig. 2-6 shows the 2D behavioral model developed by McLean and Smith [4]. This behavioral model is quite similar to Sagan et al.'s model [7] for non-contact lap splices except for the compressive strut angle which was taken as 45 degrees rather than 50 degrees considered by Sagan et al. [7].

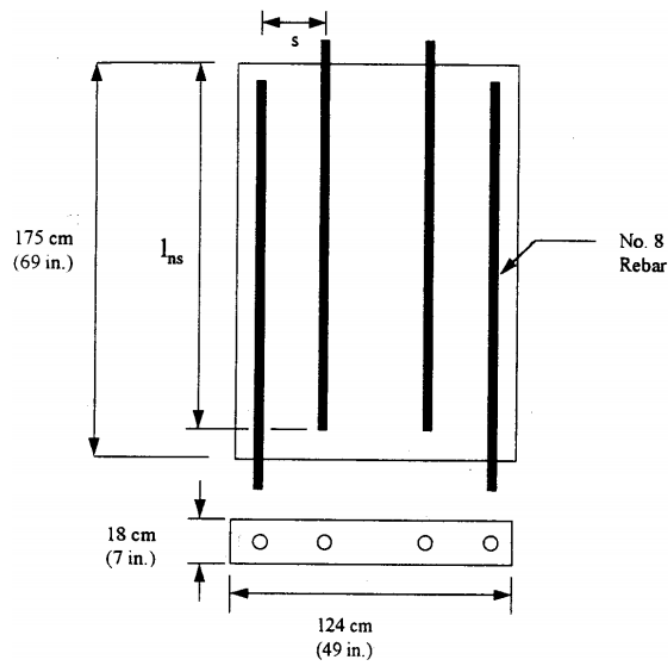


**Fig. 2-5: Flat panel specimens.**

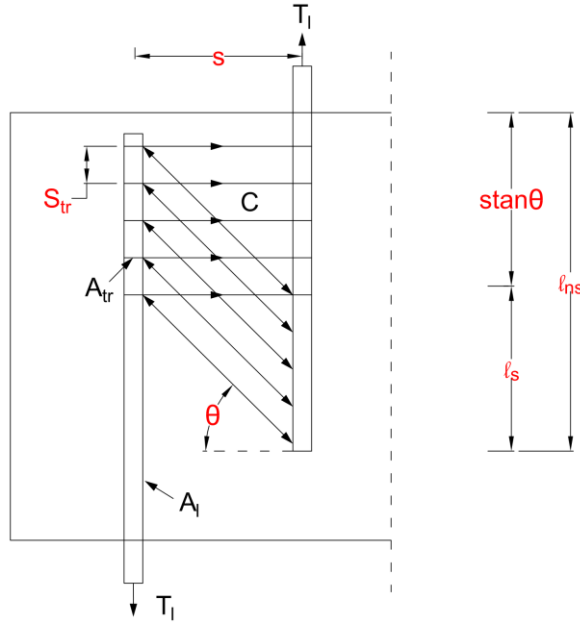


**Fig. 2-6: Two-dimensional behavioral model for non-contact lap splices.**

Based on their 2D behavioral model, McLean and Smith [4] proposed that the total non-contact lap splice length in a non-contact lap splice should be the standard required splice length plus the offset (non-contact) distance as given by (considering 45 degrees' inclination of compression struts based on the fact that majority of the cracks occurred at 45 degrees) (Fig. 2-6)

$$l_{ns} = l_s + s, \quad (3)$$

where,

$l_s$  = standard required splice length (in.);

$s$  = offset distance (in.);

$l_{ns}$  = total noncontact lap splice length (in.).

This provision was provided to ensure that the bond stresses developed in non-contact lap splices were similar to that of contact lap splices. McLean and Smith [4] also proposed the spacing of transverse reinforcement that should be provided around the spliced bars in order to develop the full capacity of the non-contact lap spliced bars by ensuring that the splice does not fail in brittle

anchorage failure. The required transverse reinforcement that should be provided around the spliced bars was given by

$$s_{tr} = \frac{A_{tr}f_{ytr}l_s}{A_l f_{ul}}, \quad (4)$$

where,

$s_{tr}$  = spacing of transverse reinforcement (in.);

$A_{tr}$  = area of transverse reinforcement (in.<sup>2</sup>);

$f_{ytr}$  = specified minimum yield strength of transverse reinforcement (ksi);

$l_s$  = standard required splice length (in.);

$A_l$  = area of longitudinal reinforcement in tension (in.<sup>2</sup>);

$f_{ul}$  = ultimate strength of longitudinal reinforcement (ksi).

The researchers further observed that non-contact lap splices designed using Equation 4 were successful in withstanding repeated cyclic tension loading and cyclic flexural loading with no strength degradation or slippage of the lapped reinforcing bars.

## **2.2.2 Behavior of Non-Contact Lap Splices in Column-Drilled Shaft Specimens**

### **2.2.2.1 McLean and Smith (1997)**

In order to predict the behavior of non-contact lap splices in the circular column-drilled shaft specimens, a three-dimensional (3D) truss model was developed by McLean and Smith [4] as shown in Fig. 2-7. Based on the 3D behavioral model, they proposed a minimum spiral reinforcement that must be provided in the bar anchorage region of the column-drilled shaft connection in order to fully develop the column reinforcing bars extended into the drilled shaft which can be calculated as

$$s_{tr} = \frac{2\pi A_{sp} f_{ytr} l_s}{A_l f_{ul}}, \quad (5)$$

where,

$s_{tr}$  = spacing of transverse shaft reinforcement (in.);

$A_{sp}$  = area of shaft spiral or transverse reinforcement ( $in.^2$ );

$f_{ytr}$  = specified minimum yield strength of shaft transverse reinforcement (ksi);

$l_s$  = Class C tension lap splice length of the column longitudinal reinforcement (in.);

$A_l$  = area of longitudinal column reinforcement ( $in.^2$ );

$f_{ul}$  = specified minimum tensile strength of column longitudinal reinforcement (ksi).

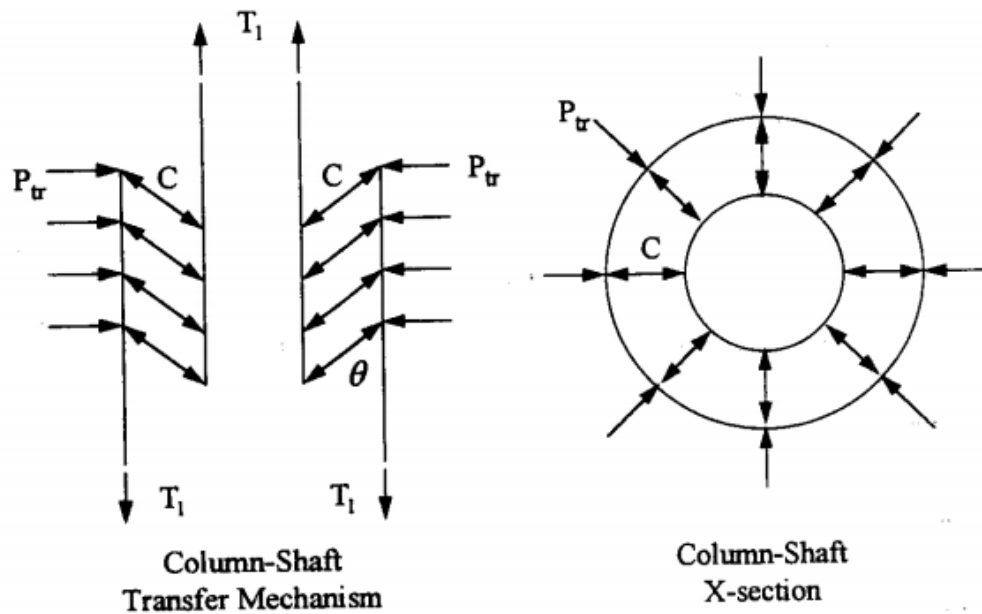


**Fig. 2-7: Three-dimensional behavioral model for non-contact lap splices in circular column-shaft specimens.**

McLean and Smith [4] further investigated the performance of non-contact lap splices in bridge column-drilled shaft connections under monotonic and cyclic loading by performing tests on two

one-fourth scale column-drilled shaft specimens with regards to lap splice length, non-contact lap splice distance, and spacing of transverse reinforcement. One of the two column-drilled shaft specimens was tested under tensile loading and the other specimen under flexural loading. It was observed during the tensile testing that cracks developed at the base of the column and along the top of the drilled shaft extending from the column to the drilled shaft. The cracks were splitting cracks which can be attributed to the bursting forces resulting from slip of the spliced bars. Similar cracks radiated from the column to the drilled shaft and down the sides of the drilled shaft during the flexural testing. Diagonal cracks were also observed in the non-contact lap splice zone where the concrete acts as inclined compression struts between the spliced bars. From the flexure test of one-fourth scale column-drilled shaft specimens, it was observed that the equations provided by the researchers based on the proposed 2D and 3D behavioral model were successful in controlling the propagation of cracks and maintaining the integrity of the splice for non-contact lap splice distances of up to six inches.

#### **2.2.2.2 Lin et al. (1998)**

Lin et al. [6] performed experimental research on the seismic behavior of bridge column non-contact lap splices with regards to non-contact lap splice distance and concrete cover. The laboratory test specimens were subjected to fully reversed (tension-compression), inelastic loadings. They tested six column specimens with varying combinations of longitudinal bar splice non-contact distance for the radial direction and concrete cover (Fig. 2-8). The non-contact lap splice distance for these columns was kept within 0 to 2 in. The researchers observed that the increased non-contact lap splice distance between dowel and column bars does not change the lap splice capacity. They reasoned that the smaller internal moment arm for the dowel bars due to non-contact lap splice distance decreases the flexural capacity of the column, but the cover to the dowel bars increased which allowed the bars to develop forces greater than that of contact splices between



$l_s$  = standard required splice length (in. );

$A_{Tl}$  = Total area of longitudinal reinforcement in tension (in.<sup>2</sup>);

$f_{ul}$  = ultimate strength of longitudinal reinforcement (ksi).

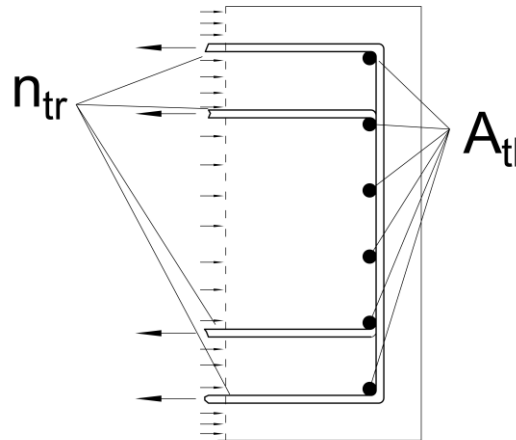


**Fig. 2-9: Behavioral model for non-contact lap splices in rectangular sections.**

#### 2.2.2.4 Murcia-Delso et al. (2013)

Murcia-Delso et al. [8 and 9] performed an experimental and analytical investigation to determine the minimum development length required for column longitudinal reinforcement extending into an oversized pile shaft and the amount of transverse reinforcement required for the pile shaft to prevent anchorage failure at the column-shaft connection. The researchers tested four full-scale column-to-shaft specimens under quasi-static cyclic lateral loading (Fig. 2-10). Investigated variables were embedment lengths for the column reinforcement, amounts of transverse reinforcement in the drilled shafts, sizes of longitudinal bars, and column-to-shaft diameter ratios. All specimens exhibited plastic deformation near the base of the columns although cone-shaped fractures and tensile splitting cracks were observed in the top portion of the drilled shafts. Based on the test results, the researchers concluded that the development length for the column reinforcement could be significantly reduced as compared to that required in AASHTO [18] and Caltrans [19] guidelines.

Based on the test results, Murcia-Delso et al. [8, 9] proposed that the development length,  $l_s$  of the column longitudinal reinforcement extended into the supporting drilled shaft should be calculated as

$$l_s = l_d + s + c, \quad (7)$$

where,

$l_d$  = Required development length for a straight bar in tension determined according to Article 5.11.2.1 of the AASHTO LRFD Bridge Design Specifications (BDS) [18];

$s$  = Bar spacing in the non-contact lap splice;

$c$  = Thickness of the concrete cover above the pile reinforcement.

Murcia-Delso et al. [8, 9] also proposed that the spacing  $s_{tr,max}$ , of the transverse reinforcement in the bar anchorage region of the drilled shaft should be no more than that given by

$$s_{tr,max} = \frac{2\pi A_{tr} f_{ytr}}{N_{col} d_{b,col} \tau_u}, \quad (8)$$

where,  $A_{tr}$ , is the cross-sectional area of a transverse reinforcing bar,  $f_{ytr}$ , is the nominal yielding stress of the transverse reinforcement,  $N_{col}$ , is the number of column longitudinal bars,  $d_{b,col}$ , is the diameter of column longitudinal bars, and  $\tau_u$ , is the ultimate bond strength of the column longitudinal reinforcing bars, which can be taken as 2.4 ksi for a concrete compressive strength of 5.0 ksi.



**Fig. 2-10: Tests on column-oversized drilled shaft assemblies.**

#### **2.2.2.5 Tran et al. (2015)**

Tran et al. [10] performed large-scale, lateral-load tests to a drift ratio of 10% on three specimens (DS-1, DS-2, and DS-3) consisting of a precast column embedded in a cast-in-place column-to-shaft transition region, which in turn was anchored to the testing rig by a base. The spiral reinforcement in Specimen DS-1 was designed using AASHTO [20] specifications. Specimen DS-2 contained half the amount of spiral in the column-to-shaft transition region compared to that of DS-1. DS-3 had a smaller diameter drilled shaft and higher percentages of shaft longitudinal reinforcement and shaft transverse reinforcement.

The test results showed that if sufficient transverse reinforcement is provided in the splice region, the plastic hinging mechanism forms in the column away from the splice region or shaft. They also observed that inadequate confinement in the splice region could cause strength deterioration under cyclic loading. That is why Specimen DS-2 with half of the conventional amount of shaft spiral reinforcement exhibited failure to occur in the shaft, by prying action of the

concrete shell surrounding the precast column. It is important to note that most of the available design guidelines provide a uniform distribution of transverse reinforcement in the splice region. However, Tran et al. [10] observed that the strains in the spiral reinforcement were higher at the top and lower at the bottom of the splice region. This led the researchers to conclude that a more efficient design could be achieved by providing a larger portion of the spiral reinforcement concentrated near the top of the splice region. Further, the researchers proposed a strut-and-tie model able to predict the mode of failure similar to the experimental results of the three specimens constructed with precast columns.

### **2.3 Provisions on the Design of Structures with Non-Contact Lap Splices**

The following design codes were examined for finding provisions on the design of structures with non-contact lap splices: American Association of State Highway and Transportation Officials (AASHTO) *Load Resistance Factor Design (LRFD) Bridge Design Specifications (BDS)* [2], American Concrete Institute *Building Code Requirements for Structural Concrete and Commentary* [16], AASHTO LRFD BDS Interim Revisions (2015) [11], Texas Department of Transportation (TxDOT) *Bridge Design Manual (2015)* [21], and AASHTO LRFD BDS Interim Revisions (2016) [12]. The relevant code provisions regarding the design of structures with non-contact lap splices are described in the following sections.

#### **2.3.1 AASHTO LRFD Bridge Design Specifications (2014)**

The following provisions of AASHTO [2] are relevant to the design of non-contact lap splices:

##### Article 5.11.5.2.1- Lap Splices

“Bars spliced by noncontact lap splices in flexural members shall not be spaced farther apart transversely than one-fifth the required lap splice length or 6.0 in.”

It also states that “For columns with longitudinal reinforcing that anchors into oversized shafts, where bars are spliced by noncontact lap splices, and longitudinal column and shaft reinforcement

are spaced farther apart transversely than one-fifth the required lap splice length or six inches, the spacing of the shaft transverse reinforcement in the splice zone shall meet the requirements of the following equation:

$$s_{max} = \frac{2\pi A_{sh} f_{ytr} l_s}{k A_l f_{ul}} \text{ (Eq. 5.11.5.2.1 - 1 [2])}, \quad (9)$$

where,

$s_{max}$  = spacing of transverse shaft reinforcement (in.);

$A_{sh}$  = area of shaft spiral or transverse reinforcement ( $in.^2$ );

$f_{ytr}$  = specified minimum yield strength of shaft transverse reinforcement (ksi);

$l_s$  = Class C tension lap splice length of the column longitudinal reinforcement (in.);

$A_l$  = area of longitudinal column reinforcement ( $in.^2$ );

$f_{ul}$  = specified minimum tensile strength of column longitudinal reinforcement (ksi) (90 ksi for ASTM A615 [22]);

$k$  = factor representing the ratio of column tensile reinforcement to total column reinforcement at the nominal resistance.”

#### Article 5.11.5.3.1- Lap Splices in Tension

“The length of lap for tension lap splices,  $l_s$  shall not be less than either 12.0 inches or the following for Class A, B or C splices:

Class A splice.....  $1.0l_d$

Class B splice.....  $1.3l_d$

Class C splice.....  $1.7l_d$ .”

“The class of lap splice required for deformed bars and deformed wire in tension shall be specified in Table 5.11.5.3.1-1.”

**Table 2-1: Classes of tension lap splices (Table 5.11.5.3.1-1 [2])**

Ratio of $\frac{(A_s \text{ as provided})}{(A_s \text{ as required})}$	Percent of $A_s$ spliced with required lap length		
	50	75	100
$\geq 2$	A	A	B
$< 2$	B	C	C

Article 5.11.2.1.1- Tension Development Length

“The basic tension development length,  $l_{db}$ , in inches shall be taken as

For No.11 bar and smaller.....  $\frac{1.25A_b f_y}{\sqrt{f'_c}}$

but no less than .....  $0.4d_b f_y$ , (10)

where,  $A_b$  is the area of the reinforcement being spliced (in<sup>2</sup>),  $f_y$  is the yield strength of the spliced reinforcement (ksi),  $d_b$  is the diameter of the rebar being spliced (in.), and  $f'_c$  is the compressive strength of the concrete (ksi).”

Article 5.8.2.5- Minimum Transverse Reinforcement

“Where transverse reinforcement is required, as specified in Article 5.8.2.4, the area of steel shall satisfy

$$A_v \geq 0.0316\sqrt{f'_c} \frac{b_v s}{f_y} \text{ (Eq. 5.8.2.5 - 1),} \quad (11)$$

where,

$A_v$  = area of transverse reinforcement within distance  $s$  ( $in.^2$ );

$b_v$  = width of web adjusted for the presence of ducts as specified in Article 5.8.2.9 ( $in.$ );

$s$  = spacing of transverse reinforcement ( $in.$ );

$f_y$  = yield strength of transverse reinforcement ( $ksi$ )  $\leq 100$   $ksi$ .”

#### Article 5.10.6.2- Spirals

“The center-to-center spacing between the bars of the spiral shall not exceed 6.0 times the diameter of the longitudinal bars or 6.0 in.”

#### Article 5.10.6.3- Ties

“The spacing of ties along the longitudinal axis of the compression member shall not exceed the least dimension of the compression member or 12.0 in.”

### **2.3.2 ACI Building Code Requirements for Structural Concrete and Commentary (2014)**

The following provisions are relevant to the design of non-contact lap splices:

#### Section 25.5.1.3

“For non-contact splices in flexural members, the transverse center-to-center spacing of spliced bars shall not exceed the lesser of one-fifth the required lap splice length and six inches.”

#### Section R25.5.1.3

“If individual bars in non-contact lap splices are too widely spaced, an unreinforced section is created. Forcing a potential crack to follow a zigzag line (5-to-1 slope) is considered a minimum precaution. The six-inch maximum spacing is added because most research available on the lap splicing of deformed bars was conducted with reinforcement within this spacing.”

### Section 25.4.2.2

“For deformed bars or deformed wires,  $l_d$  shall be calculated in accordance with Table 25.4.2.2.”

### Section 25.4.2.3

“For deformed bars or deformed wires,  $l_d$  shall be calculated by

$$l_d = \left( \frac{3f_y \Psi_t \Psi_e \Psi_s}{40\lambda \sqrt{f'_c} \left( \frac{c_b + K_{tr}}{d_b} \right)} \right) d_b \text{ (Eq. 25.4.2.3a [16])}, \quad (12)$$

where,  $l_d$  is the required development length (in.),  $f_y$  is yield strength of reinforcement being spliced (psi),  $f'_c$  is the 28-day compression strength of the concrete from cylinder testing (psi),  $\Psi_t$  is a reinforcement location factor,  $\Psi_e$  is a coating factor,  $\Psi_s$  is a bar size factor,  $\lambda$  is a factor for the weight of concrete,  $d_b$  is reinforcement diameter (in<sup>2</sup>),  $c_b$  is the smallest center-to-center cover or spacing dimension (in.), and  $K_{tr}$  is the transverse reinforcement index as follows:

$$K_{tr} = \frac{40A_{tr}}{sn} \text{ (Eq. 25.4.2.3b [16])}, \quad (13)$$

where,  $A_{tr}$  is the area of the transverse reinforcement at the section of the developing longitudinal reinforcement (in<sup>2</sup>),  $s$  is the spacing of transverse reinforcement (in.) and  $n$  is the number of bars being developed or spliced along the plane of splitting. The confinement term  $\left( \frac{c_b + K_{tr}}{d_b} \right)$  shall not be taken greater than 2.5 to limit the probability of a pullout failure.”

**Table 2-2: Development Length of Deformed Bars or Deformed Wires (Table 25.4.2.2 [16])**

Spacing and cover	No. 6 and smaller bars and deformed wires	No. 7 and larger bars
<p>Clear spacing of bars or wires being developed or spliced not less than <math>d_b</math>, clear cover not less than <math>d_b</math>, and stirrups or ties throughout <math>d_b</math>, not less than the code minimum</p> <p style="text-align: center;">or</p> <p>clear spacing of bars or wires being developed or spliced not less than <math>2d_b</math>, and clear cover not less than <math>d_b</math>.</p>	$\left( \frac{f_y \Psi_t \Psi_e}{25 \lambda \sqrt{f'_c}} \right) d_b$	$\left( \frac{f_y \Psi_t \Psi_e}{20 \lambda \sqrt{f'_c}} \right) d_b$
<p>Other cases</p>	$\left( \frac{3 f_y \Psi_t \Psi_e}{50 \lambda \sqrt{f'_c}} \right) d_b$	$\left( \frac{3 f_y \Psi_t \Psi_e}{40 \lambda \sqrt{f'_c}} \right) d_b$

Section 25.5.2.1

“Tension lap splice length,  $l_{st}$  for deformed bars and deformed wires in tension shall be in accordance with Table 25.5.2.1, where  $l_d$  shall be in accordance with 25.4.2.3(a).”

**Table 2-3: Lap Splice Lengths of Deformed Bars and Deformed Wires in Tension (Table 25.5.2.1 [16])**

$\frac{A_{s,provided}}{A_{s,required}}$	Maximum percent of $A_s$	Splice type	Tension lap splice length $l_{st}$
Over length of splice	spliced within required lap length	Class A	Greater of: $1.0l_d$ and 12 in.
		Class B	Greater of: $1.3l_d$ and 12 in.
$\geq 2.0$	50	Class A	
	100	Class B	
$< 2.0$	All cases	Class B	

### 2.3.3 AASHTO LRFD Bridge Design Specifications Interim Revisions (2015)

The following provisions are relevant to the design of non-contact lap splices:

#### Article 5.11.5.3.1 – Lap Splices in Tension

“The minimum length of lap for tension lap splices shall be as required for Class A or B lap splice, but not less than 12 in. where:

Class A lap splice  $1.0l_d$

Class B lap splice  $1.3l_d$

The tension development length,  $l_d$ , for the specified yield strength shall be taken in accordance with Article 5.11.2.”

“Except as specified herein, lap splices of deformed bars and deformed wire in tension shall be Class B lap splices. Class A lap splices may be used where:

- a) The area of reinforcement provided is at least twice that required by analysis over the entire length of the lap splice; and
- b) One-half or less of the total reinforcement is spliced within the required lap splice length.”

#### 2.3.4 TxDOT Bridge Design Manual (2015)

The following provisions discuss the design of non-contact lap splices:

Section 7 - Columns for Single Column Bents or Piers: Detailing states that “For non-contact lap splices between the column and its foundation, meet the requirements of Article 5.11.5.2.1 [2].”

#### 2.3.5 AASHTO LRFD Bridge Design Specifications Interim Revisions (2016)

The following provisions are relevant to the design of non-contact lap splices:

Article 5.11.2.1.1 – Tension Development Length

“The modified tension development length,  $l_d$ , in in. shall be taken as

$$l_d = l_{db} * \frac{\lambda_{rl} * \lambda_{cf} * \lambda_{rc} * \lambda_{er}}{\lambda} \text{ in which: } l_{db} = \frac{2.4d_b f_y}{\sqrt{f'_c}}, \quad (14)$$

where,

$l_{db}$  = basic development length (in.);

$\lambda_{rl}$  = reinforcement location factor;

$\lambda_{cf}$  = coating factor;

$\lambda$  = concrete density modification factor as specified in Article 5.4.2.8;

$\lambda_{rc}$  = reinforcement confinement factor;

$\lambda_{er}$  = excess reinforcement factor;

$f_y$  = specified yield strength of reinforcing bars or wire (ksi);

$f'_c$  = specified compressive strength of concrete for use in design (ksi);

$d_b$  = diameter of bar or wire (in.).”

## 2.4 Summary

A thorough background of the design and behavior of non-contact lap splices in flat plate specimens and column-drilled shaft specimens was presented in this chapter. Also, an overview of the provisions on the design of structures with non-contact lap splices as per AASHTO LRFD code [2, 11 and 12], ACI 318-14 [16], and TxDOT Bridge Design Manual [21] were summarized.

The current AASHTO LRFD code [2, 11-12] does not take into account the reduction of transfer length due to the non-contact splice distance between the spliced bars for determining the required non-contact lap splice length. Article 5.11.5.3.1 of AASHTO LRFD code [2] only states that lap splices must be classified into Class A, B or C splices in order to determine the required splice length of the bars [2, 14]. However, AASHTO LRFD Interim Revisions [11] have removed the use of Class C type lap splices and recommended using Class A or B lap splices for lap splices of deformed bars and deformed wire in tension.

McLean and Smith [4] provided a 2D behavioral model to find out the required spacing of transverse reinforcement in the non-contact lap splice zone of 2D non-contact lap splices. However, Maksoud [17] proposed a modification of the McLean and Smith’s model to determine the required amount of transverse reinforcement for rectangular sections constructed with non-contact lap splices. Still, the effect of these different amounts of transverse reinforcement in the non-contact lap splice zone on the performance of non-contact lap splices in non-circular columns has not been investigated thoroughly.

It is important to note that Article 5.11.5.2.1 of AASHTO [2] adopted McLean and Smith’s 3D behavioral model with a simple modification as given by Equation 9. A modification factor,  $k$ , was added due to the fact that McLean and Smith’s behavioral model [4] assumed all spliced bars to be

in tension but in reality, the spliced bars could be experiencing tension and compression depending on the location of the bars in flexural members. Based on the provisions of Article 5.11.5.2.1, very large spacing (up to 24 inches) for non-contact lap splices has been provided in practice which is much greater than six inches. However, McLean and Smith [4] observed that the proposed 3D behavioral model was successful in controlling the propagation of cracks and maintaining the integrity of the splice for non-contact splices of up to six inches. The effect of such large spacing of up to 24 inches on the performance of non-contact splices has not been investigated.

## Chapter 3 Experimental Program

### 3.1 Overview

In this chapter, details of the test variables, design, fabrication, test setup, instrumentation and testing procedures of the specimens in the experimental program are provided. Eleven tests were conducted on the column-drilled shaft specimens with various non-contact lap splice distances, non-contact lap splice lengths, and amounts of transverse reinforcement in the non-contact lap splice zone of rectangular columns.

### 3.2 Representative Full-Scale Column-Drilled Shaft Connection

Throughout the state of Texas, a significant number of rectangular bridge columns are supported by circular drilled shafts. A lot of these rectangular bridge columns are connected to cantilever bridge bent caps as shown in Fig. 1-2(a). Due to the eccentricity of the girders on these bent caps from the centerline of the bridge columns, these column-drilled shaft connections could experience significant flexural demand. Quite a few of these column-drilled shaft connections, e.g., Bent 17 column-drilled shaft connection on State Highway 99 (SH 99), were constructed with non-contact lap splices as shown in Fig. 1-2(b). As the Bent 17 column-drilled shaft connection has a geometrically dissimilar column-drilled shaft interface, consists of non-contact lap splices and is subjected to significant flexural demand, it was selected as the representative column-drilled shaft connection for this study.

### 3.3 Test Variables

#### 3.3.1 Non-Contact Lap Splice Distance

Several studies concluded that there was little or no behavioral difference between spaced and contact splices [24-27]. However, the scope of these experimental works was limited because the maximum spacing between the spliced bars was not more than three bar diameters ( $3d_b$ ), or 2 inches. Also, Sagan et al. [7] concluded that the ultimate load capacity of a splice was independent of the splice-bar spacing up to at least six bar diameters for monotonic loading and under repeated

loading up to the yield strength of the splice bars. Hence, the non-contact lap splice distance for the spliced bars of the proposed test specimens was designed by incorporating the aforementioned findings from the previous researchers.

AASHTO [2] and ACI [16] guidelines limit the maximum non-contact lap splice distance to the smaller of one-fifth of the required lap splice length or 6 inches based on the experimental results from previous researchers [4, 7]. Hence, a non-contact lap splice distance greater than the limit was also used to design the test specimens in order to understand how the non-contact lap spliced specimens would perform when the non-contact lap splice distance is greater than 6 inches.

### **3.3.2 Non-Contact Lap Splice Length**

Based on their 2D behavioral model of non-contact lap splices (Fig. 2-6), McLean and Smith [4] proposed that non-contact lap splice length,  $l_{ns}$  should be equal to a standard required lap splice length,  $l_s$  plus non-contact lap splice distance  $s$ . The reason behind this is the reduced transfer length of non-contact lap splices observed by Sagan et al. [7]. Based on a truss analogy, Sagan et al. [7] proposed that in order to compensate for this reduction of transfer length, an additional length,  $stanA$ , should be added to the required lap splice length as shown in Fig. 2-3. McLean and Smith [4] and Murcia-Delso et al. [8, 9] supported the concept of adding  $stanA$  to the standard required lap splice length to determine the lap splice length of non-contact lap splices. This 2D behavioral model was adopted to determine the lap splice length of non-contact lap splices of the test specimens.

### **3.3.3 Amount of Transverse Reinforcement in the Non-Contact Lap Splice Zone of Rectangular Columns**

Based on the findings from the tests on the flat plate specimens, McLean and Smith [4] proposed that the relationship given by Equation 4 should be used to find out the spacing of transverse reinforcement around the spliced bars in order to develop the full capacity of the non-contact lap spliced bars by ensuring that the splice does not fail in brittle anchorage failure. Maksoud [17]

proposed a modification of the McLean and Smith's [4] model to determine the transverse reinforcement for rectangular sections constructed with non-contact lap splices as given by Equation 6 (Fig. 2-9). For each non-contact lap splice distance used for the test specimens, two separate test specimens were designed using the equations proposed by McLean and Smith [4] and Maksoud [17] in order to find out the influence of different amounts of transverse reinforcement on the behavior of non-contact lap splices.

### **3.4 Design of the Test Specimens**

The experimental investigation was divided into two phases. The Phase I experimental program focused on the effect of the non-contact lap splice distance between the spliced bars, non-contact lap splice length, and the amount of transverse reinforcement in the lap splice zone of rectangular columns. In the Phase II experimental program, in addition to studying the effect of the non-contact lap splice distance between the spliced bars and the non-contact lap splice length, the interim revisions in the AASHTO LRFD codes [11, 12] were incorporated in the test specimens to study the effect of the changes made to the current AASHTO LRFD code provisions [2].

#### **3.4.1 Design of the Test Specimens in Phase I**

The test specimens were designed based on the design of the full-scale representative structure-Bent 17 column-drilled shaft connection. The test specimens were 1/4-scale of the Bent 17 column-drilled shaft connection. An unconfined concrete compressive strength of 3.6 ksi and a steel rebar yield strength of 60 ksi were used for the design of the Bent 17 column-drilled shaft connection. The same material properties were adopted for designing the test specimens. Seven column-drilled shaft specimens were designed and tested in Phase I: Specimens 1 to 7. Each specimen consisted of a rectangular column and a circular drilled shaft with a rectangular footing as shown in Fig. 3-1. The rectangular column had a depth of 28 inches and a width of 21 inches. The drilled shaft had a diameter of 34 inches and a height of 42 inches. Specimen 1 consisted of contact lap splices in which the dowel bars and the column longitudinal bars were in contact with each other. Specimens

2 to 7 consisted of non-contact splices where the distance between the dowel bars and column longitudinal bars ranged from 4 inches to 8 inches. The lap splice length for the specimens was calculated by considering the lap spliced connection having Class C lap splice as per AASHTO LRFD 5.11.5.3.1 [2]. The lengths for non-contact lap splices were calculated using Equation 3. The transverse reinforcement (ties) within the non-contact lap splice zone of the column of Specimens 2 to 4 was designed using Equation 4 recommended by McLean and Smith [4] whereas Equation 6 recommended by Maksoud [17] was used for Specimens 5 to 7. The transverse reinforcement (spirals) within the lap splice zone of the drilled shaft was designed using Equation 9 for all the specimens. Grade 60 No. 5 bars were used for the longitudinal reinforcing bars in the column and the drilled shaft. The bar size of the transverse reinforcement in the column and the drilled shaft was No. 3. Each specimen consisted of twenty column longitudinal bars and thirty drilled shaft longitudinal bars. The details of the test specimens are presented in Table 3-1. A typical elevation and cross-sections of the specimens in Phase I are shown in Fig. 3-1. The elevation and cross-sections of the specimens in Phase I are provided in Appendix A.

**Table 3-1: Details of test specimens in Phase I**

Specimen type	Specimen No.	Non-contact lap splice distance in the column, $s$ (in.)				Lap splice length <sup>a</sup> , $l_{ns}$ (in.)	Spacing of transverse reinforcement in column, $s_{tr}$ (in.)	Spacing of transverse reinforcement in drilled shaft <sup>e</sup> , $s_{max}$ (in.)
		0	4	6	8			
Contact	1	x				25.5	10 <sup>b</sup> (2-legged)	3.75
Non-contact	2	x				29.5	6 <sup>c</sup> (2-legged)	3.75
Non-contact	3			x		31.5	6 <sup>c</sup> (2-legged)	3.75
Non-contact	4				x	33.5	6 <sup>c</sup> (2-legged)	3.75
Non-contact	5	x				29.5	4.0 <sup>d</sup> (4-legged)	3.75
Non-contact	6			x		31.5	4.0 <sup>d</sup> (4-legged)	3.75
Non-contact	7				x	33.5	4.0 <sup>d</sup> (4-legged)	3.75

<sup>a</sup> $l_s = 1.7 * l_{db}$  \* modification factors of Articles 5.11.2.1.2 and 5.11.2.1.3 of AASHTO [2]

where,  $l_{db} = \frac{1.25A_b f_y}{\sqrt{f'_c}} \geq 0.4d_b f_y$  as per AASHTO LRFD code [2] and the factor of 1.7 is used to

convert the basic tension development length,  $l_{db}$ , into the required lap splice length for Class C lap splices as per Article 5.11.5.3.1 of AASHTO LRFD code [2]

<sup>b</sup> For Specimen 1 with contact lap splice,  $S_{tr}$  was calculated using the minimum of AASHTO LRFD code [2] Articles 5.8.2.5 and 5.10.6.3.

$${}^c S_{tr} = \frac{A_{tr} f_y t_r l_s}{A_t f_{ul}} \text{ (Equation 4)}$$

$${}^d S_{tr} = \frac{n_{tr} A_{tr} f_y t_r l_s}{A_t f_{ul}} \text{ (Equation 6)}$$

$${}^e S_{max} = \frac{2\pi A_{sp} f_y t_r l_s}{k A_t f_{ul}} \text{ (Equation 9)}$$

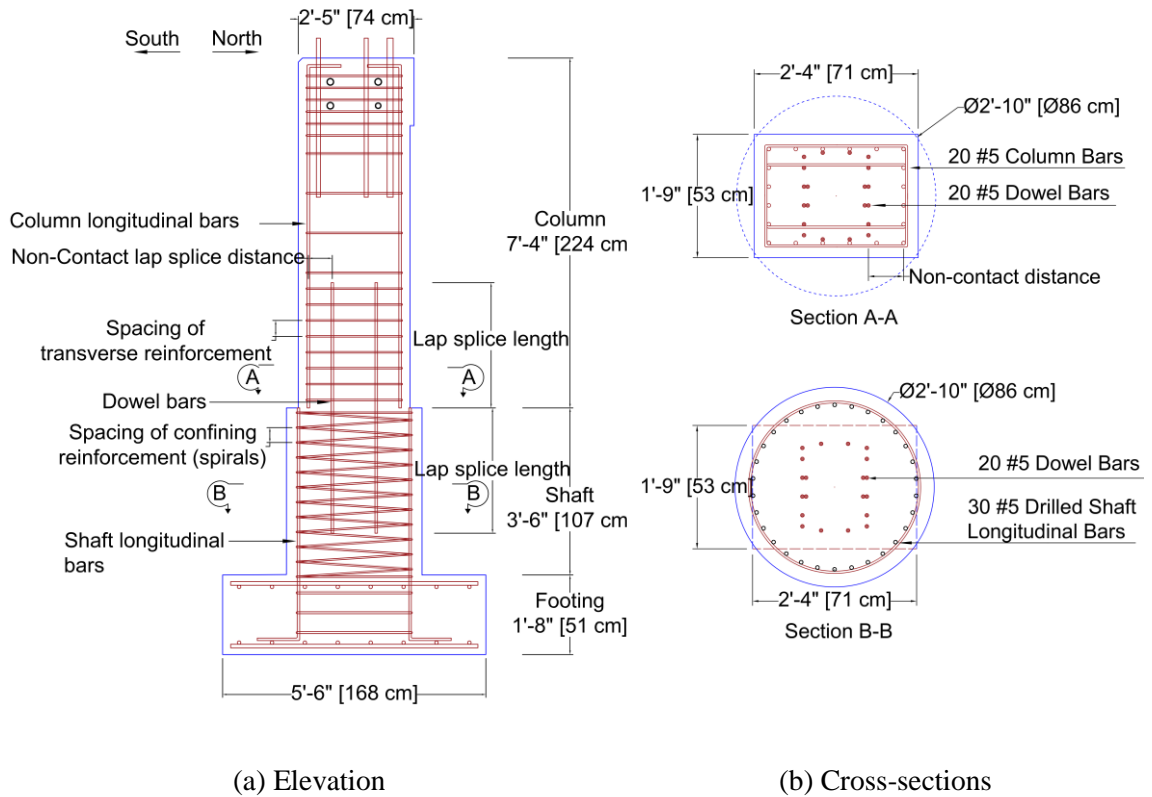


**Fig. 3-1: Typical reinforcement details of test specimens in Phase I.**

### 3.4.2 Design of the Test Specimens in Phase II

Four column–drilled shaft specimens were designed and tested in the Phase II experimental program: Specimens 8 to 11. In the Phase II experimental program, in addition to studying the effect of the non-contact lap splice distance between the spliced bars and the non-contact lap splice length, the interim revisions in the AASHTO codes [11, 12] were incorporated in the test specimens to study the effect of the changes made to the current AASHTO LRFD code provisions [2].

Specimens 8 to 11 consisted of non-contact lap splices with a non-contact lap splice distance ranging from 4 inches to 6 inches. The lap splice length for the specimens was calculated by considering the lap spliced connection as Class B lap splice as per AASHTO LRFD Article 5.11.5.3.1 [11]. The non-contact lap splice lengths in Specimens 8 and 10 were calculated using Equation 3 as per the AASHTO LRFD code [2]. On the other hand, the lap splice length in Specimens 9 and 11 were calculated using Equation 3 as per AASHTO LRFD Interim Revisions [11, 12]. The transverse reinforcement within the lap splice zone of the column of Specimens 8 to 11 was designed using Equation 6 proposed by Maksoud [17]. The transverse reinforcement within the lap splice zone of the drilled shaft was designed using Equation 9 as per the current AASHTO LRFD code [2].

Grade 60 No. 7 bars were used for the longitudinal reinforcing bars in the column and the drilled shaft. The bar size of the transverse reinforcement in the column and the drilled shaft was No. 3. Each specimen consisted of ten column longitudinal bars and sixteen drilled shaft longitudinal bars. The details of the test specimens are presented in Table 3-2. A typical elevation and cross-sections of the specimens in Phase II are shown in Fig. 3-2. The elevation and cross-sections of the specimens in Phase II are provided in Appendix A.

**Table 3-2: Details of test specimens in Phase II**

Specimen type	Specimen No.	Non-contact lap splice distance in the column, $s$ (in.)	Lap splice length, $l_{ns}$ (in.)	Spacing of transverse reinforcement in column, $s_{tr}$ (in.) <sup>c</sup>	Spacing (Pitch) of transverse reinforcement in drilled shaft, $s_{max}$ (in.) <sup>d</sup>	
		4	6			
			$l_{ns} = l_s + s$ (Equation 3)	[within lap splice]	[within lap splice]	
Non-contact	8	x	44.5 <sup>a</sup>	6.5	5.25	
Non-contact	9	x	38.75 <sup>b</sup>	6.5	5.25	
Non-contact	10		x	46.5 <sup>a</sup>	6.5	5.25
Non-contact	11		x	40.75 <sup>b</sup>	6.5	5.25

<sup>a</sup>  $l_s = 1.7 * l_{db} * \text{modification factors of Articles 5.11.2.1.2 and 5.11.2.1.3 of AASHTO [2]}$

where,  $l_{db} = \frac{1.25A_b f_y}{\sqrt{f'_c}} \geq 0.4d_b f_y$  as per AASHTO [2]

<sup>b</sup>  $l_s = 1.3 * l_{db} * \frac{\lambda_{rl} * \lambda_{cf} * \lambda_{rc} * \lambda_{er}}{\lambda}$  where,  $l_{db} = \frac{2.4d_b f_y}{\sqrt{f'_c}}$  as per AASHTO Interim revisions [11, 12]

(Class C lap splice used in AASHTO BDS [2] has been removed. Instead, Class B lap splice has been used in AASHTO [11, 12])

$${}^c S_{tr} = \frac{n_{tr} A_{tr} f_{ytr} l_s}{A_{Tl} f_{ul}} \text{ (Equation 6)}$$

$${}^d S_{max} = \frac{2\pi A_{sp} f_{ytr} l_s}{k A_{l} f_{ul}} \text{ (Equation 9)}$$

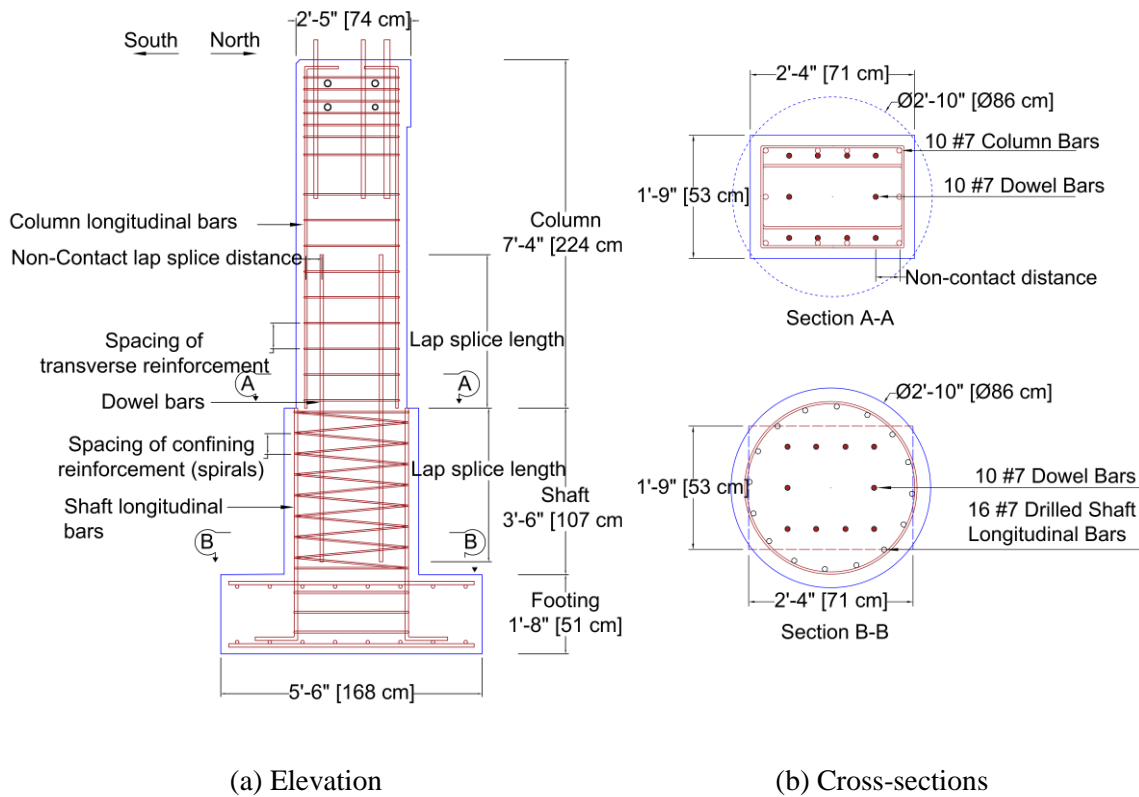


**Fig. 3-2: Typical reinforcement details of test specimens in Phase II.**

### 3.5 Fabrication of the Test Specimens

All specimens were cast in collaboration with a concrete manufacturing company located in Houston, Texas. A total of eleven large-scale column-drilled shaft specimens were cast. The specimens were cast in two stages. In the first stage, the rectangular footing and the circular drilled shaft were cast. The rectangular column was cast in the second stage. Plain cement concrete (PCC) was used for Specimens 1 to 4 in Phase I. Detailed mixture design of PCC concrete used for

Specimens 1 to 4 is provided in Table 3-3. For Specimens 5 to 7, self-consolidating concrete (SCC) was used for the rectangular column part while PCC was used for the circular drilled shaft and the footing part. Detailed mixture design of SCC and PCC concrete used for Specimens 5 to 7 are provided in Table 3-4 and Table 3-5, respectively. In Phase II, self-consolidating concrete (SCC) was also used for the rectangular column part while PCC was used for the circular drilled shaft and footing part for Specimens 8 to 11. The steel reinforcement was supplied as per design requirements by a reinforcing steel distribution company.

**Table 3-3: PCC mixture design for Specimens 1 to 4 in Phase I**

Material Specifications	Quantity per yd <sup>3</sup>
Type 3 Portland cement (ALAMO III)	310 lb
Water	27.36 gallons
Water /Cement ratio	0.44
Class F Fly ash	207 lb
CA: Pioneer Hanson Arena 1” limestone aggregate	1673 lb
FA: Pioneer Hanson Arena natural sand	1540 lb
Admixture: Sika Visco-crete 2110	21 oz
Sika Plastiment	6 oz
Ambient temperature	82 -93 °F
Entrapped air	2%
Slump	6 ± 2 inches

**Table 3-4: SCC mixture design for the column part of Specimens 5 to 11**

<b>Material Specifications</b>	<b>Quantity per yd<sup>3</sup></b>
Type 3 Portland cement (ALAMO III)	474 lb
Water	30.12 gallons
Water /Cement ratio	0.35
Class F Fly ash	255 lb
CA: Pioneer-Hanson Arena 1” limestone aggregate	1507 lb
FA: Pioneer-Hanson Arena natural sand	1441 lb
Admixture: Sika Visco-crete 2110	37.2 oz
Sika Plastiment	4 oz
High Range Water-Reducing Admixture: Sika R-4	4 oz
Air	2.5 oz
Ambient temperature	55-70 °F
Entrapped air	4.8%
Spread value	21-23”

**Table 3-5: PCC mixture design for the drilled shaft and footing part of Specimens 5 to 11**

<b>Material Specifications</b>	<b>Quantity per yd<sup>3</sup></b>
Type 3 Portland cement (ALAMO III)	600 lb
Water	30.2 gallons
Water/Cement ratio	0.34
Class F Fly ash	150 lb
CA: Pioneer Hanson Arena 1” limestone aggregate	1694 lb
FA: Pioneer Hanson Arena natural sand	1251 lb
Admixture: Sika Visco-crete 2110	30 oz
Sika Plastiment	10 oz
Ambient temperature	55-70 °F
Entrapped air	1.7%
Slump	7 ± 2 inches

As mentioned earlier, in the first stage, the footing and the circular drilled shaft were cast together. The footing was cast in plywood forms, and the circular drilled shaft was cast in a ½ inches thick round card-board form [Fig. 3-3(b)]. Before the concrete casting, the steel cages of the footing and the circular shaft were assembled and placed in their proper position inside the formwork. Once the concrete had been poured inside the circular shaft formwork, the dowel bars were placed in their positions with respect to the drilled shaft steel cage. The rectangular column was cast in a plywood form reinforced with a steel angle frame in the second stage. The column cage was carefully positioned with respect to the dowel bars and the drilled shaft bars. Nine 4-inch. by 8-inch. control cylinders were cast for each stage for determining the concrete material properties. The entire concrete fabrication procedure of the specimens is illustrated in Fig. 3-3.



(a) Drilled shaft and footing rebar cage



(b) Drilled shaft and footing formwork



(c) Drilled shaft and footing casting



(d) Placement of dowel bars



(e) Drilled shaft and footing - after casting



(f) Placement of column bars



(g) Column formwork



(h) Column casting



(i) Completed specimen

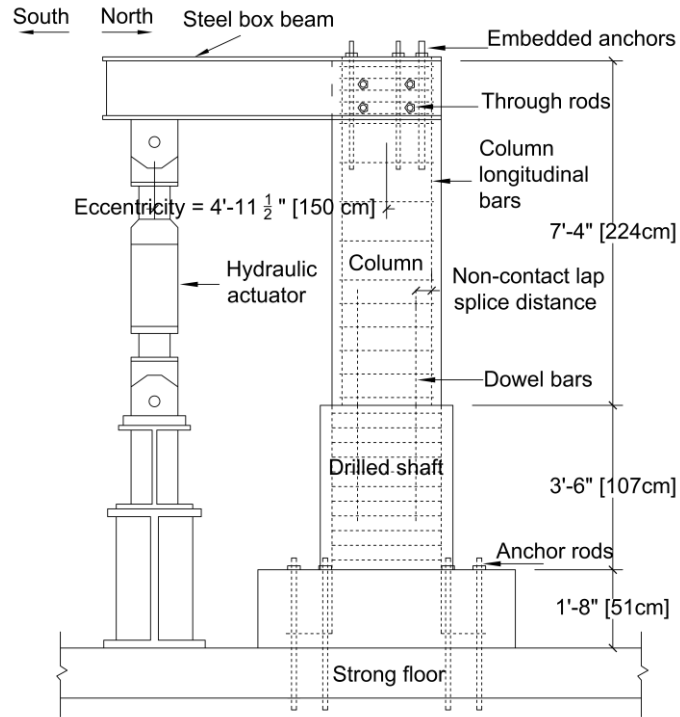
**Fig. 3-3: Various stages of fabrication of the specimens.**

Electrical resistance strain gages were pasted on the column longitudinal bars, column ties, dowel bars, drilled shaft longitudinal bars and drilled shaft spirals before concrete casting. The locations and designations of the strain gages are discussed in Section 3.7. Each strain gage pasting

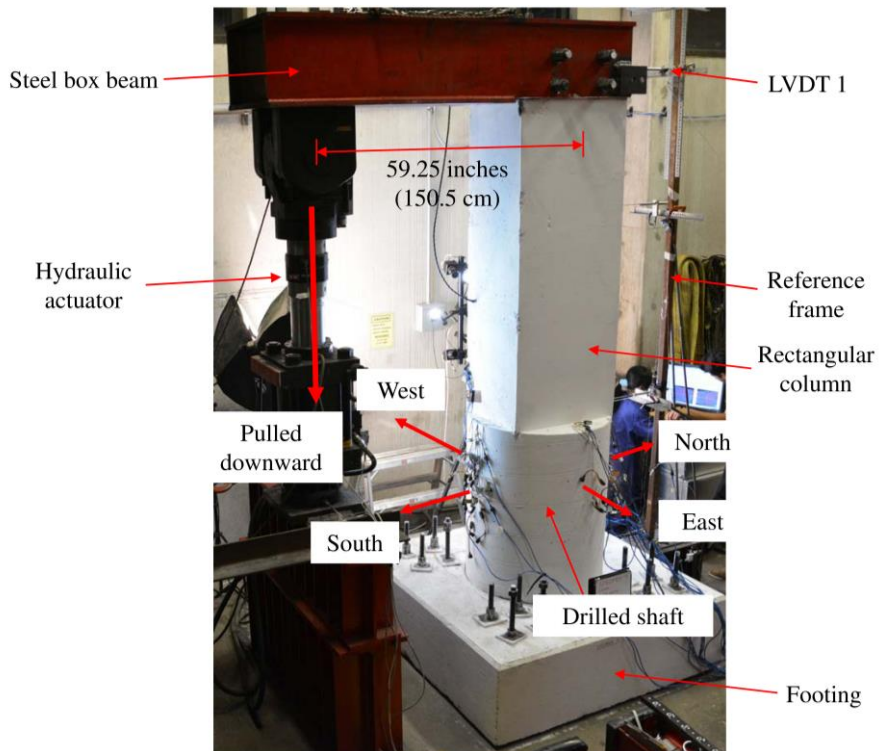
location was polished and well prepared before pasting. The strain gages were water-proofed with several coatings so that they would survive the casting of concrete around them.

### **3.6 Laboratory Test Setup**

The test setup was designed to reflect the behavior of the representative column-drilled shaft structure which experiences a uniform bending moment. The test setup for producing the uniform bending moment on the test specimens is shown in Fig. 3-4. The footing of the drilled shaft was tension-anchored to the laboratory strong-floor using sixteen 1.25 inch-diameter high strength threaded rods. A steel box beam was designed and constructed to replicate the actual cantilever bent cap for the test specimens as shown in Fig. 3-4(b). Each specimen consisted of six high strength threaded rods embedded at the top of the column. These embedded rods were used to anchor the top flange of the steel beam to the column. During the fabrication of the specimens, four through holes were made near the top end of the column on the East and West side. Through these holes, four high strength threaded rods were inserted, and then, the webs of the steel beam were anchored to the sides of the column. The load was applied on the steel box beam at an eccentricity of 59.25 inches from the centerline of the column which produced a uniform bending moment in the column-drilled shaft assembly. The downward vertical load was applied by a 220.0 kips' capacity hydraulic actuator that reacted against a steel reaction beam bolted to the laboratory strong floor as shown in Fig. 3-4(b).



(a) Schematic of setup



(b) Typical test setup

**Fig. 3-4: Test setup.**

### 3.7 Instrumentation

#### 3.7.1 Linear Variable Differential Transformers (LVDTs)

Shown in Fig. 3-5 is the arrangement of the Linear Variable Differential Transformers (LVDTs) which were used to measure the lateral displacement at four different locations on the tension side of the specimens. The LVDTs were fixed to a separate reference frame adjacent to the specimen, as shown in Fig. 3-5.

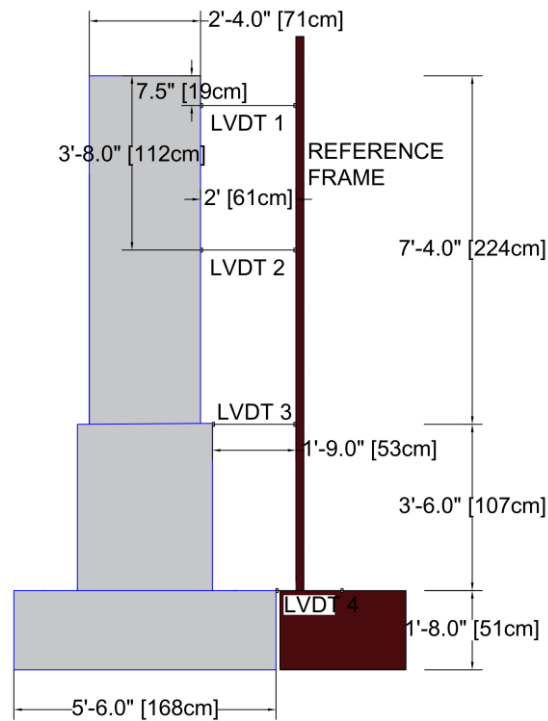


Fig. 3-5: Location of LVDTs.

#### 3.7.2 Strain Gages on the Reinforcing Bars

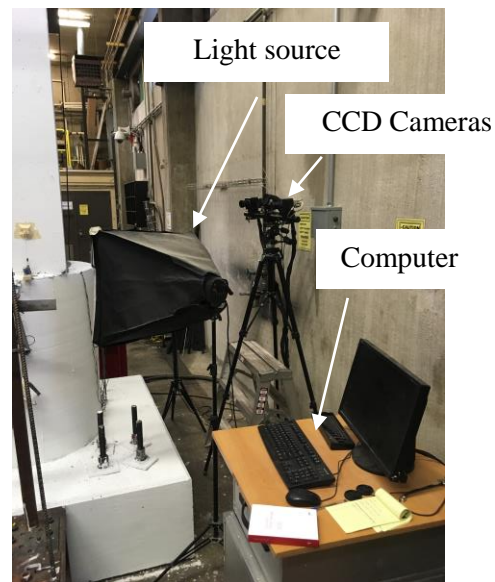
The strains in the longitudinal reinforcement, transverse reinforcement, and dowel bars in the column and drilled shaft were measured with electrical resistance strain gauges. The locations of all the strain gages are provided in Appendix B.

### 3.7.3 Digital Image Correlation (DIC)-Based Non-contact Measurement System

The Digital Image Correlation (DIC)-based non-contact measurement system was placed on the west side of the column in order to obtain the strain measurements, crack propagation and crack width in the non-contact lap splice zone. A random speckle pattern was applied on the surface of the column as shown in Fig. 3-6(a) using black spray paint. The following hardware were used for the DIC-based non-contact measurements: a pair of 12 megapixel charge-coupled device (CCD) cameras (4096 × 3072 image resolution) with 50 mm fixed focal lenses for capturing images and a high-performance computer. An external light source was also provided in order to maintain a constant brightness on the measurement surface. The positioning and components of the DIC-based non-contact measurement system are shown in Fig. 3-6(b).



(a) Speckle pattern



(b) Positioning and components

**Fig. 3-6: DIC-based non-contact measurement system (West side).**

### 3.7.4 Data Acquisition

The applied load was obtained from the built-in load cell of the hydraulic actuator. The vertical load obtained from the load cell and the lateral displacement of the specimens obtained from LVDTs 1 to 4 were recorded using the HBM Spider 8 data acquisition system (Fig. 3-7). The strains

on the reinforcing bars obtained from the electrical resistance strain gauges were recorded using the Vishay data acquisition system (Fig. 3-8).

Before the actual test, all the instruments were set to zero at their balance points and care was taken to ensure that all were working properly. During each test, the vertical load and the lateral displacement from LVDT 1 were plotted versus one another on the HBM Spider 8 computer screen. That plot provided a means for controlling the test program by providing immediate feedback on the behavior of each column-drilled shaft specimen during testing.



**Fig. 3-7: HBM Spider 8 data acquisition system.**



**Fig. 3-8: Vishay data acquisition system.**

### **3.8 Loading Protocol**

In order to design the loading protocol for the test specimens, a preliminary finite element analysis (FEA) of the Bent 17 column-drilled shaft connection and a preliminary laboratory test were performed on Specimen 1.

#### **3.8.1 Preliminary Finite Element Analysis of the Bent 17 Column-Drilled Shaft Connection**

An FEA was performed on the Bent 17 column-drilled shaft connection to investigate the performance of the connection under service load. A three-dimensional finite element model of the Bent 17 column-drilled shaft connection was developed using Abaqus [28]. The FEA model of the structure is shown in Fig. 3-9(a). Fig. 3-9(b) shows the reinforcement layout in the column and the drilled shaft.

The Concrete Damaged Plasticity (CDP) model [29] was used as the constitutive model of concrete in the FEA models. The uniaxial stress-strain curves proposed by Hsu and Mo [30] were adopted for the definition of the CDP model (Fig. 3-10). Equation 15 was used to develop the

parabolic compression stress-strain curve. Equations 16 [31] and 17 [32] defined the ascending and descending branch of the tensile stress-strain curve, respectively.

Concrete in compression is given by

$$\sigma_c = f_c' \left[ \frac{2\varepsilon_c}{\varepsilon_0} - \left( \frac{\varepsilon_c}{\varepsilon_0} \right)^2 \right]. \quad (15)$$

Concrete in tension is given by

$$\text{Ascending branch: } \sigma_c = E_c \varepsilon_c \text{ and} \quad (16)$$

$$\text{Descending branch: } \sigma_c = f_{cr} \left( \frac{\varepsilon_{cr}}{\varepsilon_c} \right)^{0.4}, \quad (17)$$

where,  $\sigma_c$  = stress of concrete (ksi);  $\varepsilon_c$  = strain of concrete (in/in);  $f_c'$  = peak compressive stress (ksi);  $\varepsilon_0$  = strain at the peak stress of  $f_c'$  taken as 0.002 in/in;  $E_c$  = modulus of elasticity of concrete (ksi);  $f_{cr}$  = cracking stress of concrete (ksi); and  $\varepsilon_{cr}$  = cracking strain of concrete taken as 0.00008 in/in.

An unconfined concrete compressive strength of 3.6 ksi and concrete tensile strength of 0.2736 ksi was used for the CDP model. The modulus of elasticity of concrete was 3,420 ksi, and its Poisson's ratio was 0.2. The stress-strain curve of the reinforcing steel was a bilinear elastoplastic model with a linear strain hardening as shown in Fig. 3-11 [30]. The yield strength of the steel reinforcement was 60 ksi. The modulus of elasticity of steel was 29,000 ksi, and its Poisson's ratio was 0.3. An 8-node linear brick, reduced integration, hourglass control element (C3D8R) was used to mesh the concrete material [33]. A 2-node linear 3-D truss element (T3D2) was used to implement the steel reinforcement [33]. The reinforcing bars in the FEA model were "embedded" in the concrete. By "embedding" the reinforcing bars in concrete, it was assumed that there is a perfect bond between the rebar and the surrounding concrete.

For highway bridges, the columns and drilled shafts are constructed in separate stages, and hence the connections are typically not a monolithic connection. Therefore, the column-drilled

shaft interface was simulated by assuming a “Surface to Surface” [33] contact between the column bottom surface and the drilled shaft top surface. Also, a friction coefficient of 0.4 was used as per PCA recommendations [34] to simulate the tangential behavior of the interface.

The service load (dead load plus live load) corresponding to the Bent 17 column-drilled shaft connection was applied to the FEA model as shown in Fig. 3-9(a). Due to the loads, a uniform bending moment was produced in the column-drilled shaft assembly. From the FEA results, the stresses in the column longitudinal bars on the tension side were studied as shown in Fig. 3-12. Due to the dead load (DL), the maximum tensile stress in the column longitudinal bars on the “tension side” of the column-drilled shaft structure was 6.2 ksi as shown in Fig. 3-13(a). Due to the dead and live loads (LL), the maximum tensile stress in the column longitudinal bars on the “tension side” was 9.8 ksi as shown in Fig. 3-13(b).

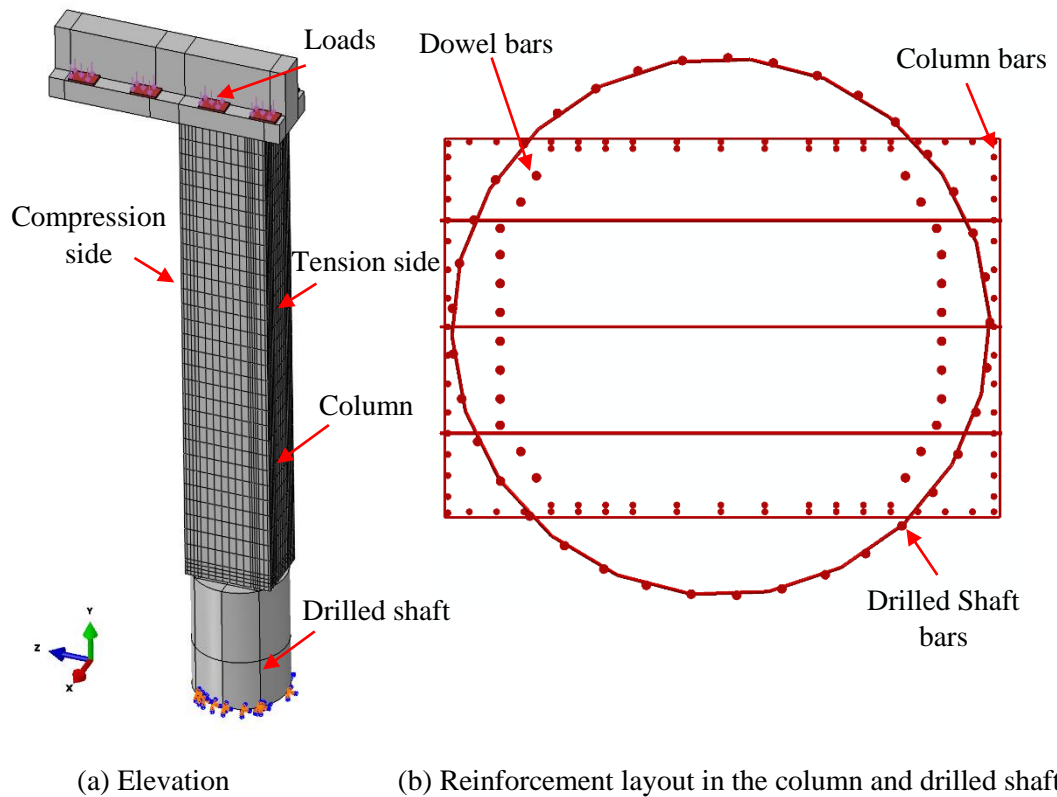


**Fig. 3-9: Three-dimensional (3D) finite element model of the Bent 17 column-drilled shaft structure.**

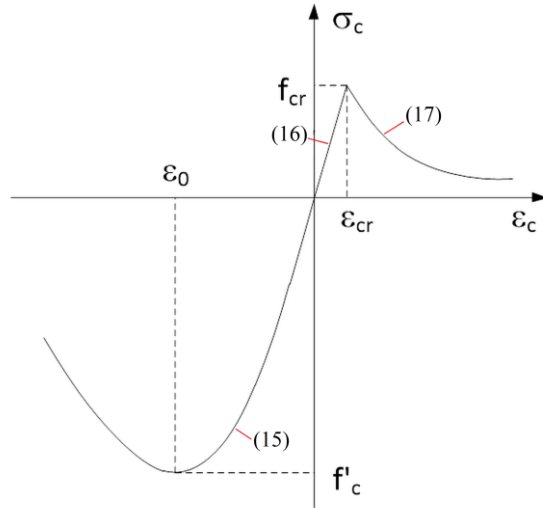


**Fig. 3-10: Stress-strain curves of concrete in compression and tension.**

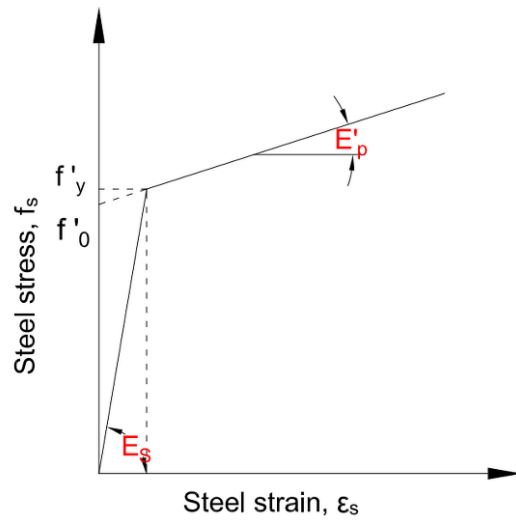


**Fig. 3-11: Stress-strain relationship of reinforcing steel using bilinear elastoplastic model.**

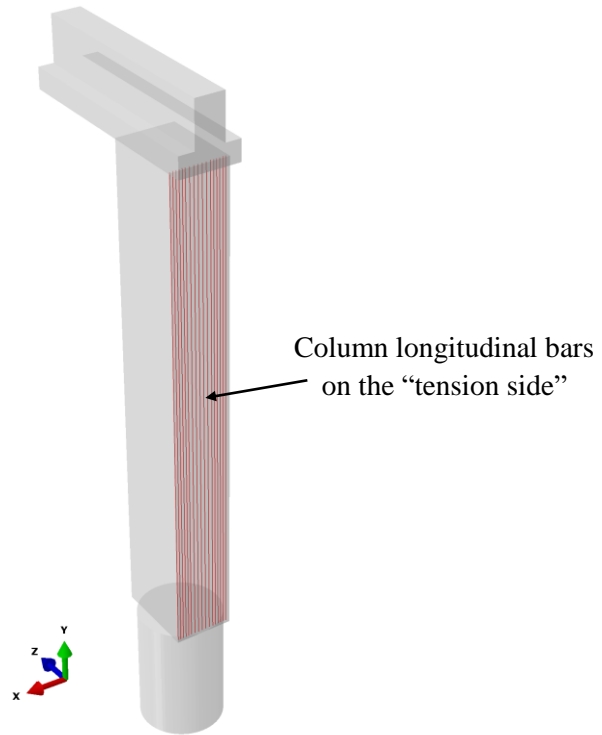


**Fig. 3-12: Column longitudinal bars on the “tension side” of the FEA model of the Bent 17 column-drilled shaft structure.**

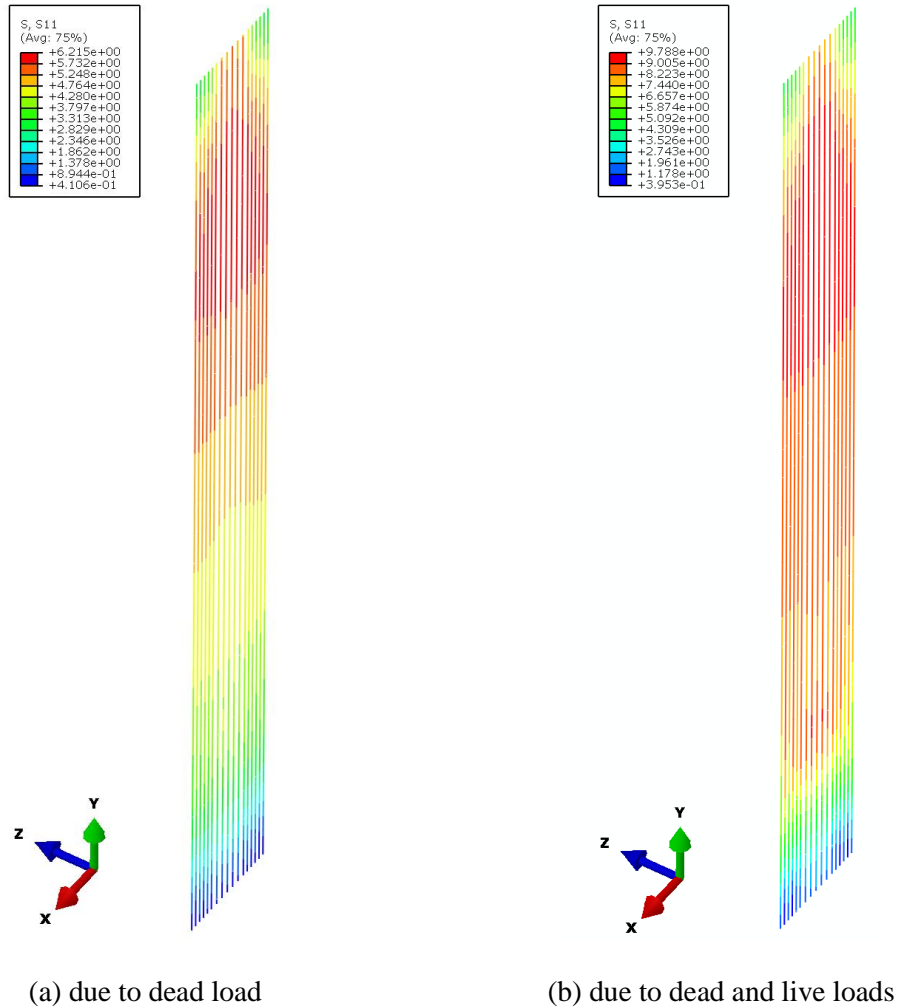


**Fig. 3-13: Stresses in the column longitudinal bars of Bent 17 column-shaft structure.**

### 3.8.2 Preliminary Test on Specimen 1

A preliminary laboratory test was performed on Specimen 1 in which the specimen was monotonically loaded till the maximum tensile stress in the column longitudinal bars on the north side reached a value of 6.2 ksi (measured by Strain Gages C1 and C2). The applied load during the test corresponding to the stress of 6.2 ksi was found to be 56.25 kips which was selected as Load Level A. Further the monotonic loading was continued until the maximum tensile stress in the column longitudinal bars on the north side reached 9.8 ksi. The applied load corresponding to the stress of 9.8 ksi was 66.75 kips which was selected as Load Level B. It is important to note that

Load Levels A and B for the test specimens correspond to the DL and DL + LL of the Bent 17 column-drilled shaft connection, respectively.

### **3.8.3 Test Procedure**

Fig. 3-14 shows the loading procedure for the test specimens. The loading protocol consisted of both monotonic and cyclic loading. The loading was implemented in three stages. In Stage 1, the load was applied monotonically up to the Load Level A of 56.25 kips. The quasi-static loading was applied using a load-control procedure at a rate of 2 kips/minute. In Stage 2, cyclic loading of 10.5 kips which is the difference between Load Level A and Load Level B was applied to the specimens. The cyclic loading was applied at a rate of 0.5 Hz for three days. The decision to limit the application of the cyclic loading for three consecutive days was based on the research project schedule. In three days, a total of 125,000 cycles of a 10.5 kips load was applied on the specimens to compare the performance of the specimens under cyclic loading. It is important to note that this cyclic loading was not applied to find out the fatigue behavior of the specimens. After the application of the cyclic loading, in Stage 3 the loading was switched to a displacement-control procedure and continued until concrete crushing was observed at the toe of the column and on the drilled shaft. The loading rate at Stage 3 was 0.033 inches/minute. The loads and displacements of the actuator were precisely controlled by an MTS “Multiplex” system during the test. A data acquisition system was used to record data at a rate of 2 Hz throughout the entire loading procedure.

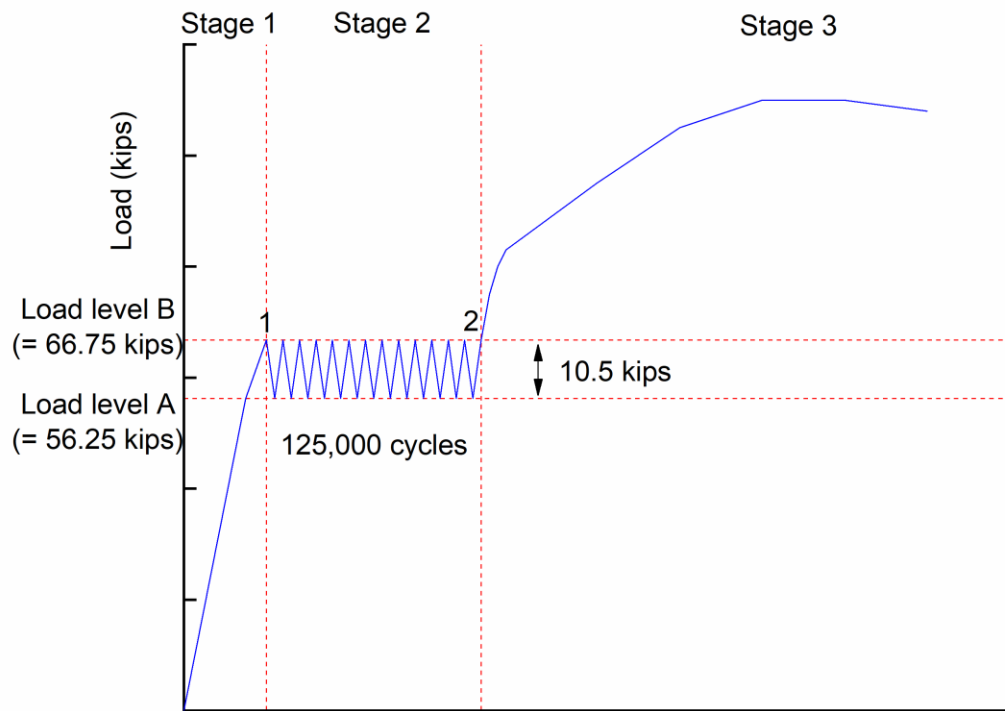


**Fig. 3-14: Loading procedure.**

## **Chapter 4 Experimental Results**

### **4.1 Overview**

In this chapter, the test results of the experimental program are presented in detail. Eleven tests were conducted on the column-drilled shaft specimens with the following three parameters investigated: non-contact lap splice distance, lap splice length of spliced bars, and amount of transverse reinforcement in the non-contact lap splice zone in non-circular columns.

### **4.2 Material Properties**

The compressive strengths of the specimens were measured from the unconfined compression test of 4-inch. by 8-inch. cylinder specimens one day before the loading test. The compressive strengths of the specimens are provided in Table 4-1. The deformed steel bars were selected according to the ASTM A615 standards [22], with the material strength of Grade 60. The yield strength and tensile strength of different sizes of bars used in the construction of the specimens are provided in Table 4-2.

**Table 4-1: Material properties of concrete**

Specimen number	Unconfined compressive strength, ksi	
	Column	Drilled Shaft
Specimen 1	7.0	6.5
Specimen 2	6.7	6.1
Specimen 3	6.5	6.8
Specimen 4	7.5	7.1
Specimen 5	6.7	7.4
Specimen 6	6.9	8.0
Specimen 7	7.1	7.7
Specimen 8	7.3	8.1
Specimen 9	7.6	7.9
Specimen 10	7.1	7.4
Specimen 11	7.9	7.7

**Table 4-2: Material properties of deformed steel bars**

Bar size	Yield strength, ksi	Tensile strength, ksi
No. 3	63.0	97.0
No. 5	66.1	105.5
No. 7	68.3	111.9

### 4.3 Summary of Experimental Results

#### 4.3.1 Specimens in Phase I

##### 4.3.1.1 Specimen 1

The vertical load vs. lateral displacement relationship of Specimen 1 is shown in Fig. 4-1(a). The lateral displacement was plotted from the measurements of LVDT 1 located on the north side of the column as shown in Fig. 3-5. As shown in Fig. 4-2(a), an opening (Crack 1) was observed at the column-drilled shaft interface at a load of 10.0 kips. The first flexural crack on the column (Crack 2) was observed outside the non-contact lap splice zone at a load of 28.6 kips. At a load of 66.75 kips, a splitting crack (Crack 3) was observed on the drilled shaft as shown in Fig. 4-4(a). The splitting crack originated from the column-drilled shaft interface and propagated downwards from the top of the drilled shaft. At this loading stage, another splitting crack (Crack 4) was observed on the column which propagated upwards from the column-drilled shaft interface. These splitting cracks formed due to the splitting forces caused by the slip of dowel bars from the surrounding concrete. At this loading stage, a total of 125,000 cycles of cyclic loading was applied to Specimen 1. At Point 1 of the cyclic loading (Fig. 3-14), the lateral displacement of the specimen was found to be 0.402 inches, and at Point 2 of the cyclic loading, the lateral displacement was 0.424 inches. Due to the cyclic loading, the lateral displacement of the specimen was increased by 5.47%. When the load applied by the actuator was progressively increased, the dowel bars started

yielding at a load of 77.1 kips. At this loading stage, the strains in the dowel bars (Strain Gage D2) reached the yield strain of 0.0023. At a load of 105.0 kips, the strains in the column longitudinal bars (Strain Gage C1 and C2) remained elastic and well below the yield strain of 0.0023. The strains in the transverse reinforcement in the column (Strain Gages T1 and T7) and the transverse reinforcement in the drilled shaft (Strain Gages S1 and S2) also remained elastic and well below the yield strain. At this loading stage, concrete crushing was not observed on the specimen.

#### **4.3.1.2 Specimen 2**

The vertical load vs. lateral displacement relationship of Specimen 2 is shown in Fig. 4-1(b). As shown in Fig. 4-2(b), the opening (Crack 1) was observed at the column-drilled shaft interface on the North side of the specimen at a load of 8.5 kips. The first flexural crack (Crack 2) was observed on the column at a load of 29.0 kips as shown in Fig. 4-2(b). As shown in Fig. 4-4(b), a splitting crack was observed (Crack 3) on the column at a load of 56.25 kips. At the same loading stage, another splitting crack (Crack 4) was observed on the drilled shaft. At this loading stage, an inclined crack (Crack 5) was observed between the non-contact distance of the column longitudinal and dowel bars as shown in Fig. 4-4(b). The inclined crack propagated further into the compression zone at a maximum inclination angle of 12 degrees with the horizontal. As shown in Fig. 4-3(b), the first flexural crack on the drilled shaft (Crack 6) was also observed at a load of 56.25 kips. When the load applied by the actuator was progressively increased, the dowel bars started yielding (Strain Gage D2) at a load of 63.5 kips. It was found that due to the cyclic loading, the lateral displacement of the specimen was increased by 9.03%. As the loading progressed, the cracks on the specimen propagated more and more. At a load of 68.9 kips, the strains in the column ties (Strain Gage T1) were found to have reached the yield strain of 0.0023. At a load of 103.7 kips, the column longitudinal bars started yielding (Strain Gage C1). At a load of 112.0 kips, concrete crushing failure was observed on the south side of the drilled shaft (Crack 7) which originated from the column-drilled shaft interface and propagated down the south side of the shaft. At this loading

stage, the strains in the drilled shaft longitudinal bars and the drilled shaft transverse reinforcement remained elastic. The loading was stopped at a load of 112.0 kips, and the specimen was considered to have failed due to concrete crushing in the drilled shaft.

#### **4.3.1.3 Specimen 3**

The vertical load vs. lateral displacement relationship of Specimen 3 is shown in Fig. 4-1(c). As shown in Fig. 4-2(c), the opening (Crack 1) was observed at the column-drilled shaft interface on the north side of the specimen at a load of 7.5 kips. The first flexural crack (Crack 2) was observed on the column at a load of 30.0 kips. As shown in Fig. 4-4(c), a splitting crack was observed (Crack 3) at a load of 37.5 kips on the column. At a load of 50.0 kips, another splitting crack (Crack 4) was observed on the drilled shaft. At this loading stage, the first flexural crack on the drilled shaft (Crack 5) was observed as shown in Fig. 4-3(c). Shortly after, an inclined crack (Crack 6) was observed at a load of 56.25 kips between the non-contact distance of the column longitudinal and dowel bars as shown in Fig. 4-4(c). The inclined crack propagated further into the compression zone at a maximum inclination angle of 33 degrees with the horizontal. At a load of 66.5 kips, the strains in the dowel bars (Strain Gage D3) were found to have reached the yield strain of 0.0023. Due to the cyclic loading, the lateral displacement of the specimen was increased by 8.32%. At a load of 81.2 kips, the column ties (Strain Gage T1) started yielding near the column-shaft interface. At a load of 92.0 kips, concrete crushing failure was also observed on the south side of the drilled shaft (Crack 7). At this loading stage, the strains in the column longitudinal bars (Strain Gage C1) reached the yield strain. Afterward, the strains in the transverse reinforcement (Strain Gage S1) in the vicinity of the column-drilled shaft interface reached the yield strain. Finally, concrete crushing failure was observed at the toe of the column (Crack 8) on the south side of the specimen at a load of 100.0 kips. At this loading stage, the strains in the drilled shaft longitudinal bars (Strain Gage DS1) remained elastic.

#### **4.3.1.4 Specimen 4**

The vertical load vs. lateral displacement relationship of Specimen 4 is shown in Fig. 4-1(d). As shown in Fig. 4-2(d), the opening (Crack 1) was observed at the column-drilled shaft interface on the north side of the specimen at a load of 7.0 kips. The first flexural crack (Crack 2) was observed on the column at a load of 33.0 kips. At this loading stage, a splitting crack was also observed (Crack 3) on the column. At a load of 50.0 kips, an inclined crack (Crack 4) was observed between the non-contact distance of the column longitudinal bars and the dowel bars as shown in Fig. 4-4(d). The inclined crack propagated further into the compression zone at a maximum inclination angle of 43 degrees with the horizontal. As shown in Fig. 4-3(d), the first flexural crack on the drilled shaft (Crack 5) was observed at a load of 56.25 kips. At this loading stage, another splitting crack (Crack 6) was observed on the drilled shaft. At a load of 58.8 kips, the column ties started yielding near the column-shaft interface (Strain Gage T1). Due to the cyclic loading, the lateral displacement of the specimen was increased by 9.35%. When the load applied by the actuator was progressively increased, the dowel bars started yielding (Strain Gage D1) at a load of 72.5 kips. At a load of 89.3 kips, the strains in the column longitudinal bars (Strain Gage C1) were found to have reached the yield strain of 0.0023. At a load of 90.0 kips, the loading could not be continued due to technical difficulties with the actuator. The specimen was not loaded again as the results would have been affected due to the unloading. Therefore, the ultimate capacity of Specimen 4 could not be observed. The strains in the drilled shaft longitudinal bars and the drilled shaft transverse reinforcement remained elastic up to this loading stage. Moreover, at this loading stage concrete crushing failure was not observed on the specimen.

#### **4.3.1.5 Specimen 5**

The vertical load vs. lateral displacement relationship of Specimen 5 is shown in Fig. 4-1(e). As shown in Fig. 4-2(e), the opening (Crack 1) was observed at the column-drilled shaft interface at a load of 8.0 kips. The first flexural crack (Crack 2) was observed on the column at a load of 29.0

lips. As shown in Fig. 4-4(e), a splitting crack was observed (Crack 3) at a load of 44.0 kips on the column. At this loading stage, an inclined crack (Crack 4) was observed between the non-contact distance of the column longitudinal and dowel bars. The inclined crack propagated further into the compression zone at a maximum inclination angle of 24 degrees with the horizontal. As shown in Fig. 4-3(e), the first flexural crack on the drilled shaft (Crack 5) was observed at a load of 56.25 kips. When the load applied by the actuator was progressively increased, the dowel bars started yielding (Strain Gage D3) at a load of 63.75 kips. At a load of 66.75 kips, another splitting crack (Crack 6) was observed on the drilled shaft which propagated from the column-drilled shaft interface to the edge of the shaft radially and then extended downwards along the dowel bars inside the drilled shaft. At the 5,570<sup>th</sup> cycle of the cyclic loading, the strains in the column longitudinal bars (Strain Gage C1) were found to have reached the yield strain of 0.0023. Due to the cyclic loading, the lateral displacement of the specimen was increased by 10.2%. At a load of 100.5 kips, the column ties started yielding near the column-shaft interface (Strain Gage T4). At this loading stage, concrete crushing failure was observed at the toe of the column (Crack 7) on the south side of the specimen. At a load of 108.2 kips, concrete crushing failure was observed on the south side of the drilled shaft (Crack 8) which originated from the column-drilled shaft interface and propagated down the south side of the shaft. At this loading stage, the strains in the drilled shaft longitudinal bars and the drilled shaft transverse reinforcement remained elastic.

#### **4.3.1.6 Specimen 6**

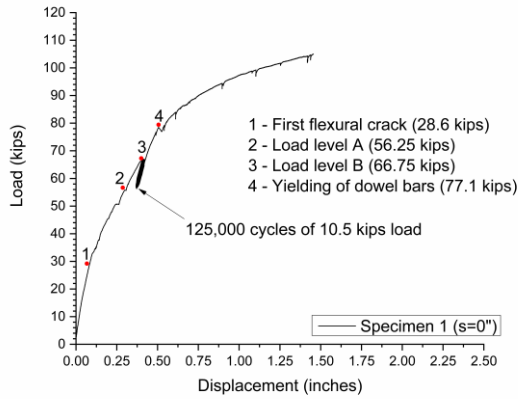
The vertical load vs. lateral displacement relationship of Specimen 6 is shown in Fig. 4-1(f). As shown in Fig. 4-2(f), the opening (Crack 1) was observed at the column-drilled shaft interface at a load of 8.5 kips. The first flexural crack (Crack 2) was observed on the column at a load of 28.5 kips. As shown in Fig. 4-4(f), a splitting crack was observed (Crack 3) at a load of 49.0 kips on the column. Shortly after, an inclined crack (Crack 4) was observed at a load of 52.0 kips between the non-contact distance of the column longitudinal and dowel bars which propagated further into the

compression zone at a maximum angle of 40 degrees with the horizontal. As shown in Fig. 4-3(f), the first flexural crack on the drilled shaft (Crack 5) was observed at a load of 56.25 kips. At a load of 64.0 kips, another splitting crack (Crack 6) was observed on the drilled shaft. When the load applied by the actuator was progressively increased, the dowel bars started yielding (Strain Gage D2) at a load of 64.4 kips. Due to the cyclic loading, the lateral displacement of the specimen was increased by 13.3%. At a load of 77.9 kips, the strains in the column longitudinal bars (Strain Gage C3) were found to have reached the yield strain of 0.0023. Shortly after, at a load of 80.8 kips, the column ties started yielding near the column-shaft interface (Strain Gage T3). At a load of 98.3 kips, the transverse reinforcement in the vicinity of the column-drilled shaft interface started yielding (Strain Gage S1). Finally, concrete crushing failure was observed at the toe of the column (Crack 7) on the south side of the specimen at a load of 108.0 kips. At this loading stage, concrete crushing failure was also observed on the south side of the drilled shaft (Crack 8). The strains in the drilled shaft longitudinal bars remained elastic up to this stage.

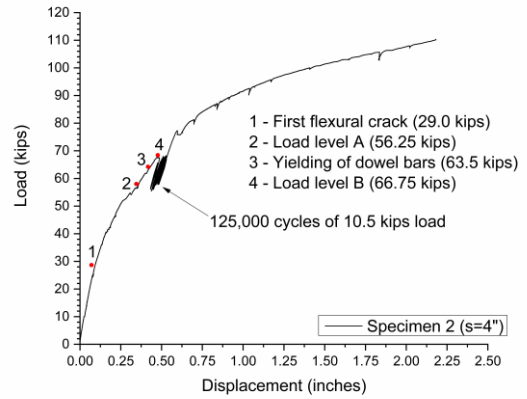
#### **4.3.1.7 Specimen 7**

The vertical load vs. lateral displacement relationship of Specimen 7 is shown in Fig. 4-1(g). As shown in Fig. 4-2(g), the opening (Crack 1) was observed at the column-drilled shaft interface at a load of 6.0 kips. The first flexural crack (Crack 2) was observed on the column at a load of 34.0 kips. As shown in Fig. 4-4(g), a splitting crack was observed (Crack 3) at a load of 37.0 kips on the column. Shortly after, an inclined crack (Crack 4) was observed at a load of 51.0 kips which propagated further into the compression zone at a maximum inclination angle of 34 degrees with the horizontal. As shown in Fig. 4-3(g), the first flexural crack on the drilled shaft (Crack 5) was observed at a load of 60.0 kips. At a load of 64.9 kips, the column ties started yielding near the column-shaft interface (Strain Gage T3). Shortly after, at a load of 65.6 kips, the dowel bars started yielding (Strain Gage D1). At a load of 66.75 kips, another splitting crack (Crack 6) was observed on the drilled shaft. Due to the cyclic loading, the lateral displacement of the specimen was

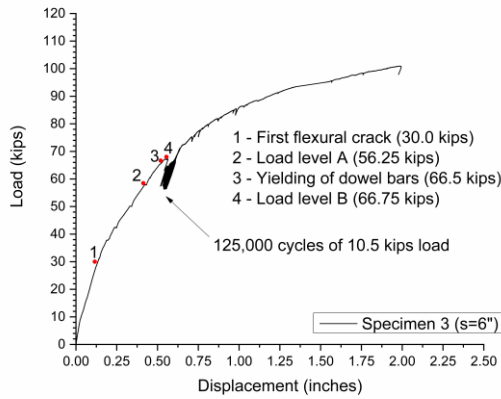
increased by 13.0%. At a load of 82.3 kips, the strains in the column longitudinal bars (Strain Gage C3) were found to have reached the yield strain of 0.0023. Finally, concrete crushing failure was observed at the toe of the column (Crack 7) on the south side of the specimen at a load of 110.0 kips. At this loading stage, concrete crushing failure was also observed on the south side of the drilled shaft (Crack 8).



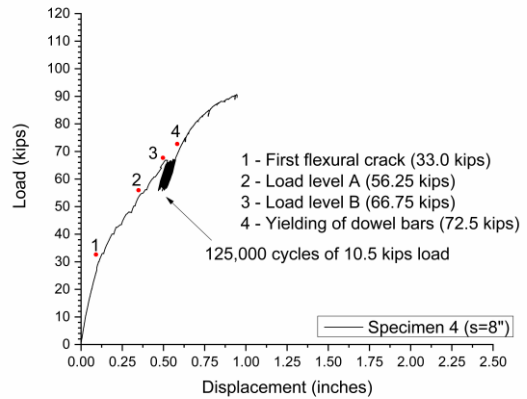
(a) Specimen 1



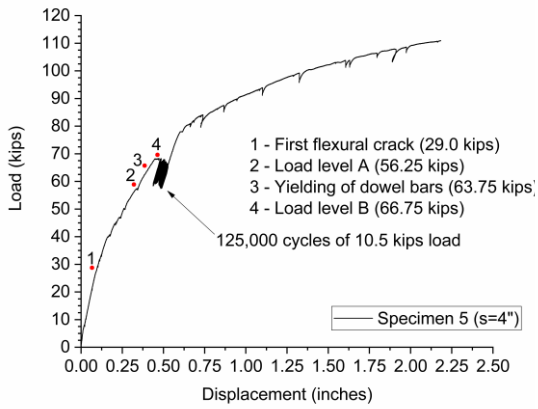
(b) Specimen 2



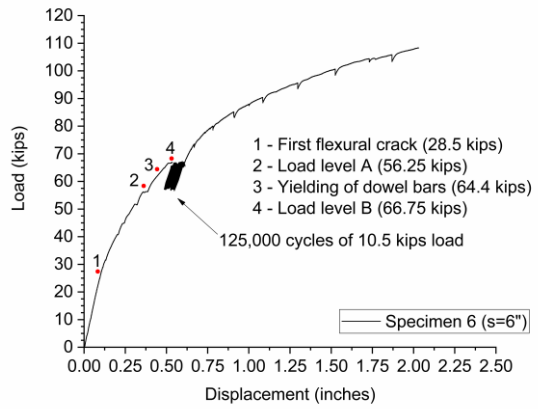
(c) Specimen 3



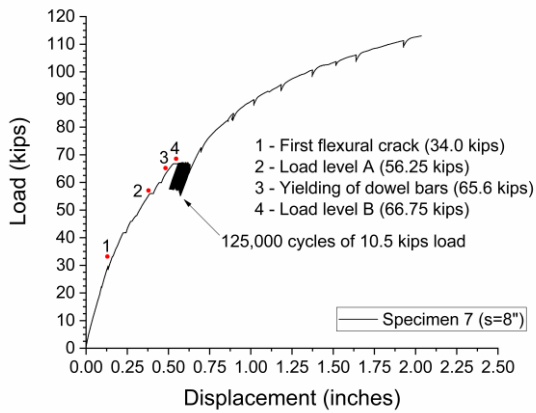
(d) Specimen 4



(e) Specimen 5

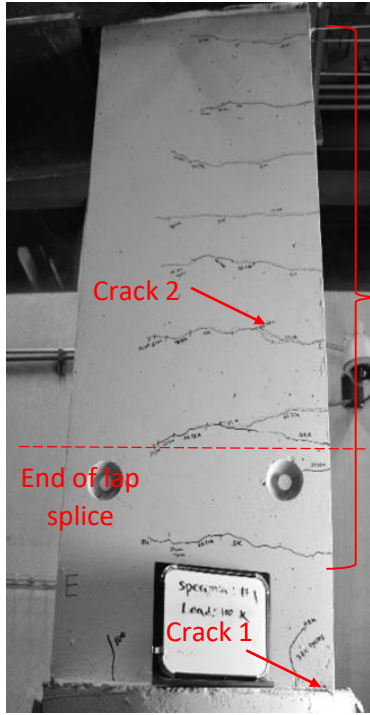


(f) Specimen 6

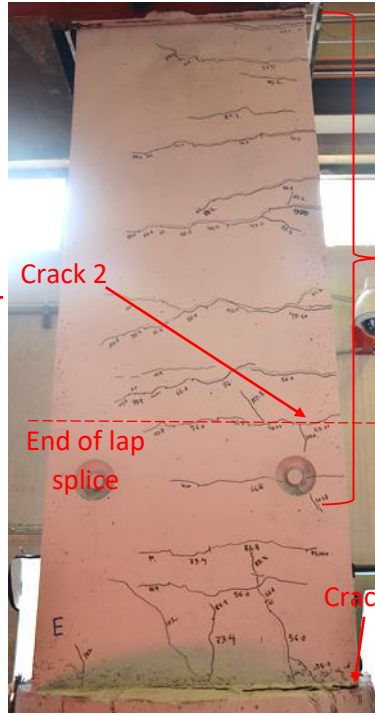


(g) Specimen 7

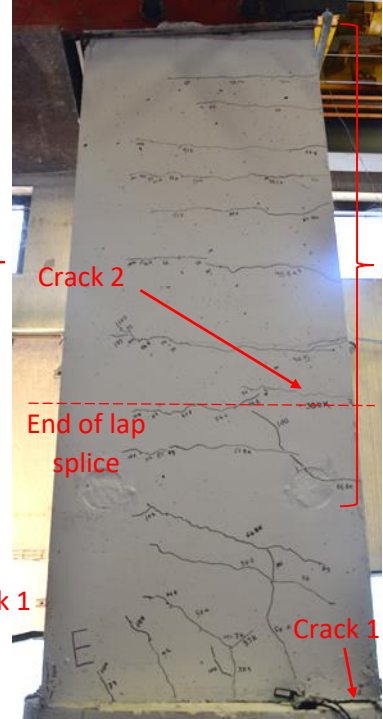
**Fig. 4-1: Load vs. displacement relationship of the specimens in Phase I.**



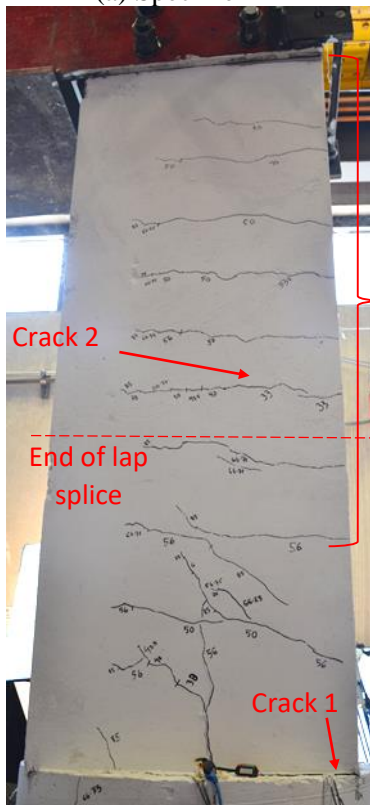
(a) Specimen 1



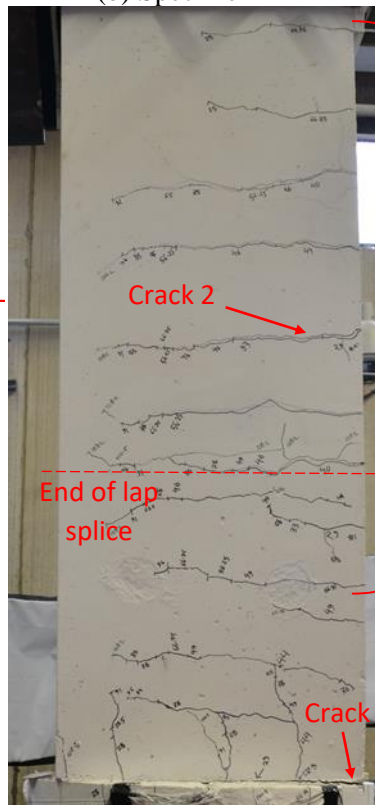
(b) Specimen 2



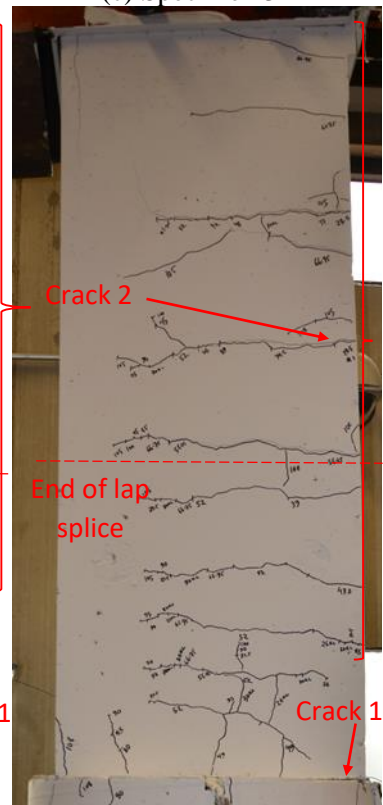
(c) Specimen 3



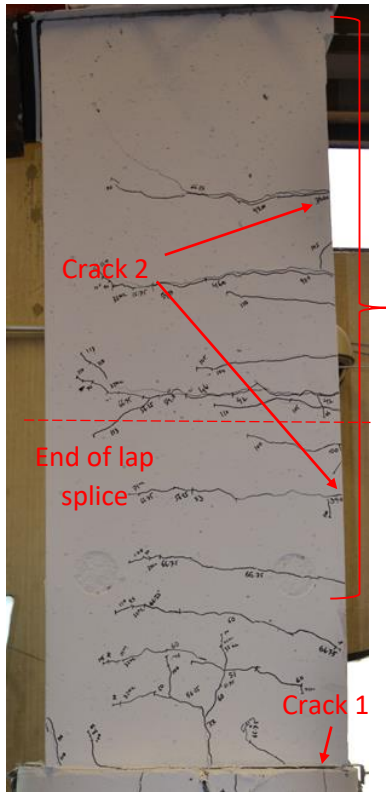
(d) Specimen 4



(e) Specimen 5

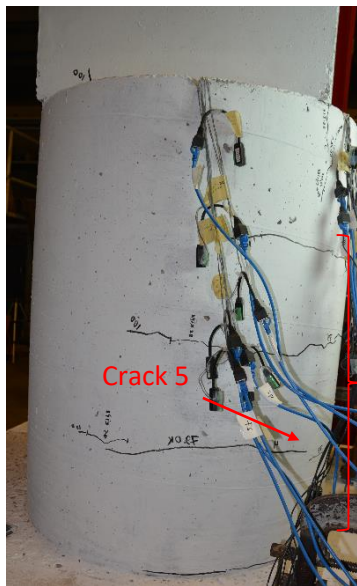


(f) Specimen 6

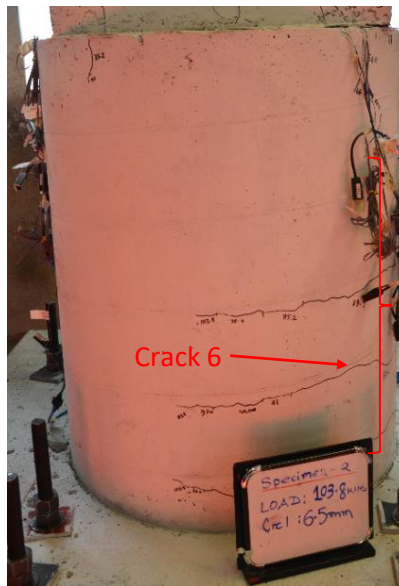


(g) Specimen 7

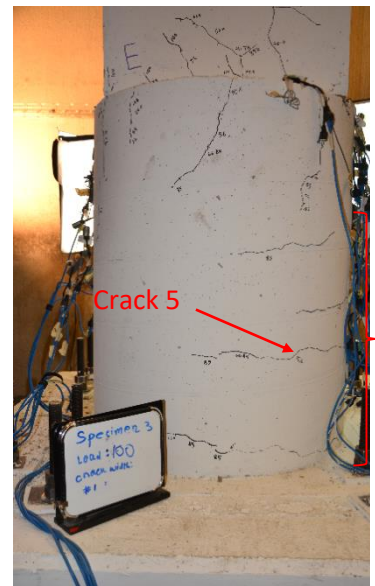
**Fig. 4-2: Flexural cracks on the column (east face)**



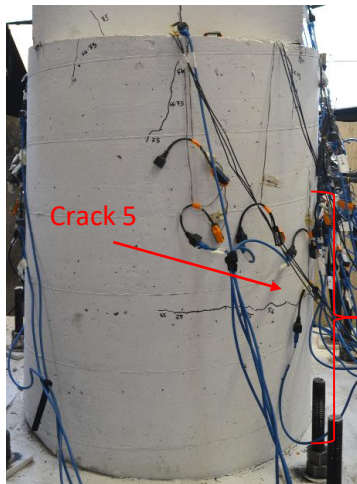
(a) Specimen 1



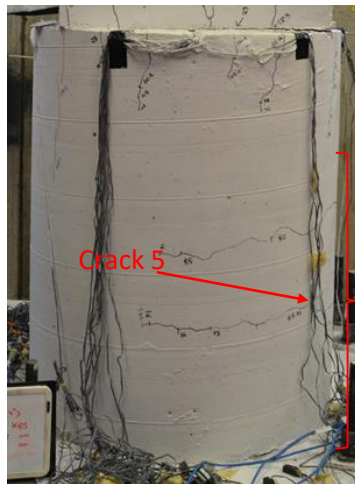
(b) Specimen 2



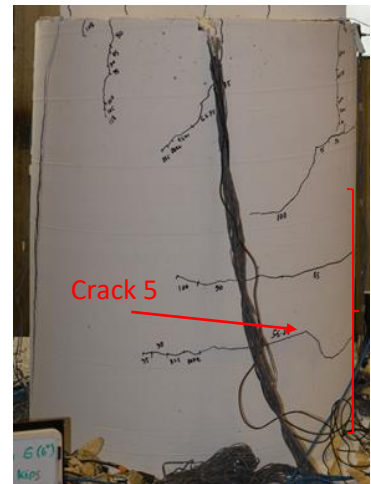
(c) Specimen 3



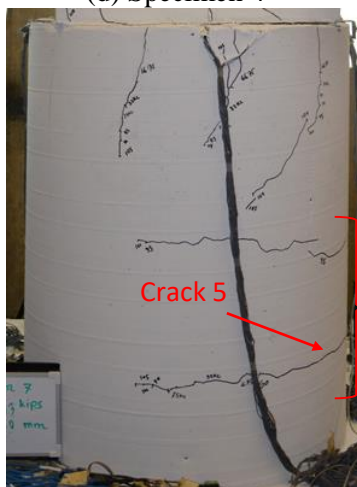
(d) Specimen 4



(e) Specimen 5

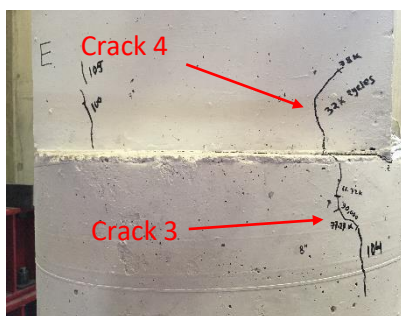


(f) Specimen 6

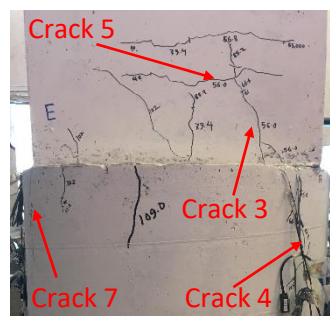


(g) Specimen 7

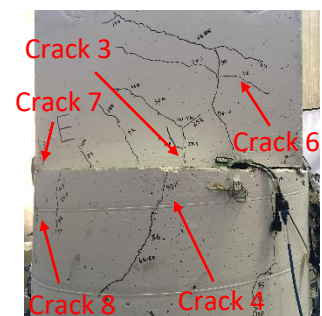
**Fig. 4-3: Flexural cracks on the drilled shaft (east face)**



(a) Specimen 1



(b) Specimen 2



(c) Specimen 3

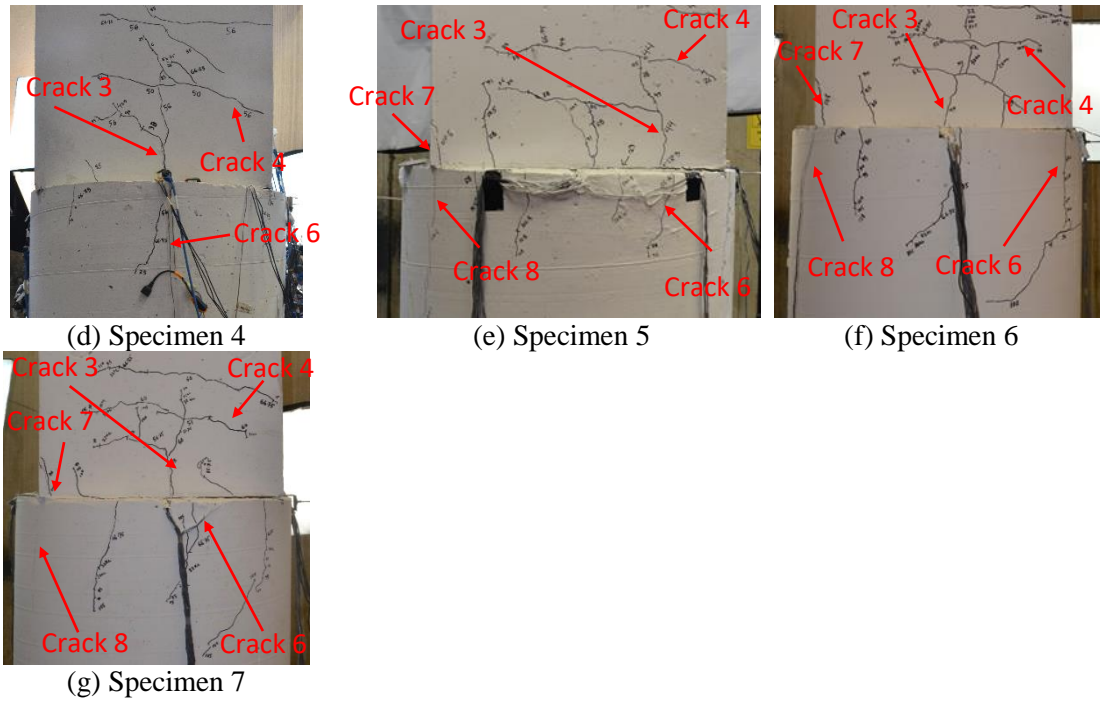


**Fig. 4-4: Splitting and inclined cracks on the column (east face).**

#### 4.3.2 Specimens in Phase II

##### 4.3.2.1 Specimen 8

The vertical load vs. lateral displacement relationship of Specimen 8 is shown in Fig. 4-5(a). As shown in Fig. 4-6(a), an opening (Crack 1) was observed at the column-drilled shaft interface at a load of 7.0 kips. The first flexural crack (Crack 2) was observed on the column at a load of 25.5 kips. As shown in Fig. 4-8(a), a splitting crack was observed (Crack 3) at a load of 37.0 kips on the column. As shown in Fig. 4-7(a), the flexural crack (Crack 5) on the drilled shaft was observed at a load of 46.5 kips. An inclined crack (Crack 4) was observed at a load of 51.5 kips which propagated further into the compression zone at a maximum inclination angle of 19 degrees with the horizontal. At a load of 63.0 kips, another splitting crack (Crack 6) was observed on the drilled shaft. At a load of 62.9 kips, the dowel bars started yielding (Strain Gage D1). Due to the cyclic loading, the lateral displacement of the specimen was increased by 9.9%. At a load of 89.5 kips, the strains in the column longitudinal bars (Strain Gage C4) were found to have reached the yield strain of 0.0023. At a load of 97.0 kips, the column ties started yielding near the column-shaft

interface (Strain Gage T3). Finally, concrete crushing failure was also observed on the south-west side of the drilled shaft [Crack 7 – not visible in Fig. 4-8(a)].

#### **4.3.2.2 Specimen 9**

The vertical load vs. lateral displacement relationship of Specimen 9 is shown in Fig. 4-5(b). As shown in Fig. 4-6(b), an opening (Crack 1) was observed at the column-drilled shaft interface at a load of 6.9 kips. The first flexural crack (Crack 2) was observed on the column at a load of 25.5 kips. As shown in Fig. 4-8(b), a splitting crack was observed (Crack 3) at a load of 35.0 kips on the column. An inclined crack (Crack 4) was observed at a load of 45.0 kips which propagated further into the compression zone at a maximum inclination angle of 37 degrees with the horizontal. As shown in Fig. 4-7(b), the flexural crack (Crack 5) on the drilled shaft was observed at a load of 50.0 kips. At a load of 58.0 kips, the dowel bars started yielding (Strain Gage D1). At a load of 60.4 kips, another splitting crack (Crack 6) was observed on the drilled shaft. Due to the cyclic loading, the lateral displacement of the specimen was increased by 9.98%. At a load of 71.6 kips, the column ties started yielding near the column-shaft interface (Strain Gage T2). At a load of 78.0 kips, the strains in the column longitudinal bars (Strain Gage C3) were found to have reached the yield strain of 0.0023. Finally, concrete crushing failure was observed at the toe of the column (Crack 7) on the south side of the specimen at a load of 107.0 kips. At this loading stage, concrete crushing failure was also observed on the south side of the drilled shaft (Crack 8).

#### **4.3.2.3 Specimen 10**

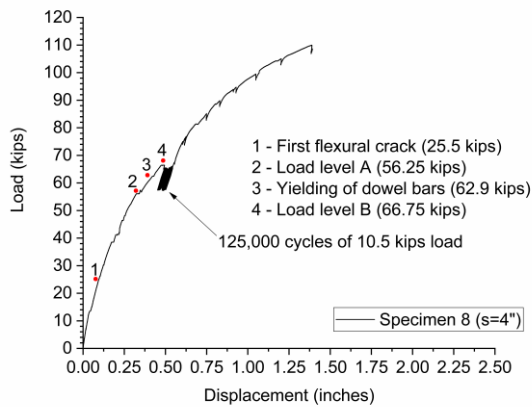
The vertical load vs. lateral displacement relationship of Specimen 10 is shown in Fig. 4-5(c). As shown in Fig. 4-6(c), an opening (Crack 1) was observed at the column-drilled shaft interface at a load of 6.7 kips. The first flexural crack (Crack 2) was observed on the column at a load of 25.0 kips. As shown in Fig. 4-8(c), a splitting crack was observed (Crack 3) at a load of 34.0 kips on the column. An inclined crack (Crack 4) was observed at a load of 40.0 kips which propagated further into the compression zone at a maximum inclination angle of 32 degrees with the horizontal.

As shown in Fig. 4-7(c), the flexural crack (Crack 5) on the drilled shaft was observed at a load of 45.0 kips. At a load of 56.25 kips, another splitting crack (Crack 6) was observed on the drilled shaft. At a load of 55.8 kips, the column ties started yielding near the column-shaft interface (Strain Gage T3). At a load of 63.95 kips, the dowel bars started yielding (Strain Gage D1). Due to the cyclic loading, the lateral displacement of the specimen was increased by 11.25%. At a load of 89.1 kips, the strains in the column longitudinal bars (Strain Gage C4) were found to have reached the yield strain of 0.0023. Finally, concrete crushing failure was observed (Crack 8) on the south side of the drilled shaft at a load of 105.0 kips. At a load of 110.0 kips, concrete crushing failure was also observed at the toe of the column on the south side of the specimen (Crack 7).

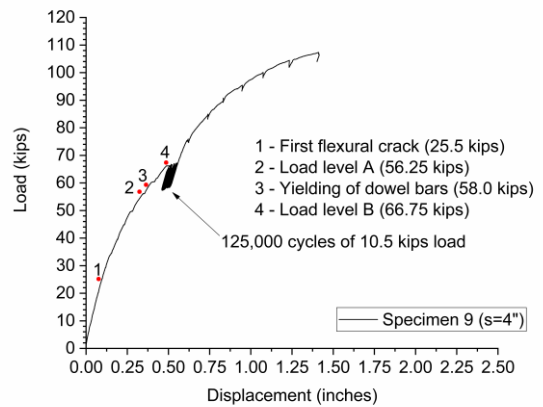
#### **4.3.2.4 Specimen 11**

The vertical load vs. lateral displacement relationship of Specimen 10 is shown in Fig. 4-5(d). As shown in Fig. 4-6(d), an opening (Crack 1) was observed at the column-drilled shaft interface at a load of 7.5 kips. The first flexural crack (Crack 2) was observed on the column at a load of 29.0 kips. As shown in Fig. 4-8(d), a splitting crack was observed (Crack 3) at a load of 40.0 kips on the column. As shown in Fig. 4-7(d), the flexural crack (Crack 5) on the drilled shaft was observed at a load of 45.0 kips. At this loading stage, another splitting crack (Crack 6) was observed on the drilled shaft. An inclined crack (Crack 4) was observed at a load of 50.0 kips which propagated further into the compression zone at a maximum inclination angle of 47 degrees with the horizontal. Specimen 11 was subjected to 2,000,000 cycles of the cyclic loading rather than only 125,000 cycles of the cyclic loading. The cyclic loading was applied at a rate of 1 Hz for 24 days. At the 3,440<sup>th</sup> cycle of the cyclic loading, the column ties started yielding near the column-shaft interface (Strain Gage T2). Between the first and 125,000<sup>th</sup> cycle of the cyclic loading, the lateral displacement of the specimen was increased by 9.7%. The lateral displacement increased at an average rate of 0.448 inches per million cycles between the first and 125,000<sup>th</sup> cycle. Between the 125,000<sup>th</sup> and 2,000,000<sup>th</sup> cycle of the cyclic loading, the lateral displacement of the specimen

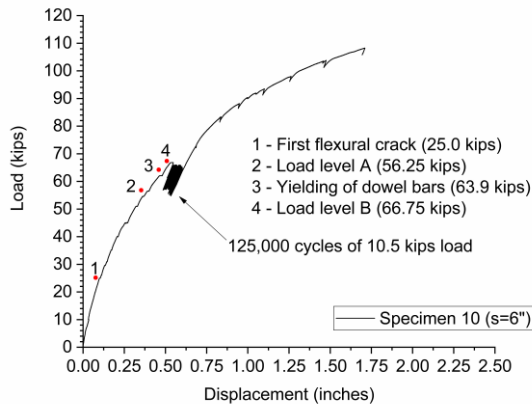
was increased by 10.11%. The lateral displacement increased at an average rate of 0.034 inches per million cycles between the 125,000<sup>th</sup> and 2,000,000<sup>th</sup> cycle. At the 282,966<sup>th</sup> cycle of the cyclic loading, the dowel bars started yielding near the column-shaft interface (Strain Gage D1). At a load of 76.8 kips, the strains in the column longitudinal bars (Strain Gage C3) were found to have reached the yield strain of 0.0023. Finally, concrete crushing failure was observed (Crack 7) on the south side of the drilled shaft at a load of 100.0 kips.



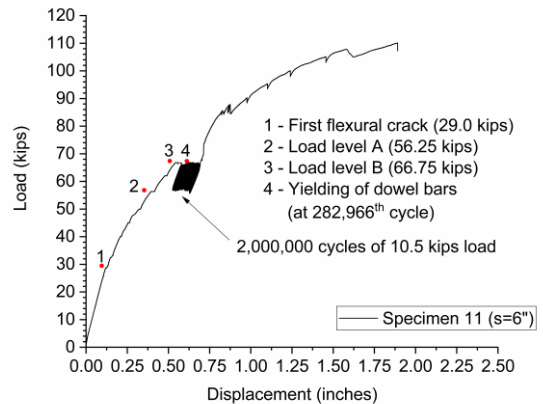
(a) Specimen 8



(b) Specimen 9

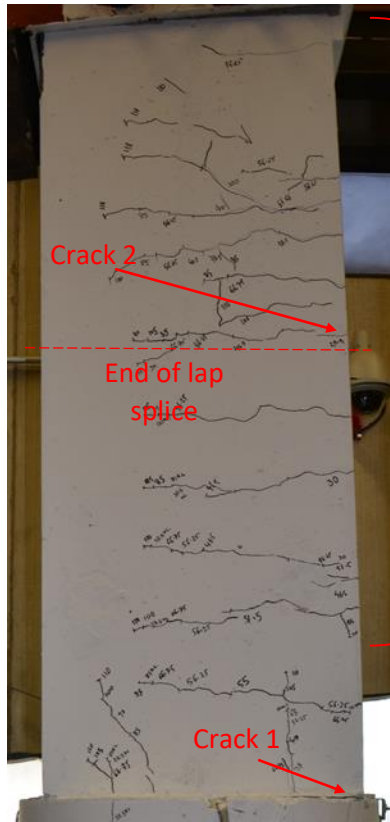


(c) Specimen 10

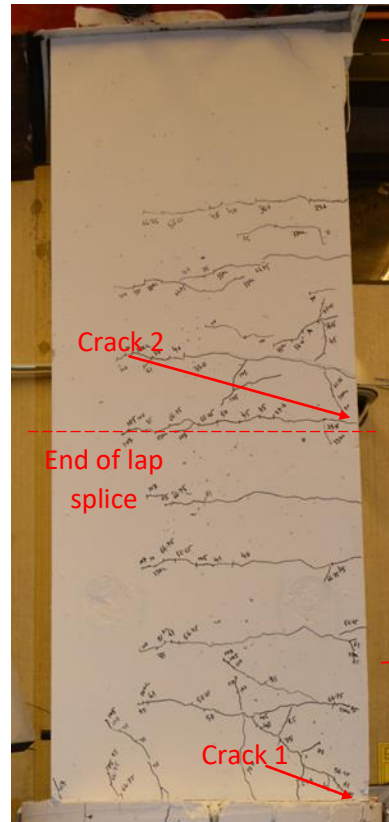


(d) Specimen 11

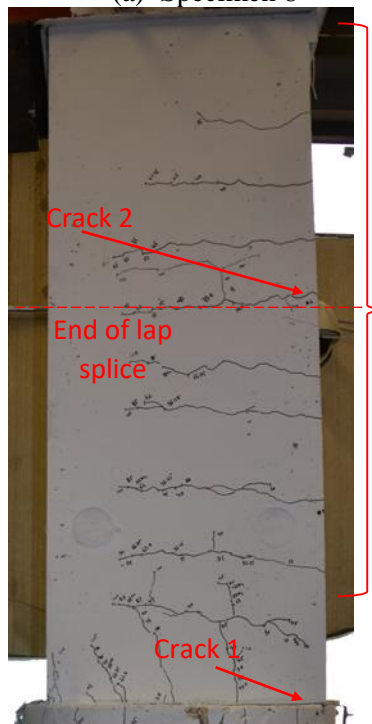
**Fig. 4-5: Load vs. displacement relationship of the specimens in Phase II.**



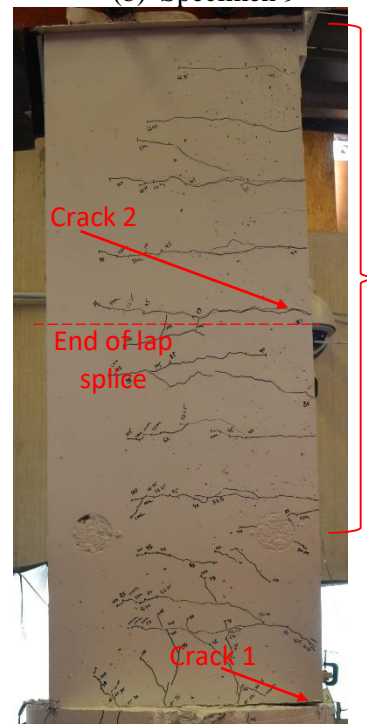
(a) Specimen 8



(b) Specimen 9

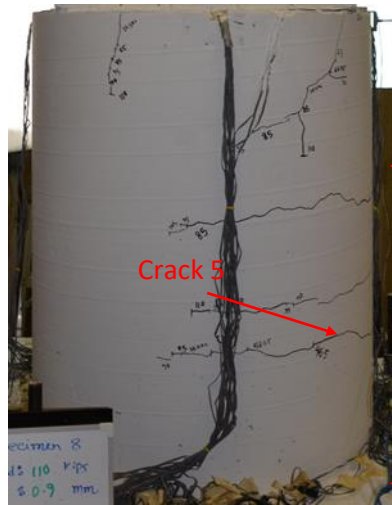


(c) Specimen 10

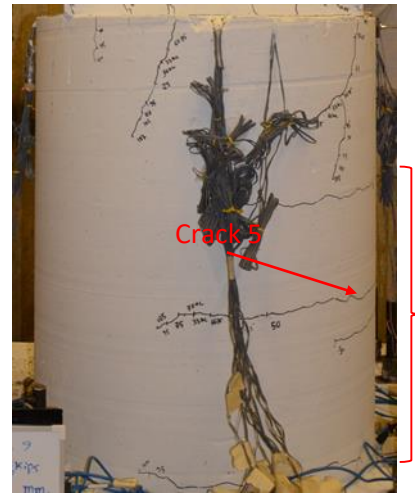


(d) Specimen 11

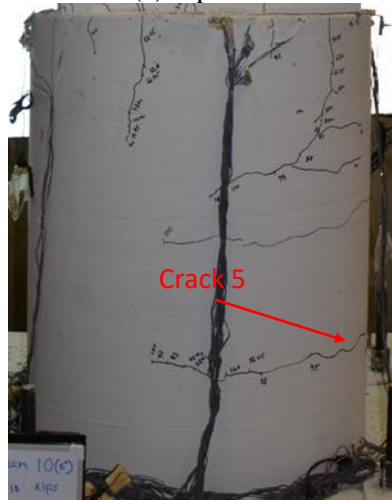
**Fig. 4-6: Flexural cracks on the column (east face).**



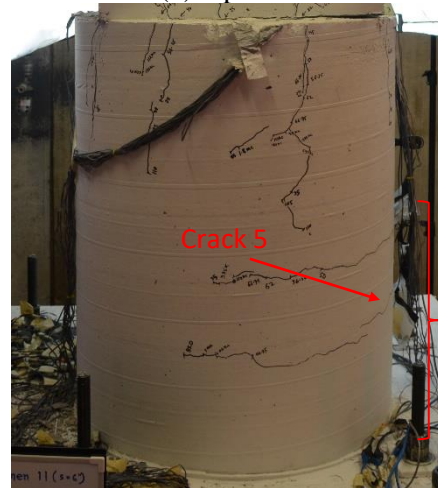
(a) Specimen 8



(b) Specimen 9

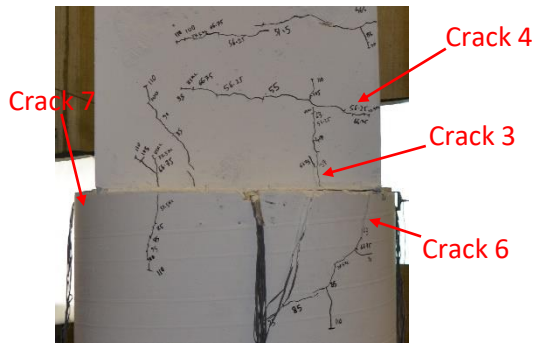


(c) Specimen 10

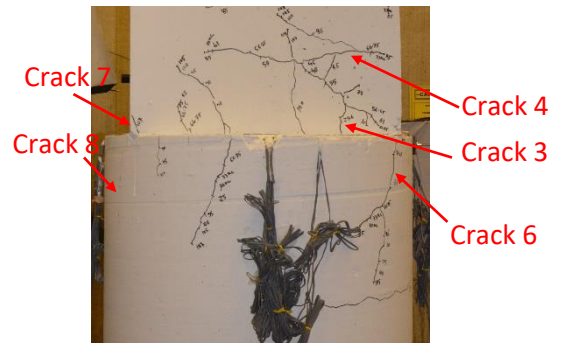


(d) Specimen 11

**Fig. 4-7: Flexural cracks on the drilled shaft (east face).**



(a) Specimen 8



(b) Specimen 9

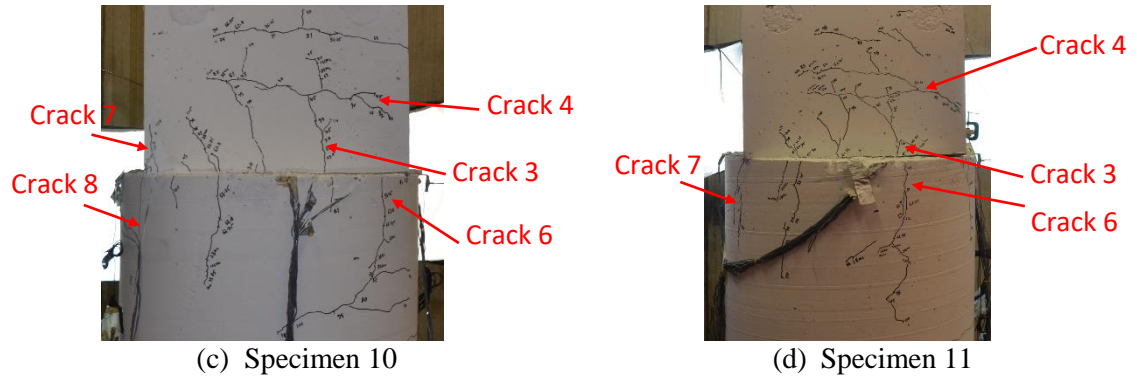


**Fig. 4-8: Splitting and inclined cracks on the column (east face).**

#### **4.4 Discussion of Experimental Results**

##### **4.4.1 Load vs. Displacement Relationships**

The applied load vs. lateral displacement relationships of Specimens 1 to 4 have been compared in Fig. 4-9. From the comparison, it is evident that Specimen 1, constructed with the contact lap splice, exhibited higher stiffness than Specimens 2 to 4 which consisted of the non-contact lap splice. Specimen 2 with 4 inches of non-contact splice distance exhibited higher stiffness than Specimens 3 and 4 with 6 inches and 8 inches of non-contact lap splice distance, respectively. However, Specimen 4 with 8 inches of non-contact lap splice distance showed slightly higher stiffness than Specimen 3 with 6 inches of non-contact lap splice distance. Similarly, the applied load vs. lateral displacement relationships of Specimens 1, 5, 6 and 7 have been compared in Fig. 4-10. As shown in Fig. 4-10, the capacities and lateral stiffnesses of the specimens slightly decreased with increasing the non-contact lap splice distance except for Specimen 7.

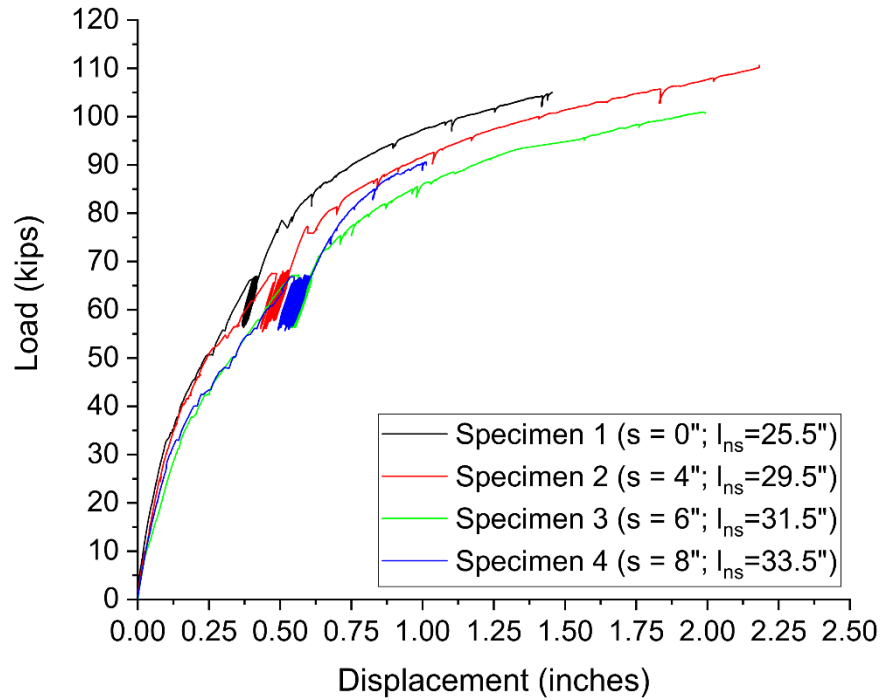


**Fig. 4-9: Applied load vs. lateral displacement relationships of Specimens 1 to 4.**

The lateral stiffnesses of the specimens with 8 inches of non-contact lap splice distance (Specimens 4 and 7) were higher than the specimens with 6 inches of non-contact lap splice distance (Specimens 3 and 6) mostly in Stage 3 of the loading procedure due to the location of the dowel bars. For example, as shown in Fig. 4-11, the dowel bars located on the north side moved away from the extreme tension fiber, and the dowel bars located on the south side moved away from the extreme compression fiber with increasing the non-contact splice distance. As a result, while the lever arm (the centroid of the compressive block to the centroid of the bars) of the dowel bars located on the north side was decreasing, the lever arm of the dowel bars located on the south side was increasing with increasing the non-contact splice distance. Hence, the dowel bars located on the south side of Specimen 7 had a larger lever arm than the respective dowel bars in Specimens 5 and 6. Consequently, the contribution of the dowel bars located on the south side of the column of Specimen 7 in increasing the capacity and the stiffness is greater than the respective dowel bars in

Specimens 5 and 6. The increase in lateral stiffness of Specimen 7 could be attributed to the contribution of the dowel bars located on the south side of the column of Specimen 7.

It is also important to note that the lap splice length for the specimens was increased based on the 2D behavioral model (given in Equation 3) proposed by McLean and Smith [4] with increasing the non-contact splice distance. This increase in the lap splice length also might have contributed to the increase of lateral stiffnesses of Specimens 4 and 7 because Specimens 4 and 7 have the longest lap splice lengths among all the test specimens.

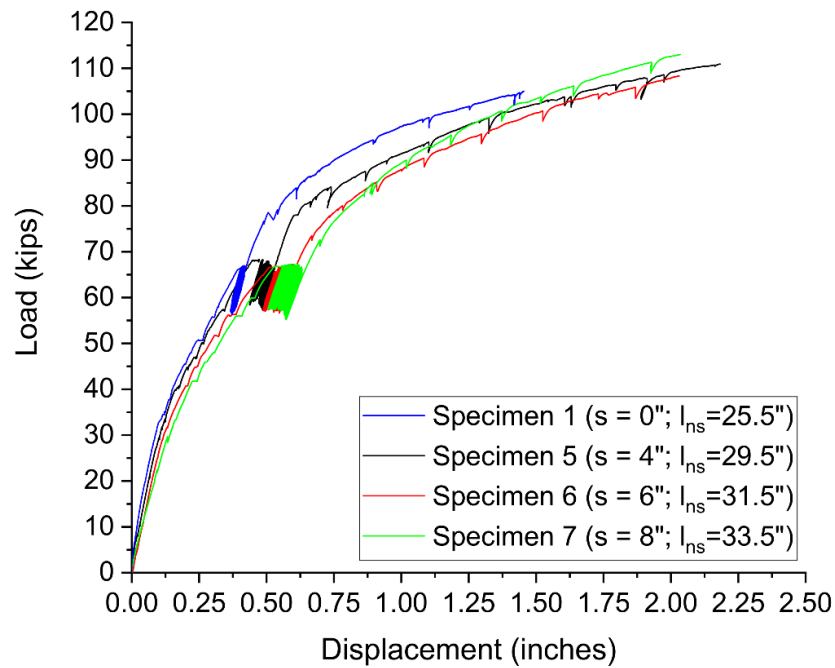


**Fig. 4-10: Applied load vs. lateral displacement relationships of Specimens 1, 5, 6 and 7.**

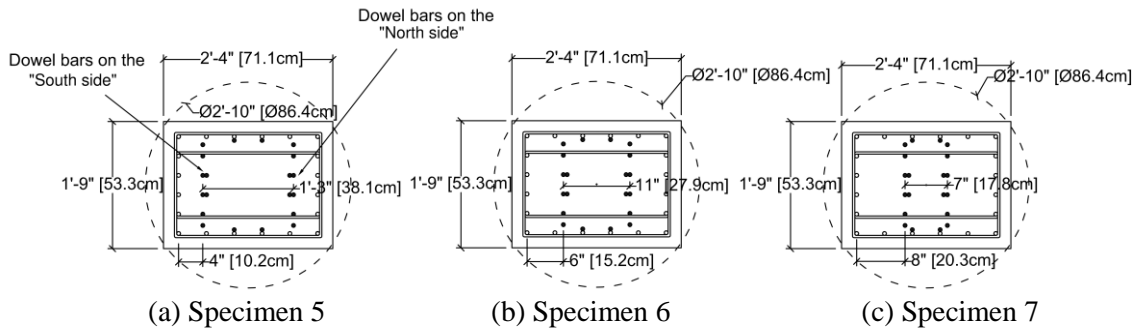


**Fig. 4-11: Location of the dowel bars.**

The applied load vs. lateral displacement relationships of Specimens 8 to 11 have been presented in Fig. 4-12. It is evident from Fig. 4-12 that Specimen 8 with 4 inches of non-contact lap splice distance and 44.50 inches of lap splice length exhibited similar behavior to Specimen 9 with 4 inches of non-contact lap splice distance and 38.75 inches of lap splice length. The application of AASHTO LRFD Interim Revisions [11, 12] for designing lap splice lengths yielded shorter lap splice length for Specimen 9 while older AASHTO code provisions [2] were used for Specimen 8. But the shorter splice length of Specimen 9 did not influence the performance of the connection significantly. Similarly, Specimen 10 with 6 inches of non-contact lap splice distance and 46.50 inches of lap splice length exhibited similar behavior to Specimen 11 with 6 inches of non-contact lap splice distance and 40.75 inches of lap splice length. It is also important to note that Specimens 8 and 9 with 4 inches of non-contact lap splice distance exhibited higher stiffness than Specimens 10 and 11 with 6 inches of non-contact lap splice distance. It is evident from the results of Specimens 8 to 11 that the lateral stiffness is mainly influenced by the non-contact lap splice distance and the specimens with larger non-contact lap splice distance generally exhibited lower lateral stiffness.

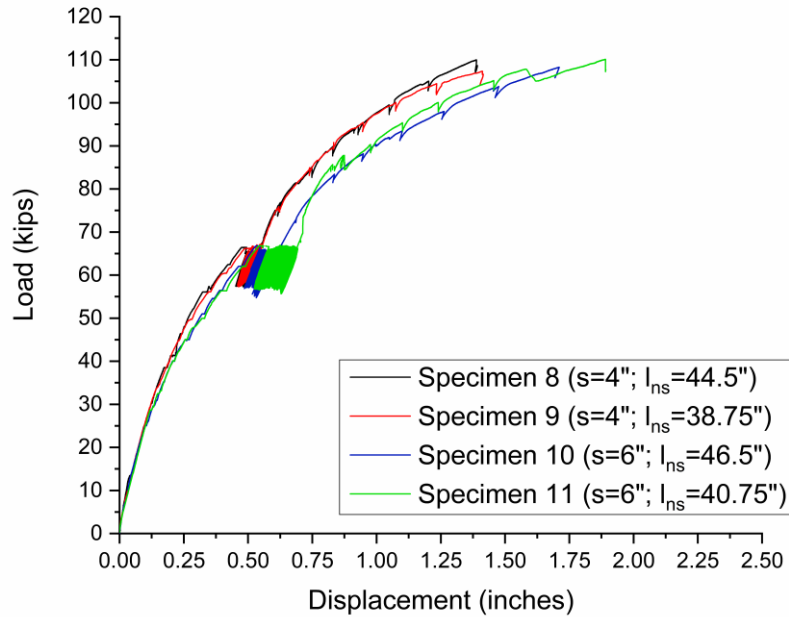


**Fig. 4-12: Applied load vs. lateral displacement relationships of Specimens 8 to 11.**

#### 4.4.2 Effect of Cyclic loading

The rate of increase of the lateral displacement of the specimens was generally higher under the same 125,000 cycles of cyclic loading when the non-contact lap splice distance was larger as shown in Table 4-3. For example, due to the cyclic loading, the lateral displacement of Specimens 1, 5, 6, and 7 was increased by 5.47%, 10.2%, 13.3%, and 13.0%. Except for Specimen 7, Specimens 1, 5, and 6 exhibited a higher rate of increase of the lateral displacement due to the cyclic loading with increasing the non-contact lap splice distance.

**Table 4-3: Change in lateral displacement of the specimen due to the cyclic loading**

Specimen No.	Lateral displacement of the specimen, inches		Change in displacement, %
	First cycle	125,000 <sup>th</sup> cycle	
1	0.402	0.424	+5.47 <sup>a</sup>
2	0.487	0.531	+9.03
3	0.565	0.612	+8.32
4	0.524	0.573	+9.35
5	0.480	0.529	+10.2
6	0.532	0.603	+13.3
7	0.560	0.633	+13.0
8	0.495	0.544	+9.9
9	0.501	0.551	+9.98
10	0.542	0.603	+11.25
11	0.577	0.633	+9.70

<sup>a</sup> positive value represents an increase.

#### 4.4.3 Strains in the Reinforcing Bars

The strains in the longitudinal reinforcement, transverse reinforcement, and dowel bars in the column and the drilled shaft were measured with electrical resistance strain gages. Only some of the most significant results from the strain gages are discussed in this section. The results from all the strain gages are provided in Appendix C.

#### **4.4.3.1 Strains in the column longitudinal bars**

Fig. 4-13(a) and (b) show the strains in the column longitudinal bars of Specimens 1 to 7 at Strain Gages C1 and C3. In the case of Specimens 2 to 7, the column longitudinal bars reached the yield strain of 0.0023 only after the dowel bars had yielded. Except for Specimen 5, the strains in the column longitudinal bars (Strain Gages C1 and C3) exhibited larger strains with increasing non-contact splice distance.

Fig. 4-14(a) and (b) show the strains in the column longitudinal bars of Specimens 8 to 11 at Strain Gages C1 and C3. The strains in the column longitudinal bars (Strain Gages C1 and C3) exhibited larger strains with increasing non-contact splice distance.

#### **4.4.3.2 Strains in the dowel bars**

The strains in the dowel bars of Specimens 1 to 7 from Strain Gages D5, D1, and D3 are presented in Fig. 4-13(c), (d), and (e). It is evident from Fig. 4-13(d) and (e) that plastic strains developed in the dowel bars near the column-shaft interface. These dowel bars experienced extensive yielding and subsequently strain hardening at higher loading stages. Strains measured by Strain Gage D5 showed that the strains in the dowel bars propagated into the non-contact lap splice zone and reached near the yield strain of 0.0023 at a distance of 59% of the standard splice length of these bars.

The strains in the dowel bars of Specimens 8 to 11 from Strain Gages D5, D1, and D3 are presented in Fig. 4-14(c), (d), and (e). It is evident from Fig. 4-14(d) and (e) that plastic strains developed in the dowel bars near the column-shaft interface. These dowel bars also experienced extensive yielding and subsequently, strain hardening at higher loading stages. Strains measured by Strain Gage D5 showed that the strains in the dowel bars propagated into the lap splice zone and either yielded or reached near the yield strain of 0.0023 at a distance of 59% of the standard splice length of these bars.

#### 4.4.3.3 Strains in the column ties

The strains in the column ties of Specimens 1 to 7 from Strain Gages T13, T7, and T1 are presented in Fig. 4-13(f), (g), and (h), respectively. For a non-contact lap splice distance of up to 6 in. (Specimens 2, 3, 5, and 6), the transverse reinforcement near the column-shaft interface in the columns exhibited yielding after the yielding of the dowel bars. On the other hand, for a non-contact lap splice distance greater than 6 in. (Specimens 4 and 7), the transverse reinforcement near the column-shaft interface in non-circular columns exhibited yielding before the yielding of the dowel bars. Therefore, the distance between the non-contact splices in the non-circular column to circular drilled shaft connections should be limited to 6 inches. As shown in Fig. 4-13(h), the column ties closest to the column-shaft interface exhibited the highest tensile stress among the column ties within the non-contact splice zone. The higher tensile stresses can be attributed to the presence of splitting cracks which propagate upwards from the column-shaft interface. These splitting cracks were intercepted by the column ties and subsequently, as loading was progressively increased, the column ties experienced high tensile stresses due to the increasing width of the splitting cracks. The tensile stresses in the column ties away from the interface were significantly lower than the ones near the interface. It can also be observed from Fig. 4-13(f), (g), and (h) that in general the higher the non-contact lap splice distance, the higher the contribution of the column ties. With increasing non-contact lap splice distance, the column ties experienced larger stresses as the force transferred from the column longitudinal bars to the dowel bars, which is evident from larger strains in the column ties (Strain Gages T7 and T1). It is also evident from Fig. 4-13(g) and (h) that the strains in the column ties of Specimens 5 to 7 were considerably smaller than that of Specimens 2 to 4, respectively. This is because Specimens 5 to 7 consisted of a higher amount of transverse reinforcement in the column than Specimens 2 to 4.

The strains in the column ties of Specimens 8 to 11 from Strain gages T13, T7, and T1 are presented in Fig. 4-14(f), (g) and (h). Similar to Specimens 1 to 7, the column ties closest to the

column-shaft interface exhibited the highest tensile stress among the column ties within the non-contact splice zone of Specimens 8 to 11. It was also observed that the tensile stresses in the column ties of Specimens 8 and 9 (4 in. of lap splice distance) were generally lower than that of Specimens 10 and 11 (6 in. lap splice distance).

#### **4.4.3.4 Strains in the shaft spirals**

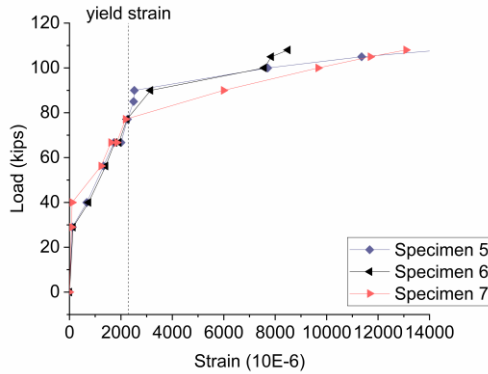
The strains in the drilled shaft spirals of Specimens 1 to 7 from Strain Gages S1, S2, and S3 are presented in Fig. 4-13(i), (j), and (k), respectively. It is evident from Fig. 4-13(i) that the shaft spirals closest to the column-shaft interface exhibited the highest tensile stress. The higher tensile stresses can be attributed to the presence of splitting cracks which were intercepted by the shaft spirals and subsequently, as loading was progressively increased, experienced high tensile stresses due to the increasing width of the splitting cracks. The tensile stresses in the shaft spirals away from the interface were significantly lower than the ones near the interface. It can also be observed from Fig. 4-13(i), (j), and (k) that in general the higher the non-contact lap splice distance, the higher the contribution of shaft spirals. With increasing non-contact lap splice distance, the shaft spirals were loaded more as evident from larger strains in the shaft spirals (Strain Gage S1 and S2). However, the strains in the shaft spirals (Strain Gages S1, S2, and S3) of Specimens 4 and 7 were found lower than that of Specimens 2, 3, 5, and 6. This is because in the case of a non-contact lap splice distance of 8 inches, the dowel bars in Specimens 4 and 7 were located almost near the centerline of the specimen and therefore the splitting cracks also emerged along those dowel bars. As the locations of the Strain Gages S1, S2, and S3 were away from the location of the splitting cracks, the exact strain values in the vicinity of the splitting cracks could not be measured.

#### **4.4.3.5 Strains in the shaft longitudinal bars**

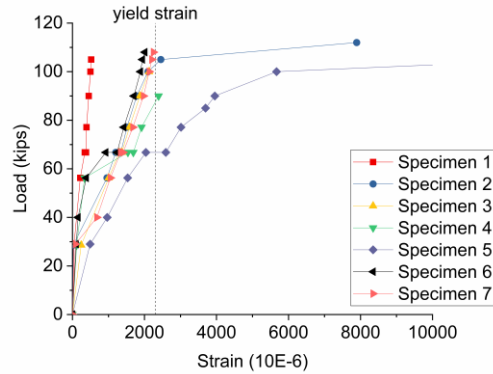
As shown in Fig. 4-13(l), the drilled shaft longitudinal bar of Specimens 1 to 7 remained elastic (Strain Gage DS1) throughout the tests. It can also be observed that the bars were stressed more

with increasing non-contact lap splice distance because with increasing non-contact lap splice distance, the dowel bars moved away from the shaft longitudinal bars.

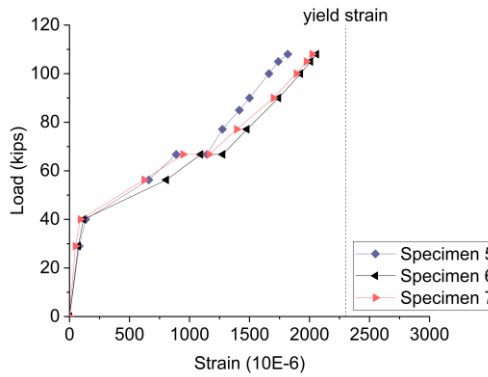
As shown in Fig. 4-14(i), the drilled shaft longitudinal bar of Specimens 8 to 11 remained elastic (Strain Gage DS1) throughout the tests. It can be observed from Fig. 4-14(i) that the stresses in the bars were not significantly influenced by increasing lap splice distance.



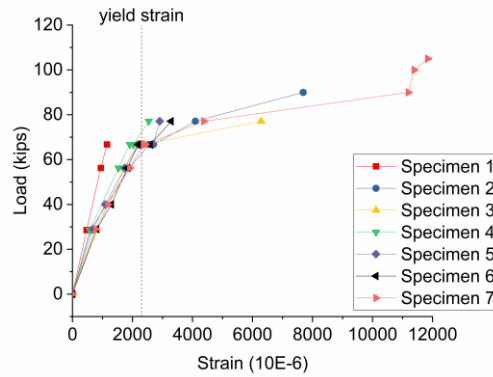
(a) Strain Gage C3 on column longitudinal bars



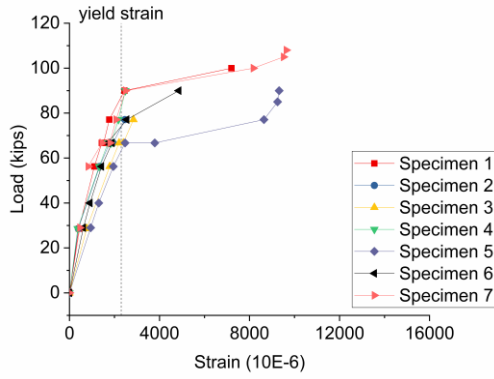
(b) Strain Gage C1 on column longitudinal bars



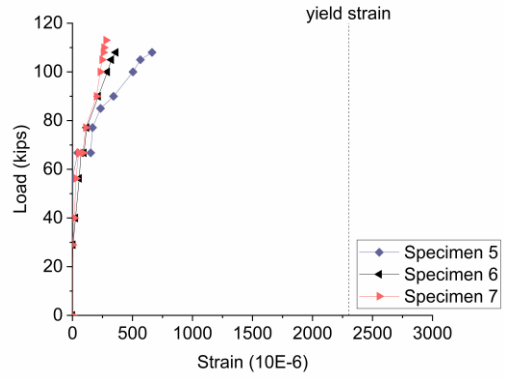
(c) Strain Gage D5 on dowel bars



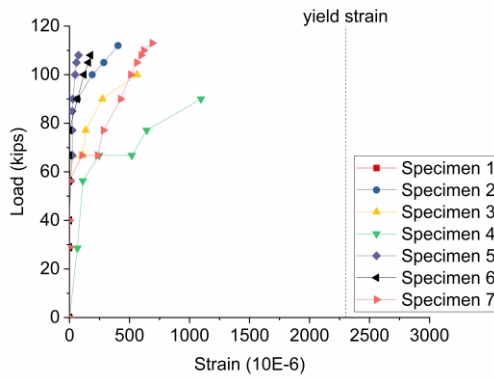
(d) Strain Gage D1 on dowel bars



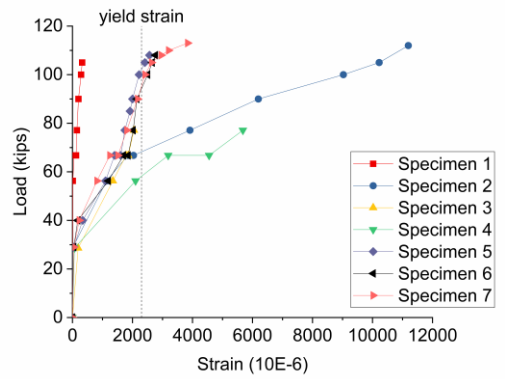
(e) Strain Gage D3 on dowel bars



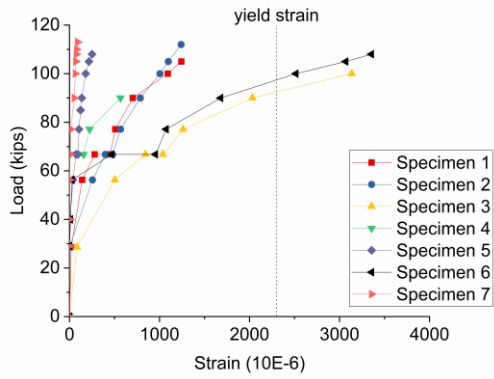
(f) Strain Gage T13 on column ties



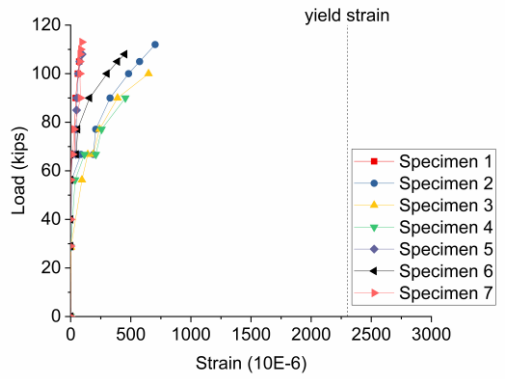
(g) Strain Gage T7 on column ties



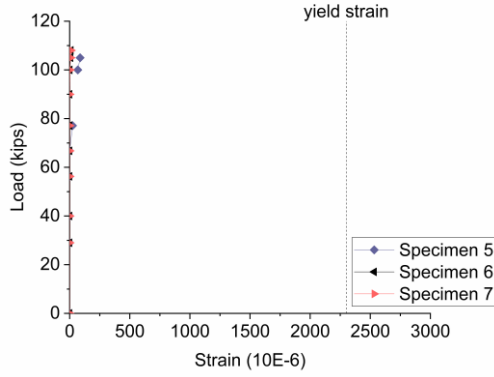
(h) Strain Gage T1 on column ties



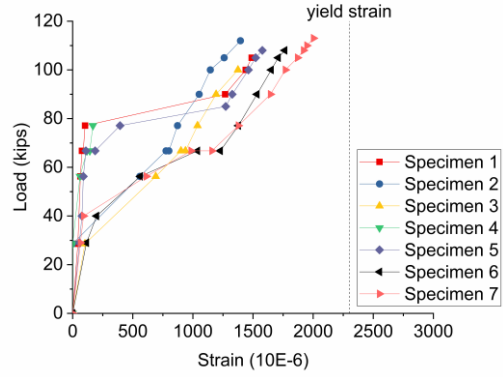
(i) Strain Gage S1 on shaft spirals



(j) Strain Gage S2 on shaft spirals

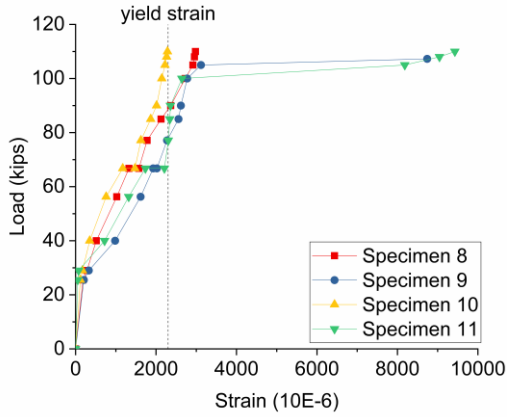


(k) Strain Gage S3 on shaft spirals

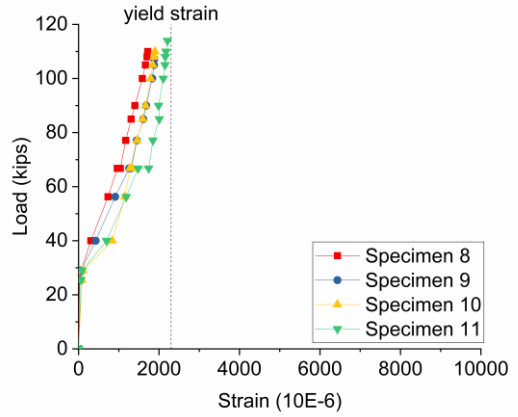


(l) Strain Gage DS1 on shaft longitudinal bars

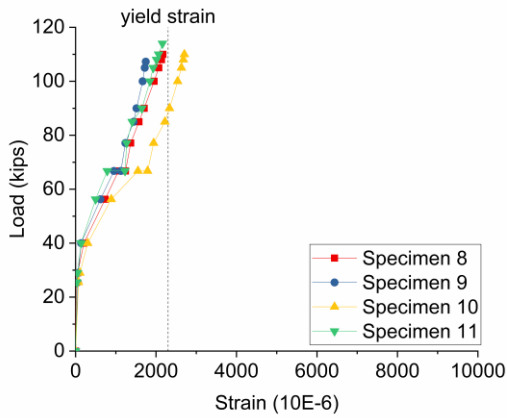
**Fig. 4-13: Strains in the reinforcing bars in Phase I**



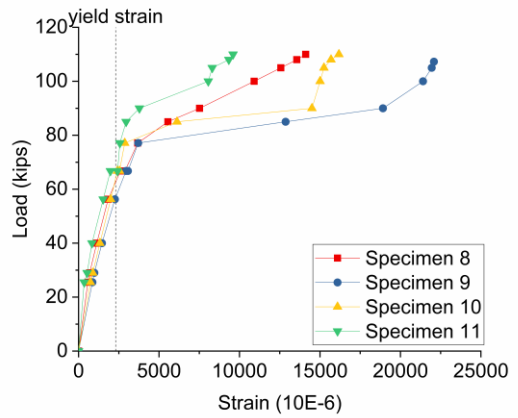
(a) Strain Gage C3 on column longitudinal bars



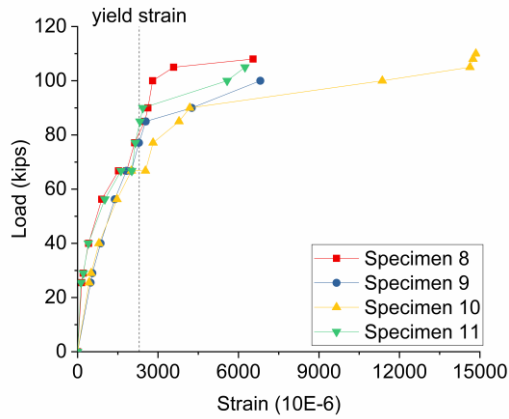
(b) Strain Gage C1 on column longitudinal bars



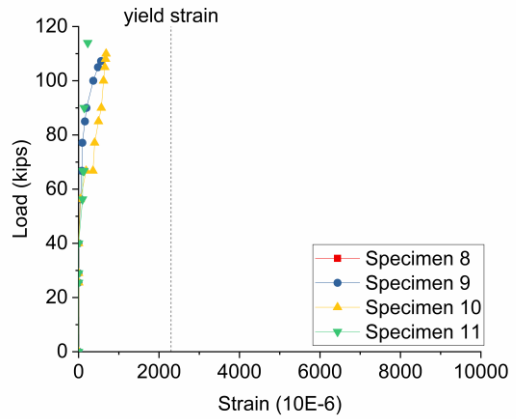
(c) Strain Gage D5 on dowel bars



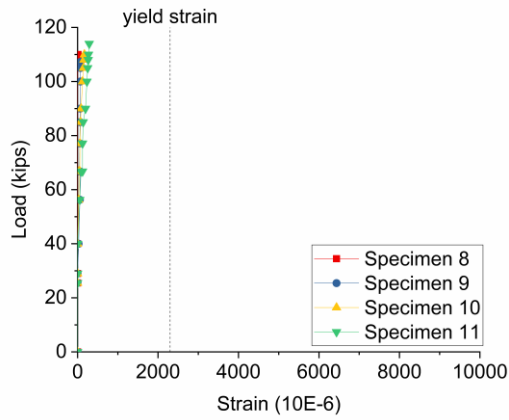
(d) Strain Gage D1 on dowel bars



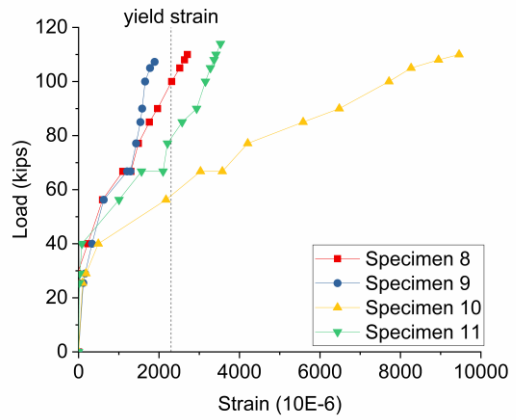
(e) Strain Gage D3 on dowel bars



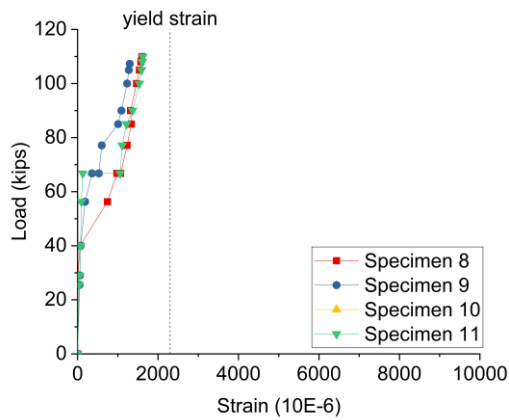
(f) Strain Gage T13 on column ties



(g) Strain Gage T7 on column ties



(h) Strain Gage T1 on column ties



(i) Strain Gage DS1 on shaft longitudinal bars

**Fig. 4-14: Strains in the reinforcing bars in Phase II**

The loads corresponding to the yielding of the reinforcing bars are tabulated in Table 4-4.

**Table 4-4: Summary of yielding of different types of bars and the corresponding applied loads**

Specimen Designation	Applied load, kips			Ultimate load, kips
	Yielding of dowel bars	Yielding of column longitudinal bars	Yielding of column ties	
Specimen 1	77.1	No yielding	No yielding	105.0
Specimen 2	63.5	103.7	68.9	112.0
Specimen 3	66.5	92.0	81.2	100.0
Specimen 4	72.5	89.3	58.8	90.0
Specimen 5	63.75	5,570 <sup>th</sup> cycle	100.5	110.0
Specimen 6	64.4	77.9	80.8	108.0
Specimen 7	65.6	82.3	64.9	113.0
Specimen 8	62.9	89.5	97.0	110.0
Specimen 9	58.0	77.98	71.6	108.0
Specimen 10	63.9	89.1	55.8	110.0
Specimen 11	282,966 <sup>th</sup> cycle	76.8	3,440 <sup>th</sup> cycle	110.0

#### 4.4.4 Crack Patterns

##### 4.4.4.1 Opening at the Column-Drilled Shaft Interface

Each specimen exhibited an opening at the column-drilled shaft interface. The opening typically appeared within an applied load of 6.0 to 10.0 kips. Fig. 4-15 shows a typical opening at the column-drilled shaft interface. Fig. 4-16(a) shows the applied load vs. opening relationship for Specimens 1 to 7. It can be observed from Fig. 4-16(a) that the specimens with non-contact splices consistently exhibited a larger opening than the specimen with the contact splice. A comparison of the opening

among Specimens 1 to 4 showed that the opening increased with increasing the non-contact lap splice distance except for Specimen 4. Similar comparisons made among Specimens 5 to 7 showed that the opening was quite similar despite changing the non-contact lap splice distance.

Fig. 4-16(b) shows the applied load vs. opening relationship for Specimens 8 to 11. A comparison of the opening among Specimens 8 to 11 showed that the opening increased with increasing the non-contact splice distance.

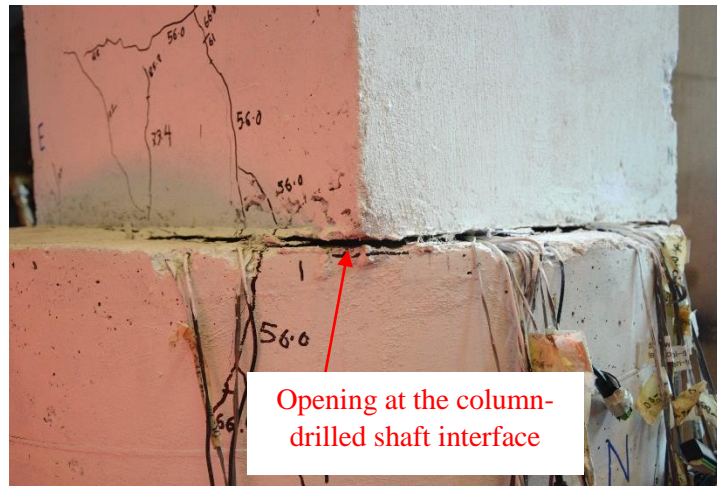


**Fig. 4-15: Typical opening at the column-drilled shaft interface (North-east face of Specimen 2).**

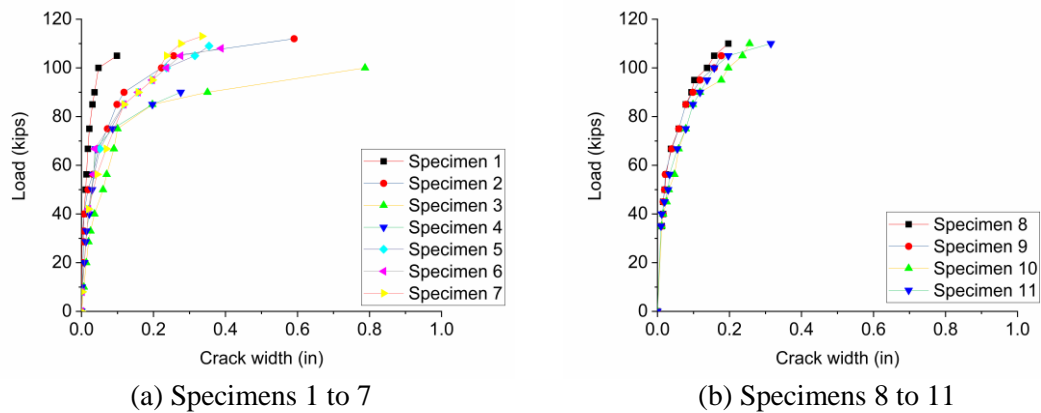


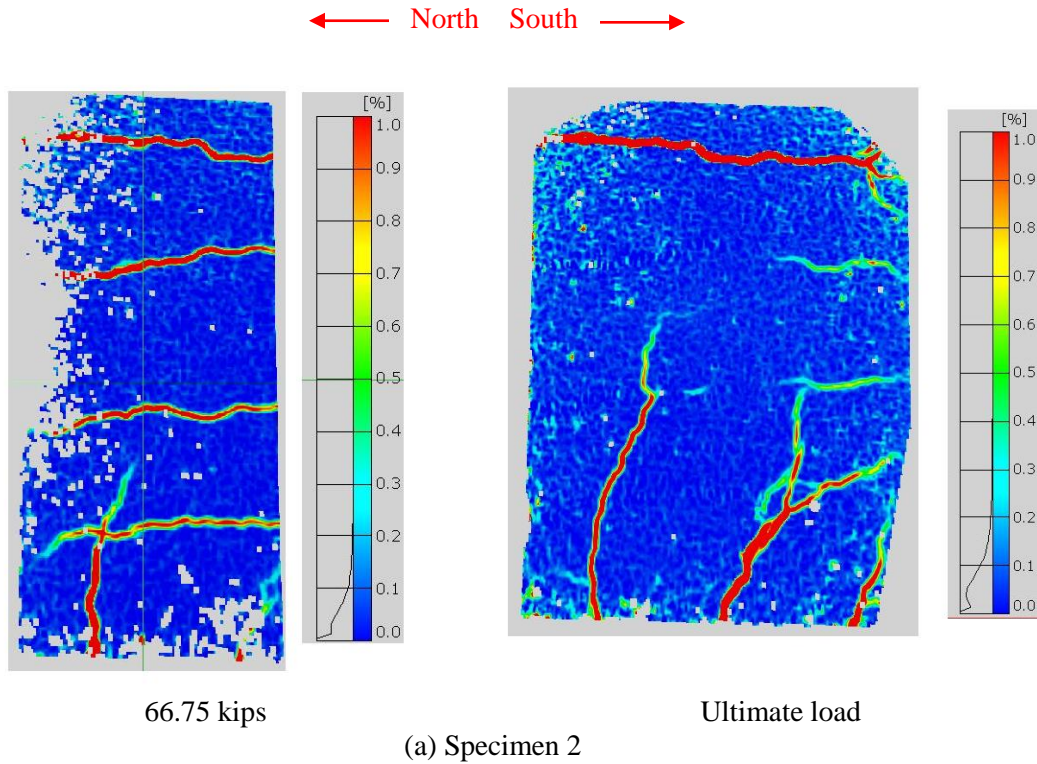
**Fig. 4-16: Opening at the column-drilled shaft interface.**

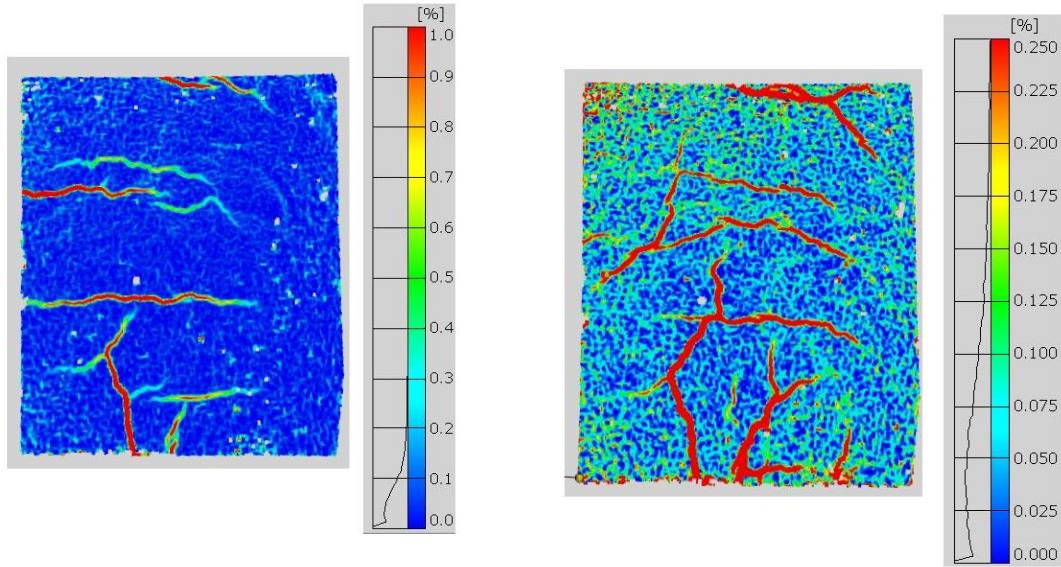
#### 4.4.4.2 Inclined Cracking in the Non-Contact Lap Splice Zone

As shown in Fig. 4-4 and Fig. 4-8, inclined cracking was observed in the non-contact lap splice zone of the specimens. The inclined cracks appeared first within the spliced bars and propagated

further into the compression zone at varying inclination angles of up to 47 degrees. It can be observed from the comparison that the inclination angle of the inclined cracks, in general, would increase with increasing the non-contact splice distance.

Digital Image Correlation–based (DIC) non-contact measurement system was used to observe the locations of major (tensile) principal strains on the West side of the specimens which resulted in inclined cracks on the concrete in the non-contact lap splice zone in the column. Also, the crack widths of the inclined cracks were measured using the DIC-based measurement system. Fig. 4-17 shows the major (tensile) principal strains on the West side of the Specimens 2 to 7. Fig. 4-18 shows the crack widths of the inclined cracks on the columns of Specimens 2 to 7. It is evident from Fig. 4-18 that the crack widths of the inclined cracks increased with the increase of the non-contact lap splice distance.

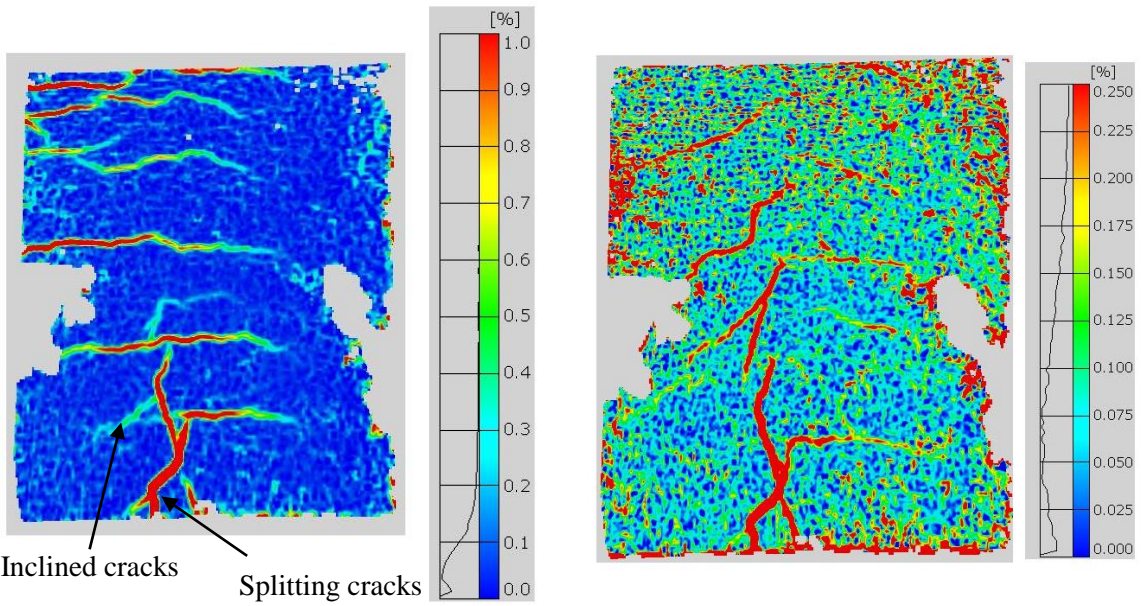




66.75 kips

Ultimate load

(b) Specimen 3



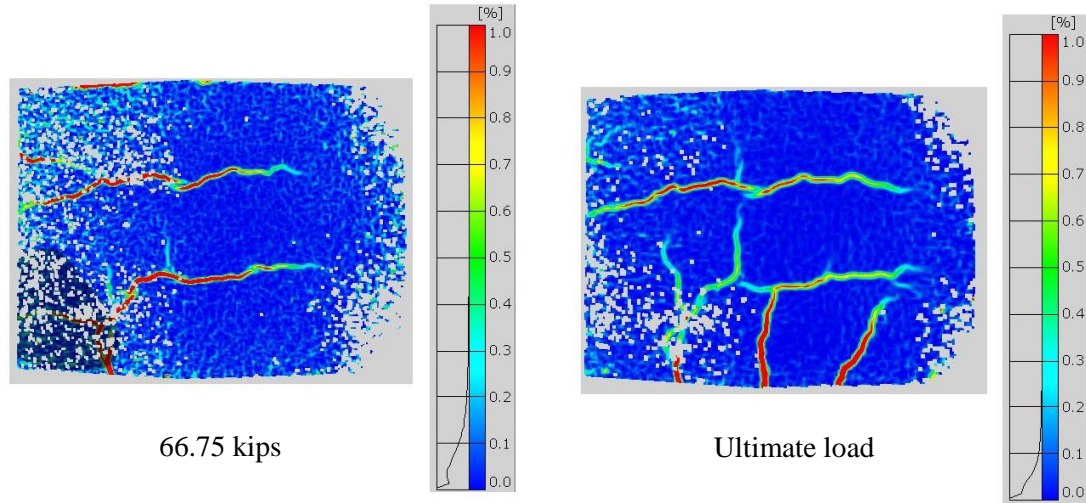
Inclined cracks

Splitting cracks

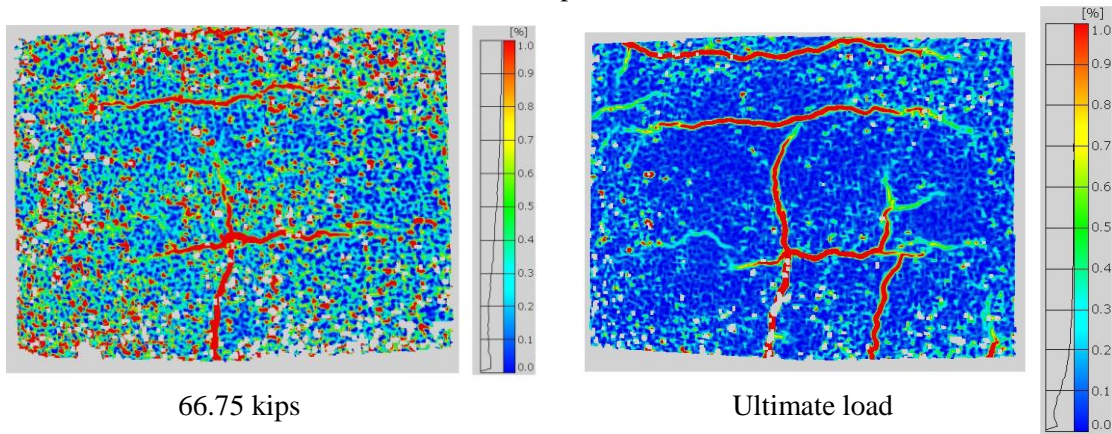
66.75 kips

Ultimate load

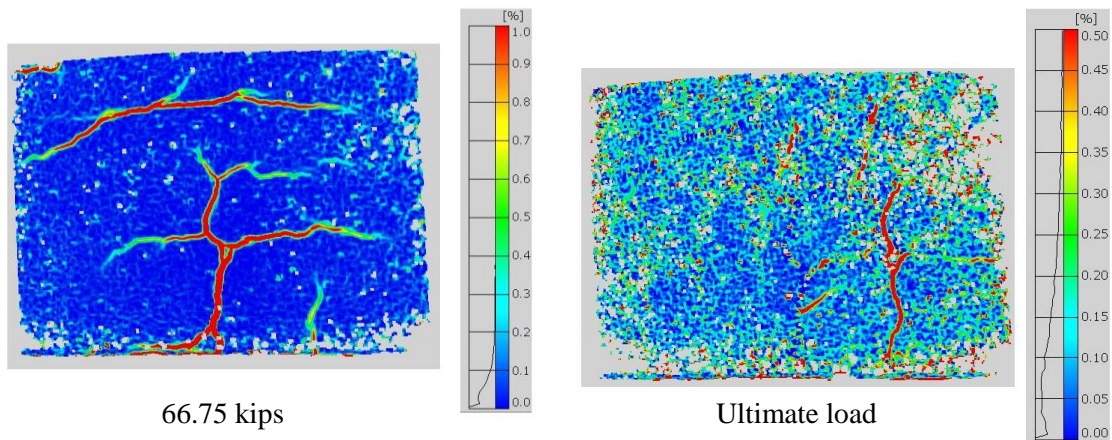
(c) Specimen 4



(e) Specimen 5

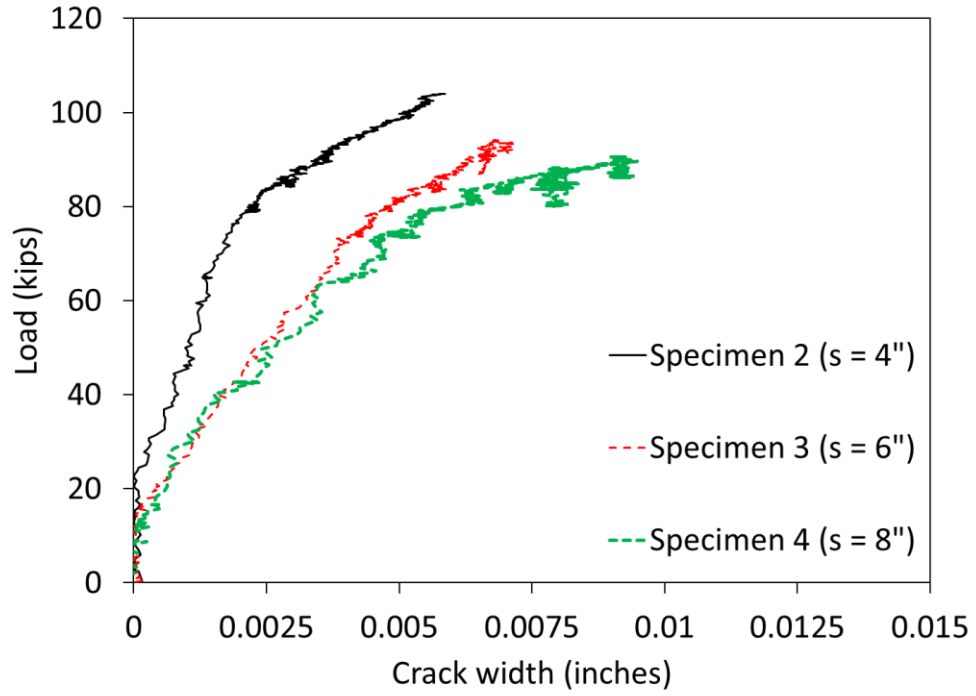


(e) Specimen 6

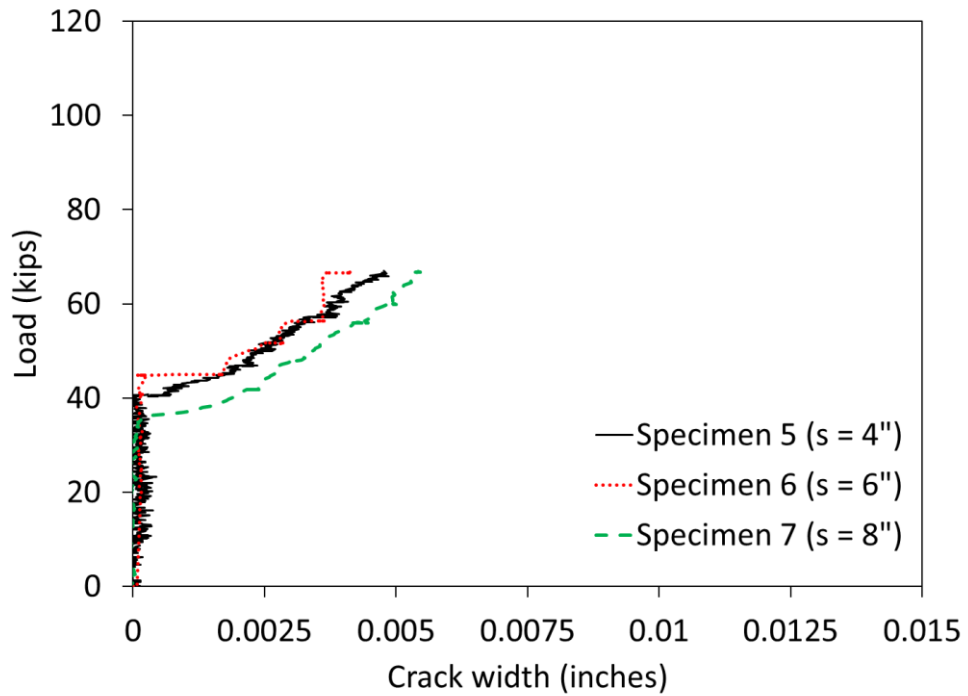


(f) Specimen 7

**Fig. 4-17: Major (tensile) principal strain in the non-contact lap splice zone in the rectangular column (West side).**



(a) Specimens 2 to 4



(b) Specimens 5 to 7

**Fig. 4-18: Crack widths of the inclined cracks.**

#### 4.4.4.3 Splitting Cracks

Every specimen exhibited splitting cracks near the column-drilled shaft interface. These splitting cracks formed mainly due to the dowel bar slip. The splitting cracks on the column propagated upwards from the column-drilled shaft interface. The splitting cracks on the column propagated vertically upwards along the dowel bars as far as 60.1% of the standard splice length from the column-drilled shaft interface. On the other hand, the splitting cracks on the drilled shaft propagated from the column-drilled shaft interface to the edge of the shaft radially (Fig. 4-19) and then extended downwards along the length of the drilled shaft. The splitting cracks on the drilled shaft propagated vertically downwards along the dowel bars as far as 64.3% of the standard splice length from the column-drilled shaft interface.

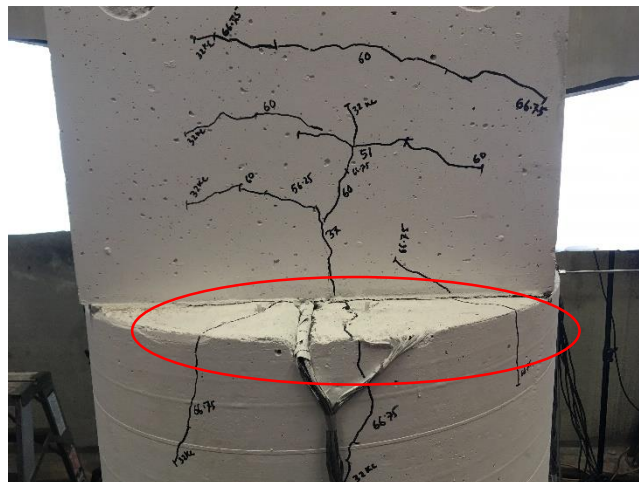
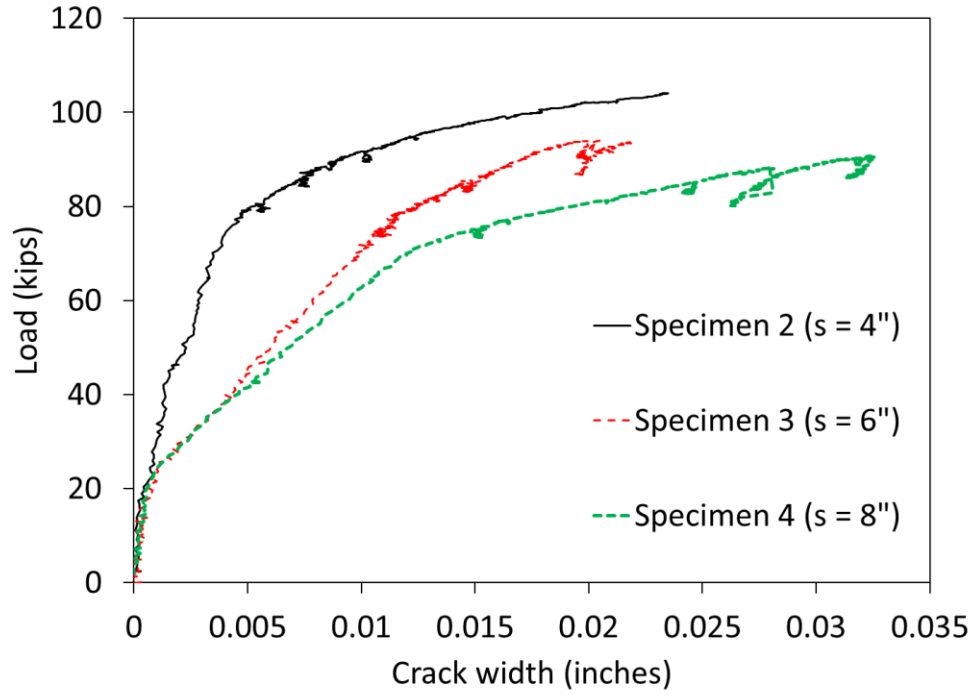
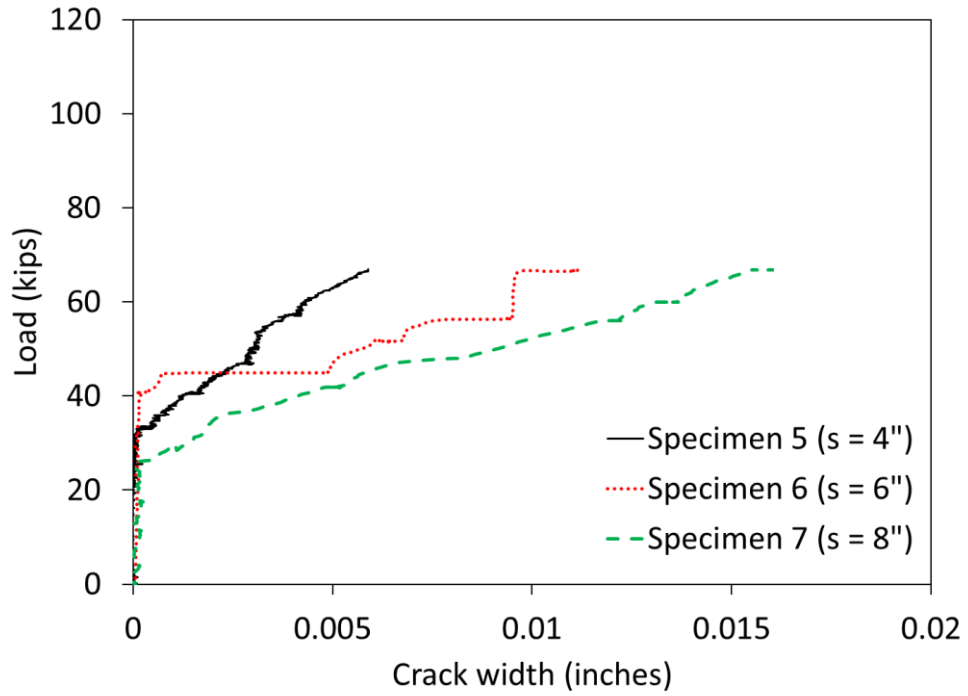


**Fig. 4-19: Splitting crack propagation atop the drilled shaft of Specimen 7.**

Digital Image Correlation – based (DIC) non-contact measurement system was used to observe the locations of major (tensile) principal strains on the West side of the specimens which result in splitting cracks on the concrete in the non-contact lap splice zone in the column. Also, the crack widths of the splitting cracks were measured using the DIC-based measurement system. Fig. 4-20 shows the crack widths of the splitting cracks on the columns of Specimens 2 to 7. It is evident from Fig. 4-20 that the crack widths of the splitting cracks generally increased with the increase of the non-contact lap splice distance.



(a) Specimens 2 to 4



(b) Specimens 5 to 7

**Fig. 4-20: Crack widths of the splitting cracks.**

Table 4-5 tabulates the applied loads corresponding to the different types of cracks observed during the test.

**Table 4-5: Summary of crack patterns and their corresponding applied loads**

Specimen Designation	Applied load, kips						
	Flexural cracks		Inclined cracking	Splitting cracks		Concrete Crushing	
	Column	Shaft	in column	Column	Shaft	Column	Shaft
Specimen 1	28.6	79.0	No inclined cracking	66.75	66.75	-	-
Specimen 2	29.0	56.0	56.0	56.0	56.0	112.0	112.0
Specimen 3	30.0	50.0	56.0	37.5	50.0	100.0	92.0
Specimen 4	33.0	56.0	50.0	33.0	56.0	-	-
Specimen 5	29.0	56.25	44.0	44.0	66.75	100.5	108.2
Specimen 6	28.5	56.25	52.0	49.0	64.0	108.0	108.0
Specimen 7	34.0	60.0	51.0	37.0	66.75	110.0	110.0
Specimen 8	25.5	46.5	51.5	37.0	63.0	110.0	110.0
Specimen 9	25.5	50.0	45.0	35.0	56.25	107.0	107.0
Specimen 10	25.0	45.0	40.0	34.0	56.25	110.0	105.0
Specimen 11	29.0	45.0	50.0	40.0	45.0	-	100.0

#### 4.5 Summary

Based on the experimental investigation of the column-drilled shaft connections with contact and non-contact lap splices, the following outcomes can be reported:

- 1) The specimens with larger non-contact lap splice distance generally exhibited lower lateral stiffness and lower capacity.

- 2) Further, the rate of increase of lateral displacement due to the cyclic loading increased with increasing the non-contact lap splice distance.
- 3) In the case of Specimen 11, the lateral displacement increased at a significantly higher rate between the first and 125,000th cycles of the cyclic loading than between the 125,000th and 2,000,000th cycles of the cyclic loading. In other words, after 125,000 cycles of the cyclic loading, the lateral displacement did not increase significantly despite applying an additional 1,850,000 cycles of the cyclic loading. These results indicated an increase in the incremental displacements in the early stages of the cyclic loading and subsequent tendency to stabilize without much increase in the accumulated displacements.
- 4) Non-contact lap splices constructed with splice lengths equaling standard lap splice length as per the AASHTO LRFD code [2] plus the non-contact lap splice distance were effective in developing yielding and strain hardening of the spliced bars provided that the transverse reinforcements are designed according to the proposed guidelines.
- 5) The specimens with Class B lap splices as per the AASHTO LRFD codes [11, 12] exhibited quite similar structural performance to the specimens with Class C lap splices as per the AASHTO LRFD code [2] for bar sizes of up to No. 7.
- 6) The transverse reinforcement in the column and the drilled shaft near the column-drilled shaft interface exhibited the highest tensile stress within the non-contact lap splice zone. The tensile stresses in the transverse reinforcement located away from the interface were significantly lower than the ones located near the interface.
- 7) For a non-contact lap splice distance of up to 6 in. (Specimens 2, 3, 5, and 6), the transverse reinforcement near the column-shaft interface in columns exhibited yielding after the dowel bars had yielded. On the other hand, for a non-contact lap splice distance greater than 6 in. (Specimens 4 and 7), the transverse reinforcement near the column-shaft interface in non-circular columns exhibited yielding before the dowel bars had yielded. Therefore,

the distance between the non-contact lap splices in the non-circular column connected to circular drilled shaft connections should not exceed 6 inches.

- 8) The increase of non-contact lap splice distance yielded significant inclined cracks and splitting cracks in the non-contact lap splice zone. The angle of inclined cracks was observed to increase with increasing the non-contact splice distance. Also, the opening at the column-drilled shaft interface increased with increasing the non-contact splice distance. Due to the large opening at the column-drilled shaft interface, the dowel bars and the column longitudinal bars could be subjected to corrosion over time.
- 9) Overall, the outcomes of the experimental investigation provide a basic understanding of the behavior of non-contact lap splices in non-circular columns to circular drilled shaft connections. The experimental investigation also provided significant information for performing a thorough finite element analysis of the specimens to study the performance of non-contact lap splices.

## **Chapter 5 Finite Element Analysis**

### **5.1 Overview**

In this chapter, the finite element analyses of the test specimens are thoroughly discussed. The details of the finite element modeling of the test specimens and constitutive models of materials are discussed in this chapter. The finite element simulated results are compared with the test outcomes, and the comparisons are reported. A thorough parametric study of the critical parameters is also performed and reported in this chapter. Lap splice length, non-contact lap splice distance, and the amount of transverse reinforcement in the non-circular columns were the variables used in the parametric analysis. Also, the outcomes of finite element analyses of the Bent 17 column-drilled shaft connection are provided.

### **5.2 Finite Element Analysis of the Test Specimens**

#### **5.2.1 Three-dimensional Finite Element Modeling of the Specimens**

##### **5.2.1.1 Element Types**

The finite element model of the test specimens was developed using Abaqus [28]. Fig. 5-1(a) and (b) show the finite element model and the reinforcement layout of the column-drilled shaft specimens, respectively. An 8-node linear brick, reduced integration, hourglass control element (C3D8R) was used to mesh the concrete material. The steel box beam was also modeled using the C3D8R element. A 2-node linear three-dimensional (3-D) truss element (T3D2) was used to implement the steel reinforcement. Most of the elements in the FEA models had an aspect ratio equal to or less than 4:1. Near the column-drilled shaft interface, the elements were meshed finer than other locations of the model. This was done to ensure the accuracy of the FEA results at the location of the discontinuity. Overall, the aspect ratios of the elements were less than the aspect ratio limit of 10:1 as mentioned in the Abaqus user's guide [33].

### **5.2.1.1 Boundary Conditions**

It is important to note that the top flange of the steel beam was anchored to the column using the embedded rods at the top of the column whereas the webs of the steel beam were anchored to the sides of the column using four high strength threaded rods inserted through the sides of the column. The modeling of these embedded anchors and threaded rods were quite complex. To simplify the model, the flanges and webs of the steel box beam were connected to the concrete surface of the column using tie constraints (A tie constraint ties two separate surfaces together so that there is no relative motion between them).

The column-drilled shaft interface was simulated by assuming a surface to surface “hard” contact relationship between the column bottom and the shaft top surfaces. A “hard” contact relationship minimizes the penetration of the connected surfaces at the constraint locations and does not allow the transfer of tensile stress across the interface [33]. In addition, to simulate the tangential behavior of the interface, a friction coefficient of 0.4 was used for the friction formulation as recommended by PCA guidelines [34]. These assumptions were based on the fact that the connection between the column and the drilled shaft is not a monolithic connection. Moreover, a ‘fixed’ boundary condition was provided at the base of the rectangular footing [Fig. 5-1(a)].

### **5.2.1.2 Bond-Slip between Concrete and Steel Reinforcement**

To simulate the bond-slip behavior in tension between the column longitudinal bars/dowel bars and the surrounding concrete, the column longitudinal bars and the dowel bars on the north side of the column were connected to the concrete using spring elements. For the definition of the bond stress vs. slip behavior of the spring elements, an average “local bond” stress vs. “local slip” relationship can be considered as per European CEB-FIP Model Code 90 as shown in Fig. 5-2 [35]. It is important to note that the bond stress-slip curve as shown in Fig. 5-2 can be considered as a statistical mean curve, applicable for a broad range of cases [35]. As the FEA models consisted of material and geometric nonlinearities and contact formulation at the column-drilled shaft interface,

the entire bond stress vs. slip curve was not simulated in order to avoid convergence issues during the analysis. As shown in Fig. 5-2, linear bond stress vs. slip relationship was assumed by considering the initial stiffness of the curve. Other reinforcing bars, e.g., column ties, drilled shaft spirals, etc. in the FEA models were “embedded” in the concrete. By “embedding” the reinforcing bars in concrete, it was assumed that there is a perfect bond (slip of bars was restricted) between the rebar and the surrounding concrete.

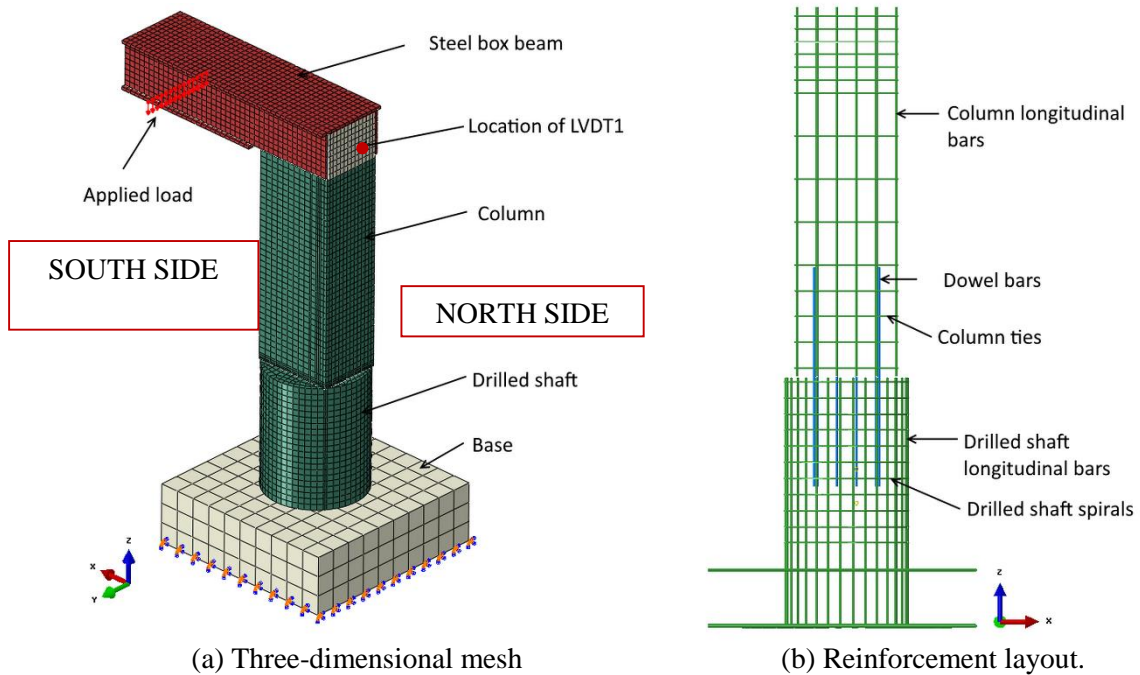


**Fig. 5-1: Finite element model of the column-drilled shaft specimens.**

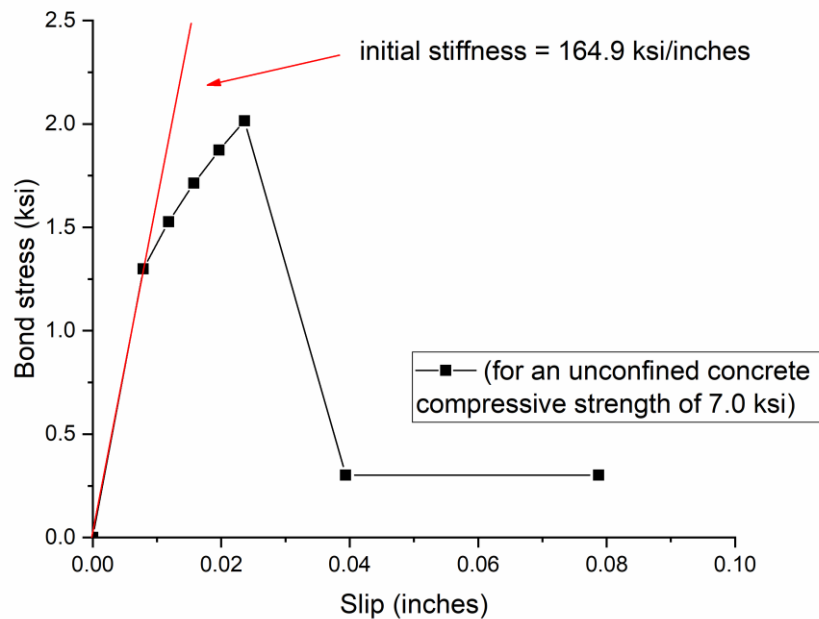


**Fig. 5-2: Typical bond stress vs. slip relationship.**

## 5.2.2 Constitutive Models of Materials

The Concrete Damaged Plasticity (CDP) model was used as the constitutive model of concrete in the FEM model [29]. The CDP model requires the definition of uniaxial behavior in compression and tension. The uniaxial stress-strain curves proposed by Hsu and Mo [30] were adopted for the definition of the CDP model as shown in Fig. 3-10. Equation 14 was used to develop the parabolic compression stress-strain curve. Equations 15 [31] and 16 [32] define the ascending and descending branch of the tensile stress-strain curve, respectively.

The stress-strain curve of the reinforcing bar (steel reinforcement) was bilinear elastoplastic as shown in Fig. 3-11. A bilinear steel model with a linear strain hardening proposed by Hsu and Mo [30] was utilized for the constitutive model of the steel reinforcement.

The CDP model also requires the definition of damage variables in tension and compression. When the concrete specimen is unloaded from any point on the strain softening branch of the stress-strain curves, the unloading response is weakened which means that the elastic stiffness of the

material appears to be damaged (or degraded) [36]. The degradation of the elastic stiffness is characterized by two damage variables, the compressive and tensile damage coefficients,  $d_c$  and  $d_t$ , respectively. The compressive and tensile damage coefficients,  $d_c$  and  $d_t$  were calculated by using the mathematical Equations 18 and 19, respectively [37] which are as

$$d_c = 1 - \frac{\frac{\sigma_c}{E_c}}{\varepsilon_c^{pl} \left( \frac{1}{b_c} - 1 \right) + \frac{\sigma_c}{E_c}} \text{ and} \quad (18)$$

$$d_t = 1 - \frac{\frac{\sigma_t}{E_c}}{\varepsilon_t^{pl} \left( \frac{1}{b_t} - 1 \right) + \frac{\sigma_t}{E_c}}, \quad (19)$$

where,  $\sigma_c$  = compressive stress of concrete;  $\varepsilon_c^{pl}$  = plastic compressive strain;  $b_c$  = experimentally determined factor for compressive damage;  $\sigma_t$  = tensile stress of concrete;  $\varepsilon_t^{pl}$  = plastic tensile strain; and  $b_t$  = experimentally determined factor for tensile damage.

The details of the material parameters of the CDP model and steel bilinear elastoplastic model for Specimens 1 to 11 are provided in Table 5-1 and Table 5-2, respectively.

### 5.2.3 Loading

The load was applied on the steel beam at an eccentricity of 59.25 inches from the centerline of the column as shown in Fig. 5-1(a). From the applied load vs. displacement curves of the test specimens, it can be observed that the cyclic loading did not reduce the stiffness of the specimens significantly. Therefore, the influence of the cyclic loading was ignored, and the cyclic loading portion of the experiments was not simulated in the FEA: only the monotonic loading portion with a uniform loading rate was simulated in the finite element simulation.

**Table 5-1: Material parameters for the concrete damaged plasticity model**

<b>Specimen designation</b>	<b>Young's modulus (ksi)</b>	<b>Poisson's ratio</b>	<b>Compressive strength (ksi)</b>	<b>Tensile strength (ksi)</b>	<b>Density (lb/ft<sup>3</sup>)</b>	<b>Dilation<sup>a</sup> angle (°)</b>
Specimen 1	4771	0.2	7.0	0.31	150	31
Specimen 2	4670	0.2	6.7	0.30	150	31
Specimen 3	4598	0.2	6.5	0.29	150	31
Specimen 4	4936	0.2	7.5	0.32	150	31
Specimen 5	4666	0.2	6.7	0.30	150	31
Specimen 6	4735	0.2	6.9	0.30	150	31
Specimen 7	4803	0.2	7.1	0.31	150	31
Specimen 8	4870	0.2	7.3	0.31	150	31
Specimen 9	4969	0.2	7.6	0.32	150	31
Specimen 10	4803	0.2	7.1	0.31	150	31
Specimen 11	5066	0.2	7.9	0.32	150	31

<sup>a</sup> Abaqus user's manual [33]

**Table 5-2: Material parameters for the bilinear elastoplastic steel model**

<b>Bar size</b>	<b>Yield stress (ksi)</b>	<b>Tensile strength (ksi)</b>	<b>Young's modulus (ksi)</b>	<b>Poisson's ratio</b>	<b>Density(lb/ft<sup>3</sup>)</b>
#3 rebar	63.0	97.0	27,400.0	0.3	502.54
#5 rebar	66.1	105.5	28,800.0	0.3	502.54
#7 rebar	68.3	111.9	29,188.0	0.3	502.54

## **5.2.4 Finite Element Simulated Results of the Test Specimens**

### **5.2.4.1 Load vs. Displacement Relationships**

The relationship between the lateral displacement at the top of the column (at the location of LVDT 1 as shown in Fig. 5-1(a) and the vertical force on the steel box beam was obtained from the finite element simulated results of the test specimens. The load vs. lateral displacement curves of Specimens 1 to 11 obtained from the experiment and the finite element analysis are shown in Fig. 5-3(a) to (k), respectively. Fig. 5-3 indicates that the results of the three-dimensional numerical analysis are in good agreement with the experimental findings.

#### **5.2.4.1.1 Specimens 1 to 4**

The initial stiffness of the FEA models matched very well with the test results. The post-crack behavior matched reasonably well with the test results except for Specimen 4. The ultimate load capacities obtained from the FEA models were 3.3%, 4.6%, 2.6%, and 4.5% lower than that of the tested Specimens 1, 2, 3 and 4, respectively.

During the laboratory test of Specimen 4, the loading stopped abruptly because the hydraulic pump fuses which were used to power the hydraulic actuator were blown. As a result, the maximum

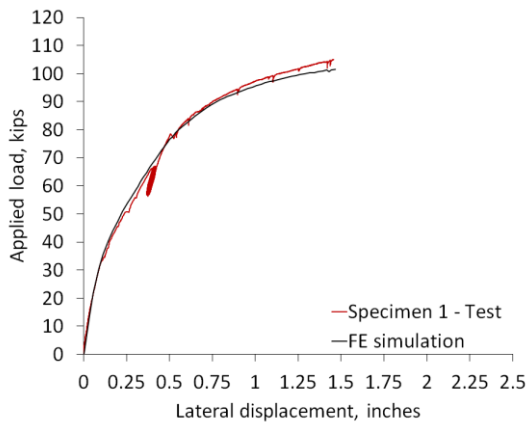
load of 90.0 kips was reached during the test, and the lateral displacement of the specimen corresponding to the load of 90.0 kips was 0.947 inches. It was found from the FEA results of Specimen 4 that the load corresponding to the displacement of 0.947 inches is 4.5% smaller than that of the tested specimen.

#### 5.2.4.1.2 Specimens 5 to 7

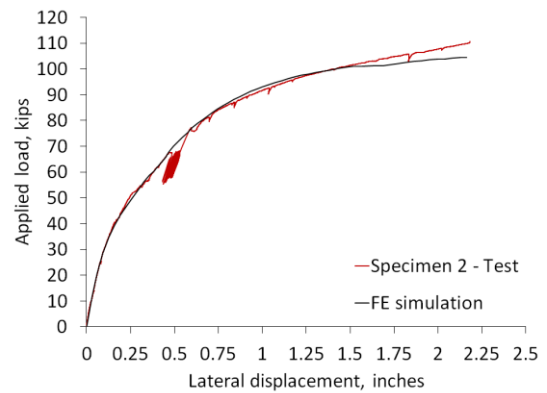
The initial stiffness of the FEA models matched very well with the test results. The post-crack behavior also matched reasonably well with the test results. The ultimate load capacities obtained from the FEA models were 3.5%, 4.3%, and 1.9% lower than that of the tested Specimens 5, 6 and 7, respectively.

#### 5.2.4.1.3 Specimen 8 to 11

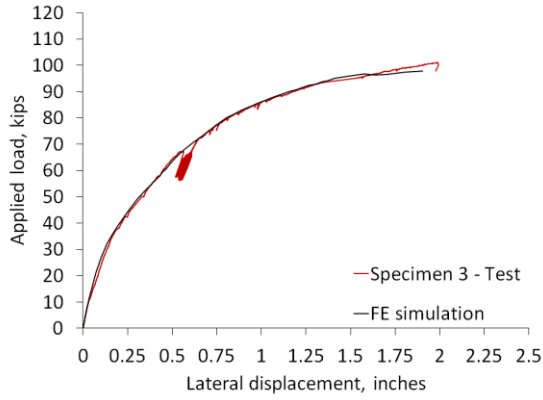
The initial stiffness of the FEA models matched very well with the test results. The post-crack behavior matched reasonably well with the test results. The ultimate load capacities obtained from the FEA model was 4.6%, 4.9%, 2.6%, and 0.9% higher than that of the tested Specimens 8, 9, 10 and 11, respectively.



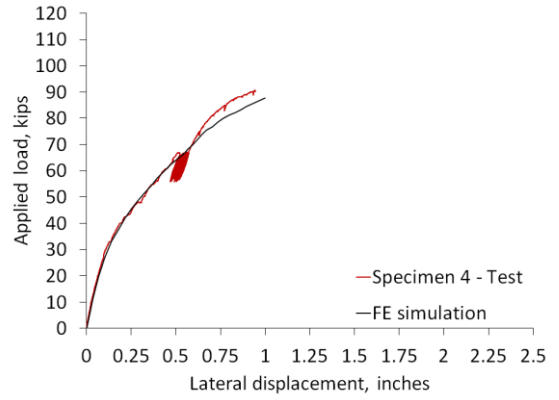
(a) Specimen 1



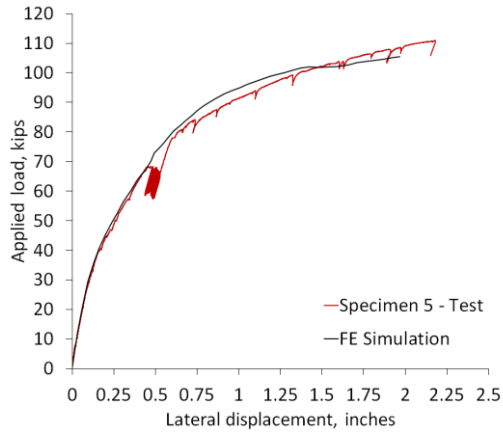
(b) Specimen 2



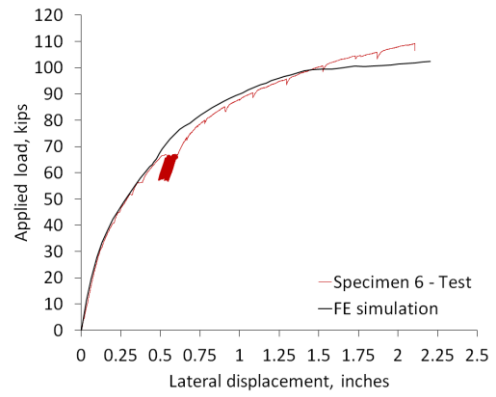
(c) Specimen 3



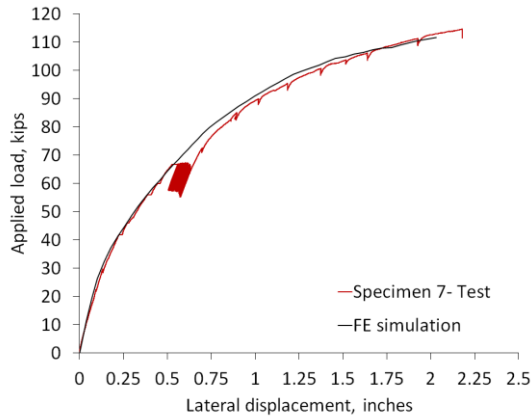
(d) Specimen 4



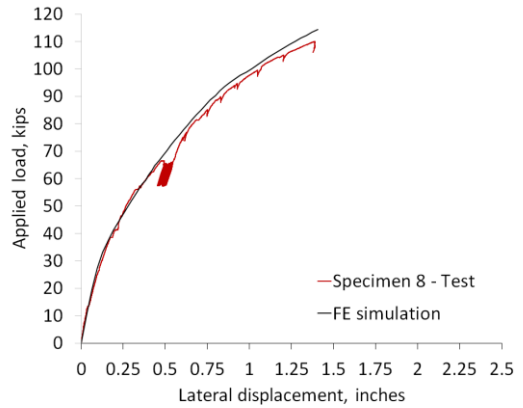
(e) Specimen 5



(f) Specimen 6



(g) Specimen 7



(h) Specimen 8

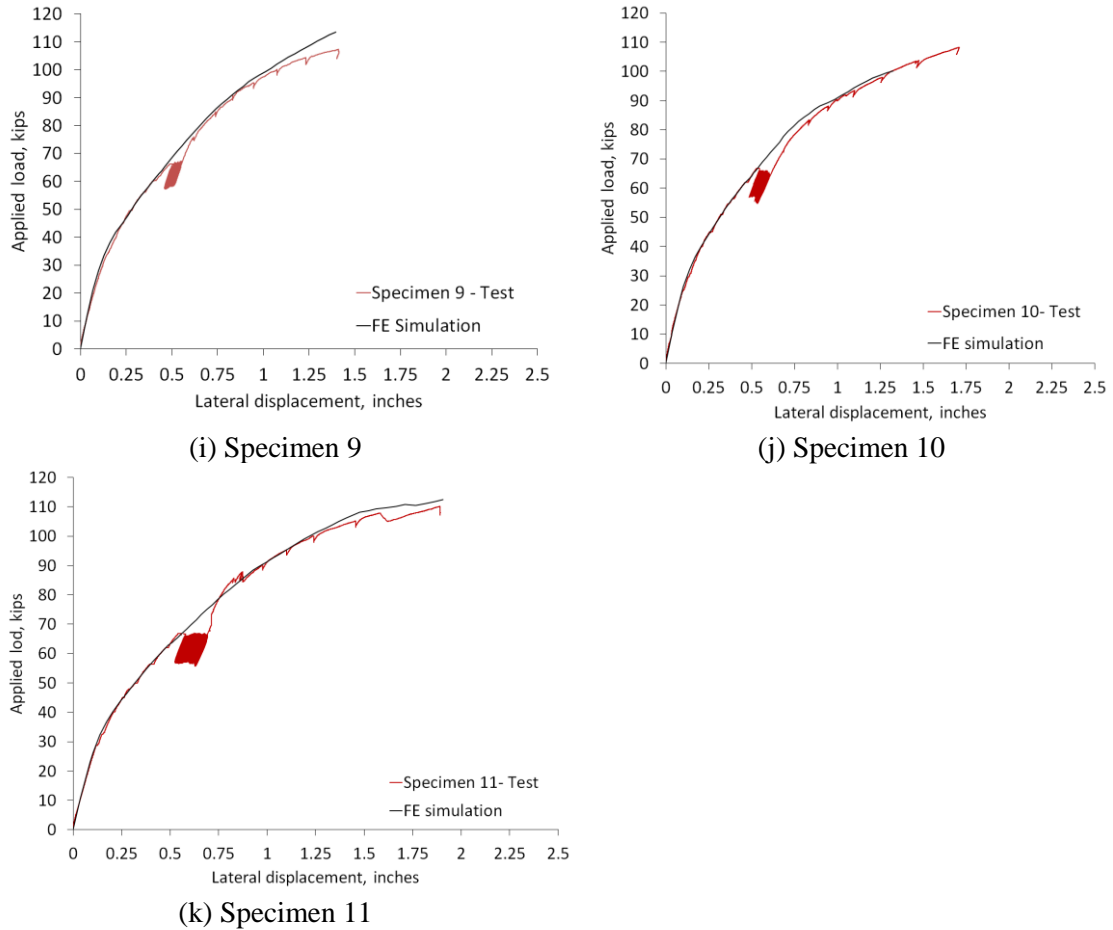


**Fig. 5-3: Comparison of simulated results with test outcomes: load vs. lateral displacement relationship.**

#### 5.2.4.2 Opening at the column-drilled shaft interface

Similar to the tests, each simulated specimen exhibited a significant opening at the column-drilled shaft interface. Fig. 5-4 shows the typical opening at the column-drilled shaft interface of the simulated specimens. Fig. 5-5 shows the load vs. opening relationship for the specimens. It can be observed from Fig. 5-5(a) and (b) that the specimens with the non-contact lap splice consistently exhibited wider opening at the interface than the specimen with the contact splice. A comparison of the opening among Specimens 1 to 4 showed that the opening increased with increasing the non-contact lap splice distance.

It is important to note that the rectangular column to circular drilled shaft connection is typically constructed in separate stages during the fabrication. As a result, the column-drilled shaft connection is a “cold joint,” which is a joint or discontinuity resulting from a delay in placement of sufficient duration to preclude intermingling and bonding of the concrete material [38]. Based on the FEA results, it is evident that a specimen with non-contact lap splice would exhibit a larger opening at the column-drilled shaft interface than that of a specimen with contact lap splice. In reality, due to the large opening at the column-drilled shaft interface, the dowel bars connecting the column and the drilled shaft could be exposed to weathering. More importantly, the column longitudinal bars would also be exposed to weathering because the bars have zero concrete cover at the bottom of the column. Hence, both the dowel bars and the column bars would be subjected to corrosion over time.

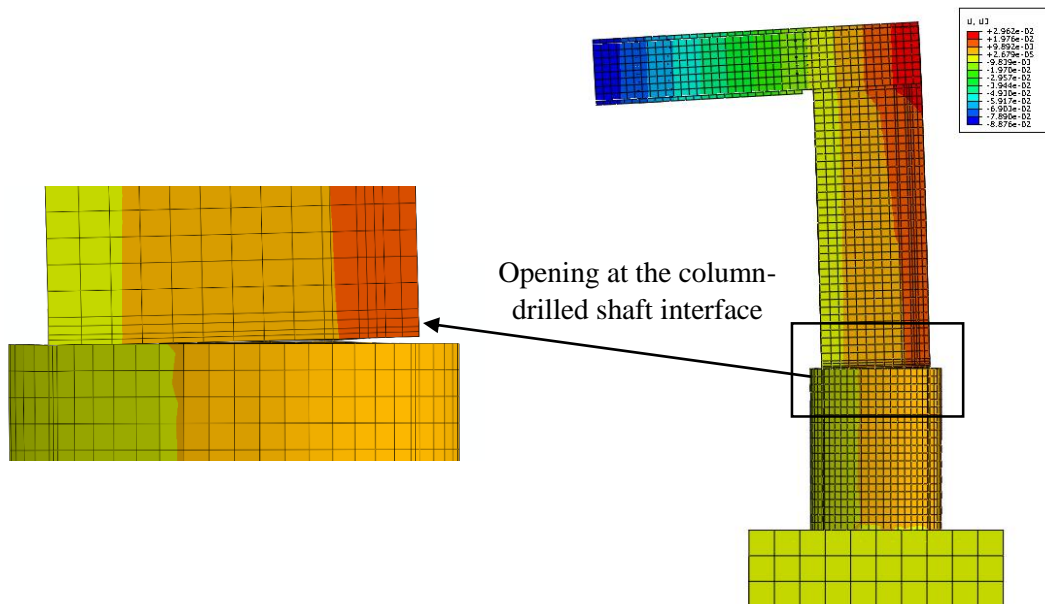


**Fig. 5-4: Typical opening at the bridge column-to-drilled shaft interface.**

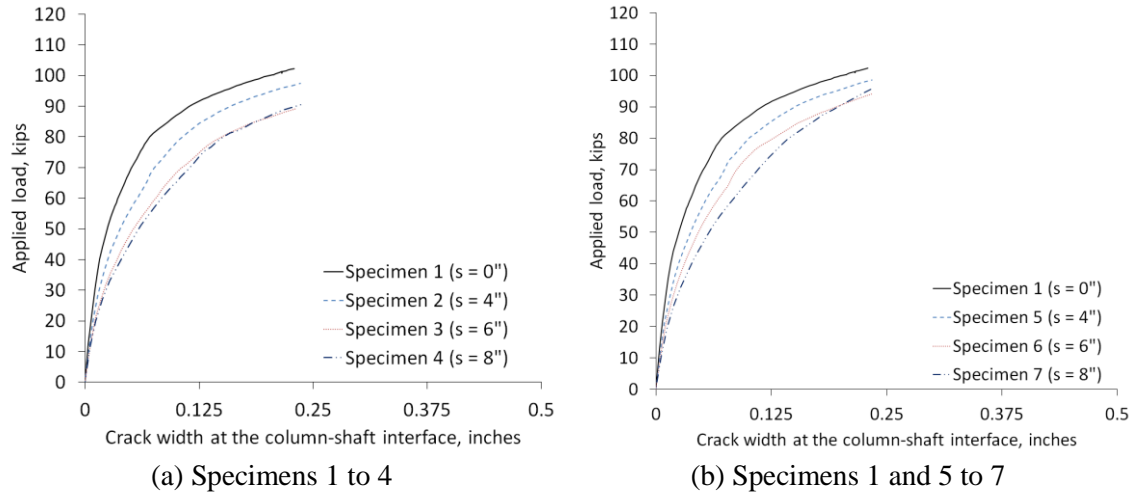
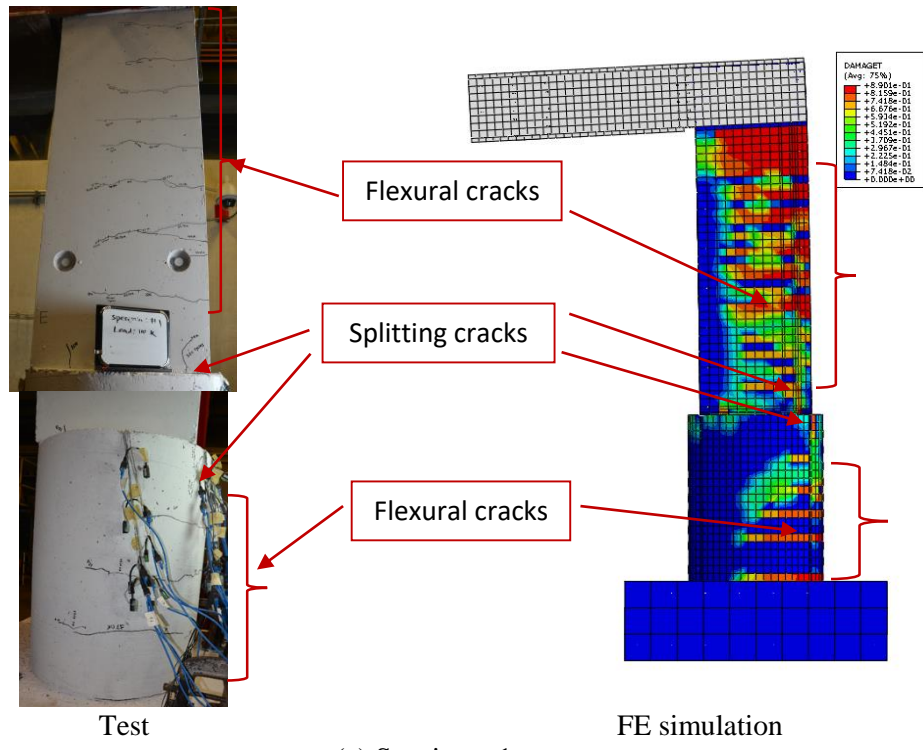


**Fig. 5-5: Opening at the column-drilled shaft interface.**

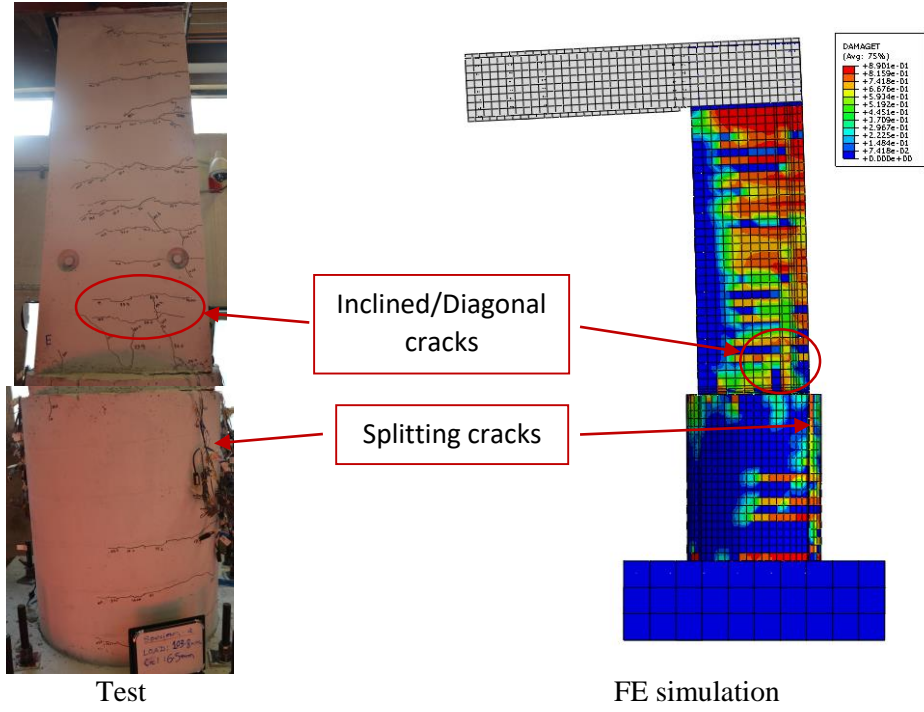
### 5.2.4.3 Crack patterns

The distribution of the tensile damage in the three-dimensional numerical models is shown in Fig. 5-6(a) to (k). No damage is observed in the rectangular footing. The tensile damage is mainly concentrated in the non-contact lap splice zone, which is in good agreement with the experimental findings. The flexural cracks in the column shown in Fig. 5-6(a) to (k) are mostly consistent with the actual cracking patterns. The location and length of flexural cracks in the circular drilled shafts obtained from the FEM simulation also match the experimental observations. In addition to the flexural cracks in the rectangular column and circular shaft, vertical splitting cracks are observed at the interface of the tensile side, as shown in Fig. 5-6. It can be observed from Fig. 5-6 that the quantity and length of splitting cracks are significantly increased with the increment of lap splice distance. The splitting cracks are mainly caused by the bond slip between the lap spliced bars and the concrete during the force transfer process. The splitting cracks appeared along the length of the dowel bars, parallel to the longitudinal column bars. Significant inclined (diagonal) cracks with inclined angles in the lap spliced zone of the column and drilled shaft are also observed. The location of inclined (diagonal) cracks is in good agreement with the experimental observations.

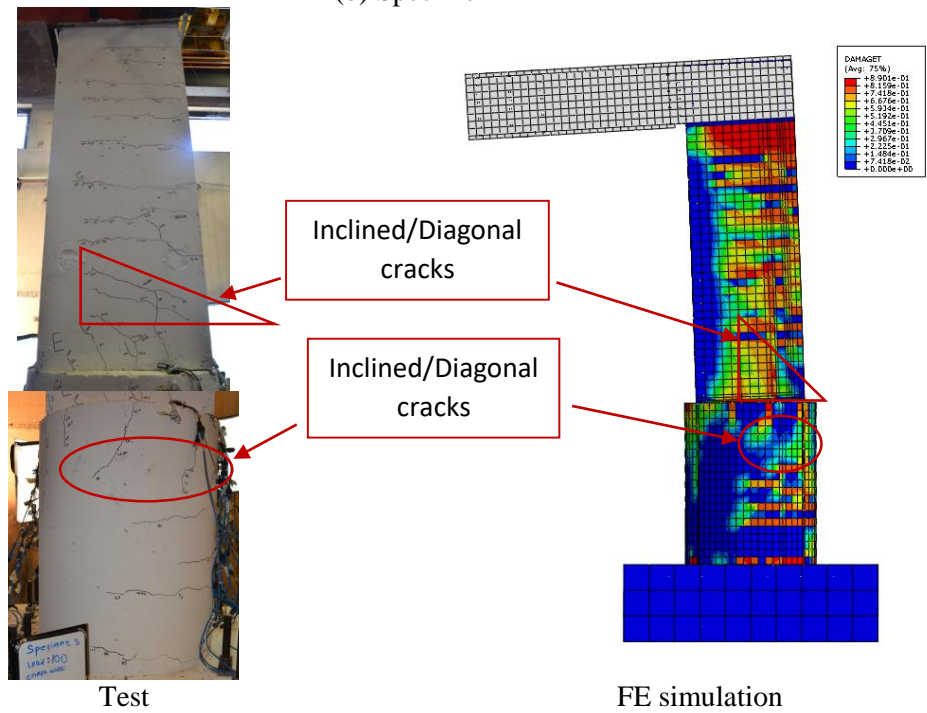
It is important to note that the modeling of the connection between the steel box beam and column, connected by several embedded anchors and through rods in the actual test, was quite complex. To simplify the model, the steel box beam flanges and webs of the FEA model were connected to the concrete surface of the column using tie constraints. As a result, it can be observed in Fig. 5-6 that the tensile stress level is higher near the connection between the column and steel box beam than other parts, presenting serious tensile damage.



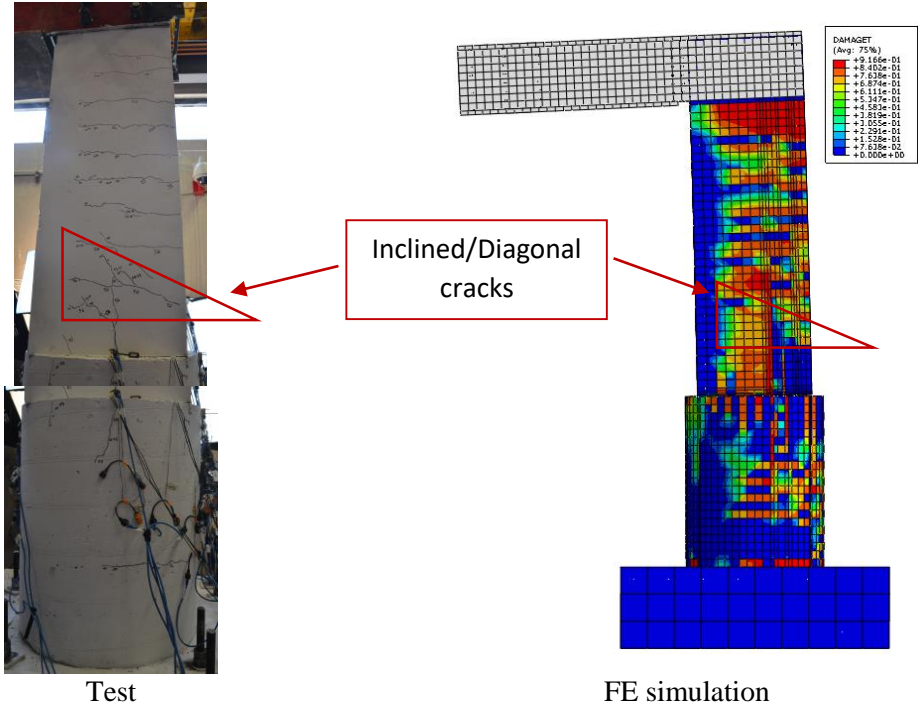
(a) Specimen 1



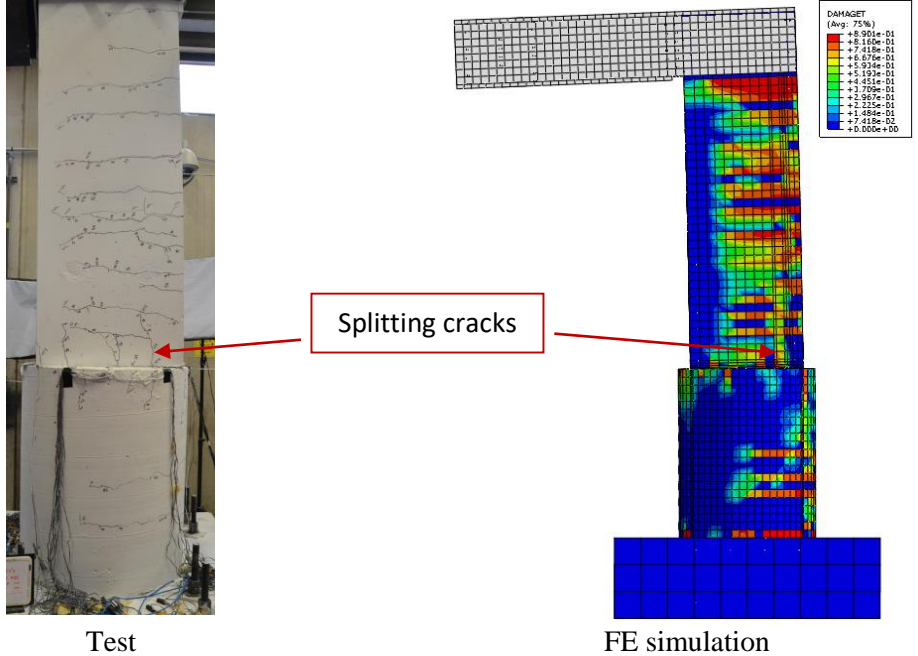
(b) Specimen 2



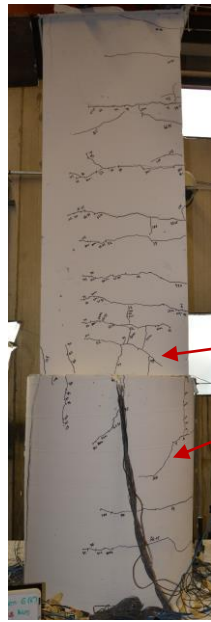
(c) Specimen 3



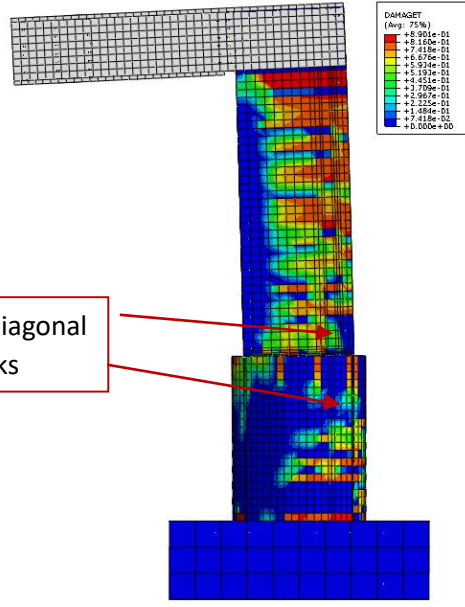
(d) Specimen 4



(e) Specimen 5

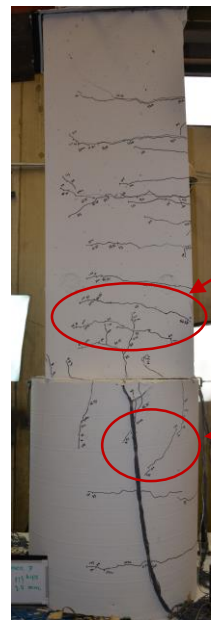


Test

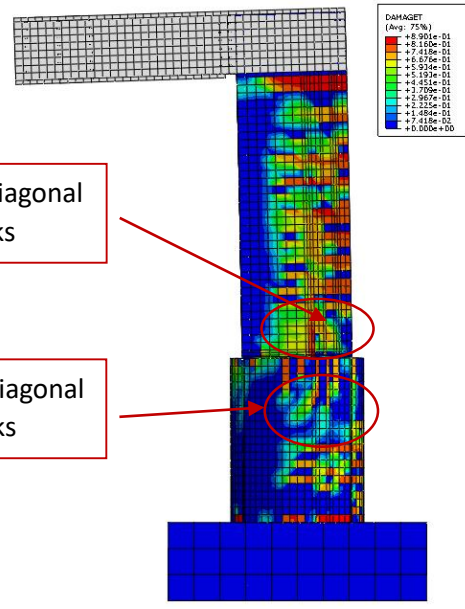


FE simulation

(f) Specimen 6

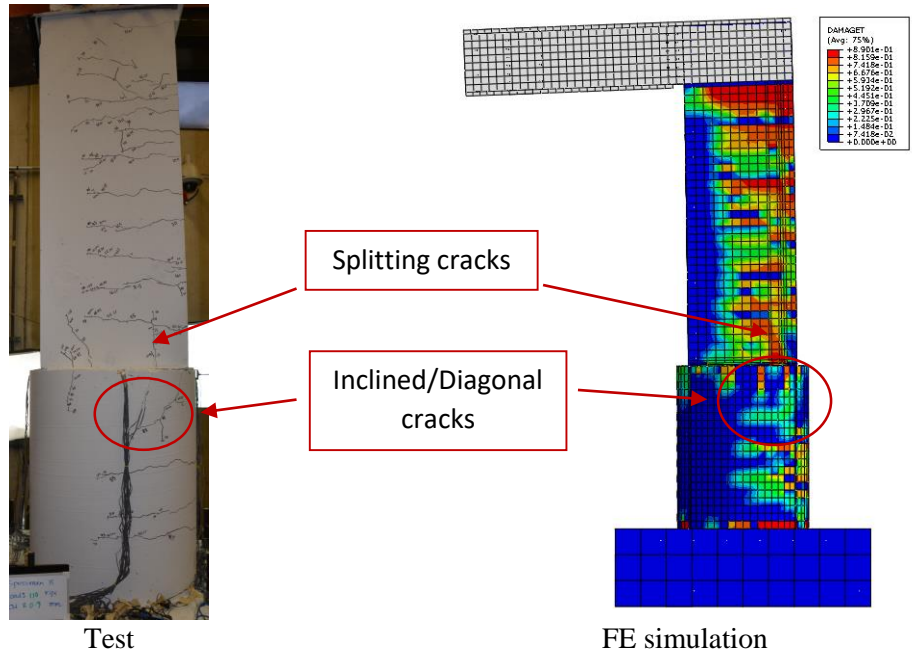


Test

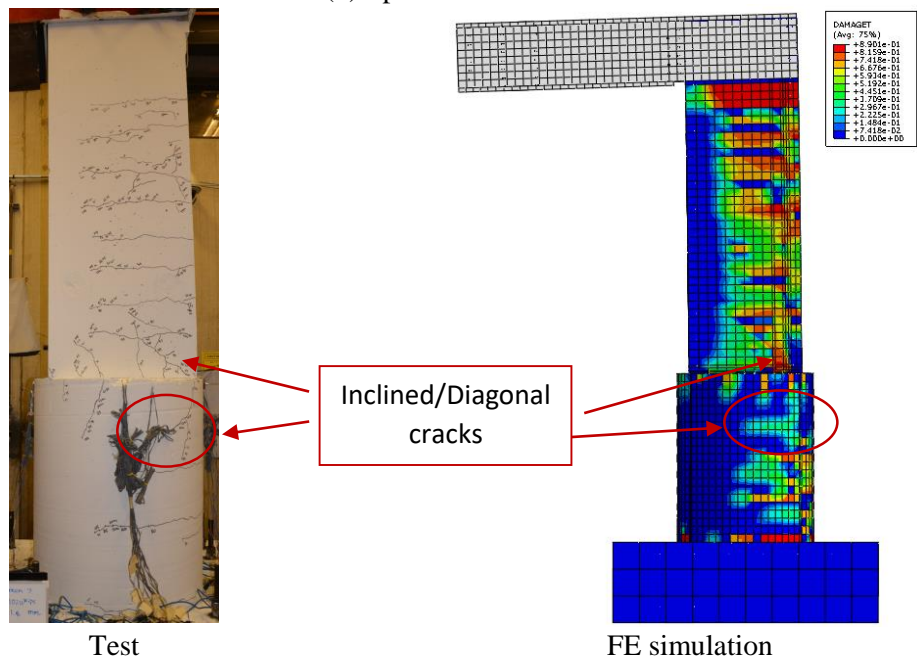


FE simulation

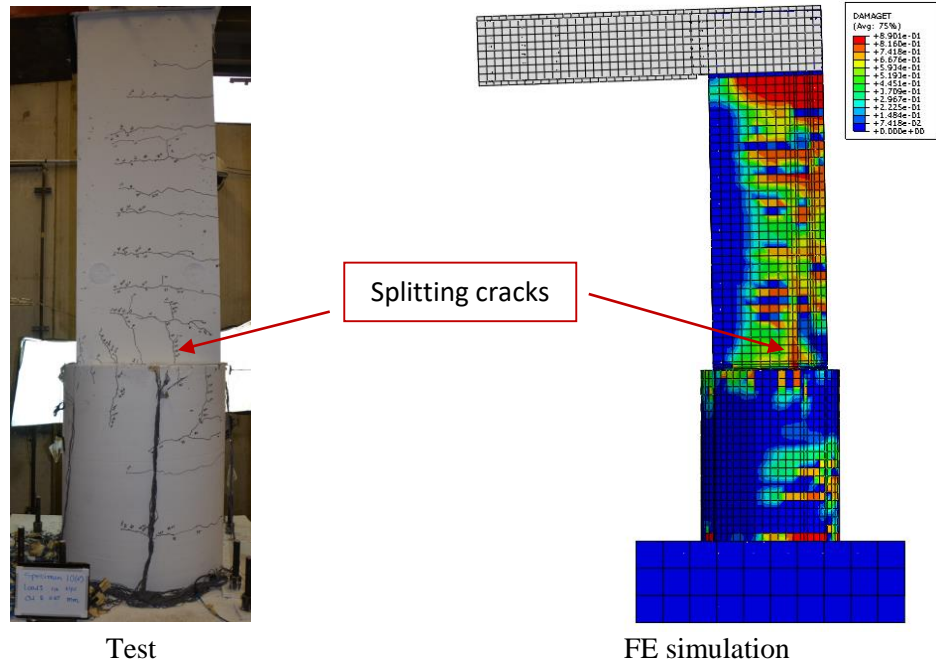
(g) Specimen 7



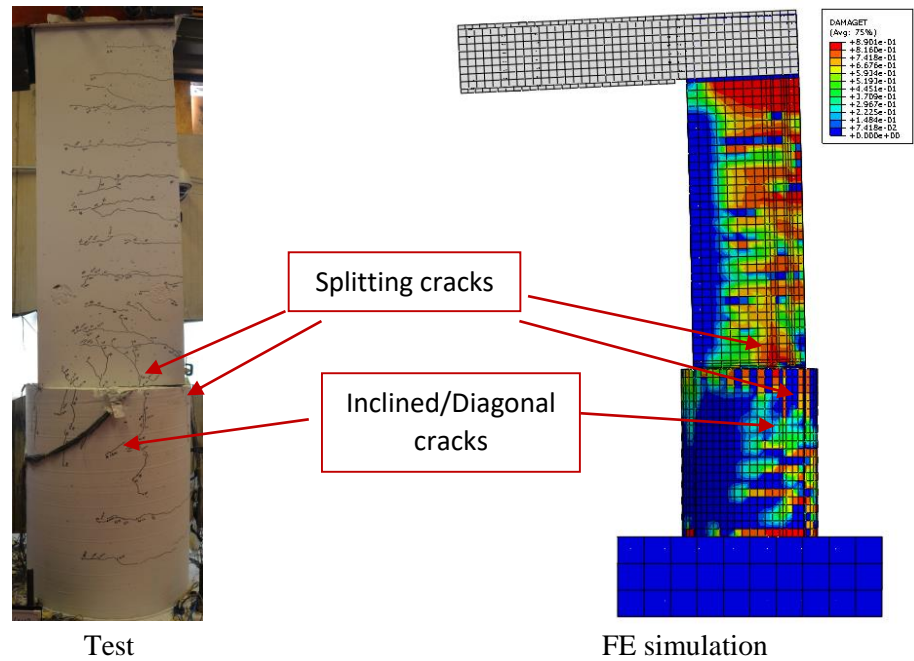
(h) Specimen 8



(i) Specimen 9



(j) Specimen 10



(k) Specimen 11

**Fig. 5-6: Cracks patterns and failure modes on the simulated specimens.**

### 5.3 Parametric Study on the Test Specimens

A comprehensive finite element method-based parametric study was performed on the test specimens to investigate the effects of the critical parameters: lap splice length, non-contact lap

splice distance, and amount of transverse reinforcement in the non-contact lap splice zone of rectangular columns.

### **5.3.1 Effect of Lap Splice Length**

The laboratory test Specimens 2 to 11 consisted of non-contact lap splice length,  $l_{nS}$  which is equal to standard lap splice length,  $l_s$  plus their respective non-contact lap splice distance,  $s$ . So the non-contact lap splice length,  $l_{nS}$  differed by 4 inches to 8 inches depending on their respective lap splice distance,  $s$  for the test specimens. The effect of lap splice length on the structural behavior of the test specimens can be understood clearly by comparing the responses of the FEA models with the same lap splice distance and transverse reinforcement, but varying lap splice length.

Specimens 2-7 were chosen for this parametric study. To study the effect of lap splice length, twelve FEA models were developed -- two models for each of Specimens 2 to 7. For example, in the case of Specimen 2, Specimens 2LS and 2L FEA models were developed. Specimen 2LS consisted of non-contact lap splices with a length equaling 25.5 inches of standard lap splice length,  $l_s$  plus 4 inches of non-contact lap splice distance,  $s$  whereas Specimen 2L consisted of non-contact splices with a length equaling 25.5 inches standard lap splice length,  $l_s$  only. Specimens 2LS and 2L had the same lap splice distance of 4 inches and the same amount of transverse reinforcement. As a result, a comparison between Specimens 2LS and 2L would be helpful in identifying the influence of lap splice length on the structural behavior of the specimens. The details of all the other FEA models developed for studying the effect of lap splice length are provided in Table 5-3.

**Table 5-3: Details of FEA models for studying the effects of lap splice length and lap splice distance**

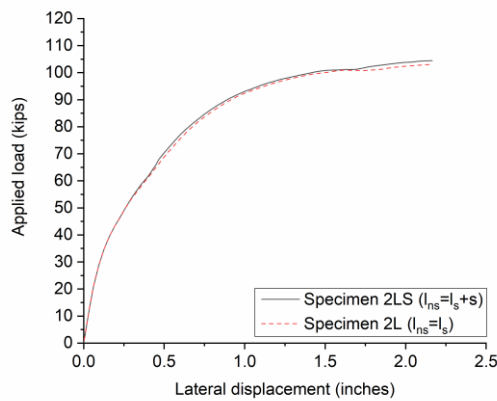
<b>FEA model designation</b>	<b>Lap splice distance, <math>s</math> (in)</b>	<b>Lap splice length, <math>l_{ns}</math> (in)</b>	<b>Spacing of transverse reinforcement in column, <math>s_{tr}</math> (in) [within lap splice]</b>	<b>Spacing (pitch) of transverse reinforcement in drilled shaft, <math>s_{max}</math> (in) [within lap splice]</b>
Specimen 2LS <sup>a</sup>	4	29.5	6 (2-legged)	3.75
Specimen 2L <sup>b</sup>	4	25.5	6 (2-legged)	3.75
Specimen 3LS	6	31.5	6 (2-legged)	3.75
Specimen 3L	6	25.5	6 (2-legged)	3.75
Specimen 4LS	8	33.5	6 (2-legged)	3.75
Specimen 4L	8	25.5	6 (2-legged)	3.75
Specimen 5LS	4	29.5	4 (4-legged)	3.75
Specimen 5L	4	25.5	4 (4-legged)	3.75
Specimen 6LS	6	31.5	4 (4-legged)	3.75
Specimen 6L	6	25.5	4 (4-legged)	3.75
Specimen 7LS	8	33.5	4 (4-legged)	3.75
Specimen 7L	8	25.5	4 (4-legged)	3.75

<sup>a</sup> LS is used to represent standard lap splice length,  $l_s$  plus non-contact lap splice distance,  $s$

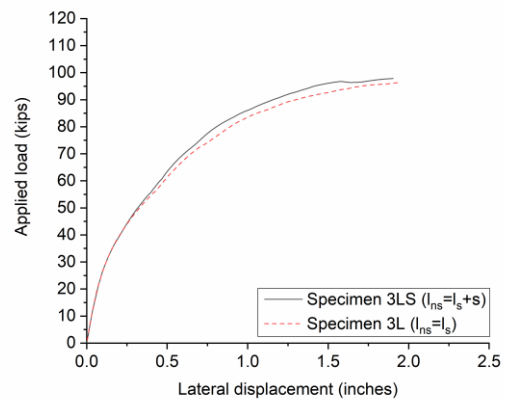
<sup>b</sup> L is used to represent standard lap splice length,  $l_s$ .

The load vs. lateral displacement relationships of Specimens 2L and 2LS are shown in Fig. 5-7(a). It is evident from Fig. 5-7(a) that the initial stiffness of the specimens is quite similar, but

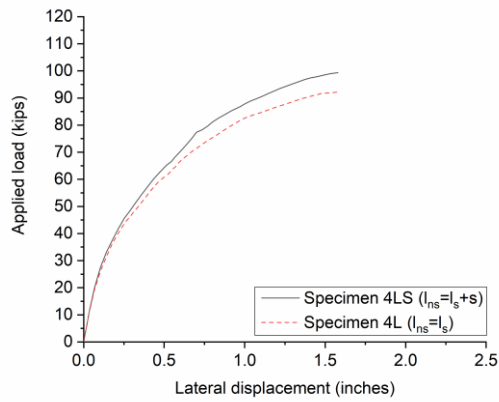
the post-crack lateral stiffness is slightly lower in the case of Specimen 2L. The post-crack lateral stiffness of Specimen 2LS is slightly higher (maximum difference of lateral stiffness is about 1.4%) than that of Specimen 2L. It can be observed from Fig. 5-7(b) that Specimen 3LS also exhibited a slightly higher lateral stiffness (about 3.5% higher) than that of Specimen 3L. It can be observed from Fig. 5-7(c) that Specimen 4LS exhibited a higher lateral stiffness (about 7.7% higher) than that of Specimen 4L. A similar trend was also observed for Specimens 5 to 7. The lateral stiffness of Specimen 5LS is 1.0% higher than that of Specimen 5L, Specimen 6LS is 2.65% higher than that of Specimen 6L and Specimen 7LS is 4.7% higher than that of Specimen 7L. It is evident from the parametric study of Specimens 2 to 7 that by providing a lap splice length consisting of standard lap splice length,  $l_s$  plus non-contact lap splice distance,  $s$ , the lateral stiffness of the specimens could be increased compared to the specimens with a lap splice length of standard lap splice length,  $l_s$  only. It is also observed that the contribution of increased lap splice length in increasing lateral stiffness of the specimens is more evident with increasing lap splice distance. This indicates that the specimens with lap splice distances  $\geq 4$  inches should be designed with lap splices with a length equaling standard lap splice length,  $l_s$  plus non-contact lap splice distance,  $s$ , because, the larger the lap splice distance, the greater the contribution of longer lap splice length in increasing lateral stiffness of the specimens designed with non-contact lap splices.



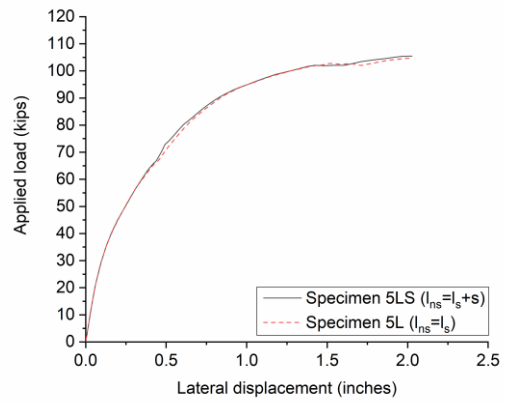
(a) Specimens 2LS and 2L



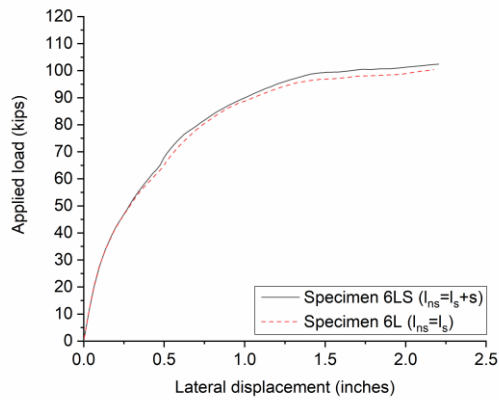
(b) Specimens 3LS and 3L



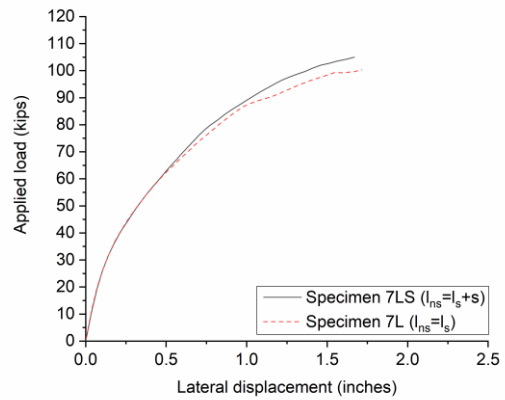
(c) Specimens 4LS and 4L



(d) Specimens 5LS and 5L



(e) Specimens 6LS and 6L



(f) Specimens 7LS and 7L

**Fig. 5-7: Load vs. lateral displacement relationship.**

### 5.3.2 Effect of Non-Contact Lap Splice Distance

The effect of lap splice distance on the structural behavior of the test specimens can be understood clearly by comparing the response of FEA models having the same lap splice length and amount of transverse reinforcement but varying lap splice distance. For example, the FEA models Specimens 2L, 3L, and 4L consisted of the same lap splice length of 25.5 inches, but the lap splice distances are 4 inches, 6 inches, and 8 inches, respectively. The load vs. lateral displacement relationships of Specimens 2L to 4L are shown in Fig. 5-8(a). The load vs. lateral displacement relationships of Specimens 5L to 7L are shown in Fig. 5-8(b).

From the comparison of Specimens 5L to 7L, it can be observed that Specimen 5L with 4 inches of non-contact splice distance showed the highest lateral stiffness. The lateral stiffness of Specimen 6L (6 inches of lap splice distance) was generally higher than Specimen 7L (8 inches of lap splice distance), but near the ultimate load level, the lateral stiffness of Specimen 7L was slightly higher than that of Specimen 6L. This increase in lateral stiffness was caused by the location of the dowel bars in Specimen 7L. As shown in Fig. 4-11, the dowel bars located on the south side of Specimen 7 had a larger lever arm than the respective dowel bars in Specimens 5 and 6. Consequently, the contribution of the dowel bars located on the south side of the column of Specimen 7 in increasing the capacity and the stiffness is greater than the respective dowel bars in Specimens 5 and 6. So, the increase in lateral stiffness of Specimen 7L could be attributed to the contribution of the dowel bars located on the south side of the column of Specimen 7L. Fig. 5-9 shows the dowel bars (highlighted in red) on the south side of the FEA model of the specimens. Fig. 5-10 shows a comparison of the stresses in the dowel bars located on the south side of the specimens at the Load Level B (66.75 kips). It can be observed from Fig. 5-10 that the maximum tensile stress induced in the dowel bars on the south side of Specimens 5, 6, and 7 are 5.95 ksi, 15.63 ksi, and 23.11 ksi, respectively. It can be observed from the FEA results that the tensile stresses induced in the dowel bars on the south side of Specimen 7L at the load level B are up to 288.4% and 47.9% higher than that of Specimens 5L and 6L, respectively. As a result, the lateral stiffness of Specimen 7L was higher than Specimens 5L and 6L.

In reality, the dowel bars in a column-drilled shaft connection might not be located so close to each other. Hence, the aforementioned effect of closely spaced dowel bars might not be expected in full-scale structures. For example, in the Bent 17 column on SH 99, the distance between the dowel bars on the “compression side” and “tension side” was 93.0 inches which was 77.5% of the depth (120 inches) of the column section. In the case of Specimens 4 and 7, the distance between the dowel bars on the south side and north side was 7 inches which was only 25.0% of the depth

(28 inches) of the column section. In contrast, for Specimens 2 (or 5) and 3 (or 6), the distance between the dowel bars on the south side and north side was 53.6% and 39.3% of the depth of the column section, respectively. Based on these results, it can be stated that except for the unique case of Specimen 7 (or 4), the lateral stiffness and ultimate load capacity would generally decrease with increasing the non-contact lap splice distance.

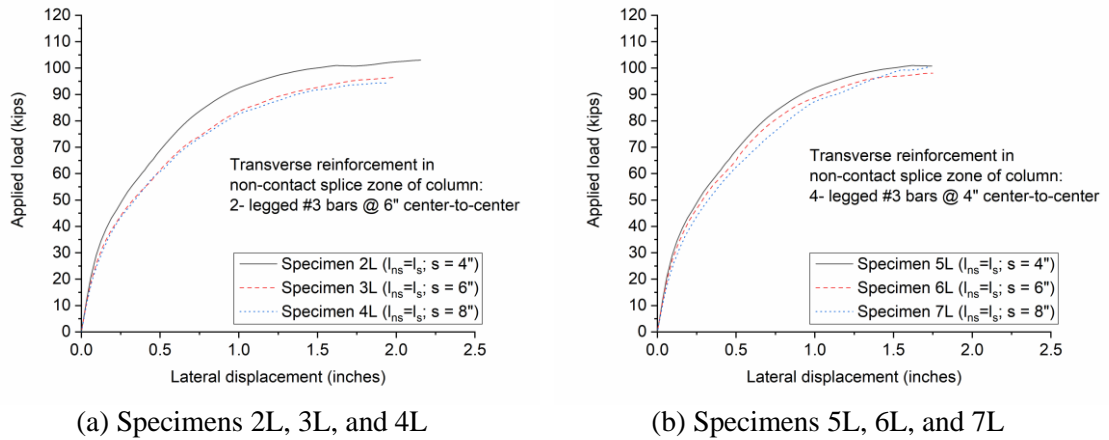


**Fig. 5-8: Load vs. lateral displacement relationship.**

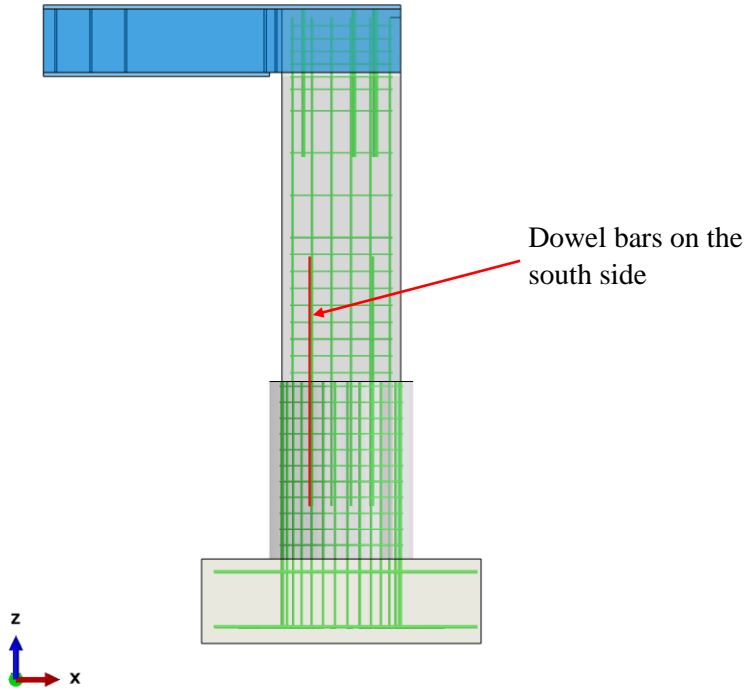


**Fig. 5-9: Location of dowel bars on the south side of the FEA models.**

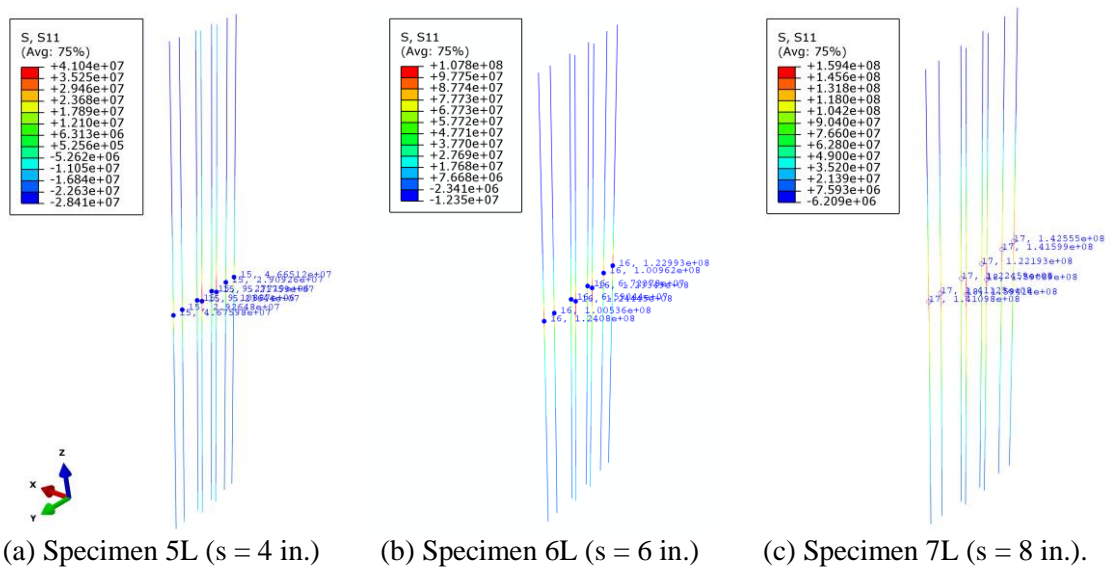


**Fig. 5-10: Stresses on the dowel bars located on the south side of the FEA models at the Load Level B (66.75 kips).**

Note: S11 represents axial stresses in the reinforcing bars. Please note that the unit of stresses in this figure is  $\text{N/m}^2$  [1 ksi = 6894757.3  $\text{N/m}^2$ ].

### **5.3.3 Effect of Amount of Transverse Reinforcement in the Non-Contact Lap Splice Zone of Rectangular Columns**

To identify the effect of the amount of transverse reinforcement in the non-contact lap splice zone of the rectangular column, a thorough FEA-based parametric study was performed on Specimens 5, 6, and 7. For each test specimen, two FEA models were developed with two different amounts of transverse reinforcement.

The transverse reinforcement in the column of the test Specimens 2 to 4 was designed with the two-dimensional behavior model of non-contact lap splices proposed by McLean and Smith [4] which can be represented as Equation 4. On the other hand, the transverse reinforcement in the column of the test Specimens 5 to 7 was designed with the behavior model of non-contact lap splices in a rectangular section proposed by Maksoud [17] which can be expressed as Equation 6.

In this parametric study, six FEA models were developed--two models for each of Specimens 5 to 7. For example, in the case of Specimen 5, Specimens 5S2D and 5S3D FEA models were developed. Specimen 5S2D consisted of transverse reinforcement designed with the two-dimensional behavior model of non-contact lap splices proposed by McLean and Smith [4]. Specimen 5S3D consisted of transverse reinforcement designed with the three-dimensional behavior model of non-contact lap splices for rectangular sections proposed by Maksoud [17]. Specimens 5S3D and 5S2D have the same lap splice distance, lap splice length and amount of transverse reinforcement in the drilled shaft but varying amounts of transverse reinforcement in the column lap splice zone. The details of the FEA models for studying the effect of the amount of transverse reinforcement in the rectangular column are presented in Table 5-4.

**Table 5-4: Details of the FEA models for studying the effect of the amount of transverse reinforcement in the rectangular columns**

<b>Model Designation</b>	<b>Lap splice distance, <math>s</math> (in)</b>	<b>Lap splice length, <math>l_{ns}</math> (in)</b>	<b>Spacing of transverse reinforcement in column, <math>s_{tr}</math> (in) [within lap splice]</b>	<b>Spacing (pitch) of transverse reinforcement in drilled shaft, <math>s_{max}</math> (in) [within lap splice]</b>
Specimen 5S3D <sup>a</sup>	4	29.5	4 (4-legged)	3.75
Specimen 5S2D <sup>b</sup>	4	29.5	6 (2-legged)	3.75
Specimen 6S3D	6	31.5	4 (4-legged)	3.75
Specimen 6S2D	6	31.5	6 (2-legged)	3.75
Specimen 7S3D	8	33.5	4 (4-legged)	3.75
Specimen 7S2D	8	33.5	6 (2-legged)	3.75

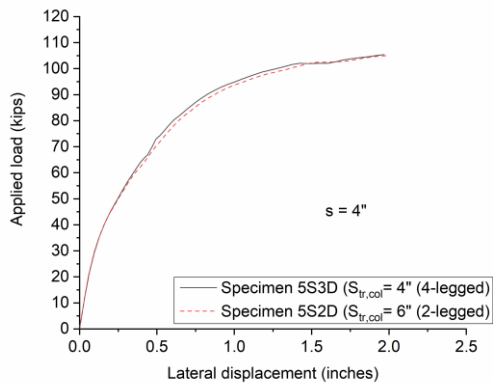
<sup>a</sup> S3D represents that the transverse reinforcement in the lap splice zone of the column was calculated using Eq. 6.

<sup>b</sup> S2D represents that the transverse reinforcement in the lap splice zone of the column was calculated using Eq. 4.

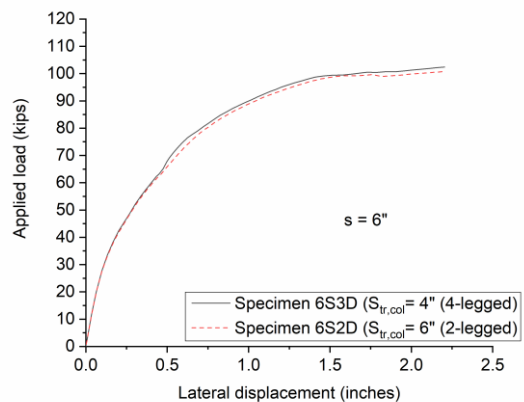
The load vs. lateral displacement relationships of Specimens 5S2D and 5S3D are shown in Fig. 5-11(a). From the comparison, it can be observed that the lateral stiffness of Specimen 5S2D was slightly lower than that of Specimen 5S3D. However, the difference in lateral stiffness and ultimate load capacity of Specimens 5S2D and 5S3D is less than 1%. The load vs. lateral displacement relationships of Specimens 6S2D and 6S3D are shown in Fig. 5-11(b). The load vs. lateral displacement relationships of Specimens 7S2D and 7S3D are shown in Fig. 5-11(c). From Fig.

5-11(a), (b), and (c), it can be observed that the lateral stiffness of specimens consisting of 2-legged ties at 6 in. center-to-center (c/c) spacing is slightly lower than the specimens consisting of 4-legged ties at 4 in. c/c spacing. From these observations, it is evident that the global response, i.e., load vs. lateral displacement relationship of the specimens is not significantly influenced by the increased amount of transverse reinforcement in the non-contact lap splice zone of the column.

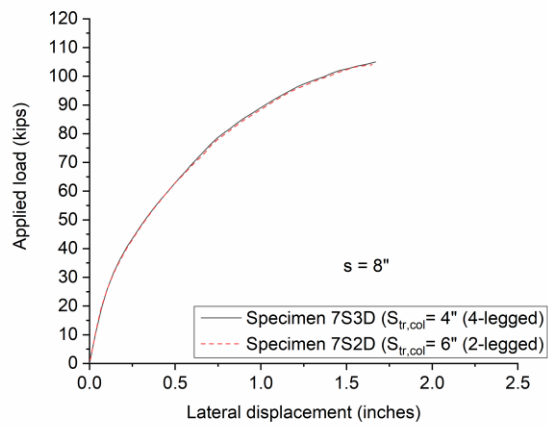
As little difference was observed between the specimens with a varying amount of transverse reinforcement in the non-contact lap splice zone of rectangular columns, the local response, i.e., tensile stresses in the column ties located at the non-contact lap splice zone was studied further. A comparison of the tensile stresses in the column ties at the non-contact lap splice zone at load level B and ultimate load level is provided in Table 5-5. It can be observed from Table 5-5 that the column ties in the specimens with a higher amount of transverse reinforcement, Specimens 5S3D, 6S3D, and 7S3D exhibited smaller stresses at load level B and ultimate load stage than that of Specimens 5S2D, 6S2D, and 7S2D, respectively. The tensile stresses in the ties of the non-contact lap splice zone of the column are illustrated in Fig. 5-12. From Fig. 5-12, it is also evident that the column ties near the column-drilled shaft connection exhibited the highest tensile stresses among all of the column ties within the lap splice zone of the rectangular column. This observation is consistent with the experimental results as discussed in Chapter 4.



(a) Specimens 5S3D and 5S2D



(b) Specimens 6S3D and 6S2D



(c) Specimens 7S3D and 7S2D

**Fig. 5-11: Simulated load vs. lateral displacement relationship.**

**Table 5-5: Comparison of tensile stresses in the ties of non-contact lap splice zone of the column**

Model designation	Tensile stresses in the column ties, ksi	
	Load level B (66.75 kips)	Ultimate load
Specimen 5S2D	17.5	41.3
Specimen 5S3D	17.1	37.5
Specimen 6S2D	46.6	59.7
Specimen 6S3D	36.0	54.4
Specimen 7S2D	58.3	76.4
Specimen 7S3D	49.2	54.5

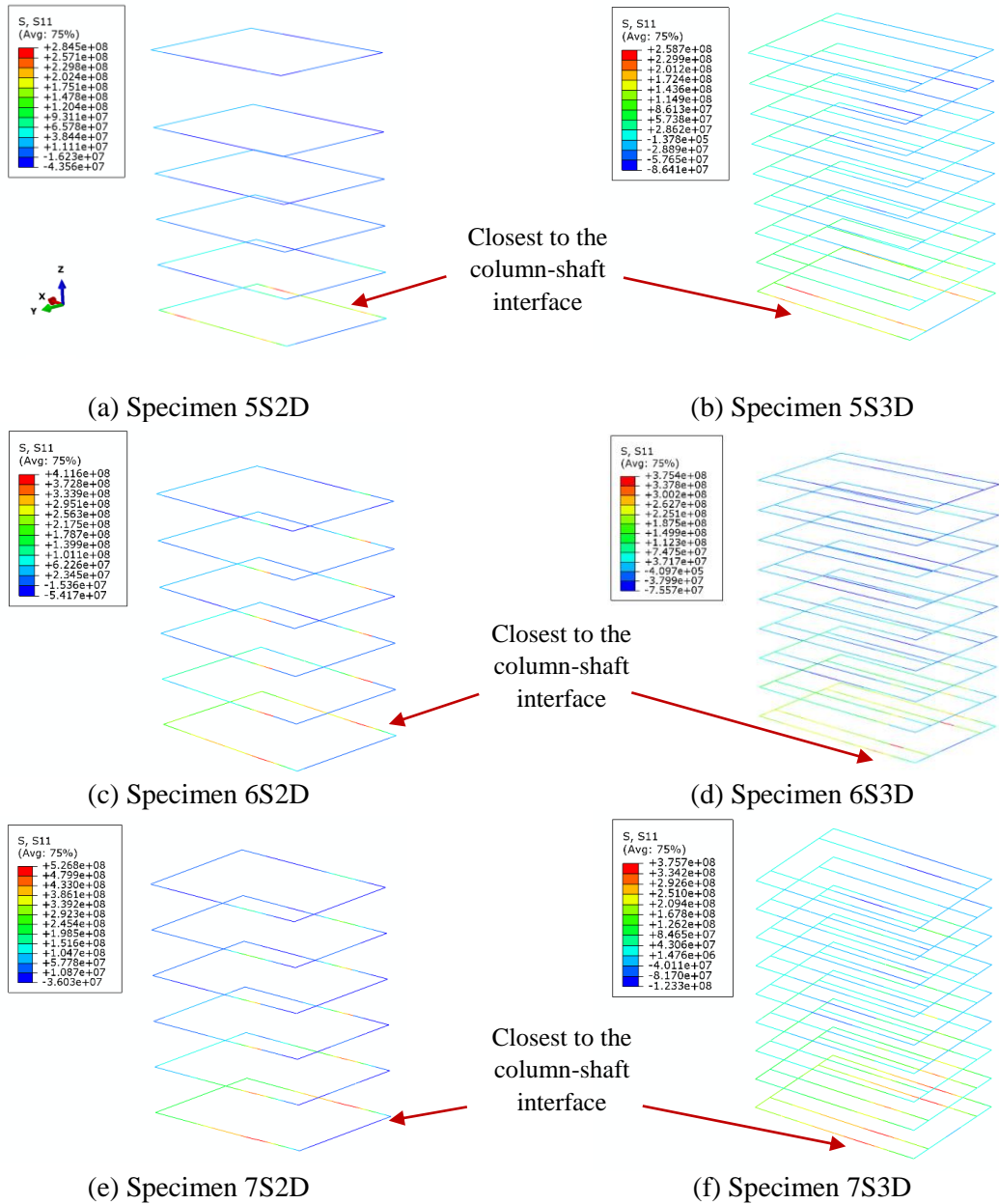


**Fig. 5-12: Tensile stresses in the ties of non-contact lap splice zone of the column.**

#### 5.4 Finite Element Analysis of a Full-Scale Column-Drilled Shaft Structure

A finite element analysis (FEA) was performed on the Bent 17 column-drilled shaft connection of Grand Parkway (SH 99) to study the effect of non-contact splice lengths on the performance of non-contact lap splices. Five FEA models of the Bent 17 column-drilled shaft connection with varying lap splice lengths were developed using Abaqus [28]. The three-dimensional modeling of

the FEA models, e.g., material parameters, boundary conditions, etc. were mostly similar to the preliminary FEA performed on the Bent 17 column-drilled shaft connection described in Section 3.8. However, the loading consisted of only service load (dead load plus live load) during the preliminary analysis whereas the aforementioned models were loaded to find out the ultimate capacity of the structures. Furthermore, the actual Bent 17 was replaced with a rigid beam at the top of the column-drilled shaft connection of the FEA models for simplicity and reducing computation time. The details of the finite element analysis (FEA) models of the Bent 17 column-drilled shaft connection for investigating the effect of splice length on the structural behavior of non-contact lap spliced connections are shown in Table 5-6. In Table 5-6, the Bent17-L-AASHTO14-24” specimen represents the original Bent 17 column-drilled shaft connection on State Highway 99. In this specimen, the dowel bars formed non-contact splices with the column longitudinal bars because the dowel bars were located as far as 24 inches away from the column longitudinal bars. In Bent17-L-AASHTO14-CONTACT model, the dowel bars were removed, and the column longitudinal bars were extended into the drilled shaft. In order to extend the column longitudinal bars into the drilled shaft, the diameter of the drilled shaft was increased by twenty-eight inches from the original diameter of the Bent 17 column-drilled shaft connection, and the position of the drilled shaft longitudinal bars was also adjusted accordingly. The other specimens shown in Table 5-6 have the same diameter of the drilled shaft as Bent17-L-AASHTO14-24” but consisted of different splice lengths based on the AASHTO 2014 and 2016 specifications [2, 12] and WSDOT [4] guidelines. The finite element model of the Bent 17 column-drilled shaft connection is shown in Fig. 5-13.

**Table 5-6: Description of FEA models for investigating the effect of splice length on the structural behavior of non-contact lap spliced connections.**

<b>Specimen Designation</b>	<b>Lap splice length, <math>l_{ns}</math> (inches)</b>	<b>Diameter of drilled shaft, D (inches)</b>	<b>Maximum non-contact Lap splice distance in the column, s (inches)</b>	<b>Design formula for calculating Lap splice length</b>
Bent17-L <sup>a</sup> - AASHTO14- CONTACT	108	148	0	$l_s = 1.7 * l_{db}$ $\text{where, } l_{db} = \frac{1.25A_b f_y}{\sqrt{f'_c}}$ (AASHTO, 2014) [2]
Bent17-L- AASHTO14- 24"	108	120	24	$l_s = 1.7 * l_{db}$ $\text{where, } l_{db} = \frac{1.25A_b f_y}{\sqrt{f'_c}}$ (AASHTO, 2014) [2]
Bent17-LS <sup>b</sup> - AASHTO14- 24"	132	120	24	$l_{ns} = l_s + s \text{ (WSDOT, 1997) [4]}$ $l_s = 1.7 * l_{db}$ $\text{where, } l_{db} = \frac{1.25A_b f_y}{\sqrt{f'_c}}$ (AASHTO, 2014) [2]

**Table 5-6: (continued) Description of FEA models for investigating the effect of splice length on the structural behavior of non-contact lap spliced connections.**

Specimen Designation	Lap splice length, $l_{ns}$ (inches)	Diameter of drilled shaft, D (inches)	Maximum non-contact Lap splice distance in the column, s (inches)	Design formula for calculating Lap splice length
Bent17-L- AASHTO16- 24"	58	120	24	$l_s = 1.3 * l_{db} * \lambda_{rl} * \lambda_{cf} * \lambda_{lw} * \lambda_{rc} * \lambda_{er}$ $\text{where, } l_{db} = \frac{2.4d_b f_y}{\sqrt{f'_c}}$ (AASHTO, 2016) [12] where $\lambda_{rc} = 0.428$
Bent17-LS- AASHTO16- 24"	82	120	24	$l_{ns} = l_s + s \text{ (WSDOT, 1997) [4]}$ $l_s = 1.3 * l_{db} * \lambda_{rl} * \lambda_{cf} * \lambda_{lw} * \lambda_{rc} * \lambda_{er}$ $\text{where, } l_{db} = \frac{2.4d_b f_y}{\sqrt{f'_c}}$ (AASHTO, 2016) [12]

<sup>a</sup> L is used to represent standard lap splice length,  $l_s$

<sup>b</sup> LS is used to represent standard lap splice length,  $l_s$  plus non-contact lap splice distance, s

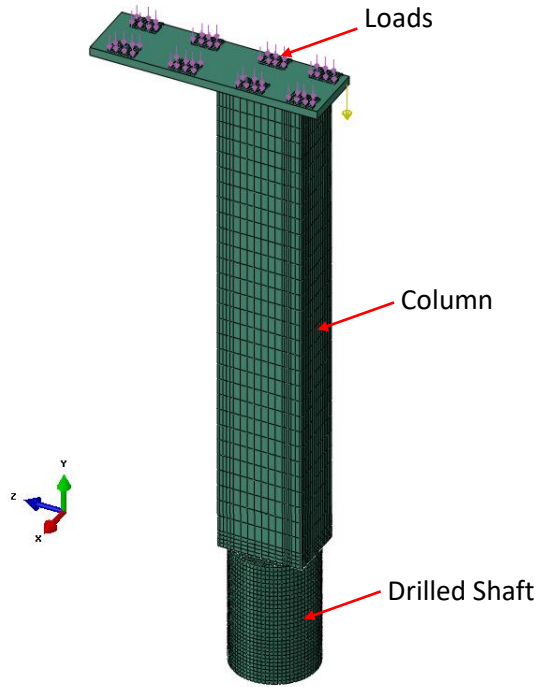


**Fig. 5-13: Finite element model of the Bent 17 column-drilled shaft connection.**

The load vs. displacement relationships of the five FEA models are presented in Fig. 5-14.

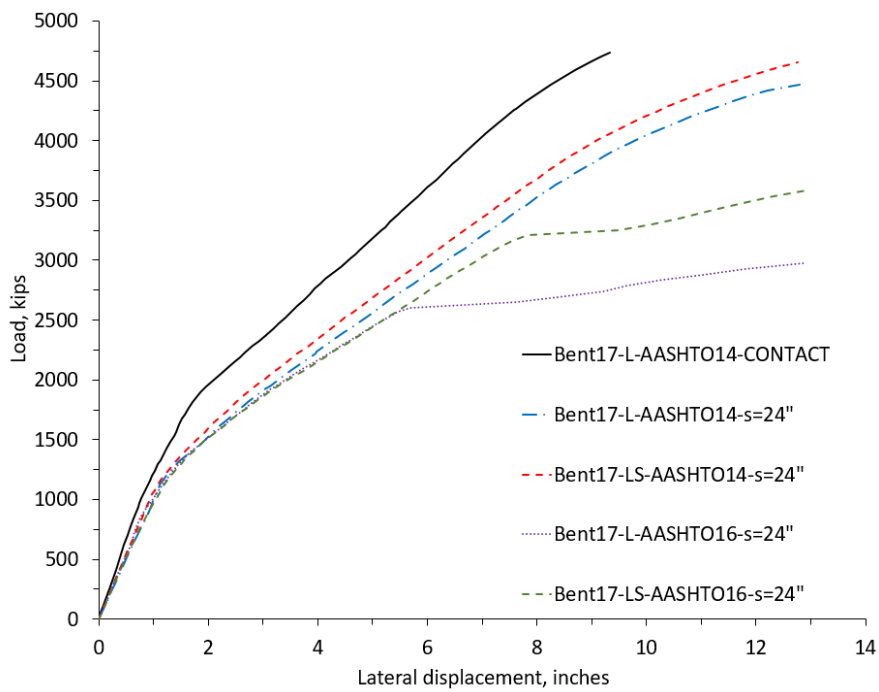
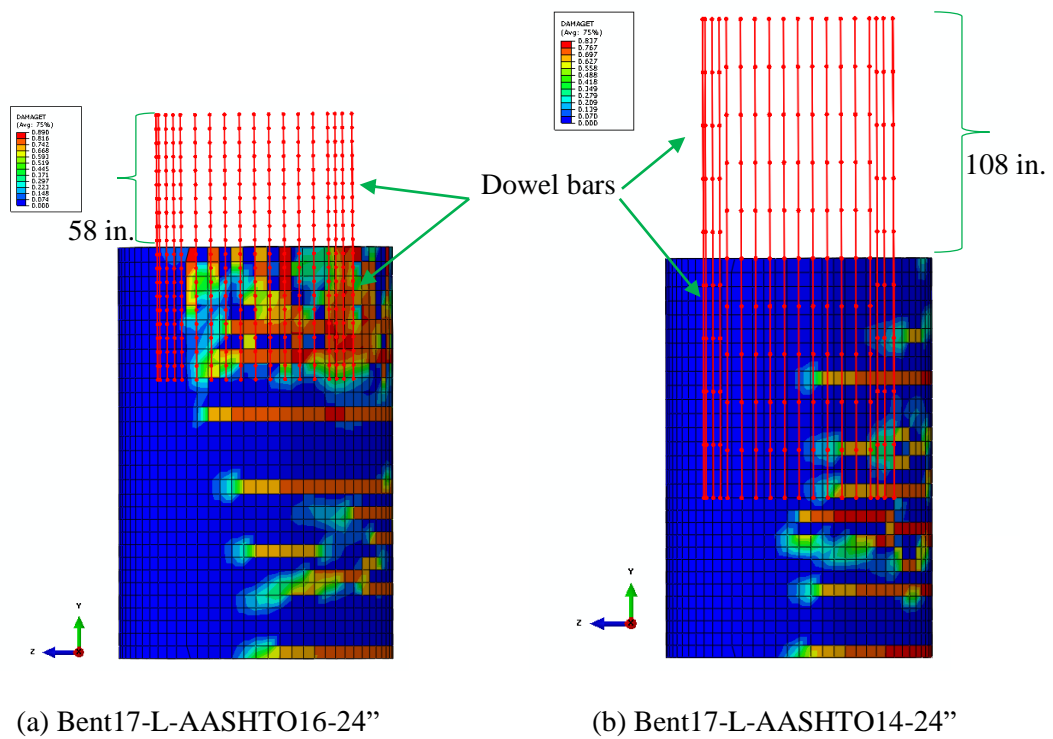


**Fig. 5-14: Load vs. displacement relationships of Bent 17 column-shaft connection FEA specimens.**

It can be observed from Fig. 5-14 that the Bent17-L-AASHTO14-CONTACT specimen exhibits the highest capacity and lateral stiffness among the specimens presented in Table 5-6. One of the primary reasons for the greater capacity and stiffness of the Bent17-L-AASHTO14-CONTACT specimen is the contact lap splices between the column longitudinal bars and the dowel bars. The capacity of the Bent17-L-AASHTO14-24” specimen (original Bent 17 column-drilled shaft connection) was 17.7% lower than the Bent17-L-AASHTO14-CONTACT specimen corresponding to a lateral displacement of 9.3 inches. Bent17-L-AASHTO14-24” and Bent17-LS-AASHTO14-24” exhibited a similar load vs. displacement relationship, but the ultimate capacity of Bent17-LS-AASHTO14-24” was 4.17% higher than that of Bent17-L-AASHTO14-24”. Except for the Bent17-L-AASHTO14-CONTACT specimen, the other models essentially exhibited quite similar lateral stiffness up to the first flexural crack. At the load level of 2,603 kips, Bent17-L-AASHTO16-24” started to exhibit significantly higher lateral displacement than that of Bent17-L-AASHTO14-24” and Bent17-LS-AASHTO14-24”. At this loading stage, Bent17-L-AASHTO16-24” exhibited extensive tensile damage in the non-contact lap splice zone of the drilled shaft due to splitting cracks [Fig. 5-15(a)]. At the load level of 3,208 kips, Bent17-LS-AASHTO16-24” started to exhibit significantly higher lateral displacement than that of Bent17-L-AASHTO14-24” and Bent17-LS-AASHTO14-24”. At this loading stage, Bent17-LS-AASHTO16-24” also exhibited extensive tensile damage in the non-contact lap splice zone of the drilled shaft due to the splitting cracks [Fig. 5-15(c)]. Bent17-L-AASHTO16-24” and Bent17-LS-AASHTO16-24” exhibited similar load vs. displacement relationships, but the ultimate capacity of Bent17-LS-AASHTO16-24” was 20.4% higher than that of Bent17-L-AASHTO16-24”. These results validate the necessity of providing a splice length equaling the standard lap splice length,  $l_s$  plus the non-contact lap splice distance,  $s$  for non-contact splices.

The tensile damage due to the splitting cracks in the non-contact lap splice zone of the drilled shaft of Bent17-L-AASHTO14-CONTACT [Fig. 5-15(d)] and Bent17-L-AASHTO14-24” was

significantly lower than that of Bent17-L-AASHTO16-24” [Fig. 5-15(b)]. This deterioration in structural performance is mainly caused by the reduced splice length when designed as per AASHTO LRFD BDS 2016 specifications [12]. Similarly, the tensile damage due to the splitting cracks in the non-contact lap splice zone of the drilled shaft of Bent17-LS-AASHTO14-24” was significantly lower than that of Bent17-LS-AASHTO16-24”. The reduction in splice length caused extensive tensile damage in the non-contact splice zone in the form of splitting cracks caused by significant bursting forces between the dowel bars and the surrounding concrete.



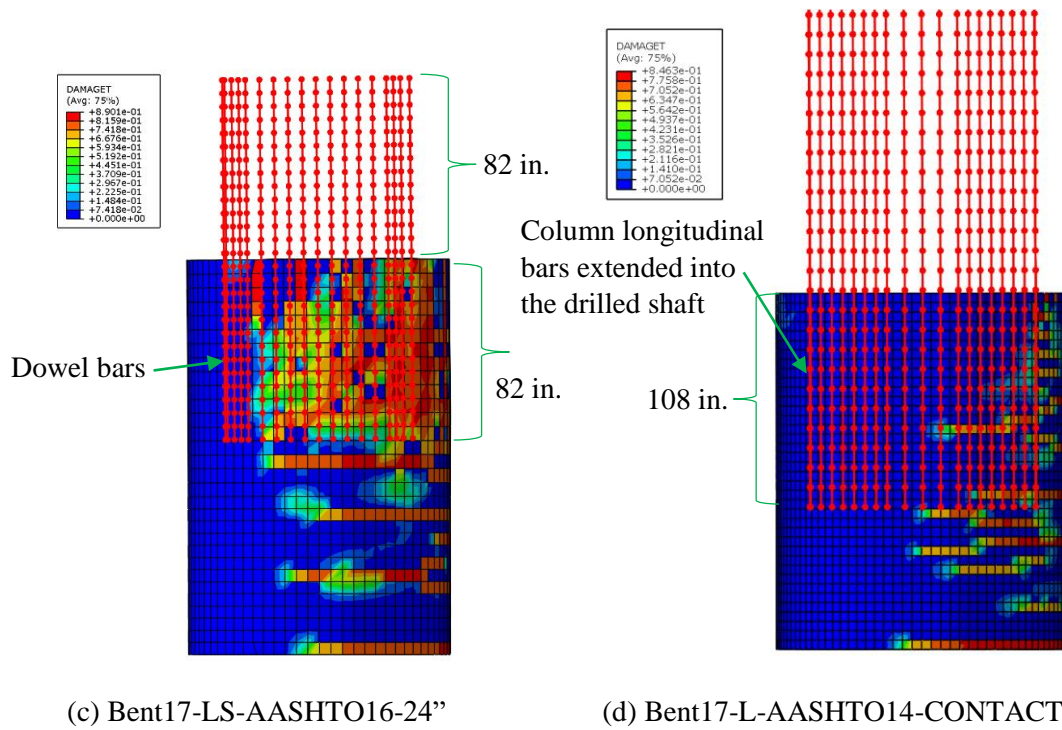


**Fig. 5-15: Tensile damage in the non-contact lap splice zone of the drilled shaft.**

The length of splice calculated using AASHTO BDS 2016 [12] guidelines was 58 inches as shown in Fig. 5-15(a) whereas the length of splice calculated using AASHTO BDS 2014 [2] guidelines was 108 inches as shown in Fig. 5-15(b). The basic development length calculated using AASHTO 2016 [12] guidelines was 104.4 inches, but the basic development length was then multiplied by the following modification factors as per AASHTO LRFD BDS [12]:

$\lambda_{rl}$  = reinforcement location factor

$\lambda_{cf}$  = coating factor

$\lambda_{lw}$  = lightweight concrete factor

$\lambda_{rc}$  = reinforcement confinement factor and

$\lambda_{er}$  = excess reinforcement factor.

It is important to note that the reduction in splice length is mainly due to the reinforcement confinement factor  $\lambda_{rc}$ . The reinforcement confinement factor  $\lambda_{rc}$  typically ranges from 0.4 to 1 depending on the cover of spliced bars and the provided confinement in the column and the drilled shaft. For the Bent 17 column, the reinforcement confinement factor  $\lambda_{rc}$  was 0.428. This resulted in a significantly reduced non-contact splice length assuming that the provided transverse reinforcement would be sufficient. Based on the simulated results, it is not recommended to reduce the calculated lap splice length as per AASHTO LRFD BDS 2016 [12] guidelines by the reinforcement confinement factor  $\lambda_{rc}$  because the lap splice length would be reduced to such an extent that the tensile damage due to splitting cracks along the spliced bars would be quite extensive and the ultimate capacity of the connection would be significantly reduced.

## 5.5 Summary

Based on the thorough finite element analysis and parametric study of the test specimens, the following conclusions can be made:

- 1) The initial stiffness of the FEA models matched very well with the test results. The post-crack behavior matched reasonably well with the test results. The ultimate load capacities predicted by the FEA models had a maximum relative error of  $\pm 5\%$  compared to that of the test specimens.
- 2) The lateral stiffness and ultimate load capacity would generally decrease with increasing the non-contact lap splice distance.
- 3) The flexural cracks and splitting cracks were predicted quite well by the FEA models. The inclined cracks were predicted reasonably well compared to the test specimens.
- 4) The specimens with non-contact lap splice consistently exhibited larger opening at the column-drilled shaft interface than the specimen with contact lap splice. A comparison of the opening among all the specimens showed that the opening would generally increase with increasing the non-contact splice distance.

- 5) Non-contact lap splices should be designed with splice lengths equaling standard lap splice length,  $l_s$  plus non-contact lap splice distance,  $s$  as recommended by WSDOT-TRAC Report WA-RD 417.1. This recommendation was verified by the results from the parametric analysis which showed that the larger the lap splice distance, the greater the contribution of longer lap splice length in increasing lateral stiffness of the specimens designed with non-contact lap splices.
- 6) It is evident that the global response, i.e., load vs. lateral displacement relationship of the specimens is not significantly influenced by the increased amount of transverse reinforcement in the non-contact lap splice zone of the column.
- 7) It can be observed from FEA simulated results that the column ties in the specimens with a higher amount of transverse reinforcement exhibited smaller stresses at the service load and ultimate load level.
- 8) It is evident that the column ties near the column-drilled shaft connection exhibited the highest tensile stresses among all the column ties within the lap splice zone of the rectangular column.

## Chapter 6 Design Recommendations and Modifications to Design Provisions

### 6.1 Overview

In this chapter, several recommendations for the design of non-contact lap splices in geometrically dissimilar column-drilled shaft connections are provided. The proposed modifications to the existing design provisions are also discussed. Moreover, an illustrative example for the design of non-contact lap splices in geometrically dissimilar column-drilled shaft connections is provided.

### 6.2 Design Recommendations

Based on the experimental and analytical investigation, the following recommendations are provided for the design of non-contact lap splices in bridge column to drilled shaft connections.

#### 6.2.1 Non-contact Lap Splice Length

The non-contact lap splice length in the non-circular column to circular drilled shaft connections should be equal to the standard lap splice length,  $l_s$  as per AASHTO [2, 11-12 ] guidelines plus the non-contact lap splice distance,  $s$  as per McLean and Smith [4] as given by

$$l_{ns} = l_s + s. \quad (3)$$

However, it is not recommended to shorten the required lap splice length as per AASHTO [12] guidelines by the reinforcement confinement factor,  $\lambda_{rc}$  because the FEA results have shown that the lap splice length could be shortened to such an extent due to the reinforcement confinement factor,  $\lambda_{rc}$  that the tensile damage due to the splitting cracks along the spliced bars would be quite extensive despite providing the required amount of transverse reinforcement in the column and the drilled shaft.

#### 6.2.2 Non-contact Lap Splice Distance

The distance between the non-contact lap splices in non-circular columns connected to circular drilled shafts should not exceed 6 inches.

### 6.2.3 Amount of Transverse Reinforcement in Non-circular Columns

The transverse reinforcement in non-circular columns connected to circular drilled shafts should be designed with the behavioral model proposed by Maksoud [17] as given by

$$S_{tr,col} = \frac{n_{tr}A_{tr}f_{ytr}l_s}{A_{Tl}f_{ul}}. \quad (6)$$

## 6.3 Validation of Modifications to Design Provisions

### 6.3.1 Non-contact Lap Splice Length

All the test specimens except Specimen 1 were constructed with non-contact lap splices with splice lengths equaling the standard lap splice length,  $l_s$  plus the non-contact lap splice distance,  $s$ . Provided that the transverse reinforcement around the spliced bars was designed with the proposed transverse reinforcement in the column and the drilled shaft, the spliced bars exhibited extensive yielding and strain hardening for all the test specimens. This proved the adequacy of the provided lap splice length in preventing brittle anchorage failure at the non-contact lap splice zone of the column-drilled shaft connections.

Also, the parametric study on the effect of lap splice length on the structural behavior of the test specimens showed that by providing a lap splice length consisting of the standard lap splice length,  $l_s$  plus the non-contact lap splice distance,  $s$ , the lateral stiffness of the specimens could be increased compared to the specimens with a lap splice length of the standard lap splice length,  $l_s$  only. It was also observed that the contribution of the increased lap splice length in increasing lateral stiffness of the specimens is more evident with the increase of lap splice distance. This indicates that the specimens with a lap splice distance  $\geq 4$  inches should be designed with lap splices with a length equaling the standard lap splice length,  $l_s$  plus the non-contact lap splice distance,  $s$  because the larger the lap splice distance, the greater the contribution of longer lap splice length in increasing lateral stiffness of the specimens designed with non-contact lap splices.

### **6.3.2 Non-contact Lap Splice Distance**

For a non-contact lap splice distance of up to 6 inches (Specimens 2, 3, 5 and 6), the transverse reinforcement located near the column-shaft interface in the columns exhibited yielding after the yielding of the dowel bars. On the other hand, for a non-contact lap splice distance greater than 6 inches (Specimens 4 and 7), the transverse reinforcement located near the column-shaft interface in the non-circular columns exhibited yielding before the yielding of the dowel bars. Yielding of transverse reinforcement is undesirable before yielding of flexural reinforcement, e.g., dowel bars, column longitudinal bars, etc. in flexural members because yielding of the transverse reinforcement before yielding of the flexural reinforcement could cause extensive inclined cracks and splitting cracks and eventually, sudden brittle anchorage failure of column-drilled shaft connections. Therefore, the distance between the non-contact lap splices in non-circular columns to circular drilled shafts should not exceed 6 inches.

### **6.3.3 Amount of Transverse Reinforcement in Non-Circular Columns**

Equation 6 was used to design the transverse reinforcement in Specimens 5 to 11 which is a modified version of the two-dimensional behavior model (Equation 4) proposed by McLean and Smith [4] for designing the transverse reinforcement in the non-contact lap splice zone of rectangular sections. Equation 6, proposed by Maksoud [17], is recommended to determine the amount of transverse reinforcement rather than the two-dimensional behavior model (Equation 4) proposed by McLean and Smith [4] because the test results have shown that the strains in the column ties of Specimens 5 to 7, designed with Equation 6, were considerably smaller than that of Specimens 2 to 4, designed with Equation 4. The test results have also shown that the larger the non-contact lap splice distance, the higher the stresses in the transverse reinforcement in the column as evident from larger strains in the column ties. This is why the increased amount of transverse reinforcement designed as per Equation 6 would be warranted.

## 6.4 Design Examples

Based on the design recommendations, the following calculations are performed as an example for the design of non-contact lap splices in a full-scale column-drilled shaft connection. For this design example, the Bent 17 column-drilled shaft connection was used.

### 6.4.1 Longitudinal Reinforcement in the Column and the Drilled Shaft

#### 6.4.1.1 Longitudinal reinforcement in the column

Assuming, Depth of the column,  $h_{col} = 120 \text{ in.}$

Width of the column,  $b_{col} = 84 \text{ in.}$

*AASHTO 5.7.4.2-Limits for reinforcement [2]*

“The minimum area of prestressed and nonprestressed longitudinal reinforcement for noncomposite compression members shall be such that:

$$\frac{A_s f_y}{A_g f'_c} + \frac{A_{ps} f_{pu}}{A_g f'_c} \geq 0.135,$$

where,

$A_s =$  area of nonprestressed tension steel ( $\text{in.}^2$ );

$A_g =$  gross area of section ( $\text{in.}^2$ );

$A_{ps} =$  area of prestressing steel ( $\text{in.}^2$ );

$f_{pu} =$  specified tensile strength of prestressing steel (ksi);

$f_y =$  specified yield strength of reinforcing bars (ksi);

$f'_c =$  specified compressive strength of concrete (ksi);

$f_{pe} =$  effective prestress (ksi).”

AASHTO C5.7.4.2 [2] states that “According to current ACI codes, the area of longitudinal reinforcement for nonprestressed noncomposite compression components should be not less than  $0.01A_g$ .”

$$A_g = \text{gross area of section (in.}^2\text{)} = h_{col} * b_{col} = 10080 \text{ in.}^2$$

$$A_{s,min}(\text{AASHTO C5.7.4.2}) = 0.01 * 10080 = 100.8 \text{ in.}^2$$

$$\text{Using \#11 bars (area of bar} = 1.56 \text{ in.}^2\text{), } A_{s,required} = \frac{100.8}{1.56} = 64.6 \approx 66 \text{ bars (provide)}$$

$$\frac{A_s f_y}{A_g f'_c} + \frac{A_{ps} f_{pu}}{A_g f'_c} = \frac{66 * 1.56 * 60}{10080 * 3.6} = 0.17 > 0.135 \text{ (OK)}$$

**Provide 66-#11 column longitudinal bars for the column reinforcement.**

#### 6.4.1.2 Longitudinal reinforcement in the drilled shaft

In order to accommodate the dowel bars within the non-contact lap splice distance limit of 6 in., the diameter of the drilled shaft is taken as  $d_{shaft} = 134 \text{ in.}$

$$A_g = \text{gross area of section (in.}^2\text{)} = \pi * \left(\frac{d_{shaft}}{2}\right)^2 = \pi * \left(\frac{134}{2}\right)^2 = 14102.6 \text{ in.}^2$$

$$A_{s,min}(\text{AASHTO C5.7.4.2}) = 0.01 * 14102.6 = 141.0 \text{ in.}^2$$

$$\text{Using \#11 bars (area} = 1.56 \text{ in.}^2\text{), } A_{s,required} = \frac{141.0}{1.56} = 90 \text{ bars (provide)}$$

$$\frac{A_s f_y}{A_g f'_c} + \frac{A_{ps} f_{pu}}{A_g f'_c} = \frac{90 * 1.56 * 60}{14102.6 * 3.6} = 0.166 > 0.135 \text{ (OK)}$$

**Provide 90-#11 drilled shaft longitudinal bars for the drilled shaft reinforcement.**

### 6.4.1.3 Non-linear section analysis of the column

A non-linear section analysis was performed for checking the adequacy of the provided reinforcement in the column. Appendix D shows the calculation of the loads on the Bent 17 column-drilled shaft connection on SH 99. A summary of the calculated loads is provided below:

**Dead Load: Total dead load on Girder 1 (see Fig. D.1 in Appendix D) = 158.51 k**

**Total dead load on Girder 2 = 151.54 k**

**Total dead load on Girder 3 = 145.68 k**

**Total dead load on Girder 4 = 126.98 k**

**Total dead load on Girder 5 = 154.98 k**

**Total dead load on Girder 6 = 157.43 k**

**Total dead load on Girder 7 = 149.21 k**

**Total dead load on Girder 8 = 121.09 k**

**Live load: Total live load,  $LL_{Rxn} = \text{Lane} + \text{Truck} * (1 + \text{IM}) = 90.24 + 68.02 * 1.33 = 180.71 \text{ k/lane}$**

**(Total number of lanes = 2)**

**Moment on the column due to dead load = 7121.5 kip – ft**

**Moment on the column due to bent cap self-weight = 1005.5 kip – ft**

**Maximum live load moment on the column = 3683.6 kip – ft**

Using the calculated axial load and bending moment on the column of the Bent 17 column-shaft connection, a non-linear section analysis was performed to obtain a Load-Moment Strength Interaction Diagram (P-M Diagram) as shown in Fig. 6-1. From the P-M diagram, it is evident that

the provided reinforcement in the column is sufficient for the combined axial load of 1,677 kips and bending moment of 11,811 kip-ft.

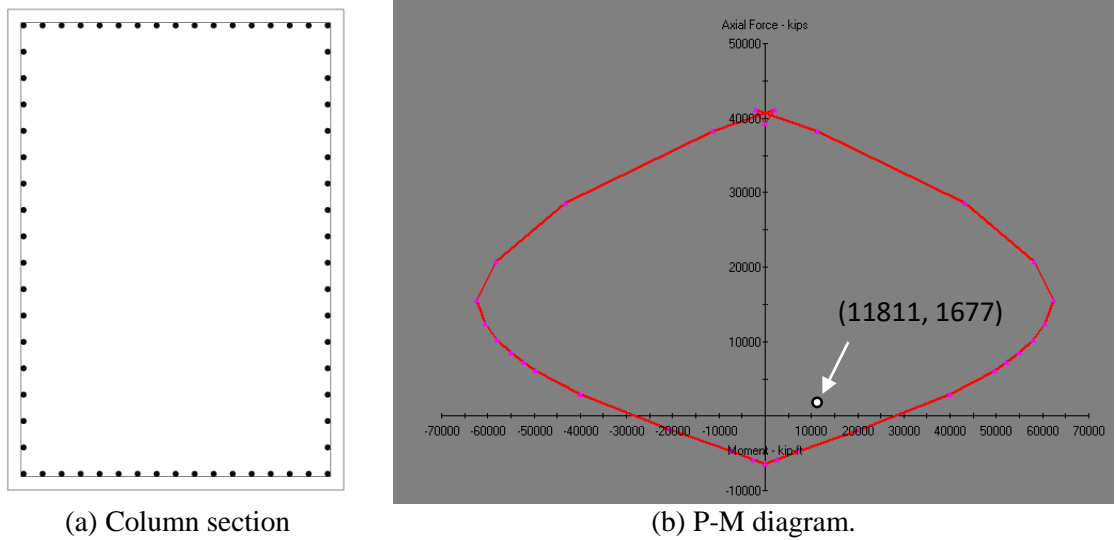


**Fig. 6-1: P-M diagram of the column of Bent 17 column-drilled shaft connection.**

Similarly, a P-M diagram could be developed for the drilled shaft for checking the adequacy of the provided reinforcement in the drilled shaft.

#### 6.4.2 Non-Contact Lap Splice Length

Article 5.11.5.3.1 of AASHTO BDS Interim Revisions 2015 [11] states that “the minimum length of lap for tension lap splices shall be as required for Class A or B lap splice, but not less than 12.0 in, where:

Class A lap splice.....  $1.0l_d$

Class B lap splice.....  $1.3l_d$ .

The tension development length,  $l_d$ , for the specified yield strength shall be taken in accordance with Article 5.11.2. Except as specified herein, lap splices of deformed bars and deformed wire in tension shall be Class B lap splices. Class A lap splices may be used where:

- (a) the area provided is at least twice that required by analysis over the entire length of the lap splice;
- (b) one-half or less of the total reinforcement is spliced within the required lap splice length.”

Article 5.11.2.1.1 of AASHTO BDS Interim Revisions 2016 [12] states that “The modified tension development length,  $l_d$ , in in. shall be taken as

$$l_d = l_{db} * \frac{\lambda_{rl} * \lambda_{cf} * \lambda_{rc} * \lambda_{er}}{\lambda} \text{ in which: } l_{db} = \frac{2.4d_b f_y}{\sqrt{f'_c}},$$

where,

$l_{db}$  = basic development length (in.)

$\lambda_{rl}$  = reinforcement location factor

$\lambda_{cf}$  = coating factor

$\lambda$  = concrete density modification factor as specified in Article 5.4.2.8

$\lambda_{rc}$  = reinforcement confinement factor

$\lambda_{er}$  = excess reinforcement factor.

$f_y$  = specified yield strength of reinforcing bars or wire (ksi)

$f'_c$  = specified compressive strength of concrete for use in design (ksi)

$d_b$  = diameter of bar or wire (in.)

Modification factors shall be applied to the basic development length to account for the various effects specified herein. They shall be taken equal to 1.0 unless they are specified to increase  $l_d$  in Article 5.11.2.1.2, or to decrease  $l_d$  in Article 5.11.2.1.3.

5.11.2.1.2 – Modification factors which increase  $l_d$

The basic development length,  $l_{db}$ , shall be multiplied by the following factor or factors, as applicable:

- For horizontal reinforcement, placed such that more than 12.0 in of fresh concrete is cast below the reinforcement,  $\lambda_{rl} = \dots \dots \dots 1.3$
- For horizontal reinforcement, placed such that no more than 12.0 in of fresh concrete is cast below the reinforcement and  $f'_c$  is greater than 10.0 ksi,  $\lambda_{rl} = \dots \dots \dots 1.3$
- For lightweight concrete, use  $\lambda$  as specified in Article 5.4.2.8
- For epoxy-coated bars with cover less than  $3d_b$  or with clear spacing between bars less than  $6d_b$ ,  $\lambda_{cf} = \dots \dots \dots 1.5$
- For epoxy-coated bars not covered above,  $\lambda_{cf} = \dots \dots \dots 1.2$

The product of  $\lambda_{rl} \times \lambda_{cf}$  need not be taken as greater than 1.7.

5.11.2.1.3 – Modification factors which decrease  $l_d$

The basic development length,  $l_{db}$ , specified in Article 5.11.2.1.1, modified by the factors specified in Article 5.11.2.1.2, as appropriate may be multiplied by the following factor or factors:

- For reinforcement being developed in the length under consideration  $\lambda_{rc}$  shall satisfy the following:

$$0.4 \leq \lambda_{rc} = \frac{d_b}{c_b + k_{tr}} \leq 1.0$$

in which:

$$k_{tr} = \frac{40A_{tr}}{sn},$$

where,

$c_b$  = the smaller of the distance from center of bar or wire being developed to the nearest concrete surface and one-half the center-to-center spacing of the bar or wires being developed (*in.*);

$k_{tr}$  = transverse reinforcement index;

$A_{tr}$  = total cross-sectional area of all transverse reinforcement which is within the spacing  $s$  and which crosses the potential plane of splitting through the reinforcement being developed (*in.*<sup>2</sup>);

$s$  = maximum center-to-center spacing of transverse reinforcement with  $l_d$  (*in.*);

$n$  = number of bars or wires developed along plane of splitting.

- Where anchorage or development for the full yield strength of reinforcement is not required, or where reinforcement in flexural members is in excess of that required

$$\text{by analysis, } \lambda_{er} = \frac{A_s \text{ required}}{A_s \text{ provided}}$$

The Bent 17 column-drilled shaft connection is designed using the following material properties:

The yield strength of steel,  $f_y = 60$  ksi and the compressive strength of concrete,  $f'_c = 3.6$  ksi.

Now, using #11 bars for the dowel bars,  $d_b = \frac{11}{8} = 1.375$  in

Basic tension development length,  $l_{db} = \frac{2.4d_b f_y}{\sqrt{f'_c}}$

$$= \frac{2.4 * \left(\frac{11}{8}\right) * 60}{\sqrt{3.6}} = 104.4 \text{ in.}$$

$\lambda_{rl} = \text{reinforcement location factor} = 1.0$

$\lambda_{cf} = \text{coating factor} = 1.0$

$\lambda = \text{concrete density modification factor as specified in Article 5.4.2.8 [2]} = 1.0$

$\lambda_{rc}$  = reinforcement location factor = 1.0 (It is not recommended to shorten the calculated lap splice length as per AASHTO LRFD BDS [12] by the reinforcement confinement factor  $\lambda_{rc}$ . That is why  $\lambda_{rc}$  is taken equal to 1.0. Nevertheless, the detailed calculation for determining the reinforcement confinement factor  $\lambda_{rc}$  is provided in Appendix D.)

$$\lambda_{er} = \text{excess reinforcement factor} = \frac{A_s \text{required}}{A_s \text{provided}} = 1.0$$

$$l_d = l_{db} * \frac{\lambda_{rl} * \lambda_{cf} * \lambda_{rc} * \lambda_{er}}{\lambda} = 104.4 \frac{1.0 * 1.0 * 1.0 * 1.0}{1.0} = 104.4 \text{ in.}$$

Standard required lap splice length,

$$l_s = 1.3 * l_d \text{ for Class B Splice (AASHTO 5.11.5.3.1 Lap Splices [12]) in Tension}$$

$$\therefore l_s = 1.3 * 104.4 = 136 \text{ in.}$$

McLean and Smith [4] proposed that the total lap splice length in a non-contact lap splice should be equal to the standard required splice length plus the offset distance as given by

$$l_{ns} = l_s + s, \tag{3}$$

where,  $l_s$  = standard required splice length;

$s$  = offset distance;

$l_{ns}$  = total noncontact lap splice length.

The non-contact lap splice distance between the spliced bars in the column is taken as  $s = 6 \text{ in.}$

Using the 134 in. diameter drilled shaft and 5 in. clear cover for the drilled shaft longitudinal bars, the non-contact lap splice distance between the spliced bars in the drilled shaft is  $s = 11 \text{ in.}$

$$\therefore \text{Non-contact lap splice length in the column, } l_{ns} = 136 + 6 = 142 \text{ in.}$$

$$\therefore \text{Non-contact lap splice length in the drilled shaft, } l_{ns} = 136 + 11 = 147 \text{ in.}$$

**Provide 70-#11 dowel bars with a splice length of 142 in. for a maximum non-contact lap splice distance of 6 in. in the rectangular column. The dowel bars should be extended inside the drilled shaft with a splice length of 147 in.**

### **6.4.3 Amount of Transverse Reinforcement in the Column**

#### **6.4.3.1 Amount of transverse reinforcement in the non-contact lap splice zone in the column**

Maksoud [17] proposed a modification (Fig. 2-9) of the McLean and Smith's model [4] to determine the required amount of transverse reinforcement for a rectangular section with non-contact lap splice as given by

$$S_{tr} = \frac{n_{tr}A_{tr}f_{ytr}l_s}{A_{Tl}f_{ul}}, \quad (6)$$

where,

$S_{tr}$  = spacing of column transverse reinforcement (in.);

$n_{tr}$  = number of legs of column transverse reinforcement;

$A_{tr}$  = area of column transverse reinforcement (in.<sup>2</sup>);

$f_{ytr}$  = specified minimum yield strength of column transverse reinforcement (ksi);

$l_s$  = standard required splice length (in.);

$A_l$  = area of longitudinal reinforcement in tension (in.<sup>2</sup>);

$A_{Tl}$  = Total area of longitudinal reinforcement in tension (in.<sup>2</sup>);

$f_{ul}$  = ultimate strength of longitudinal reinforcement (ksi).

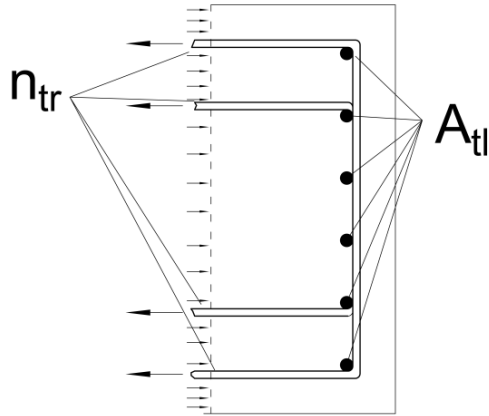


**Fig. 2-9. (Repeated) Behavioral model for non-contact lap splices in rectangular sections.**

Using 4 legs of #6 bars as the transverse reinforcement in the non-contact lap splice zone in the column,

$$\therefore s_{tr,col} = \frac{n_{tr} A_{tr} f_{ytr} l_s}{A_{tl} f_{ul}} = \frac{4 * 0.44 * 60 * 136}{22 * 1.56 * 90} = 4.65 \text{ in.} \approx 4.5 \text{ in. (provided)}$$

AASHTO 5.10.6.3-Ties [2] states that “the spacing of ties along the longitudinal axis of the compression member shall not exceed the least dimension of the compression member or 12.0 in.”

Least dimension of column = 84 in or 12 in.

So, maximum allowed spacing of ties = 12 in.

AASHTO 5.8.2.5-Minimum Transverse Reinforcement [2]

$$A_v \geq 0.0316 \sqrt{f'_c} \frac{b_v s_{tr,max}}{f_y}$$

$$2 * 0.44 = 0.0316 \sqrt{3.6} \frac{84 * s_{tr,max}}{60} \text{ (Considering 2 legs of #6 bars as the transverse reinforcement)}$$

$$\therefore s_{tr,max} = 10.5 \text{ in. (} < 12.0 \text{ in.)}$$

$$\therefore s_{tr,max} = 10.5 \text{ in.}$$

$$\therefore s_{tr,col} = 4.5 \text{ in.} < s_{tr,max} \text{ (OK)}$$

**Provide 4 legs of #6 bars as the transverse reinforcement in the column lap splice zone at a center-to-center (c/c) spacing of 4.5 in.**

**6.4.3.2 Amount of transverse reinforcement outside of the non-contact lap splice zone in the column**

Maximum allowed spacing of ties,  $s_{tr,max} = 10.5 \text{ in.}$

**Provide 2 legs of #6 bars as the transverse reinforcement outside of the column non-contact splice zone at a center-to-center spacing of 10.5 in.**

**6.4.4 Amount of Transverse Reinforcement in the Drilled Shaft**

**6.4.4.1 Amount of transverse reinforcement in the non-contact lap splice zone in the drilled shaft**

Article 5.11.5.2.1 of AASHTO BDS Interim revisions 2015 [11] states that “for columns with longitudinal reinforcing that anchors into oversized shafts, where bars are spliced by non-contact lap splices, and longitudinal column and shaft reinforcement are spaced farther apart transversely than one-fifth the required lap splice length or six inches, the spacing of the shaft transverse reinforcement in the splice zone shall meet the requirements of the following equation:

$$s_{max} = \frac{2\pi A_{sp} f_{ytr} l_s}{k A_{lf} u_l}, \quad (9)$$

where,

$s_{max}$  = spacing of transverse shaft reinforcement (in.);

$A_{sp}$  = area of shaft spiral or transverse reinforcement (in.<sup>2</sup>);

$f_{ytr}$  = specified minimum yield strength of shaft transverse reinforcement (ksi);

$l_s$  = required tension lap splice length of the column longitudinal reinforcement (in.)

$A_l$  = area of longitudinal column reinforcement ( $\text{in.}^2$ );

$f_{ul}$  = specified minimum tensile strength of column longitudinal reinforcement (ksi)

(90 ksi for ASTM A615);

$k$  = factor representing the ratio of column tensile reinforcement to total column reinforcement at the nominal resistance."

**Maximum spacing of the shaft transverse reinforcement in the splice zone:**

Using #6 bars as spirals,

$$S_{tr,shaft} = S_{max} = \frac{2\pi A_{sp} f_{ytr} l_s}{k A_l f_{ul}} = \frac{2\pi * 0.44 * 60 * 136}{0.5 * (70 * 1.56) * 90} = 4.59 \text{ in. (Provide 4.5 in.)}$$

**Maximum allowed spacing for spiral reinforcement:**

AASHTO 5.10.6.2-Spirals [2]

"The center-to-center spiral spacing shall not exceed 6.0 times the diameter of the longitudinal bars or 6.0 in."

$$\therefore S_{max} = 6 * \left(\frac{11}{8}\right) = 8.25 \text{ in. } (> 6.0 \text{ in.})$$

$$\therefore S_{max} = 6 \text{ in.}$$

$$\therefore S_{tr,shaft} = 4.5 \text{ in. } < S_{max} \text{ (OK)}$$

**Provide #6 bar spirals as the transverse reinforcement in the drilled shaft non-contact splice zone at a center to center spacing of 4.5 in.**

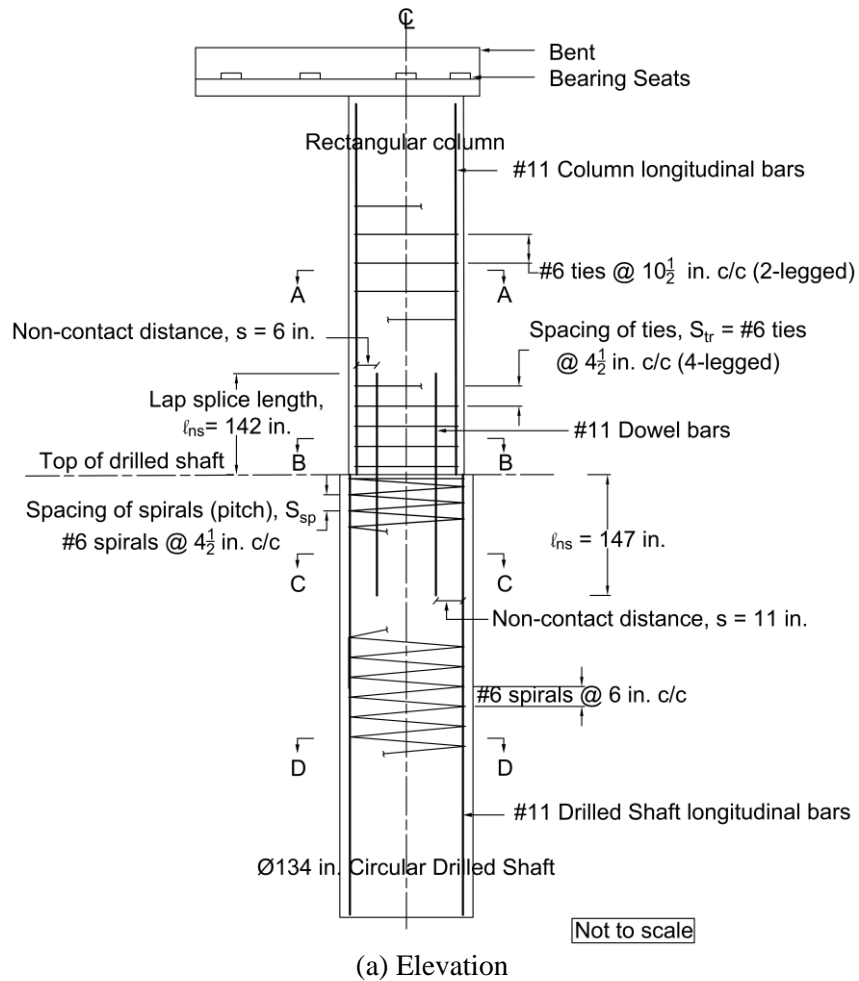
**6.4.4.2 Amount of transverse reinforcement outside of the non-contact lap splice zone in the drilled shaft**

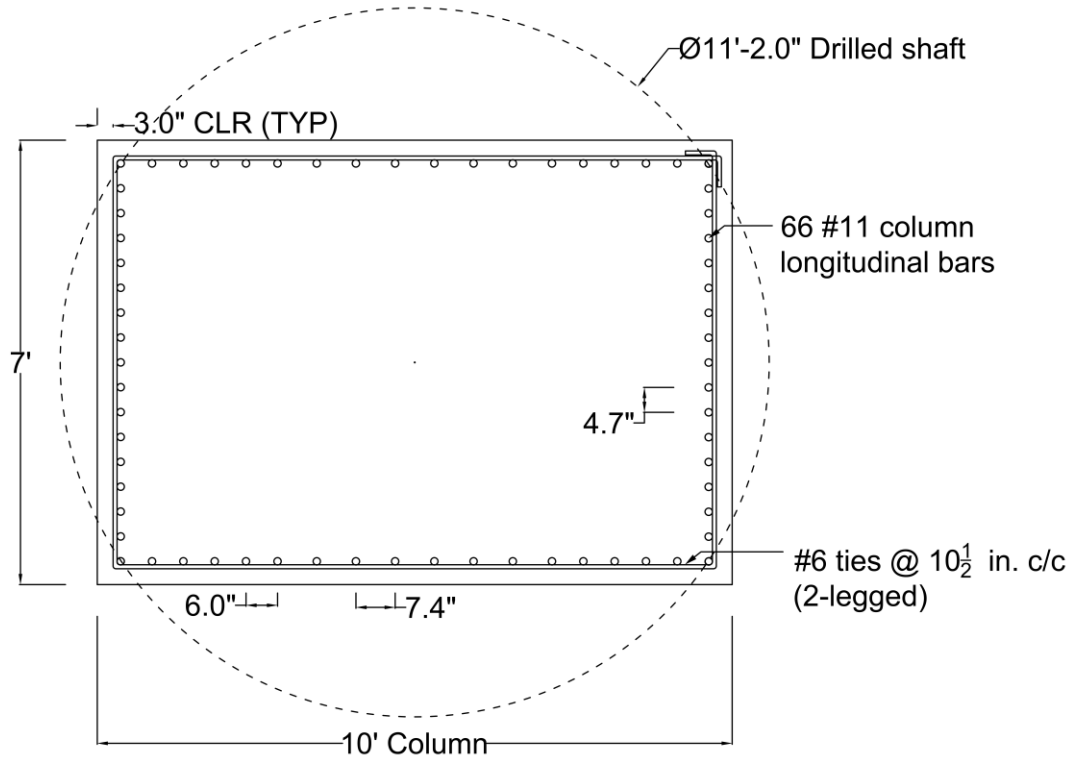
Maximum spacing of spiral reinforcement in the shaft,  $S_{max} = 6.0 \text{ in.}$

**Provide #6 bar spirals as the transverse reinforcement in the drilled shaft at a spacing of 6 in. outside of the non-contact splice zone.**

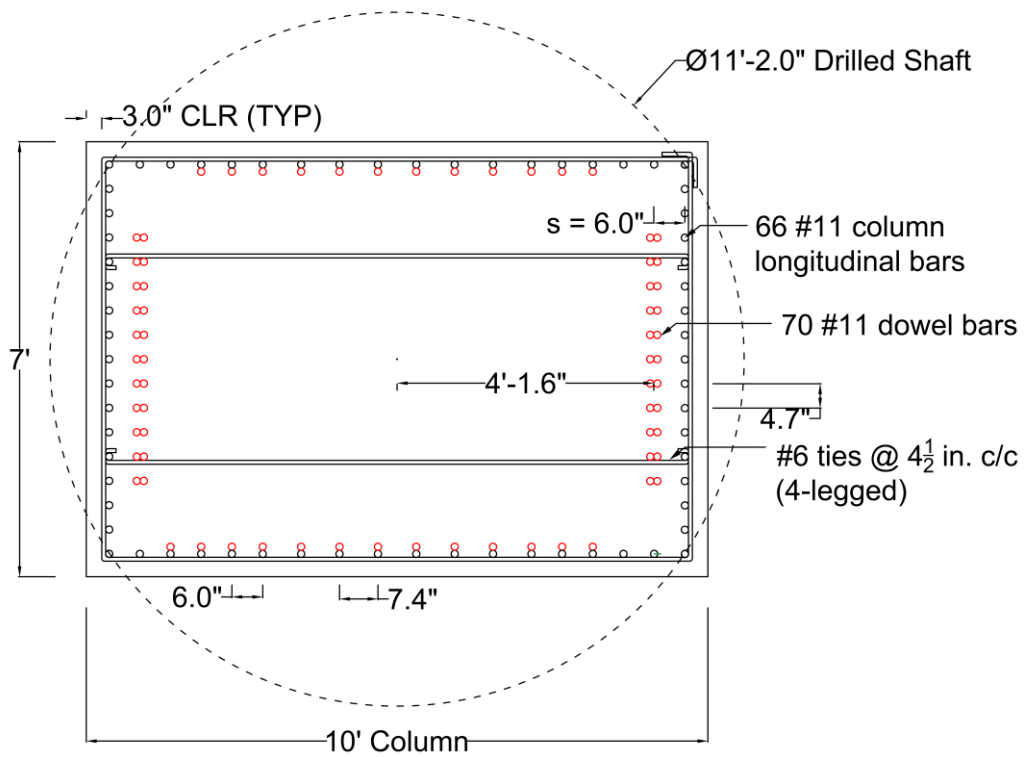
### 6.4.5 Detailed Drawings

The detailed drawings of the Bent 17 column-drilled shaft connection designed as per the design recommendations of this study are shown in Fig. 6-2.

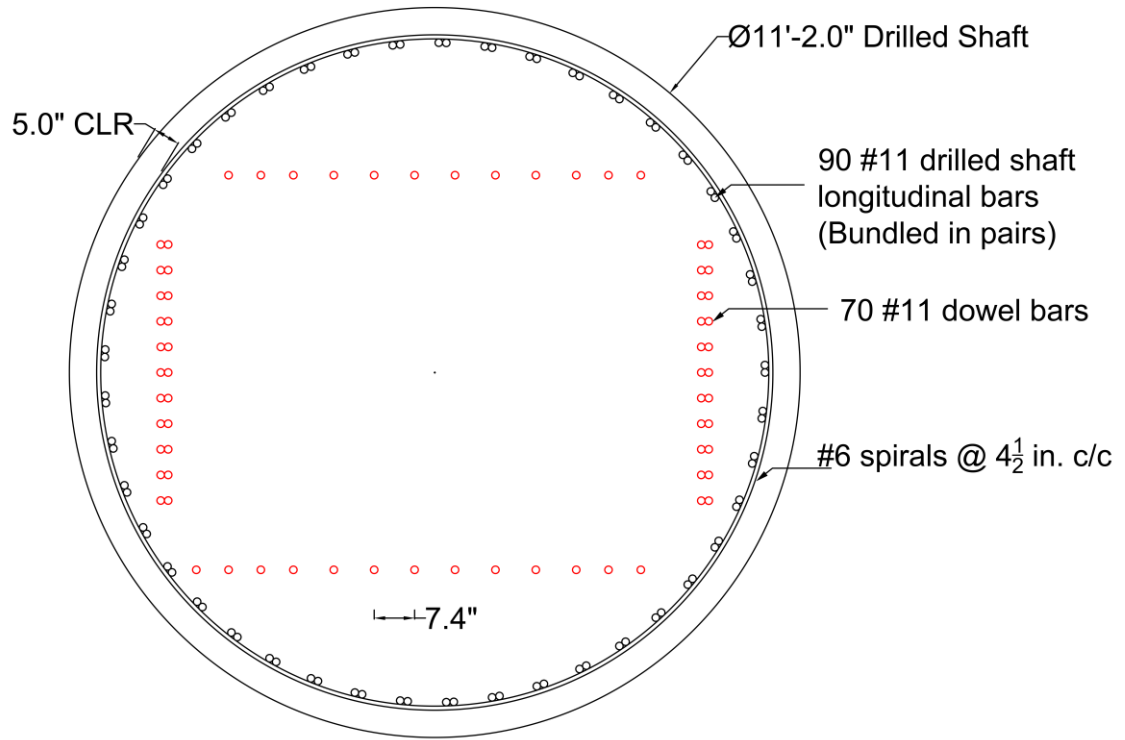




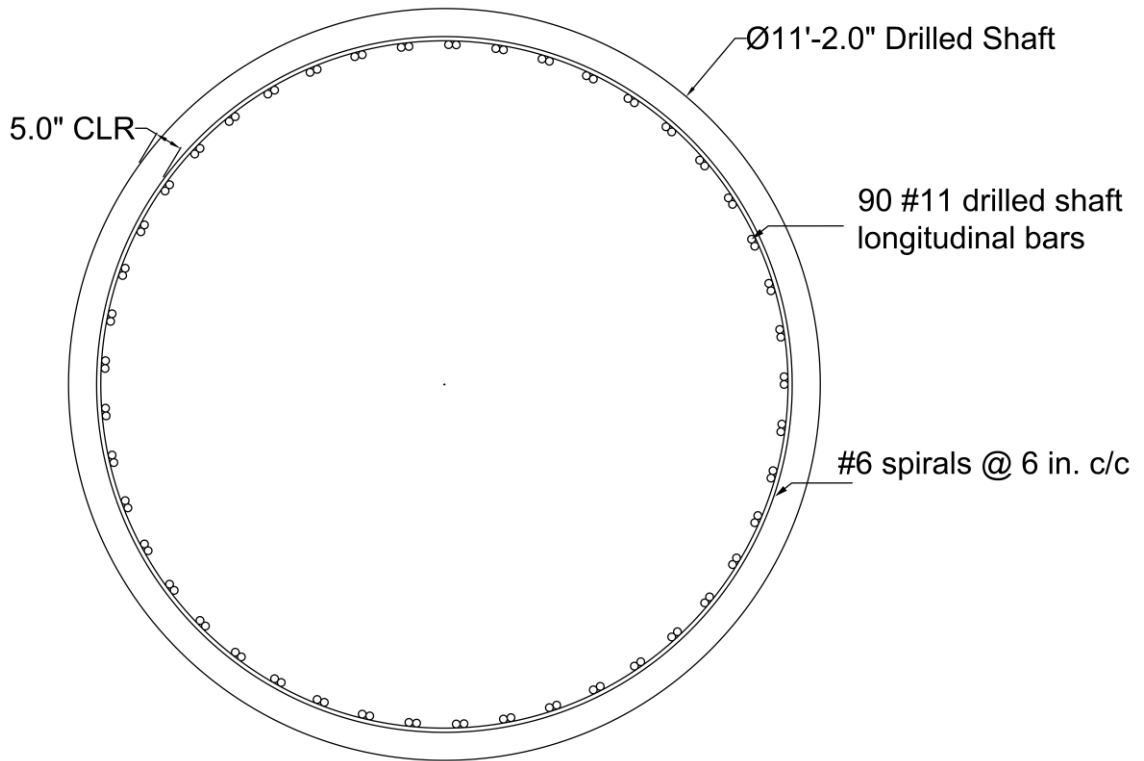
(b) Section A-A



(c) Section B-B



(d) Section C-C



(e) Section D-D

**Fig. 6-2: Details of reinforcement in the Bent 17 column-drilled shaft connection.**

## **6.5 Summary**

An analytical and experimental investigation on the behavior of non-contact lap splices at geometrically dissimilar bridge column and drilled shaft interfaces was conducted in this study with regards to non-contact lap splice distance, non-contact lap splice length and amount of transverse reinforcement in the non-contact lap splice zone. The relevant design provisions of AASHTO LRFD Codes [2, 11-12] have been reevaluated through the experimental and analytical approach. Based on the results of the analytical and experimental investigation, a set of design recommendations is provided for the design of non-contact lap splices in the non-circular column to circular drilled shaft connections. An overview of the justifications for the proposed modifications to the existing design provisions is discussed. Moreover, an illustrative example for the design of non-contact lap splices in the Bent 17 column-drilled shaft connection is provided. The detailed drawings of the Bent 17 column-drilled shaft connection designed as per the design recommendations of this study are also presented.

## Chapter 7 Conclusions and Future Work

### 7.1 Summary

Contact lap splices are widely used for the construction of reinforced concrete structures. However, it is often required to provide a reinforcing steel splicing arrangement with non-contact lap splices for the connection of non-circular bridge columns interfacing directly with circular drilled shafts. However, there is a concern on the safety and cost-effectiveness of such non-contact lap splices in the bridge column to drilled shaft connections because the guidelines in the current AASHTO code and studies on this type of connection are limited. This study presents an experimental and analytical investigation of non-contact lap splices in non-circular bridge column to circular drilled shaft connections.

During the experimental investigation, a total of eleven large-scale column-drilled shaft specimens were designed, constructed, and tested to investigate the effects of the critical parameters affecting the performance of non-contact lap splices. The investigated parameters were the non-contact distance between the spliced bars, the lap splice length of the spliced bars and the amount of transverse reinforcement in the non-contact lap splice zone. The experimental investigation was divided into two phases. The Phase I experimental program focused on the effect of the lap splice distance between the spliced bars, non-contact lap splice length and amount of transverse reinforcement in the lap splice zone. In the Phase II experimental program, in addition to the effect of the lap splice distance between the spliced bars and non-contact lap splice length, the interim revisions relevant to the design of non-contact lap splices in the AASHTO LRFD code [11-12] were also incorporated while designing the test specimens in Phase II to study the effect of the changes made to the current provisions. The specimens were subjected to flexure from both monotonic and cyclic loading. The load was applied on a steel cantilever beam, connected to the top of the column, at an eccentricity of 59.25 inches from the centerline of the column. The steel cantilever beam was designed to produce flexural stresses in the column and the drilled shaft. The

loading was implemented in three stages. First, the quasi-static loading was applied using a load-control procedure followed by the cyclic loading applied at a rate of 0.5 Hz. Finally, the loading was switched to the displacement-control procedure and continued until concrete crushing was observed at the toe of the column and on the drilled shaft.

Further, a three-dimensional finite element analysis (FEA) was performed on the test specimens. The finite element model of the test specimens was developed using Abaqus. An 8-node linear brick, reduced integration, hourglass control element (C3D8R) was used to mesh the concrete material. A 2-node linear three-dimensional (3-D) truss element (T3D2) was used to implement the steel reinforcement. To simulate the bond-slip behavior in tension between the column longitudinal bars/dowel bars and the surrounding concrete, the column longitudinal bars and the dowel bars on the north side of the column were connected to the concrete using spring elements. For the definition of the bond stress vs. slip behavior of the spring elements, an average “local bond” stress vs. “local slip” relationship was considered as per European CEB-FIP Model Code 90 [35]. The Concrete Damaged Plasticity (CDP) model was used as the constitutive model of concrete in the FEM models. The uniaxial stress-strain curves proposed by Hsu and Mo [30] were adopted for the definition of uniaxial behavior in compression and tension in the CDP model. A bilinear steel model with a linear strain hardening proposed by Hsu and Mo [30] was utilized for the constitutive model of the steel reinforcement. The definition of damage variables in tension and compression were also included in the CDP model. The finite element simulated results were compared with the test outcomes in order to validate the FEA models. Using the validated FEA models, an in-depth parametric study of the critical parameters influencing the behavior of non-contact lap splices was also performed.

Finally, a set of design recommendations for the design of non-contact lap splices in geometrically dissimilar column-drilled shaft connections is provided. An overview of the justifications for the proposed modifications to the existing design provisions is discussed.

Moreover, an illustrative example for the design of non-contact lap splices in geometrically dissimilar column-drilled shaft connections is provided.

## **7.2 Conclusions**

### **7.2.1 Conclusions from the Experimental Investigation**

Based on the experimental investigation of the column-drilled shaft connections with contact and non-contact lap splices, the following outcomes can be reported:

- 1) The specimens with larger non-contact lap splice distance generally exhibited lower lateral stiffness and lower capacity.
- 2) Further, the rate of increase of lateral displacement due to the cyclic loading increased with increasing the non-contact lap splice distance.
- 3) The lateral displacement increased at a significantly higher rate between the first and 125,000th cycles of the cyclic loading than between the 125,000th and 2,000,000th cycles of the cyclic loading. In other words, after 125,000 cycles of the cyclic loading, the lateral displacement did not increase significantly despite applying an additional 1,850,000 cycles of the cyclic loading. These results indicated an increase in the incremental displacements in the early stages of the cyclic loading and subsequent tendency to stabilize without much increase in the accumulated displacements.
- 4) Non-contact lap splices constructed with splice lengths equaling standard lap splice length as per the AASHTO LRFD code [2, 11-12] plus the non-contact lap splice distance were effective in developing yielding and strain hardening of the spliced bars provided that the transverse reinforcements are designed according to the proposed guidelines of this study.
- 5) The specimens with Class B lap splices as per the AASHTO LRFD Interim Provisions [11, 12] exhibited quite similar structural performance to the specimens with Class C lap splices as per the AASHTO LRFD code [2] for bar sizes of up to No. 7. However, it is important to note that when lap splice lengths are determined by considering the non-contact lap

splices as Class B lap splices as per the AASHTO LRFD Interim Provisions [11, 12], the lap splice lengths could be shortened due to the reinforcement confinement factor,  $\lambda_{rc}$  (which accounts for the effect of transverse reinforcement provided around the spliced bars) compared to the lap splice lengths determined by considering the non-contact lap splices as Class C lap splices as per the AASHTO LRFD code [2]. More importantly, it was observed that the larger the bar size of the spliced bars the greater would be the effect of the reinforcement confinement factor,  $\lambda_{rc}$ . As a result, the lap splice lengths could be shortened to such an extent that the tensile damage due to the splitting cracks along the spliced bars would be quite extensive despite providing the required amount of transverse reinforcement in the column and the drilled shaft. Therefore, for bar sizes larger than No. 7, the specimens with Class B lap splices as per the AASHTO LRFD Interim Provisions [11, 12] could exhibit worse structural performance than the specimens with Class C lap splices as per the AASHTO LRFD code [2].

- 6) The transverse reinforcement in the column and the drilled shaft near the column-drilled shaft interface exhibited the highest tensile stress within the non-contact lap splice zone. The tensile stresses in the transverse reinforcement located away from the interface were significantly lower than the ones located near the interface.
- 7) The distance between the non-contact lap splices in the non-circular columns connected to circular drilled shafts should not exceed 6 inches.
- 8) The increase of non-contact lap splice distance yielded significant inclined cracks and splitting cracks in the non-contact lap splice zone. The angle of inclined cracks was observed to increase with increasing the non-contact splice distance. Also, the opening at the column-drilled shaft interface increased with increasing the non-contact splice distance. Due to the large opening at the column-drilled shaft interface, the dowel bars and the column longitudinal bars could be subjected to corrosion over time. Further, the cracking or spalling of the concrete at the bottom of the column can occur due to the corrosion.

Subsequently, the serviceability of such structures could be adversely affected, and a long term maintenance issue will occur.

### **7.2.2 Conclusions from the Finite Element Analysis and Parametric Study**

Based on the thorough finite element analysis and parametric study of the test specimens, the following conclusions can be made:

- 1) The lateral stiffness and ultimate load capacity of column-drilled shaft connections would generally decrease with increasing the lap splice distance between the spliced bars.
- 2) The test specimens with non-contact lap splice consistently exhibited larger opening at the column-drilled shaft interface than the specimen with contact lap splice. A comparison of the opening among all the specimens showed that the opening at the column-drilled shaft interface would generally increase with increasing the non-contact splice distance.
- 3) The larger the lap splice distance, the greater the contribution of longer lap splice length in increasing lateral stiffness of the test specimens designed with non-contact lap splices.
- 4) It is evident that the global response, i.e., load vs. lateral displacement relationship of the specimens is not significantly influenced by the increased amount of transverse reinforcement in the non-contact lap splice zone of the non-circular columns.
- 5) It can be observed from the FEA simulated results that the column ties in the specimens with a higher amount of transverse reinforcement exhibited smaller stresses at the service load and ultimate load level.
- 6) It is evident that the column ties near the column-drilled shaft connection exhibited the highest tensile stresses within the lap splice zone of the non-circular columns.
- 7) Article 5.11.2.1.1 of AASHTO BDS Interim Revisions [12] provides several modification factors to increase  $l_d$  in Article 5.11.2.1.2, or to decrease  $l_d$  in Article 5.11.2.1.3. One of the modification factors,  $\lambda_{rc}$  (reinforcement confinement factor), accounts for the effect of transverse reinforcement provided around the spliced bars and is used to decrease  $l_d$  in

Article 5.11.2.1.3. However, it is not recommended to shorten the required lap splice length as per the AASHTO LRFD code [12] by the reinforcement confinement factor,  $\lambda_{rc}$ , because the results from the finite element analysis of the Bent 17 column-drilled shaft connection have shown that the lap splice length could be shortened to such an extent due to  $\lambda_{rc}$  that the tensile damage due to the splitting cracks along the spliced bars would be quite extensive despite providing the required amount of transverse reinforcement in the column and the drilled shaft.

- 8) It is evident from the finite element analysis of the Bent 17 column-drilled shaft connection that the capacity of the connection could be reduced by 17.7% when non-contact lap splices with a non-contact distance of 24 inches are used instead of using contact lap splices.
- 9) Overall, the analytical and experimental investigation has demonstrated that the proposed design recommendations for the design of non-contact lap splices in the non-circular column to circular drilled shaft connections would be able to ensure the structural safety, construction economy and applicability of this kind of bridge substructures.

### **7.3 Future Work**

Apart from the critical parameters investigated in this study, the investigation of the behavior of non-contact lap splices should be extended with regards to larger bar sizes, concrete cover to the spliced bars and concrete strength to understand the effect of these secondary parameters.

The loading in this study was limited to monotonic loading and cyclic loading with a limited number of cycles. The number of cycles of cyclic loading for the specimens was not sufficient to provide an insight into the fatigue behavior of the connection. It is desirable to perform tests with a greater number of cycles of cyclic loading to find out the fatigue behavior of the non-contact lap splices in the geometrically dissimilar column to drilled shaft connections. Moreover, tests could be performed under reversed cyclic loading for extending the application of the design recommendations in areas of high seismic risk.

## References

- [1] Gato-docs.its.txstate.edu. [Online] Available at: <http://gato-docs.its.txstate.edu/jcr:6f2713d4-bdf0-4184-98f8-7bffed0e8974/PS-33>. [Accessed 23 Feb. 2019].
- [2] AASHTO. AASHTO LRFD Bridge Design Specifications, 7th Ed. Washington, D.C.: American Association of State Highway Transportation Officials; 2014.
- [3] Masud M, Sawab J, Mo Y-L, Hsu TT. “Effect of noncontact lap splice on the behavior of drilled shaft–bridge column interface.” No. 18-04750. *In: Transportation research board 97th annual meeting.* Washington, DC: Transportation Research Board; 2018.
- [4] McLean DI, Smith CL. Noncontact lap splices in bridge column-shaft connections. Research Report No. WA-RD 417.1. Washington, DC: Washington State Department of Transportation; 1997.
- [5] Hamad BS, Mansour MY. “Bond strength of noncontact tension lap splices.” *ACI Structural Journal.* 1996; 93:316-26.
- [6] Lin Y, Gamble WL, Hawkins NM. Seismic behavior of bridge column non-contact lap splices. University of Illinois Engineering Experiment Station, College of Engineering, University of Illinois at Urbana-Champaign; 1998.
- [7] Sagan V, Gergely P, White R. “Behavior and design of noncontact lap splices subjected to repeated inelastic tensile loading.” *ACI Structural Journal.* 1991; 88(4):420-31.
- [8] Murcia-Delso J, Shing PB, Stavridis A, Liu Y. Required embedment length of column reinforcement extended into type II shafts. University of California, San Diego: California Department of Transportation; 2013.
- [9] Murcia-Delso J, Liu Y, Shing PB. “Development of bridge column longitudinal reinforcement in oversized pile shafts.” *Journal of Structural Engineering.* 2016; 142(11):04016114.

- [10] Tran HV. Drilled shaft socket connections for precast columns in seismic regions (Doctoral dissertation). Department of Civil and Environmental Engineering, University of Washington; 2015.
- [11] AASHTO. AASHTO LRFD Bridge Design Specifications Interim Revisions, 7th Ed. Washington, D.C.: American Association of State Highway Transportation Officials; 2015.
- [12] AASHTO. AASHTO LRFD Bridge Design Specifications Interim Revisions, 7th Ed. Washington, D.C.: American Association of State Highway Transportation Officials; 2016.
- [13] Chen H, Masud M, Sawab J, Huang HW, Xu B, Mo YL, Hsu TT. “Multiscale analysis of non-contact splices at drilled shaft to bridge column interface.” *Engineering Structures*. 2018; 176:28-40.
- [14] Crsi.org. “CRSI: Lap Splices.” [Online]. Available from: <http://www.crsi.org/index.cfm/steel/lap> [Accessed 23 Feb. 2019].
- [15] American Concrete Institute. Building Code Requirements for Reinforced Concrete (ACI 318-89) (Revised 1992) and Commentary-ACI 318R-89 (Revised 1992). Farmington Hills, MI: American Concrete Institute; 1989.
- [16] American Concrete Institute. Building Code Requirements for Structural Concrete (ACI 318-14): Commentary on Building Code Requirements for Structural Concrete (ACI 318R-14): an ACI Report. Farmington Hills, MI: American Concrete Institute; 2014.
- [17] Maksoud M. “Noncontact lap splices in rectangular columns.” Austin, Texas, U.S.: *Private correspondence to Texas Department of Transportation*; 2012.
- [18] AASHTO. AASHTO LRFD Bridge Design Specifications, 5<sup>th</sup> Ed. Washington, D.C.: American Association of State Highway Transportation Officials; 2010.

- [19] Caltrans SD. Caltrans seismic design criteria. California Department of Transportation, Sacramento, CA. 2010.
- [20] AASHTO. AASHTO LRFD Bridge Design Specifications Interim Revisions, 4th Ed. Washington, DC: American Association of State Highway Transportation Officials; 2009.
- [21] TxDOT. Bridge Design Manual (L.R.F.D.). Austin, TX: Texas Department of Transportation (TxDOT); 2015.
- [22] ASTM International. ASTM A615 / A615M-18e1. Standard Specification for Deformed and Plain Carbon-Steel Bars for Concrete Reinforcement. West Conshohocken, PA: ASTM International; 2018.
- [23] Ramirez JA, Russell BW. Transfer, development, and splice length for strand/reinforcement in high-strength concrete. NCHRP Report 603. Washington, D.C.: Transportation Research Board; 2008.
- [24] Walker WT. "Laboratory tests of spaced and tied reinforcing bars." *In Journal Proceedings* 1951 Jan 1 (Vol. 47, No. 1, pp. 365-372).
- [25] Chinn J, Ferguson PM, Thompson JN. "Lapped splices in reinforced concrete beams." *In Journal Proceedings* 1955 Oct 1 (Vol. 52, No. 10, pp. 201-213).
- [26] Chamberlin SJ. "Spacing of spliced bars in tension pull-out specimens." *In Journal Proceedings* 1952 Dec 1 (Vol. 49, No. 12, pp. 261-274).
- [27] Chamberlin SJ. "Spacing of spliced bars in beams." *In Journal Proceedings* 1958 Feb 1 (Vol. 54, No. 2, pp. 689-697).
- [28] Systèmes D. Abaqus/CAE version 6.14-3. Providence, RI: Dassault Systems Simulia Corp; 2014.

- [29] Lee J, Fenves GL. “Plastic-damage model for cyclic loading of concrete structures.” *Journal of engineering mechanics*. 1998; 124(8):892-900.
- [30] Hsu TT, Mo Y-L. Unified theory of concrete structures. Chichester, UK: John Wiley & Sons, Ltd.; 2010.
- [31] Belarbi A, Hsu TT. “Constitutive laws of concrete in tension and reinforcing bars stiffened by concrete.” *ACI Structural Journal*. 1994; 91(4):465-74.
- [32] Pang X-BD, Hsu TT. “Behavior of reinforced concrete membrane elements in shear.” *ACI Structural Journal*. 1995; 92(6):665-79.
- [33] Systèmes D. Abaqus analysis user’s manual. Providence, RI: Dassault Systems Simulia Corp; 2014.
- [34] Farny JA, Melander JM, Panarese WC. Concrete Masonry Handbook for Architects, Engineers, Builders. Skokie, Illinois: Portland Cement Association; 2008.
- [35] CEB-FIP M. 90. Design of concrete structures. CEB-FIP-Model-Code 1990. London, U.K.: British Standard Institution; 1993.
- [36] Abaqus-docs.mit.edu. “Concrete damaged plasticity.” [Online]. Available from: <https://abaqus-docs.mit.edu/2017/English/SIMACAEMATRefMap/simamat-c-concretedamaged.htm> [Accessed 23 Feb. 2019].
- [37] Birtel V, Mark P. “Parameterised finite element modelling of RC beam shear failure.” *In ABAQUS users’ conference*, (pp. 95-108). 2006.
- [38] Concrete.org. [Online]. Available from: [http://www.concrete.org/portals/0/files/pdf/ACI\\_Concrete\\_Terminology.pdf](http://www.concrete.org/portals/0/files/pdf/ACI_Concrete_Terminology.pdf) [Accessed 23 Feb. 2019].

## Appendix A

### Elevation and Cross-sections of the Test Specimens

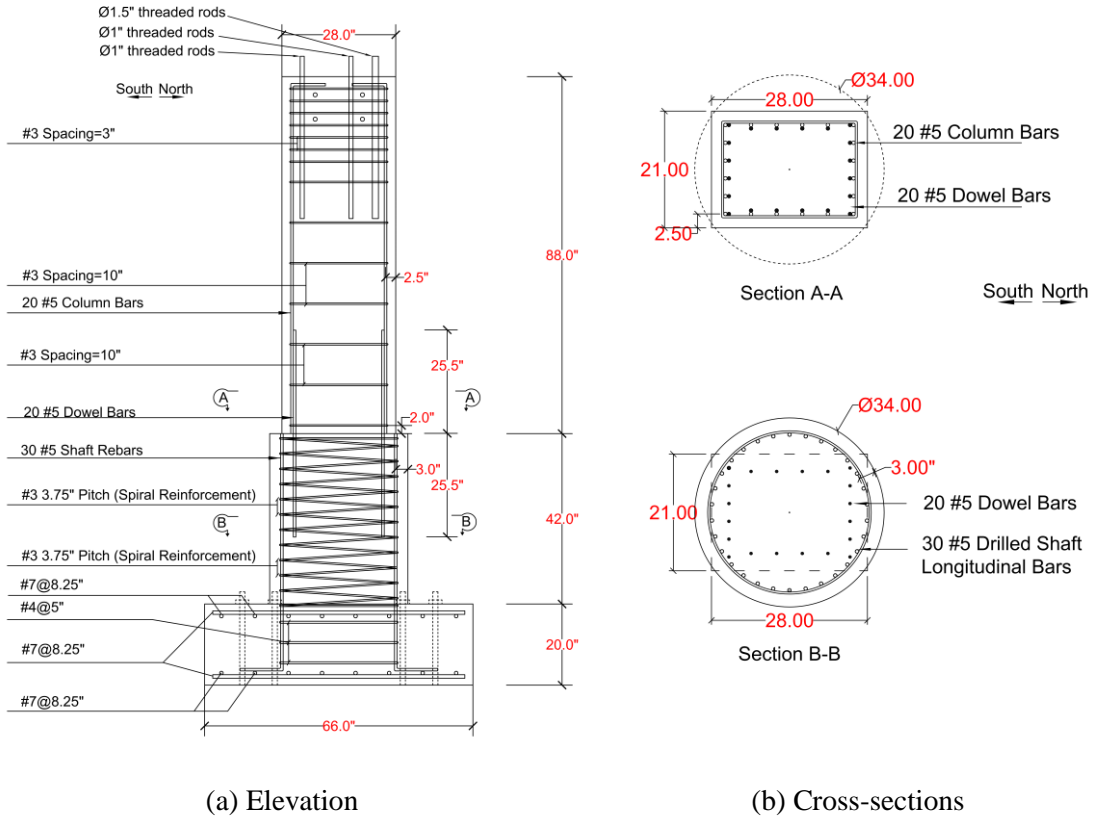
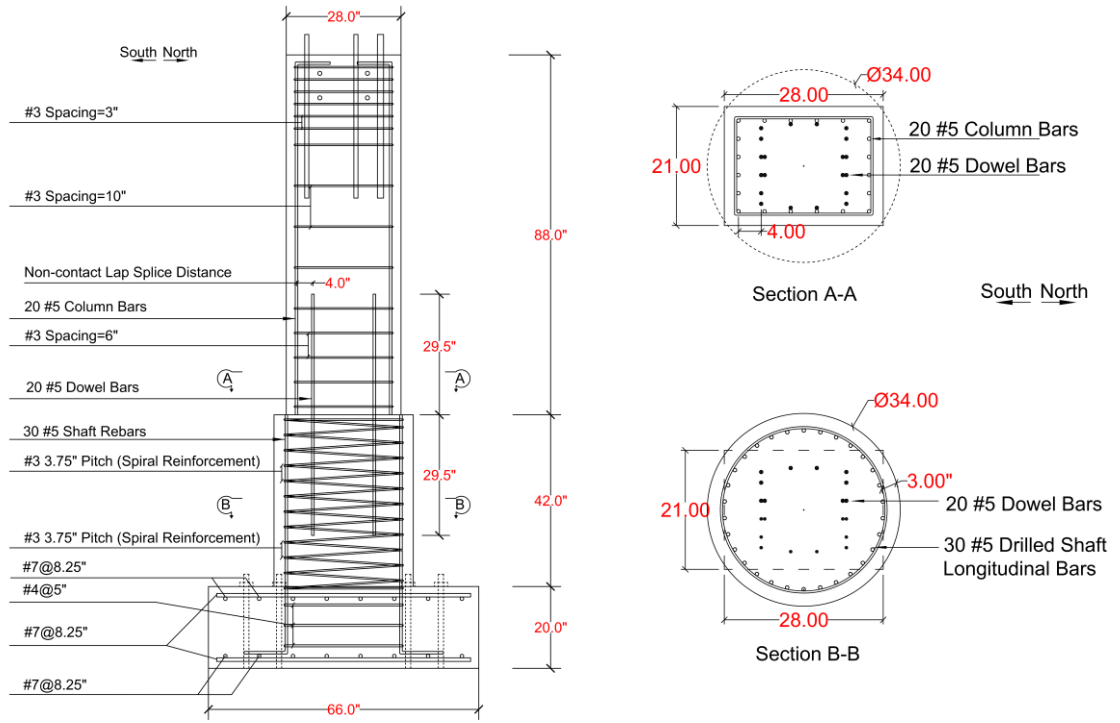


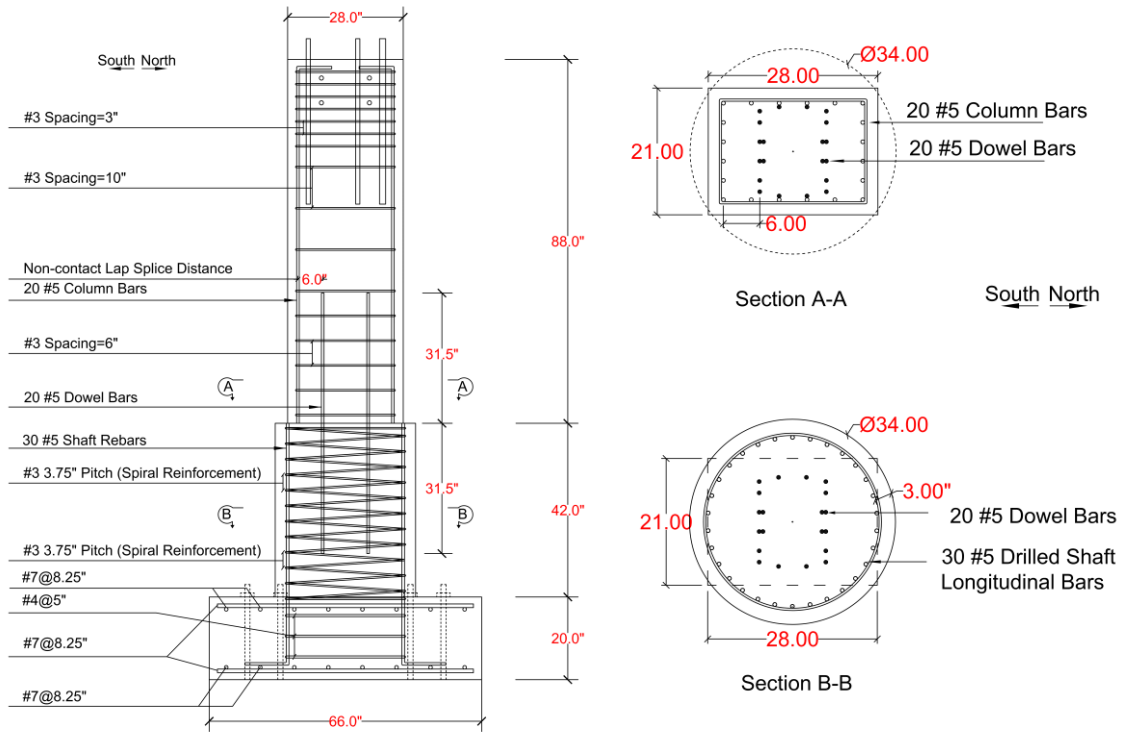
**Fig. A.1. Specimen 1.**



(a) Elevation

(b) Cross-sections

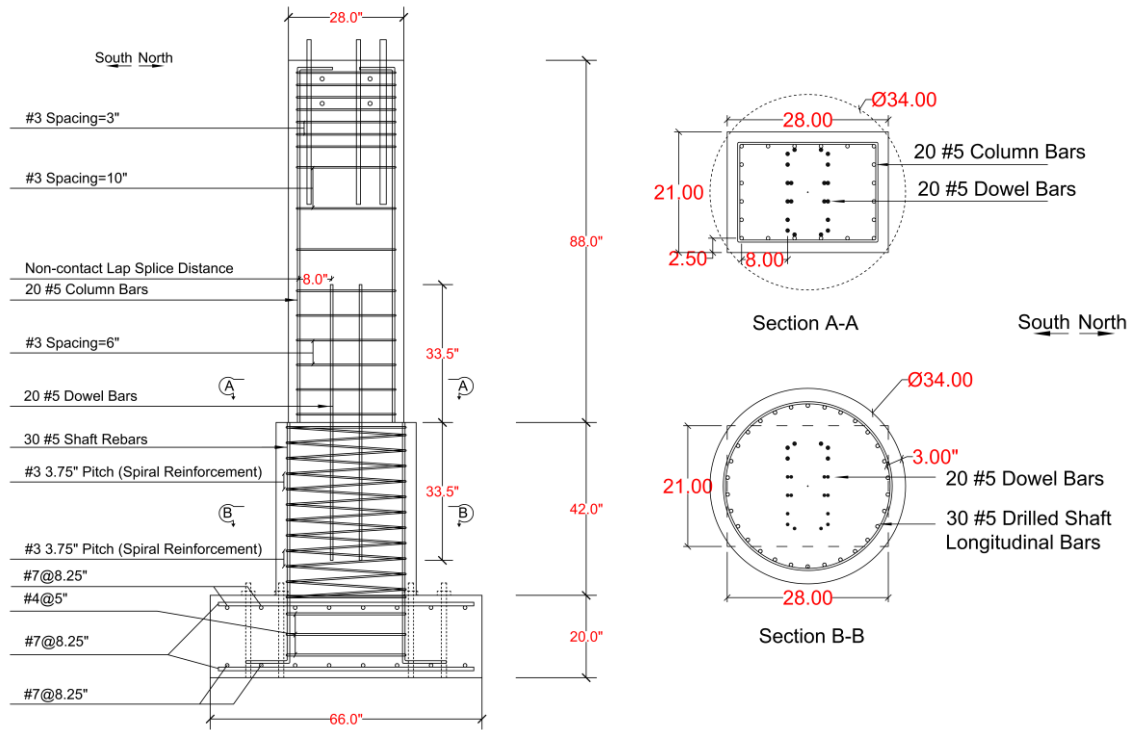
**Fig. A.2. Specimen 2.**



(a) Elevation

(b) Cross-sections

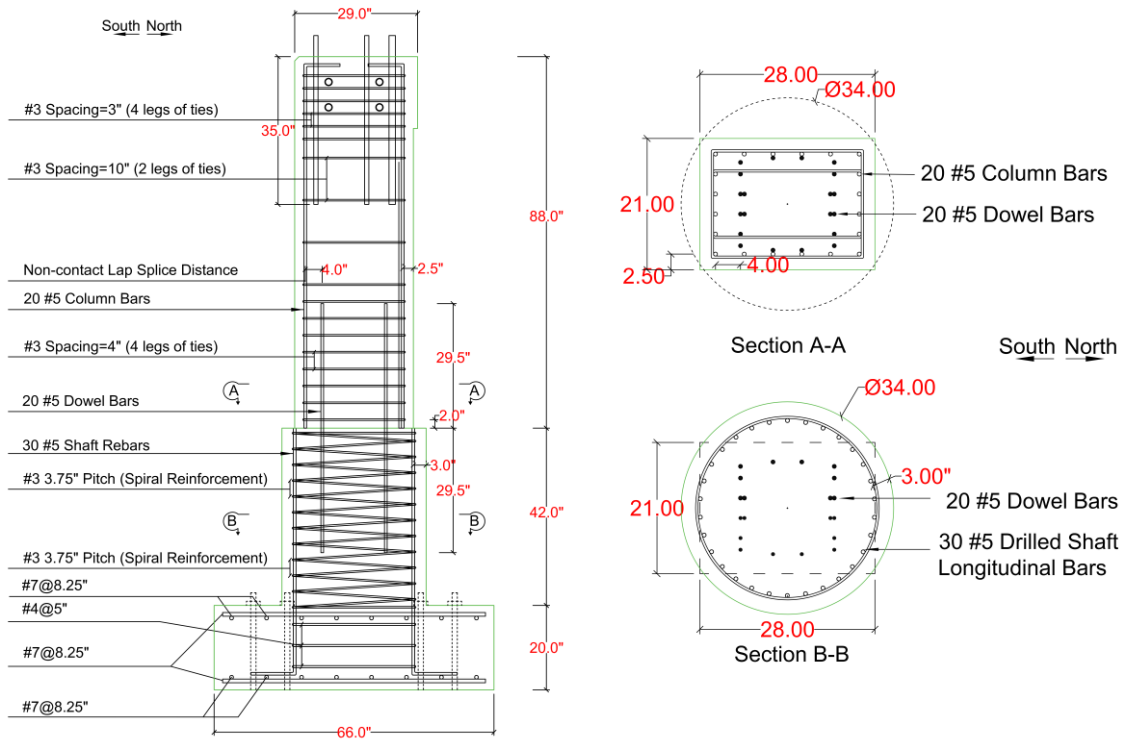
**Fig. A.3. Specimen 3.**



(a) Elevation

(b) Cross-sections

**Fig. A.4. Specimen 4.**



(a) Elevation

(b) Cross-sections

**Fig. A.5. Specimen 5.**

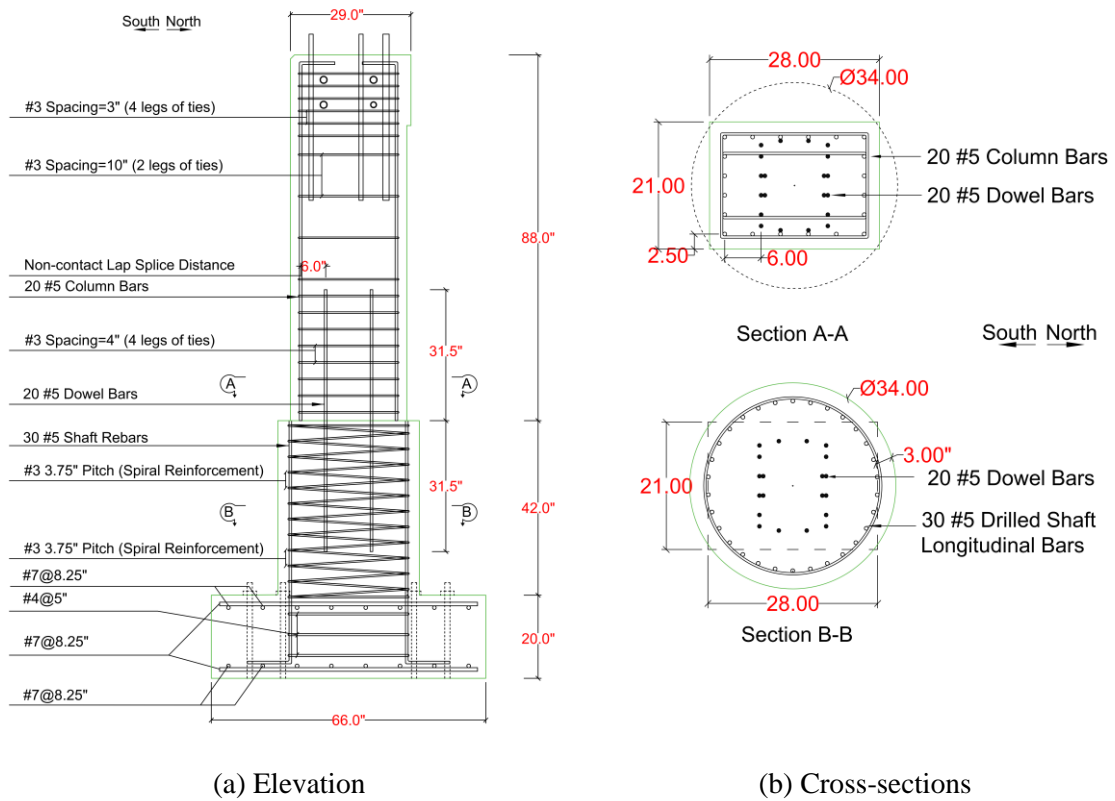
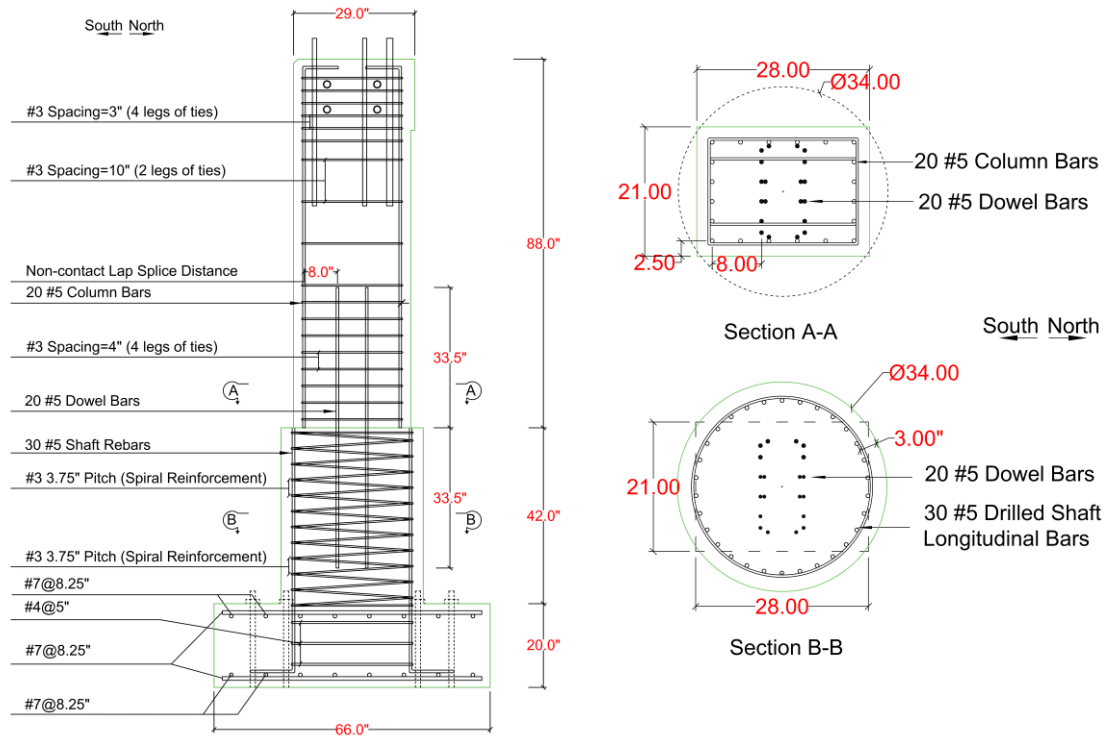


**Fig. A.6. Specimen 6.**



(a) Elevation

(b) Cross-sections

**Fig. A.7. Specimen 7.**

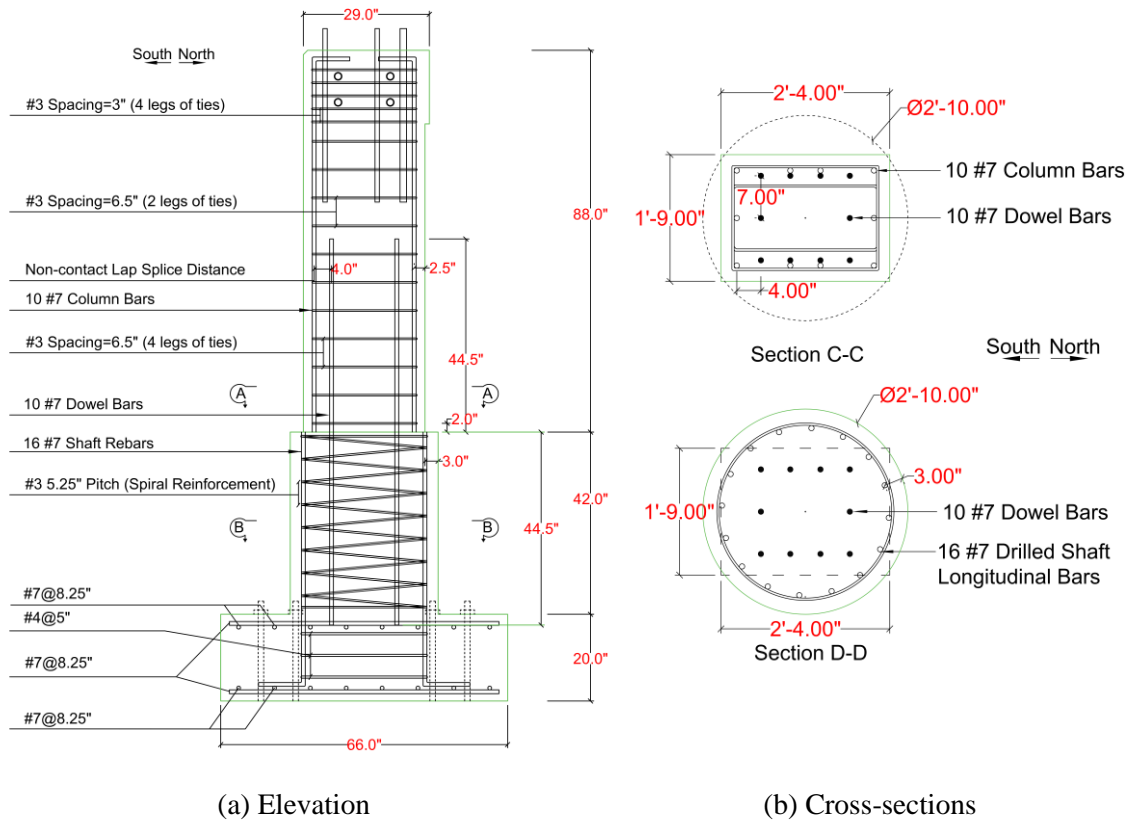
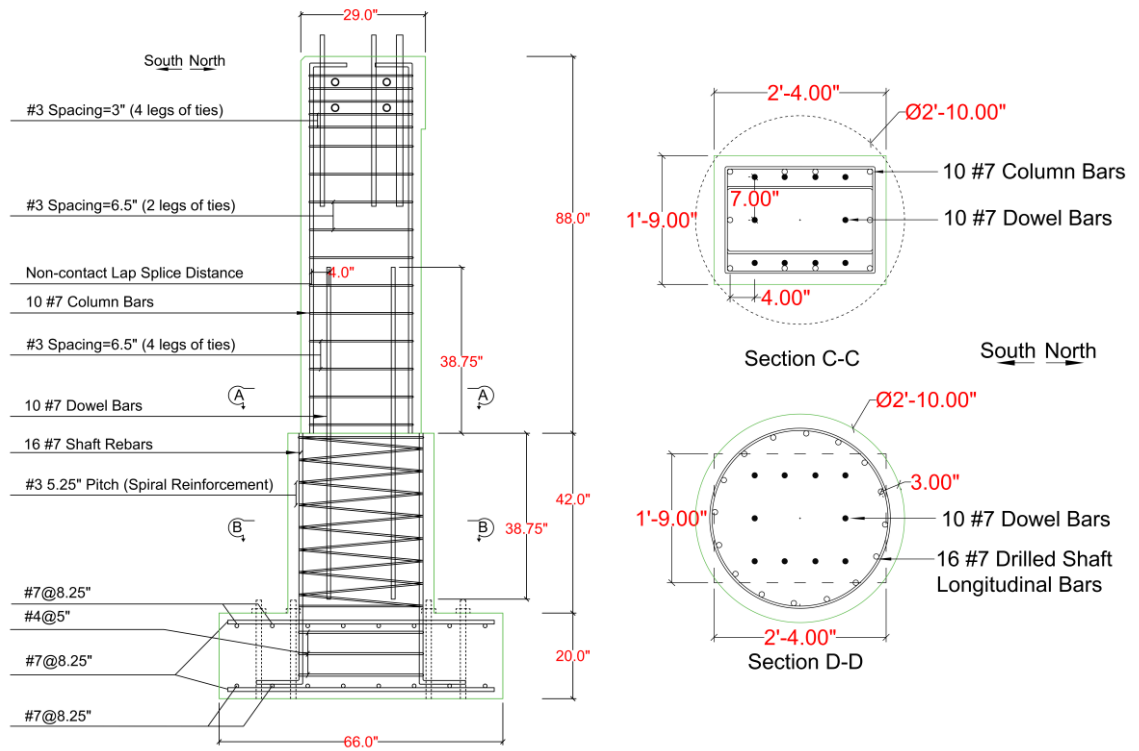


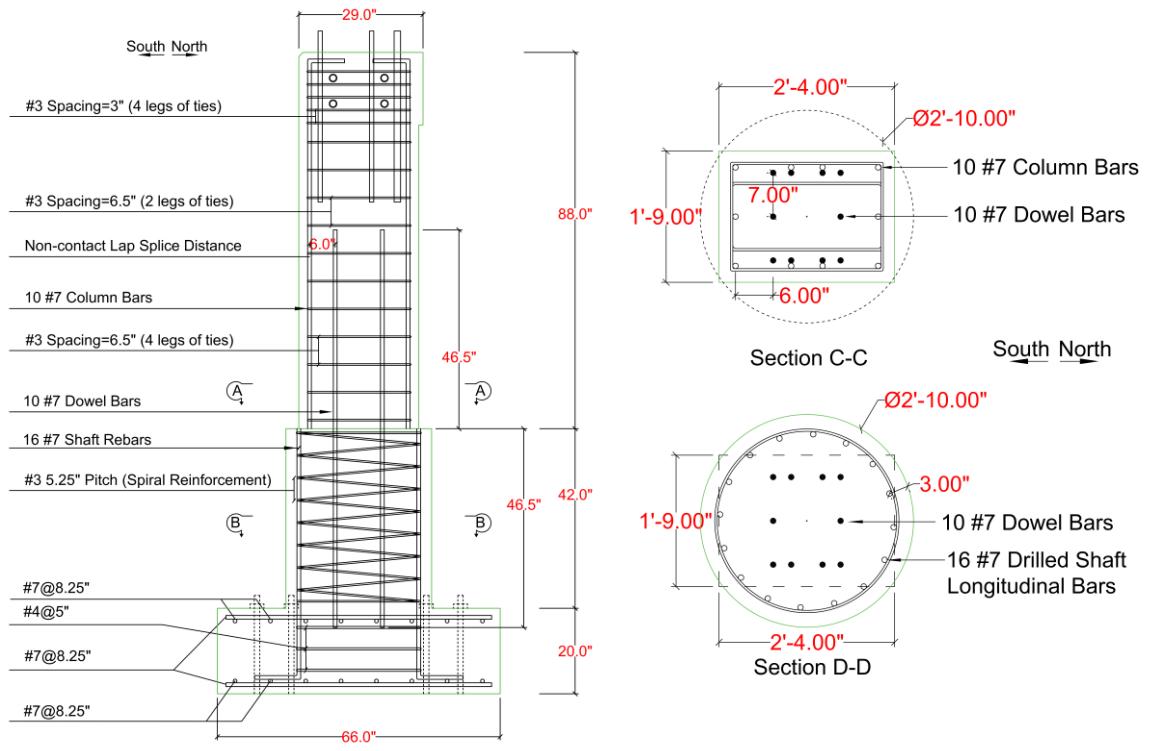
**Fig. A.8. Specimen 8.**



(a) Elevation

(b) Cross-sections

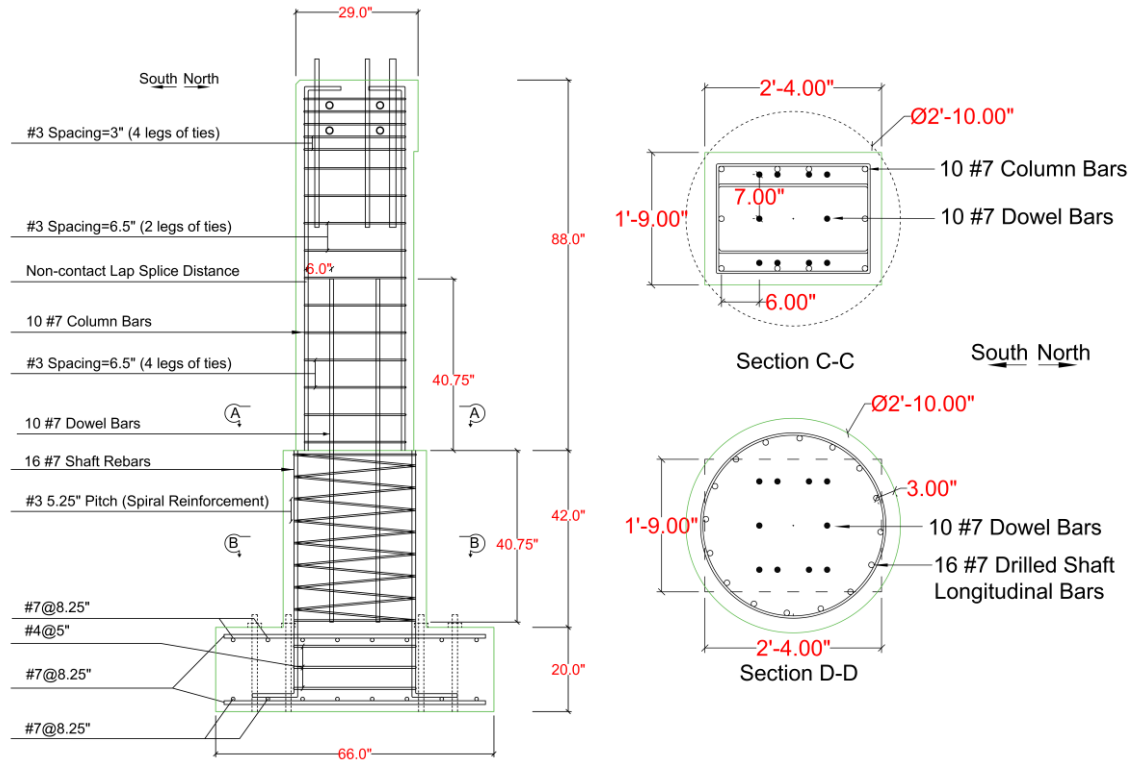
**Fig. A.9. Specimen 9.**



(a) Elevation

(b) Cross-sections

**Fig. A.10. Specimen 10.**



(a) Elevation

(b) Cross-sections

**Fig. A.11. Specimen 11.**

## Appendix B

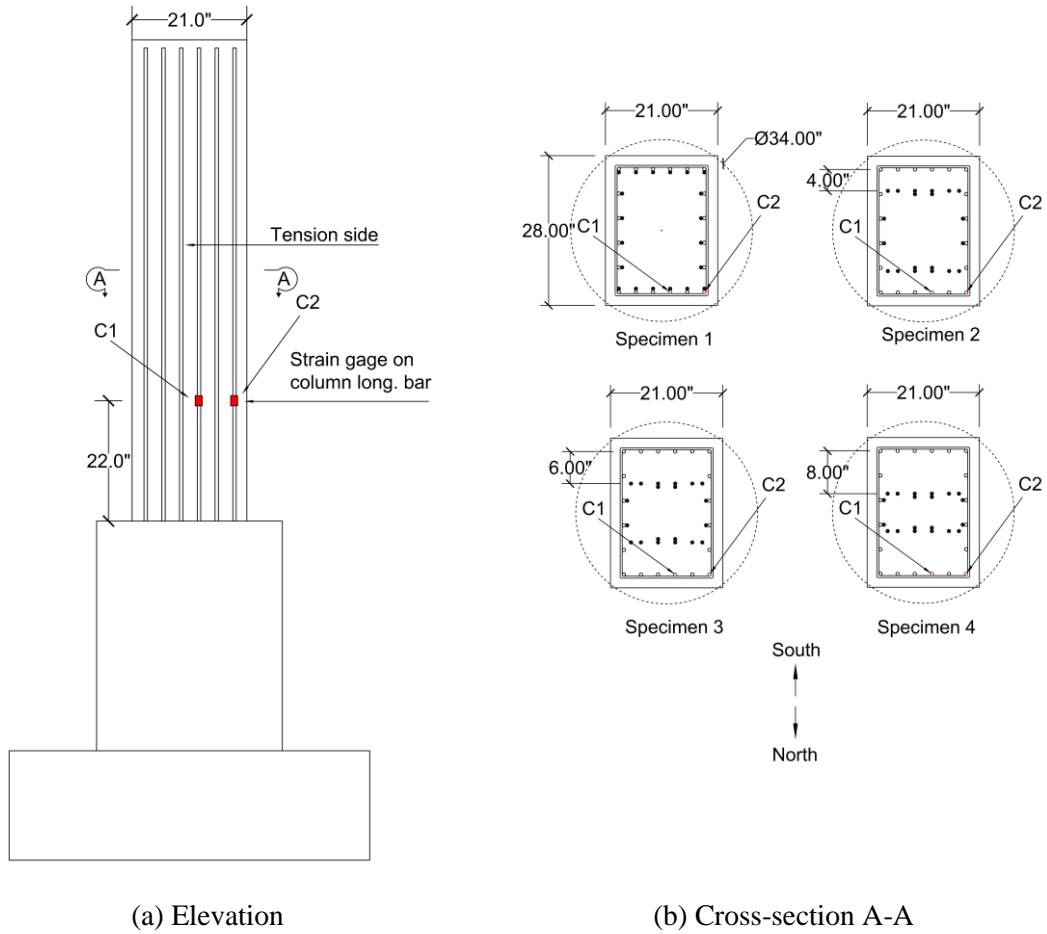
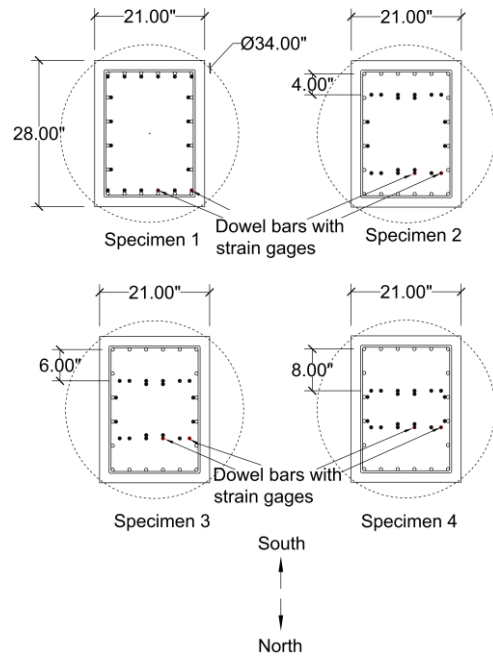
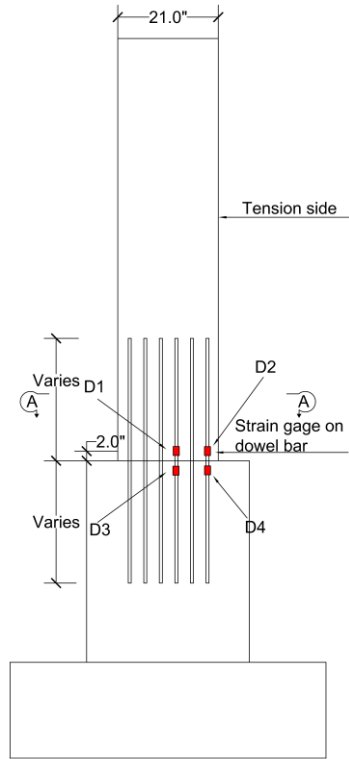


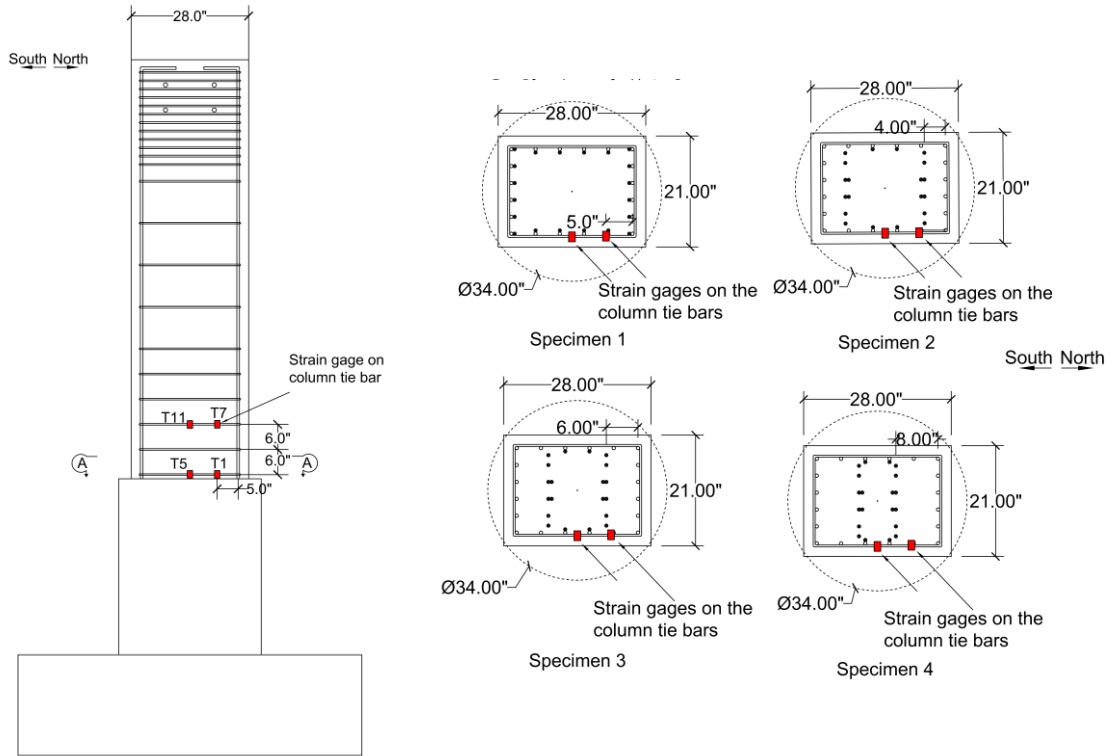
**Fig. B.1. Strain gages on the column longitudinal bars of Specimens 1 to 4.**



(a) Elevation

(b) Cross-section A-A

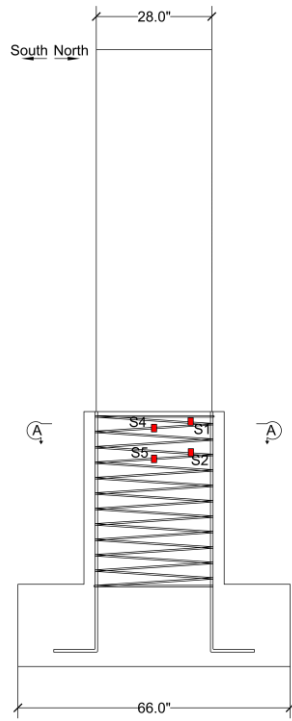
**Fig. B.2. Strain gages on the dowel bars of Specimen 1 to 4.**



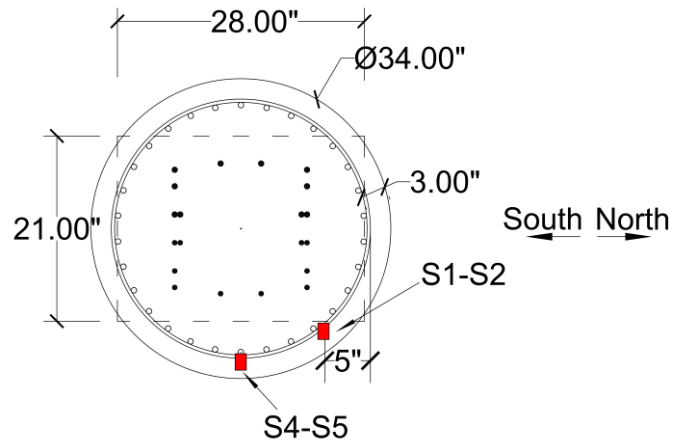
(a) Elevation

(b) Cross-section A-A

**Fig. B.3. Strain gages on the column ties of Specimen 1 to 4.**

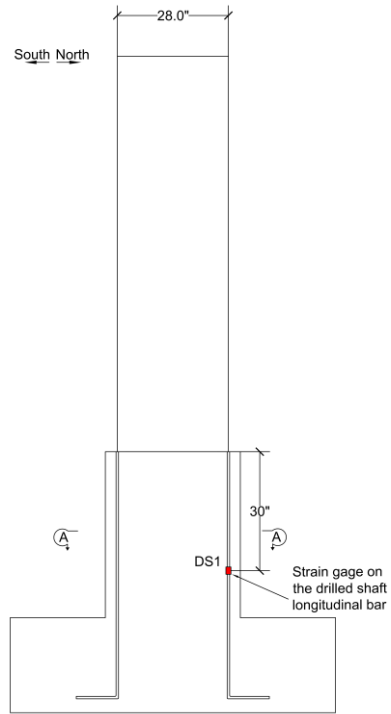


(a) Elevation

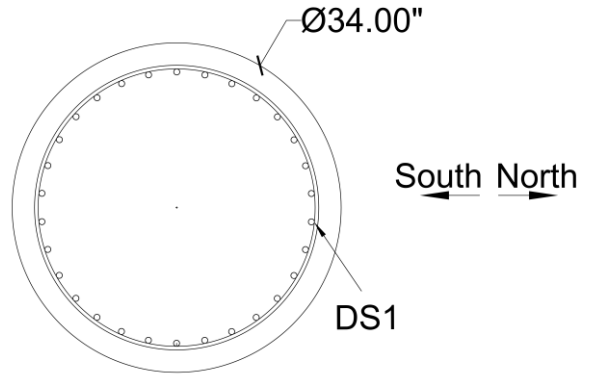


(b) Cross-section A-A

**Fig. B.4. Strain gages on the drilled shaft spirals of Specimen 1 to 4.**

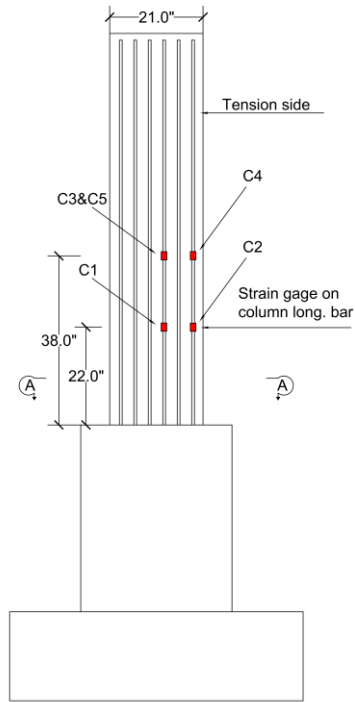


(a) Elevation

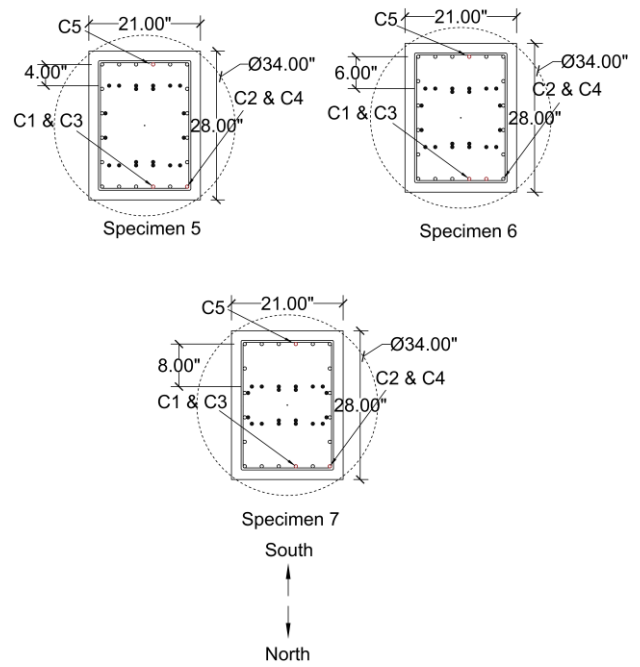


(b) Cross-section A-A

**Fig. B.5. Strain gages on the drilled shaft longitudinal bars of Specimen 1 to 4.**

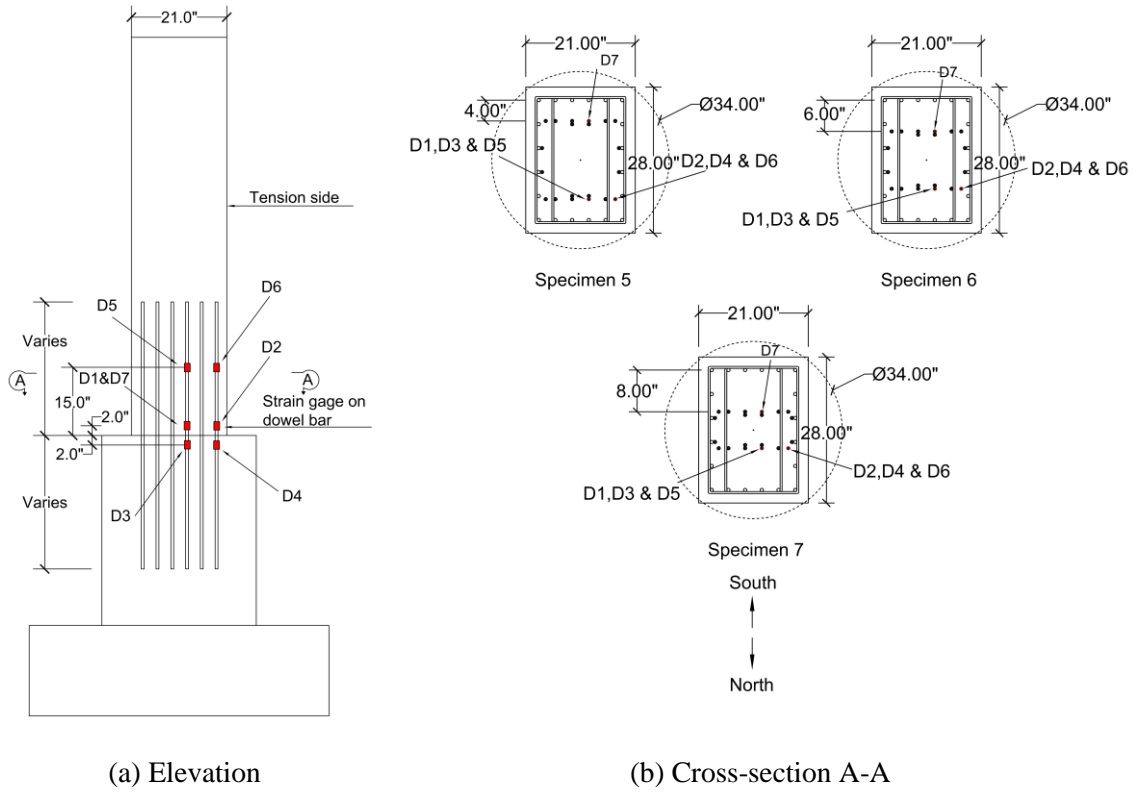


(a) Elevation



(b) Cross-section A-A

**Fig. B.6. Strain gages on the column longitudinal bars of Specimen 5 to 7.**



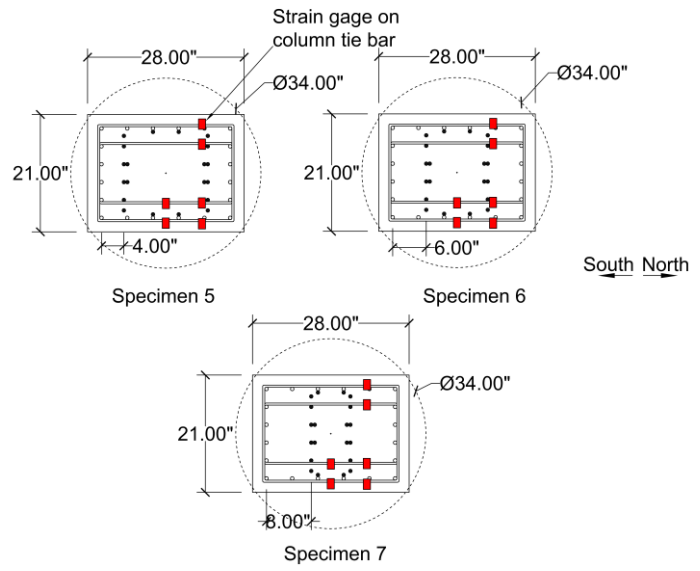
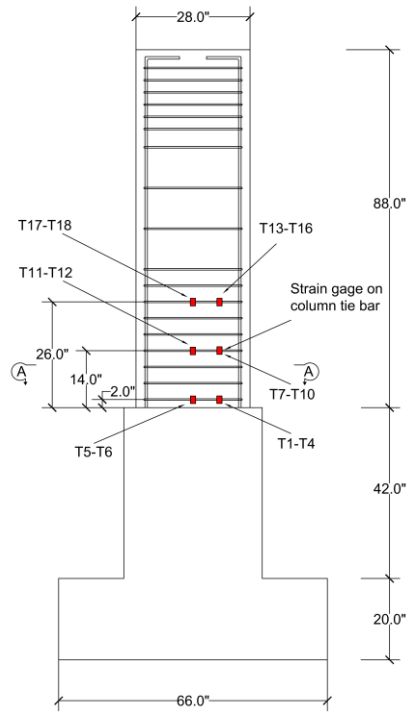
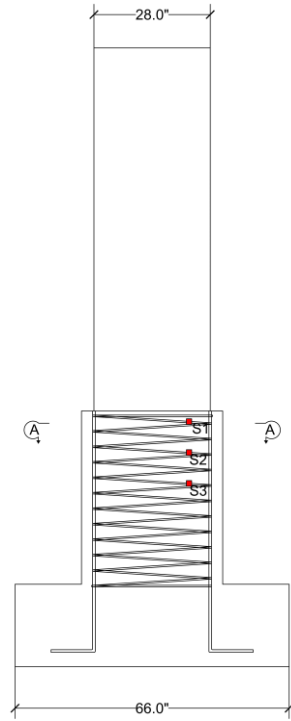
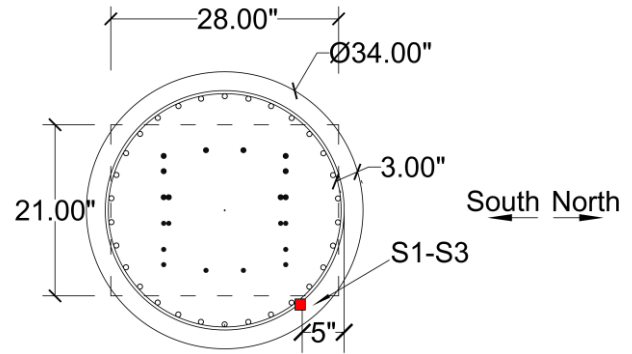


**Fig. B.8. Strain gages on the column ties of Specimen 5 to 7.**

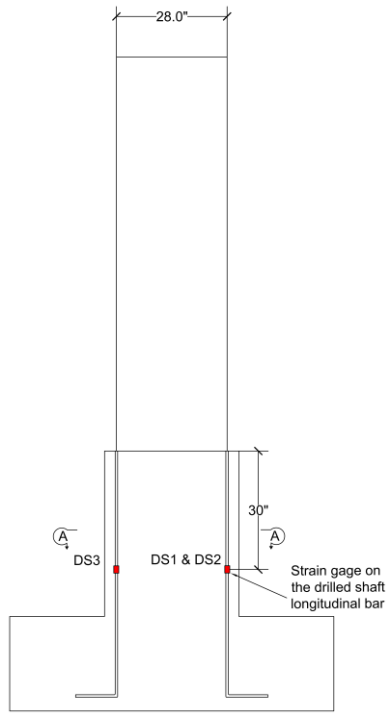


(a) Elevation

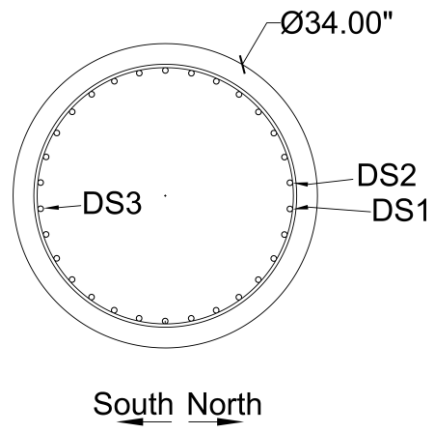


(b) Cross-section A-A

**Fig. B.9. Strain gages on the drilled shaft spirals of Specimen 5 to 7.**



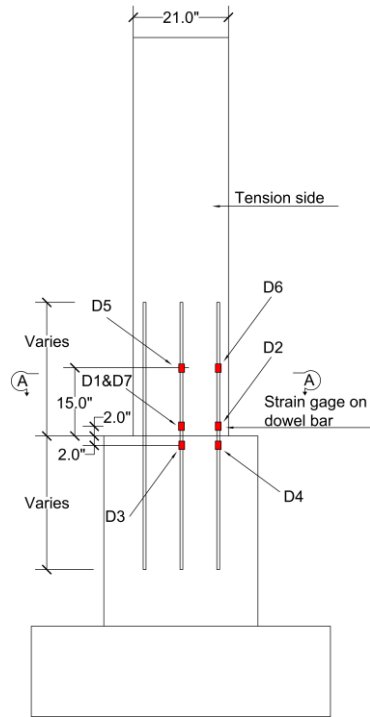
(a) Elevation



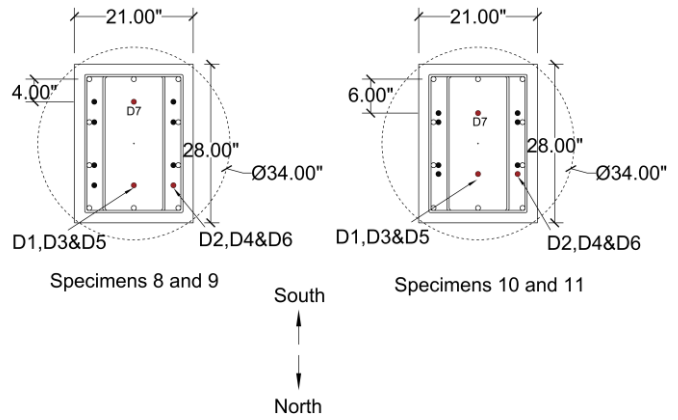
(b) Cross-section A-A

**Fig. B.10. Strain gages on the drilled shaft longitudinal bars of Specimen 5 to 7.**



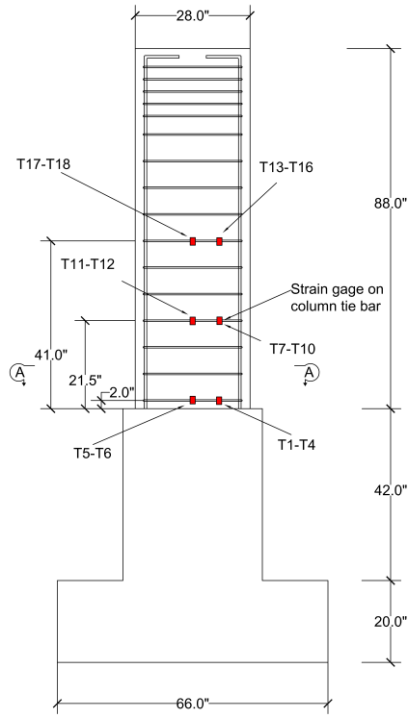


(a) Elevation

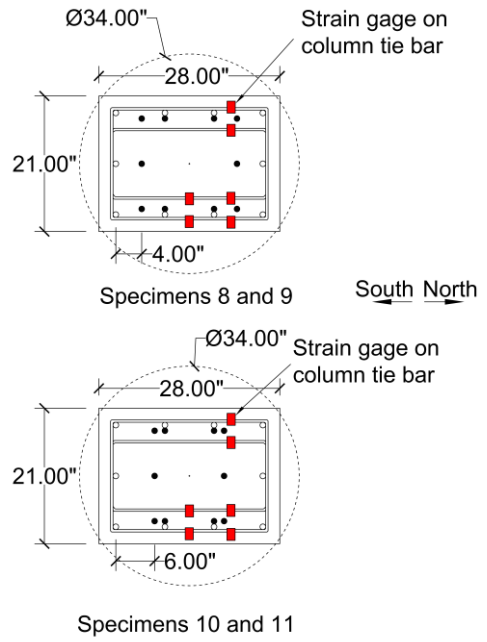


(b) Cross-section A-A

**Fig. B.12. Strain gages on the dowel bars of Specimen 8 to 11.**



(a) Elevation



(b) Cross-section A-A

**Fig. B.13. Strain gages on the column ties of Specimen 8 to 11.**

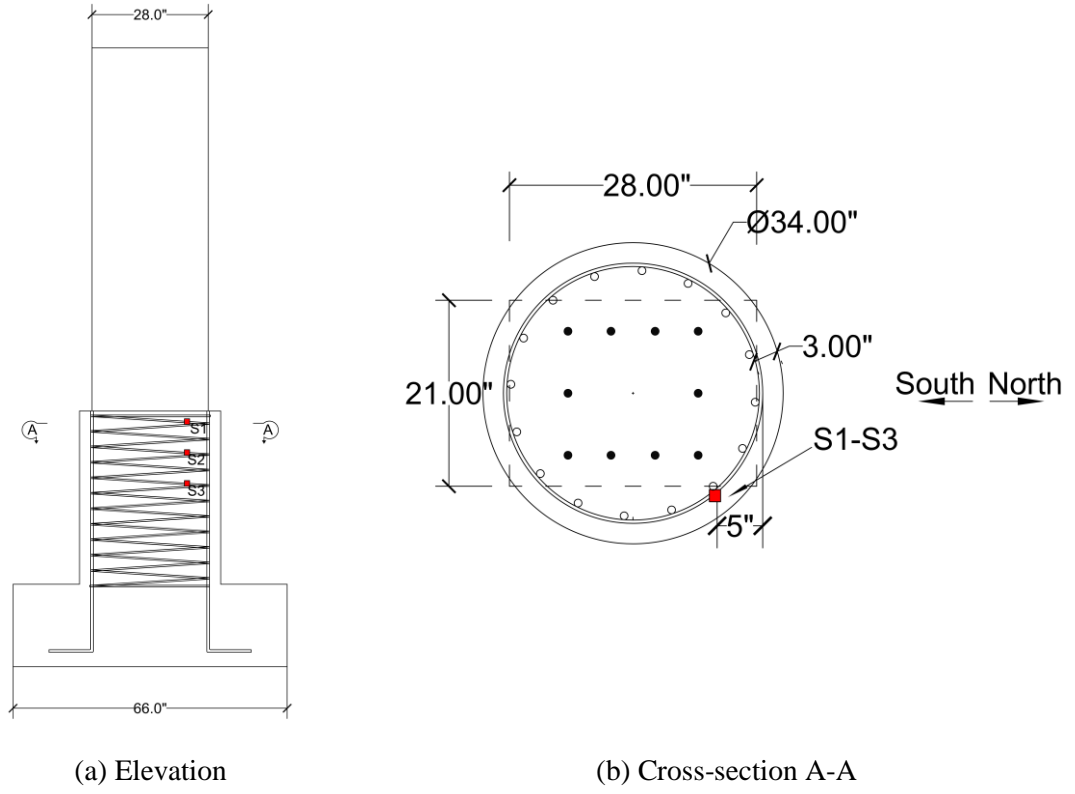


**Fig. B.14. Strain gages on the drilled shaft spirals of Specimen 8 to 11.**

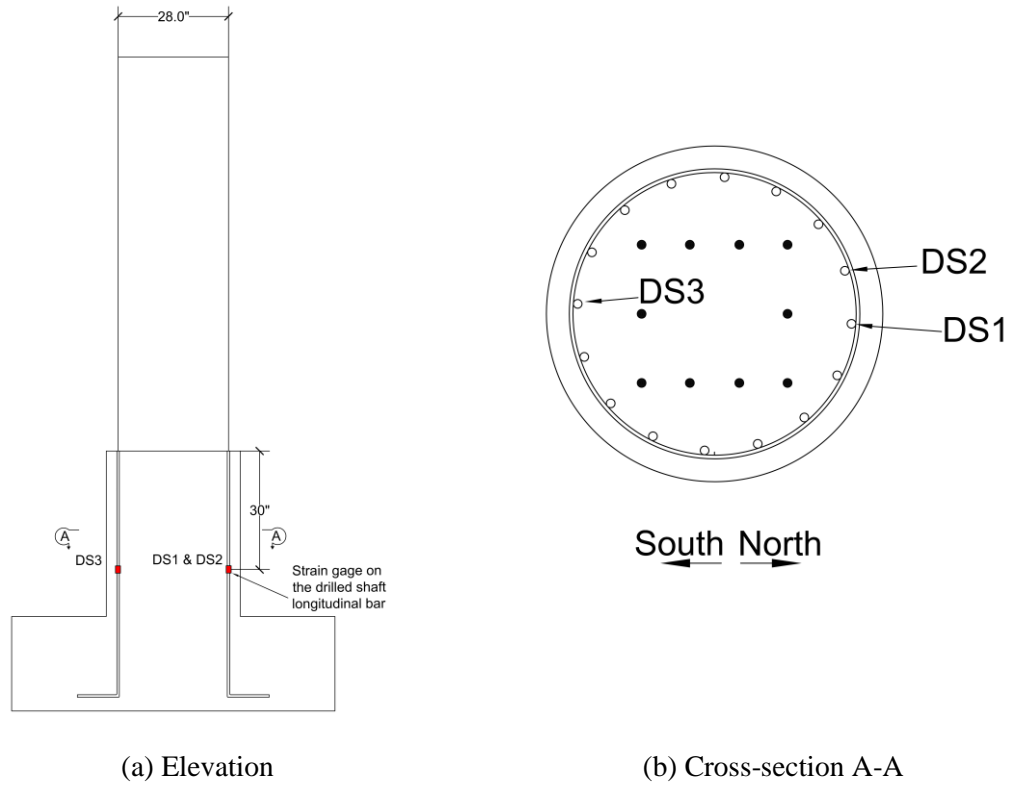


**Fig. B.15. Strain gages on the drilled shaft longitudinal bars of Specimen 8 to 11.**

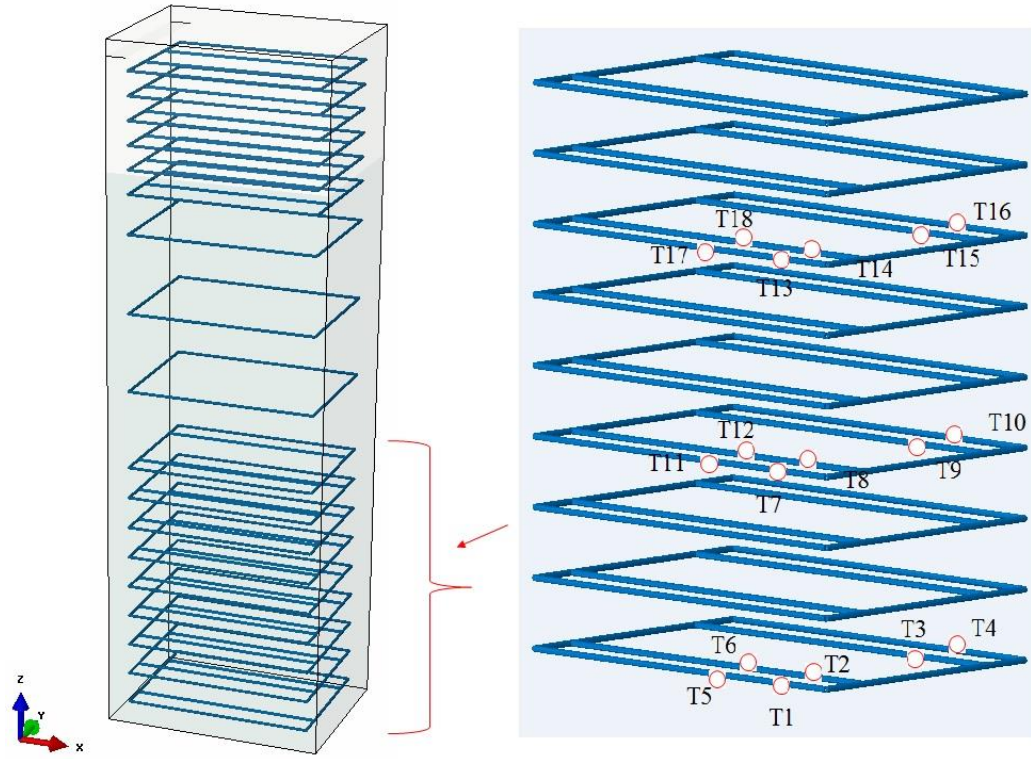


**Fig. B.16. Location of strain gages on the column ties of Specimens 5-11: Isometric view.**

## Appendix C

### Strain Gage Results from Phase I and II Specimens

**Table C.1. Strain Gage Results from Specimen 1**

Load, kips	Microstrain							
	C1	C2	D1	D2	D3	D4	T1	T5
0	0	0	0	0	0	0	0	0
28.6 <sup>a</sup>	42	60	470	697	418	338	2	0
56.25 (Load Level A)	217	110	945	1405	1104	1315	11	18
66.75 (Load Level B) 1 <sup>st</sup> cycle	341	152	1149	1750	1438	1734	52	48
66.75 (Load Level B) 125,000 <sup>th</sup> cycle	377	168	-	1882	1516	1977	120	90
77.1	391	189	-	2300	1768	2251	147	105
90	451	280	-	-	2444	4742	200	172
100	499	371	-	-	7198	-	286	235
105	520	466	-	-	-	-	323	266

Load, kips	Microstrain						
	T7*	T11	S1	S2	S4	S5	DS1
0		0	0	0	0	0	0
28.6		6	20	0	10	-1	43
56.25		23	141	0	10	-8	64
66.75 1 <sup>st</sup> cycle		30	280	15	13	-11	77
66.75 125,000 <sup>th</sup> cycle		46	451	31	19	-13	88
77.1		54	509	33	27	-15	103
90		92	704	42	84	-21	1268
100		261	1093	60	351	-25	1439
105		352	1243	71	466	-27	1489

<sup>a</sup> Lowest cracking load of specimens 1 to 4.

\* Strain gage broken

**Table C.2. Strain Gage Results from Specimen 2**

Load, kips	Microstrain							
	C1	C2	D1	D2	D3	D4	T1	T5
0	0	0	0	0	0	0	0	0
28.6	23	11	604	416	391	474	0	0
56.25	958	956	1890	1023	1340	1526	1132	156
66.75 1 <sup>st</sup> cycle	1202	1155	2560	1299	1781	1884	1845	280
66.75 125,000 <sup>th</sup> cycle	1343	1289	2698		1941	2052	2970	414
77.1	1512	1459	4093	1857	2460	2370	3916	558
90	1784	1752	7688	2542	-	-	6196	1118
100	2097	1877	-	6886	-	-	9029	2154
105	2453	2038	-	-	-	-	10221	3598
112	7893	5930	-	-	-	-	11192	5101

Load, kips	Microstrain						
	T7	T11	S1	S2	S4	S5	DS1
0	0	0	0	0	0	0	0
28.6	0	0	0	0	0	0	0
56.25	0	0	255	8	0	0	558
66.75 1 <sup>st</sup> cycle	0	0	398	85	0	0	776
66.75 125,000 <sup>th</sup> cycle	0	0	480	188	0	0	800
77.1	0	0	567	208	0	0	872
90	66	0	787	327	70	0	1052
100	190	0	1005	482	188	0	1145
105	286	29	1098	573	272	0	1260
112	404	97	1240	703	382	8	1396

**Table C.3. Strain Gage Results from Specimen 3**

Load, kips	Microstrain							
	C1	C2	D1	D2	D3	D4	T1	T5*
0	0	0	0	0	0	0	0	
28.6	242	188	649	821	761	779	189	
56.25	1005	798	1383	1737	1786	1820	1345	
66.75 1 <sup>st</sup> cycle	1294	1109	1704	2131	2309	2204	1784	
66.75 125,000 <sup>th</sup> cycle	1370	1167	1823	2333	2412	2367	1859	
77.1	1583	-	2628	6289	2841	-	2050	
90	-	-	7633	-	-	-	-	
100	-	-	10549	-	-	-	-	

Load, kips	Microstrain						
	T7	T11*	S1*	S2	S4	S5	DS1
0	0			0	0	0	0
28.6	0			3	84	9	102
56.25	0			94	504	182	691
66.75 1 <sup>st</sup> cycle	31			142	844	349	901
66.75 125,000 <sup>th</sup> cycle	108			186	1039	443	938
77.1	135			240	1263	509	1038
90	274			390	2033	677	1193
100	563			648	3136	933	1375

\* Strain gage broken

**Table C.4. Strain Gage Results from Specimen 4**

Load, kips	Microstrain							
	C1	C2	D1	D2*	D3	D4	T1	T5
0	0	0	0		0	0	0	0
28.6	117	31	574		363	297	62	10
56.25	336	1081	1532		1320	997	2101	1248
66.75 1 <sup>st</sup> cycle	1539	1416	1911		1709	1299	3190	1852
66.75 125,000 <sup>th</sup> cycle	1689	1581	2034		1852	1514	4552	2804
77.1	1918	1802	2543		2176	1698	5681	3182
90	2391	2281			2486	2719		4544

Load, kips	Microstrain						
	T7	T11*	S1	S2*	S4	S5	DS1
0	0		0		0	0	0
28.6	66		0		2	0	0
56.25	111		0		366	37	61
66.75 1 <sup>st</sup> cycle	247		1		510	115	119
66.75 125,000 <sup>th</sup> cycle	519		158		656	209	142
77.1	643		223		780	257	168
90	1096		567		1209	455	233

\* Strain gage broken

**Table C.5. Strain Gage Results from Specimen 5**

Load, kips	Microstrain										
	C1	C2	C3	C4	C5	D1	D2	D3	D4	D5	D6
0	0	0	0	0	0.0	0	0	0	0	0.0	0.0
29 <sup>a</sup>	490	313	116	93	-126	683	675	942	622	81	66
40	965	655	673	554	-230	1091	879	1301	794	135	114
56.25(Load Level A)	1533	1097	1321	1255	-365	1740	1051	1947	1426	661	606
66.75 (Load Level B) 1 <sup>st</sup> cycle	2038	1473	1729	1726	-441	2201	1163	2470	1824	889	848
66.75 (Load Level B) 125,000 <sup>th</sup> cycle	2593	1789	2003	2117	-502	2687	872	3790	2222	1145	1068
77.1	3015	1985	2254	2368	-563	2906	916	8643	2890	1274	1190
85	3696	2223	2493	2606	-634		893	9249	4505	1415	1329
90	3954	2304	2521	2757	-689		901	9316	4830	1500	1413
100	5669	2838	7709	8721	-805		986			1662	1607
105	1343 8	8894	1135 9		-855		1003			1740	1709
108		9521	1448 3		-877		1105			1819	1806

<sup>a</sup> Lowest cracking load of specimens 5 to 7.

\* Strain gage broken

Load, kips	Microstrain										
	T1	T2	T3	T4	T5	T6	T7	T8	T9	T10	T11
0	0	0	0	0	0	0	0	0	0	0	0
29 <sup>a</sup>	44	77	81	144	39	38	0	0	0	0	0
40	338	194	241	444	70	53	0	0	0	0	0
56.25(Load Level A)	1099	575	657	1098	145	199	10	28	0	0	0
66.75 (Load Level B) 1 <sup>st</sup> cycle	1401	680	889	1460	282	318	21	36	43	27	0
66.75 (Load Level B) 125,000 <sup>th</sup> cycle	1606	753	1019	1671	1235	540	23	82	108	81	5
77.1	1746	806	1185	1850	1627	617	23	88	119	93	2
85	1918	974	1264	2002	1949	791	23	116	148	134	-1
90	2001	1045	1394	2086	-	1001	28	132	161	159	-1
100	2219	1270	1494	2285	2031	1614	47	177	160	234	18
105	2414	1480	1549	2403	-	2078	58	201	169	272	35
108	2565	1682	1704	2590	-	2486	75	223	181	303	62

Load, kips	Microstrain										
	T12	T13	T14	T15	T16	T17	T18	S1	S2	S3	DS1
0	0	0	0	0	0	0	0	0.0	0.0	0.0	0.0
29 <sup>a</sup>	0	0	0	16	40	3	7	3	0	0	56
40	0	0	103	48	110	3	10	7	0	0	77
56.25(Load Level A)	0	0	151	73	168	3	29	38	1	0	89
66.75 (Load Level B) 1 <sup>st</sup> cycle	0	44	220	123	265	4	41	72	12	0	110
66.75 (Load Level B) 125,000 <sup>th</sup> cycle	0	152	319	169	334	37	64	95	44	0	187
77.1	0	167	353	188	372	40	70	106	46	24	394
85	0	234	413	217	412	54	76	123	49	-	1273
90	0	342	440	223	423	104	93	137	52	-	1327
100	0	504	478	235	450	409	171	180	64	68	1462
105	0	566	525	256	496	483	206	216	76	87	1522
108	18	663	586	296	632	609	262	251	95		1577

Load, kips	Microstrain	
	DS2	DS3
0	0.0	0.0
29 <sup>a</sup>	67	-81
40	91	-114
56.25(Load Level A)	106	-171
66.75 (Load Level B) 1 <sup>st</sup> cycle	117	-235
66.75 (Load Level B) 125,000 <sup>th</sup> cycle	162	-302
77.1	334	-354
85	1457	-458
90	1539	-496
100	1722	-562
105	1799	-592
108	1868	-622

**Table C.6. Strain Gage Results from Specimen 6**

Load, kips	Microstrain										
	C1	C2	C3	C4	C5	D1	D2	D3	D4	D5	D6
0	0	0	0	0	0	0	0	0	0	0	0
29 <sup>a</sup>	104	112	141	185	-124	804	776	618	776	73	63
40	154	131	745	510	-209	1297	1237	913	1154	116	
56.25(Load Level A)	383	315	1409	660	-317	1829	1921	1423	1799	807	96
66.75 (Load Level B) 1 <sup>st</sup> cycle	925	913	1758	788	-389	2197	2576	1888	2394	1093	736
66.75 (Load Level B) 125,000 <sup>th</sup> cycle	1238	1333	1923	1004	-414	2590	3076	1692	2737	1277	947
77.1	1424	1539	2234	1073	-471	3290	7941	2546	2989	1479	1101
90	1706	1892	3154	1417	-559		9135	4859		1742	1251
100	1887	2100	7570		-631		1245 1			1925	1421
105	1942	2178	7850		-645		1448 7			2009	1576
108	2012	2269	8497		-654		1562 6			2058	1648

<sup>a</sup> Lowest cracking load of specimens 5 to 7.

\* Strain gage broken

Load, kips	Microstrain										
	T1	T2	T3	T4	T5	T6	T7	T8	T9	T10	T11
0	0	0	0	0	0	0	0	0	0	0	0
29 <sup>a</sup>	44	195	173	42	58	28	0	0	0	0	0
40	179	527	610	335	293	37	0	0	0	0	0
56.25(Load Level A)	1195	1340	1343	906	351	92	0	0	44	0	0
66.75 (Load Level B) 1 <sup>st</sup> cycle	1700	1726	1771	1226	1226	179	0	0	100	0	0
66.75 (Load Level B) 125,000 <sup>th</sup> cycle	1854	1917	1907	1477	1298	304	0	90	165	0	0
77.1	2023	1981	2248	1705	1483	369	0	115	208	0	0
90	2148	2314	2552	1897	1792	776	66	219	315	0	0
100	2505	3393	3385	2332	2627	1116	121	296	403	0	59
105	2660	4080	3977	2648	3090	1257	158	336	447	6	99
108	2765	4576	4276	2800	3349	1347	176	354	469	15	118

Load, kips	Microstrain										
	T12*	T13	T14	T15	T16*	T17*	T18*	S1	S2	S3	DS1
0		0	0	0				0	0	0	0
29 <sup>a</sup>		4	9	0				2	0	0	115
40		25	18	24				11	0	0	199
56.25(Load Level A)		56	19	44				29	0	0	562
66.75 (Load Level B) 1 <sup>st</sup> cycle		71	37	94				470	0	0	1038
66.75 (Load Level B) 125,000 <sup>th</sup> cycle		96	56	101				955	47	0	1228
77.1		118	65	118				1074	58	0	1378
90		215	122	153				1680	157	0	1533
100		291	229	185				2516	303	2	1651
105		324	256	204				3070	389	8	1709
108		362	283	230				3354	450	11	1764

Load, kips	Microstrain	
	DS2	DS3
0	0	0
29 <sup>a</sup>	122	-58
40	163	-105
56.25(Load Level A)	724	-124
66.75 (Load Level B) 1 <sup>st</sup> cycle	1190	-201
66.75 (Load Level B) 125,000 <sup>th</sup> cycle	1404	-257
77.1	1573	-319
90	1724	-486
100	1847	-553
105	1874	-577
108	1956	-622

**Table C.7. Strain Gage Results from Specimen 7**

Load, kips	Microstrain										
	C1	C2	C3	C4	C5	D1	D2	D3	D4	D5	D6
0	0	0	0	0	0	0	0	0	0	0	0
29 <sup>a</sup>	83	73	81	76	-79	768	715	458	368	49	47
40	678	577	102	93	-130	1182	1218			90	
56.25(Load Level A)	1054	914	1230	1221	-235	1906	1822	831	667	622	95
66.75 (Load Level B) 1 <sup>st</sup> cycle	1333	1163	1612	1570	-278	2361	2203	1448	1311	946	643
66.75 (Load Level B) 125,000 <sup>th</sup> cycle	1405	1239	1839	1704	-286	2426	2398	1800	1782	1163	891
77.1	1677	1479	2178	2021	-337	4375	4828	2069	2039	1393	1068
90	1972	1733	5988	3787	-330	1118 9	9602	2493	2478	1699	1271
100	2131	1871	9664	1052 6	-321	1138 7	1001 3	8166	8534	1890	1506
105	2203	1935	1170 0	1181 3	-257	1183 7	1078 3	9509	9299	1973	1650
108	2249	1974	1308 3	1310 8	-224	1263 4	1118 0	9633	9306	2022	1719

<sup>a</sup> Lowest cracking load of specimens 5 to 7.

\* Strain gage broken

Load, kips	Microstrain										
	T1	T2	T3	T4	T5	T6	T7	T8	T9	T10	T11
0	0	0	0	0	0	0	0	0	0	0	0
29 <sup>a</sup>	44	99	93	34	120	0	0	0	0	0	0
40	223	451	479	276	344	0	0	0	0	0	0
56.25(Load Level A)	814	1457	1708	1318	1061	441	0	0	0	0	0
66.75 (Load Level B) 1 <sup>st</sup> cycle	1244	2030	2510	1801	1408	803	103	0	0	26	0
66.75 (Load Level B) 125,000 <sup>th</sup> cycle	1516	2270	3147	1987	1527		234	88	61	208	0
77.1	1812	2736	4021	2366	1901		283	118	84	252	0
90	2169	3340	5070	2677	2916		426	221	196	377	0
100	2419	3749	6002	2912	4195		510	277	268	459	29
105	2634	4136	7043	3107	4731		560	312	308	509	68
108	2957	4697	8613	3273	5130		597	339	337	550	110
110	3205	5117	9673	3460	5446		618	355	353	572	137
113	3839	6110	1180 5	4015	5870		689	409	395	623	195

Load, kips	Microstrain										
	T12*	T13	T14	T15	T16	T17	T18*	S1	S2	S3	DS1
0	0	0	0	0	0	0		0	0	0	0
29 <sup>a</sup>	0	0	0	0	0	0		0	0	0	64
40	0	16	0	0	18	43		0	0	0	90
56.25(Load Level A)	0	29	0	15	47	19		3	2	0	612
66.75 (Load Level B) 1 <sup>st</sup> cycle	0	51	0	44	90	27		6	6	0	984
66.75 (Load Level B) 125,000 <sup>th</sup> cycle	0	86	0	149	171	15		-	17	5	1158
77.1	0	110	0	195	203	17		-	29	6	1378
90	14	200	22	374	313	26		-	81	16	1645
100	44	231	50	443	362	27		-	77	18	1769
105	68	246	98	478	378	30		-	76	18	1870
108	94	257	134	510	396	32		-	79	18	1920
110	113	262	157	528	404	34		-	84	18	1948
113	157	279	217	587	443	40		-	94	16	2003

Load, kips	Microstrain	
	DS2	DS3
0	0	0
29 <sup>a</sup>	66	-76
40	92	-111
56.25(Load Level A)	785	-187
66.75 (Load Level B) 1 <sup>st</sup> cycle	1228	-243
66.75 (Load Level B) 125,000 <sup>th</sup> cycle	1413	-281
77.1	1680	-341
90	2030	-411
100	2182	-485
105	2268	-520
108	2321	-539
110	2351	-551
113	2412	-574

**Table C.8. Strain Gage Results from Specimen 8**

Load, kips	Microstrain										
	C1	C2	C3	C4	C5	D1	D2	D3	D4	D5	D6
0	0	0	0	0	0	0	0	0	0	0	0
25.5 <sup>a</sup>	23	-2	184	275	-156	573	529	155	227	13	-1
29	62	14	281	385	-178	687	644	207	283	52	8
40	306	153	515	637	-249	1131	1021	411	474	206	56
56.25(Load Level A)	732	931	1023	1112	-347	1836	1683	901	747	734	622
66.75 (Load Level B) 1 <sup>st</sup> cycle	962	1213	1327	1438	-410	2601	2334	1525	1036	1068	960
66.75 (Load Level B) 125,000 <sup>th</sup> cycle	1037	1312	1573	1666	-441	2879	2543	1830	1023	1241	1230
77.1	1173	1485	1779	1878	-488	3676	3025	2127	1243	1371	1356
85	1307	1632	2125	2184	-525	5552	5316	2506	1405	1575	1575
90	1400	1728	2365	2411	-549	7520	6973	2622	1515	1706	1707
100	1584	1903	2725	2708	-598	10908	11986	2798	2643	1951	1914
105	1663	1967	2915	2746	-623	12568	14279	3581	1158	2069	1996
108	1702	2001	2955	2752	-632	13559	15004	6543	1085	2136	2035
110	1719	2011	2980	2764	-637	14113	15549	5449	1082	2171	2056

<sup>a</sup> Lowest cracking load of specimens 8 to 11.

\* Strain gage broken

Load, kips	Microstrain										
	T1	T2	T3	T4	T5	T6	T7	T8	T9	T10	T11
0	0	0	0	0	0	0	0	0	0	0	0
25.5	-36	-39	-24	-45	-22	-29	-55	-86	-77	-64	-72
29	-25	-32	-21	-44	-20	-28	-64	-98	-86	-69	-78
40	227	44	-5	-48	-20	-5	-63	-101	-82	-67	-102
56.25	595	198	136	-31	-8	-11	-75	-83	-67	-72	-109
66.75 1 <sup>st</sup> cycle	1098	472	709	124	22	38	-71	-76	-64	-63	-108
66.75 125,000 <sup>th</sup> cycle	1302	377	1010	269	40	145	-52	-62	-58	-79	-103
77.1	1486	470	1200	409	57	177	-54	-61	-58	-81	-109
85	1761	583	1600	852	120	299	-43	-54	-58	-89	-112
90	1963	655	1904	1112	169	393	-31	-46	-56	-95	-116
100	2314	797	2513	1392	378	630	-10	-26	-52	-103	-127
105	2515	868	2873	1508	499	797	2	-15	-50	-107	-132
108	2633	929	3099	1581	561	912	9	-11	-50	-107	-138
110	2704	961	3247	1630	611	976	12	-9	-49	-104	-141

Load, kips	Microstrain										
	T12	T13*	T14	T15	T16	T17	T18	S1	S2	S3	DS1
0	0		0	0	0	0	0	0	0	0	0
25.5	-74		-47	-4	-41	-33	-32	-47	-82	-46	-1
29	-78		-47	-5	-36	-19	-26	-47	-84	-47	10
40	-112		-26	-20	-38	-29	-24	3498	-88	-52	59
56.25	-102		-13	9	14	-17	-30	-47	-98	-53	743
66.75 1 <sup>st</sup> cycle	-101		-2	36	62	-13	-23	14	-101	-55	975
66.75 125,000 <sup>th</sup> cycle	-97		-20	62	116	-27	-10	2249	-102	-57	1070
77.1	-101		-10	84	141	-23	-3	2258	-103	-58	1231
85	-102		4	124	180	10	29	2240	-54	-55	1336
90	-103		15	138	196	26	60	2247	-55	-38	1316
100	-112		41	195	244	47	115	2891	-46	-36	1467
105	-119		62	240	296	87	166	2802	-41	-37	1536
108	-126		93	284	330	156	227	2847	-37	-36	1574
110	-132		105	301	345	191	258	2868	-35	-36	1595

Load, kips	Microstrain	
	DS2	DS3
0	0	0
25.5	7	-102
29	16	-111
40	66	-143
56.25	607	-218
66.75 1 <sup>st</sup> cycle	786	-274
66.75 125,000 <sup>th</sup> cycle	879	-297
77.1	1008	-333
85	1089	-380
90	1070	-412
100	1194	-463
105	1237	-497
108	1269	-510
110	1285	-517

**Table C.9. Strain Gage Results from Specimen 9**

Load, kips	Microstrain										
	C1	C2	C3	C4	C5	D1	D2	D3	D4	D5	D6
0	0	0	0	0	0	0	0	0	0	0	0
25.5 <sup>a</sup>	59	54	205	88	-99	861	722	485	555	58	52
29	62	58	328	158	-118	979	820	550	643	66	59
40	423	217	983	862	-215	1452	1202	858	991	136	184
56.25(Load Level A)	909	633	1617	1417	-309	2260	1839	1386	1553	619	558
66.75 (Load Level B) 1 <sup>st</sup> cycle	1256	879	1930	1731	-372	2947	2287	1820	1888	952	964
66.75 (Load Level B) 125,000 <sup>th</sup> cycle	1298	944	2020	1840	-408	3066	2388	2003	1996	1126	1154
77.1	1445	1041	2274	2073	-457	3706	2812	2289	2266	1239	1262
85	1607	1163	2557	2353	-503	12865	6191	2540	2596	1440	1442
90	1681	1219	2618	2478	-528	18915	7237	4259	2789	1515	1519
100	1830	1332	2774	2518	-595	21404	8138	6812	5495	1666	1672
105	1877	1369	3117	2524	-616	21947	8887		6011	1720	1726
108	1886	1377	8739	6299	-622	22084	9486		6194	1744	1748

<sup>a</sup> Lowest cracking load of specimens 8 to 11.

\* Strain gage broken

Load, kips	Microstrain										
	T1	T2	T3	T4	T5	T6	T7	T8	T9	T10	T11
0	0	0	0	0	0	0	0	0	0	0	0
25.5	117	57	26	24	28	39	-15	-17	-11	-15	-11
29	161	70	29	27	30	45	-18	-21	-15	-19	-14
40	333	143	31	26	13	56	26	17	15	-1	0
56.25	624	584	124	64	16	53	56	24	33	51	0
66.75 1 <sup>st</sup> cycle	1207	1917	1083	982	62	91	60		39	56	0
66.75 125,000 <sup>th</sup> cycle	1290	2230	1299	1201	73	117	47		103	59	4
77.1	1430	2538	1478	1368	89	132	54		105	62	5
85	1536	2881	1716	1567	156	179	62		109	70	11
90	1581	3021	1774	1586	277	263	65		109	74	15
100	1653	3287	1902	1679	891	648	70		109	80	15
105	1776	3600	2078	1762	1157	826	73		109	82	15
108	1890	3907	2233	1851	1250	894	73		109	83	16

Load, kips	Microstrain										
	T12	T13	T14	T15	T16	T17	T18	S1*	S2*	S3	DS1
0	0	0	0	0	0	0	0			0	0
25.5	-13	-18	-18	-19	-15	0	6			-1	51
29	-17	-24	-24	-25	-23	-5	3			-1	56
40	15	-16	-48	-69	-1	43	37			-2	76
56.25	33	50	-40	-150	51	92	83			9	186
66.75 1 <sup>st</sup> cycle	31	76	-56	-143	116	133	88			14	359
66.75 125,000 <sup>th</sup> cycle	27	84	-59	-87	115	155	93			30	529
77.1	32	94	-66	-101	129	178	105			33	600
85	40	158	-66	-92	143	218	138			29	1008
90	43	196	-55	-72	169	257	175			29	1089
100	43	364	88	186		442	389			30	1232
105	44	481	156	233		638	634			31	1274
108	44	559	271			760	826			31	1297

Load, kips	Microstrain	
	DS2	DS3
0	0	0
25.5	46	-58
29	51	-65
40	70	-91
56.25	143	-172
66.75 1 <sup>st</sup> cycle	291	-220
66.75 125,000 <sup>th</sup> cycle	470	-256
77.1	582	-287
85	956	-330
90	1020	-350
100	1144	-398
105	1175	-418
108	1195	-422

**Table C.10. Strain Gage Results from Specimen 10**

Load, kips	Microstrain										
	C1	C2	C3	C4	C5	D1	D2	D3	D4	D5	D6
0	0	0	0	0	0	0	0	0	0	0	0
25.5 <sup>a</sup>	81	61	118	191	-97	736	660	426	536	73	59
29	108	80	171	294	-114	876	779	507	638	107	73
40	837	679	351	571	-175	1325	1162	796	995	301	147
56.25(Load Level A)	1152	1026	759	1060	-264	1996	1815	1469	1566	886	682
66.75 (Load Level B) 1 <sup>st</sup> cycle	1274	1170	1171	1448	-314	2410	2212	2009	2078	1551	1280
66.75 (Load Level B) 125,000 <sup>th</sup> cycle	1316	1286	1475	1752	-340	2543	2354	2532	2368	1789	1471
77.1	1454	1413	1623	1932	-376	2868	2637	2814	2589	1941	1605
85	1596	1538	1867	2190	-414	6116	4147	3783	4307	2220	1805
90	1664	1602	2013	2328	-435	1449 9	8053	4181	9533	2334	1911
100	1792	1724	2143	2500	-477	1500 7	9331	1136 0	8173	2537	2072
105	1844	1789	2223	2586	-496	1524 5	1007 8	1462 9	8122	2630	2154
108	1879	1827	2263	2631	-504	1568 7	1078 9	1474 4	8647	2678	2197
110	1899	1848	2285	2655	-507	1617 8	1140 7	1484 9	9660	2704	2224

<sup>a</sup> Lowest cracking load of specimens 8 to 11.

\* Strain gage broken

Load, kips	Microstrain										
	T1	T2	T3	T4	T5	T6	T7	T8	T9	T10	T11
0	0	0	0	0	0	0	0	0	0	0	0
25.5	98	62	48	46	45	87	-14	-38	-24	-28	-14
29	185	77	53	52	44	104	-10	-29	-20	-28	-16
40	491	194	77	121	48	163	-1	-12	97	0	10
56.25	2173	1910	2351	1727	140	209	29	-23	72	18	15
66.75 1 <sup>st</sup> cycle	3030	2697	3691	2443	226	328	37	13	71	47	10
66.75 125,000 <sup>th</sup> cycle	3572	3213	4736	2907	322	481	55	-998	15	79	29
77.1	4205	3895	5907	3344	364	538	58	-987	14	88	30
85	5582	5711	8256	4155	542	784	73	-964	14	122	34
90	6480	7031	9412	4665	732	1067	87	-945	14	142	33
100	7716	9888	1205 7	5804	1969	2063	122	-909	33	192	30
105	8266	1223 8	1409 2	6784	2518	2639	147	-887	41	214	33
108	8946	1316 5	1501 2	7214	2711	2875	158	-880	42	225	33
110	9457	1396 8	1581 4	7625	2926	3116	168	-867	50	237	35

Load, kips	Microstrain										
	T12	T13	T14	T15*	T16	T17	T18	S1	S2	S3	DS1*
0	0	0	0		0	0	0	0	0	0	
25.5	-14	4	-8		42	26	30	3	-4	-2	
29	-14	-6	-22		61	34	45	4	-4	-3	
40	52	-56	6		82	20	67	9	-7	-5	
56.25	56	44	15		208	16	150	23	-20	-9	
66.75 1 <sup>st</sup> cycle	62	188	49		352	57	205	100	-18	-1	
66.75 125,000 <sup>th</sup> cycle	83	357	72		511	125	202	315	2	18	
77.1	89	400	81		570	140	222	351	3	19	
85	98	495	143		622	184	252	428	8	36	
90	107	565	233		646	218	275	521	15	51	
100	129	620	292		674	308	344	815	53	103	
105	141	653	319		692	372	388	1021	66	134	
108	147	670	330		705	409	410	1108	70	146	
110	152	683	336		712	448	427	1210	52	162	

Load, kips	Microstrain	
	DS2*	DS3
0		0
25.5		-77
29		-88
40		-122
56.25		-212
66.75 1 <sup>st</sup> cycle		-271
66.75 125,000 <sup>th</sup> cycle		-309
77.1		-340
85		-382
90		-407
100		-466
105		-495
108		-509
110		-521

**Table C.11. Strain Gage Results from Specimen 11**

Load, kips	Microstrain										
	C1	C2	C3	C4	C5	D1	D2*	D3	D4	D5	D6
0	0	0	0	0	0	0		0	0	0	0
25.5 <sup>a</sup>	59	58	53	40	-57	374		126	60	32	28
29	87	87	76	57	-79	572		215	88	49	41
40	696	563	720	573	-150	902		400	862	136	100
56.25(Load Level A)	1184	982	1319	1185	-223	1650		1017	1485	496	361
66.75 (Load Level B) 1 <sup>st</sup> cycle	1479	1178	1734	1574	-278	2134		1616	1921	787	723
66.75 (Load Level B) 125,000 <sup>th</sup> cycle	1741	1339	2207	2030	-366	2615		2022	2412	1228	1312
77.1	1846	1421	2305	2144	-388	2772		2152	2545	1269	1365
85	2006	1561	2341	2362	-424	3187		2327	2755	1407	1519
90	1988	1418	2358	2539	-458	4082		2432	2942	1649	1795
100	2105	1502	2642	2549	-487	8705		5575	3028	1847	2135
105	2147	1531	8183	7239	-480	8967		6242	9976	1929	2272
108	2154	1537	9045	9049	-474	1008 1			1206 3	2014	2388
110	2172	1552	9428	9229	-474	1036 4			1288 4	2063	2452

<sup>a</sup> Lowest cracking load of specimens 8 to 11.

\* Strain gage broken

Load, kips	Microstrain										
	T1	T2	T3	T4	T5	T6	T7	T8	T9	T10	T11
0	0	0	0	0	0	0	0	0	0	0	0
25.5	19	19	17	19	17	28	-9	-12	-9	-8	-6
29	33	34	28	29	30	44	-13	-17	-14	-13	-9
40	83	76	53	94	49	56	3	-14	-20	-42	19
56.25	1006	1097	940	1034	118	152	55	1	6	-20	30
66.75 1 <sup>st</sup> cycle	1563	1797	1572	1705	167	222	85	4	14	-15	19
66.75 125,000 <sup>th</sup> cycle	2099	2648	2272	2486	318	423	122	8	-11	-5	45
77.1	2210	2792	2408	2617	331	440	124	8	-18	-11	45
85	2574	3406	2994	3268	430	510	138	27	-16	-3	46
90	2934	3988	3619	3998	815	695	195	117	111	120	64
100	3153	4948	4796	5062	1475	1104	233	170	157	160	72
105	3276	5440	5540	5591	1832	1426	250	198	176	178	76
108	3368	5830	6278	6143	2035	1657	265	219	185	190	80
110	3415	6016	6544	6345	2110	1741	271	229	190	195	81

Load, kips	Microstrain										
	T12	T13	T14	T15	T16	T17	T18	S1	S2	S3	DS1
0	0	0	0	0	0	0	0	0	0	0	0
25.5	-4	-9	-10	-5	-3	1	1	-5	-2	-2	40
29	-6	-15	-15	-8	-5	1	3	-6	-3	-3	52
40	42	-36	-30	-2	-11	45	72	-11	-5	-4	72
56.25	41	97	-17	88	33	35	49	1	-8	-7	94
66.75 1 <sup>st</sup> cycle	31	104	-7	120	73	33	54	46	-6	-5	128
66.75 125,000 <sup>th</sup> cycle	1	135	9	273	158	57	69		-2	32	1060
77.1	-2	132	5	282	169	54	75		-5	31	1109
85	0	128	6	314	181	60	90		-3	31	1216
90	12	141	0	412	229	57	89		3	31	1369
100	-1	96	5	697	394	86	130		15	31	1535
105	-10	109	15	923	512	142	168		30	31	1590
108	-18	51	15	794	601	147	164		56	30	1609
110	-21	77	16	789	618	154	168		49	30	1622

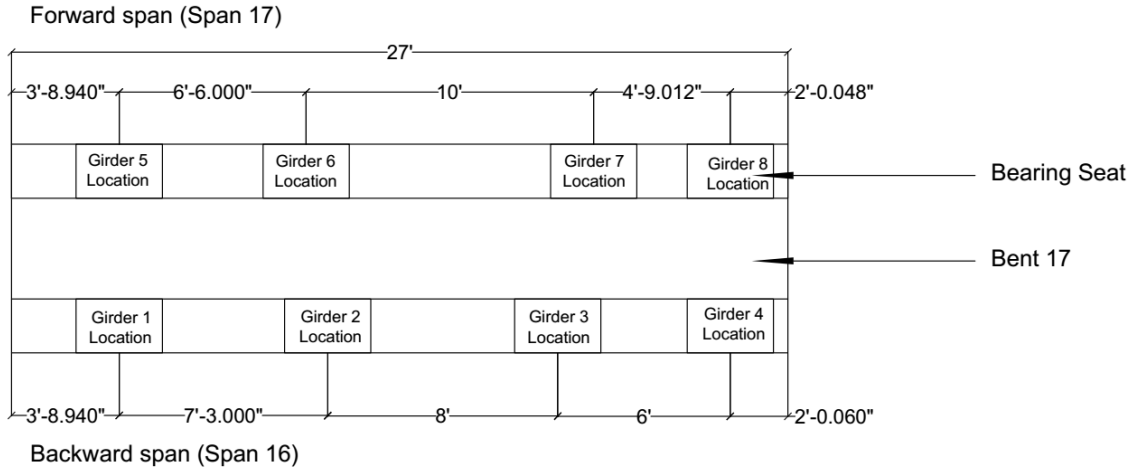
Load, kips	Microstrain	
	DS2	DS3
0	0	0
25.5	42	-44
29	56	-59
40	75	-85
56.25	87	-146
66.75 1 <sup>st</sup> cycle	111	-209
66.75 125,000 <sup>th</sup> cycle	993	-341
77.1	1042	-361
85	1146	-392
90	1300	-435
100	1465	-486
105	1518	-512
108	1529	-497
110	1538	-501

## Appendix D

### Loads on the Bent 17 Column-Drilled Shaft Connection on SH 99

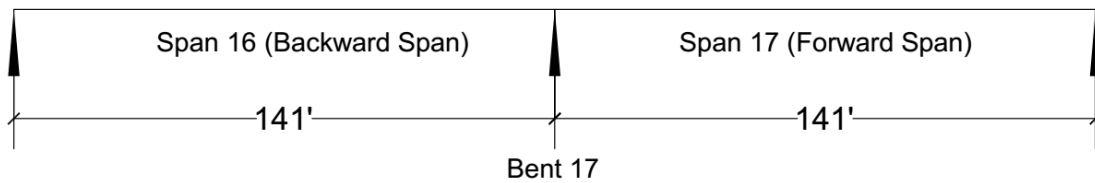
**Dead Load Calculation:**

Fig. D.1 shows the plan view of Bent 17.



**Fig. D.1: Plan view of Bent 17**

Fig. D.2 shows the location of Bent 17.



**Fig. D.2: Location of Bent 17**

**(i) Rail load:**

Rail type T221

Rail weight = 0.37 klf

$$\text{Rail load/rail} = 141 * 0.37 = 52.17 \text{ k}$$

$$\therefore \text{Rail load} = \frac{52.17 * 2}{8} = 13.0425 \text{ k/girder}$$

**(ii) Slab load:**

$$\therefore \text{Slab load} = w_c * Gdrspan * Slabthk * Span/2 * 1.10$$

$$= 0.150 * Gdrspan * \left(\frac{8}{12}\right) * \left(\frac{141}{2}\right) * 1.10 = 7.755 * Gdrspan$$

where,  $w_c$  = unit weight of concrete for loads,  $\frac{\text{kip}}{\text{ft}^3}$ ;

$Gdrspan$  = Width of slab contributing to the load applied on each girder, ft;

$Slabthk$  = Slab thickness, ft.

$$Gdrspan \text{ for Girder 1} = 8.365'$$

$$Gdrspan \text{ for Girder 2} = 7.625'$$

$$Gdrspan \text{ for Girder 3} = 7'$$

$$Gdrspan \text{ for Girder 4} = 5.011'$$

$$Gdrspan \text{ for Girder 5} = 7.99'$$

$$Gdrspan \text{ for Girder 6} = 8.25'$$

$$Gdrspan \text{ for Girder 7} = 7.3755'$$

$$Gdrspan \text{ for Girder 8} = 4.3845'$$

$$\text{Slab load on Girder 1} = 64.87 \text{ k}$$

$$\text{Slab load on Girder 2} = 59.13 \text{ k}$$

Slab load on Girder 3 = 54.285 k

Slab load on Girder 4 = 38.86 k

Slab load on Girder 5 = 61.96 k

Slab load on Girder 6 = 63.98 k

Slab load on Girder 7 = 57.2 k

Slab load on Girder 8 = 34.00 k

**(iii) Girder self-weight:**

Tx62 Girder Weight = 0.948 klf

$$\therefore \text{Girder self-weight} = 0.948 * \left(\frac{141}{2}\right) = 66.834 \text{ k/girder}$$

**(iv) Wearing surface dead load:**

$$\begin{aligned}\therefore \text{Slab load} &= w_{\text{Overlay}} * Gdrspan * Overlaythk * \frac{Span}{2} \\ &= 0.140 * Gdrspan * \left(\frac{2}{12}\right) * \left(\frac{141}{2}\right) = 1.645 * Gdrspan\end{aligned}$$

Overlay load on Girder 1 = 13.76 k

Overlay load on Girder 2 = 12.54k

Overlay load on Girder 3 = 11.52 k

Overlay load on Girder 4 = 8.24 k

Overlay load on Girder 5 = 13.14 k

Overlay load on Girder 6 = 13.57 k

Overlay load on Girder 7 = 12.13 k

Overlay load on Girder 8 = 7.21 k

**Total dead load on Girder 1 = 158.51 k**

**Total dead load on Girder 2 = 151.54 k**

**Total dead load on Girder 3 = 145.68 k**

**Total dead load on Girder 4 = 126.98 k**

**Total dead load on Girder 5 = 154.98 k**

**Total dead load on Girder 6 = 157.43 k**

**Total dead load on Girder 7 = 149.21 k**

**Total dead load on Girder 8 = 121.09 k**

(v) **Bent cap self-weight:**

Fig. D.3 shows the cross-section of the bent cap of the Bent 17 column-drilled shaft connection.

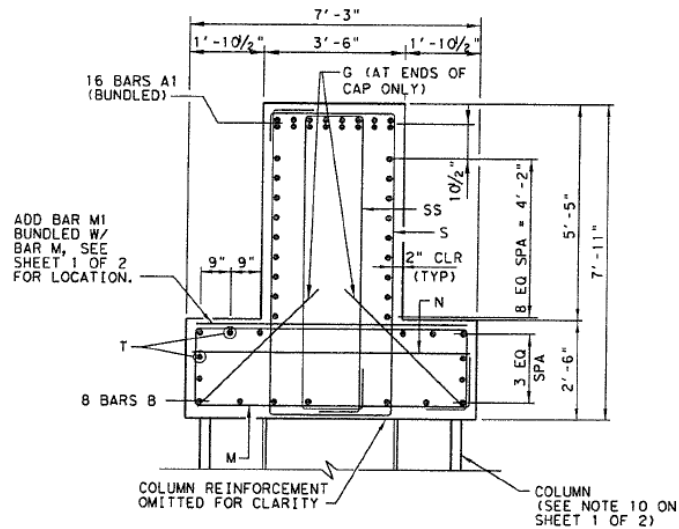


**Fig. D.3: Cross-section of the bent cap of the Bent 17 column-drilled shaft connection.**

$$\therefore \text{Bent 17 self-weight} = 27 \times (7.25 \times 2.5 + 5.42 \times 3.5) \times 0.15 = 150.25 \text{ k}$$

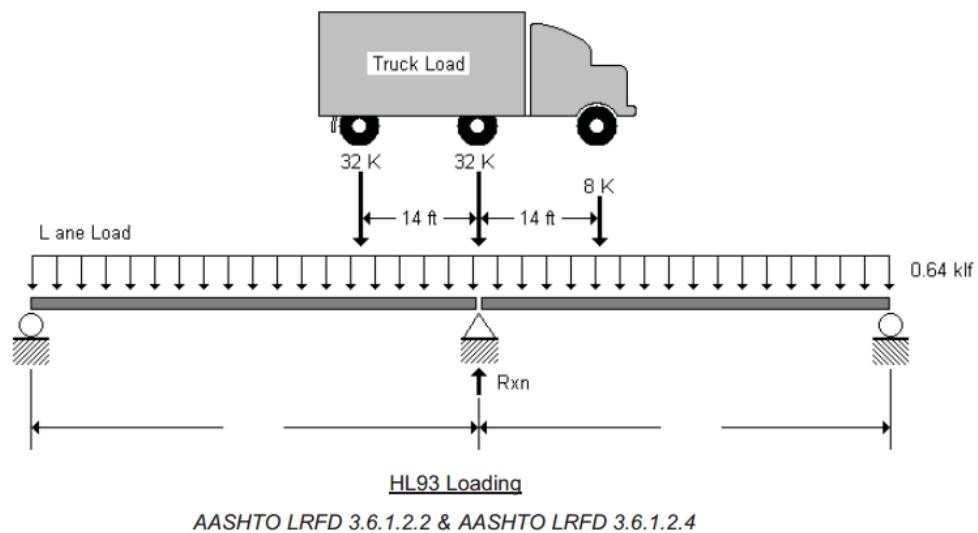
$$\text{Moment on the column due to dead load} = 158.51 \times 16.447 + 151.54 \times 9.197 + 145.68 \times 1.197 -$$

$$126.98 \times 4.802 + 154.98 \times 16.5 + 157.43 \times 10.0 - 121.09 \times 4.751 = \mathbf{7121.5 \text{ kip-ft}}$$

$$\text{Moment on the column due to bent cap self-weight} = 150.25 \times 6.692 = \mathbf{1005.5 \text{ kip-ft}}$$

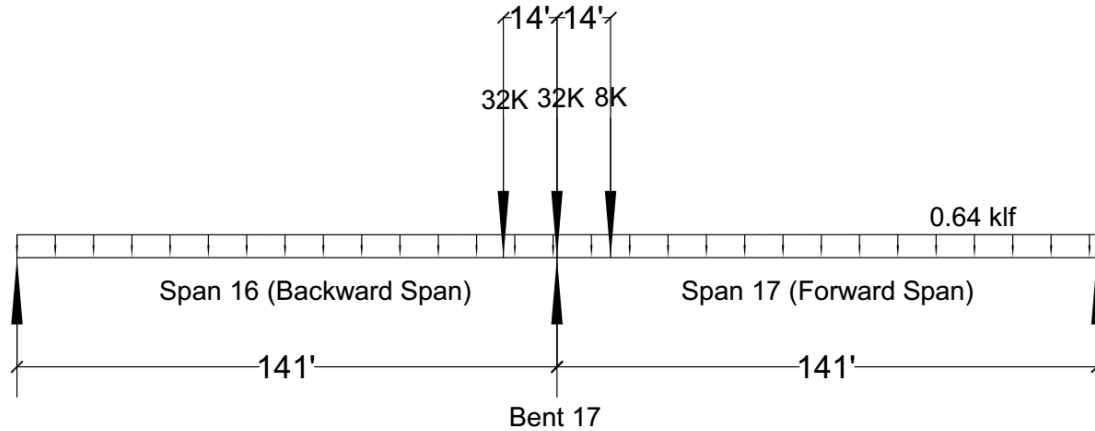
### Live Load Calculation:

Fig. D.4 shows AASHTO HL93 loading.



**Fig. D.4: HL93 Loading**

Fig. D.5 shows the HL-93 loading on SH 99 - Span 16 and 17.



**Fig. D.5: HL-93 Loading on SH 99: Span 16 and 17**

Long span = Short span = 141'

IM= 0.33

AASHTO LRFD 3.6.1.2.4 – Design Lane Load states that “The design lane load shall consist of a load of 0.64 klf uniformly distributed in the longitudinal direction.”

$$\text{Total lane load} = 0.64 * \frac{(141+141)}{2} = 90.24 \frac{k}{\text{lane}}$$

$$\text{For Span 16 (Backward span), } Truck\ load_{span\ 16} = \frac{32}{2} + 32 * \frac{141-14}{141} = 44.82\ k$$

$$\text{For Span 17 (Forward span), } Truck\ load_{span\ 17} = \frac{32}{2} + 8 * \frac{141-14}{141} = 23.2\ k$$

**Total truck load = 68.02 k/lane**

Combining “Design Truck Load” and “Design Lane” loadings AASHTO LRFD 3.6.1.3 [2],

$$\text{Total live load, } LL_{Rxn} = Lane + Truck * (1+IM) = 90.24 + 68.02 * 1.33 = 180.71\ k/lane$$

Assuming that the shoulder lane (Fig. D.6) would be loaded to truck traffic. As the aim is to simulate maximum live load on Bent 17, two loaded lanes would be considered on Bent 17.

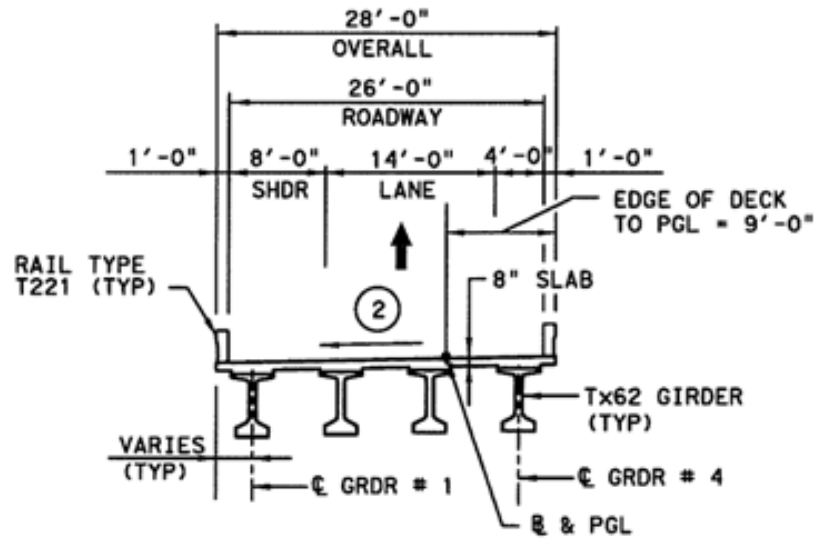


Fig. D.6: Typical section of Span 16 and 17.

Table 3.6.1.1.2-1—Multiple Presence Factors,  $m$

Number of Loaded Lanes	Multiple Presence Factors, $m$
1	1.20
2	1.00
3	0.85
>3	0.65

So, multiple presence factor,  $m = 1.00$  (Two loaded lanes) and

Multiple presence factor,  $m = 1.2$  (One loaded lane).

**Load Case 1 - Live load calculation for two loaded lanes:**

Fig. D.7 shows Live load on a 10' lane according to AASHTO LRFD 3.6.1.2.1.

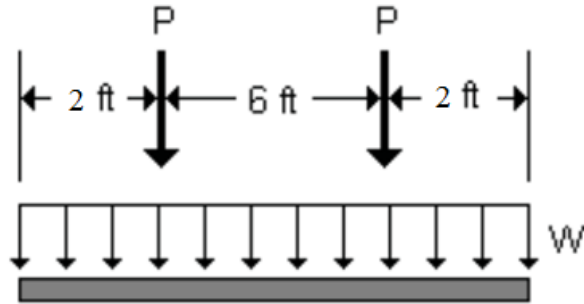


**Fig. D.7: Live load on 10' lane according to AASHTO LRFD 3.6.1.2.1 [2].**

Moment on the column due to live load on two lanes=  $180.71 (15.192 + 5.192) = 3683.6 \text{ kip} - \text{ft}$

$m$  (two loaded lanes) = 1.0

**Maximum live load moment on the column for two loaded lanes = 3683.6 kip-ft. (governs)**

**Load Case 2 - Live load calculation for one loaded lane:**

Moment on the column due to live load on one lane=  $180.71 \times 15.192 = 2745.35 \text{ kip} - \text{ft}$

$m$  (one loaded lane) = 1.2

**Maximum live load moment on the column for one loaded lane =  $2745.35 \times 1.2 = 3294.4 \text{ kip-ft}$**

**$\therefore$  Maximum live load moment on the column = 3683.6 kip-ft.**

## SUMMARY

**Moment on the column due to dead load = 7121.5 kip - ft**

**Moment on the column due to bent cap self-weight = 1005.5 kip - ft**

**Maximum live load moment on the column = 3683.6 kip - ft**

### Calculation of reinforcement confinement factor, $\lambda_{rc}$

It is not recommended to shorten the required lap splice length as per AASHTO LRFD BDS Interim Revisions [12] by the reinforcement confinement factor  $\lambda_{rc}$  because the FEA results have shown that the lap splice length would be shortened to such an extent that the tensile damage due to the splitting cracks along the spliced bars would be quite extensive despite providing the required amount of transverse reinforcement in the column and the drilled shaft.

In order to find out the effect of reinforcement confinement factor  $\lambda_{rc}$ , the reinforcement confinement factor  $\lambda_{rc}$  needs to be determined as per Article 5.11.2.1.3 of AASHTO LRFD BDS Interim Revisions [11, 12] as follows:

The reinforcement detailing of the Bent 17 column-shaft structure is used to calculate  $\lambda_{rc}$ . This factor is used to decrease the lap splice length calculated by Equation 3 by taking into consideration the contribution of the amount of transverse reinforcement in preventing sudden brittle anchorage failure of column-drilled shaft connections as per AASHTO [12] guidelines.

First of all, it is necessary to identify the potential location of splitting cracks. Fig. D.8 shows the potential splitting crack locations in the Bent 17 column as per AASHTO C5.11.2.1.3 [11] guidelines.

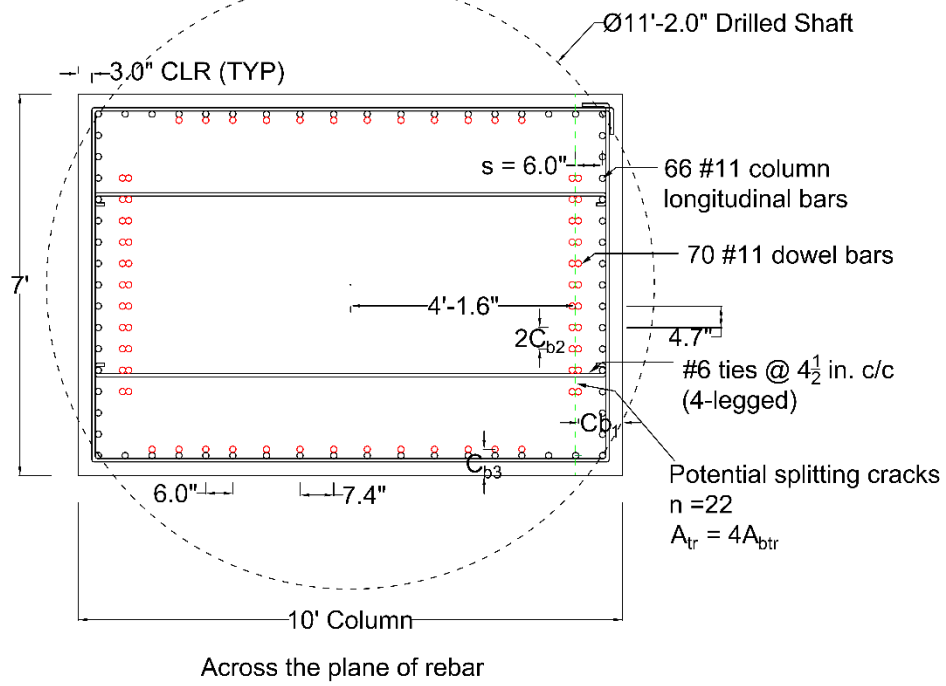
**Considering the splitting cracks occur across the plane of rebar as shown in Fig. D.8(a):**

$$C_{b1} = 9.8 \text{ in.}$$

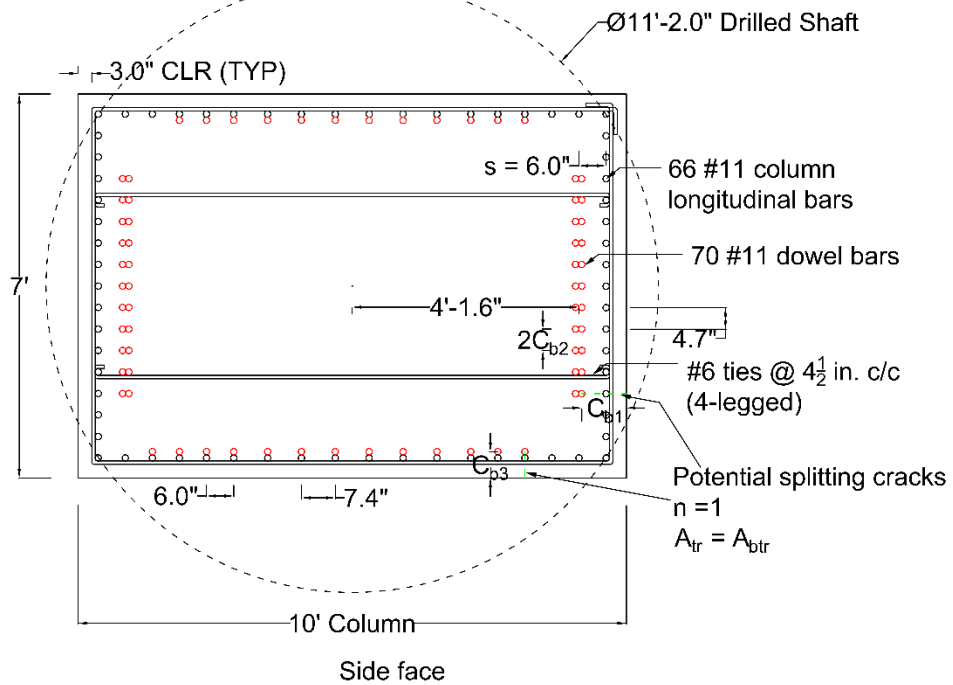
$$2C_{b2} = 4.7 \text{ in.} \therefore C_{b2} = 2.35 \text{ in.}$$

$$C_{b3} = 5.8 \text{ in.}$$

$$C_b = \min \text{ of } (C_{b1}, C_{b2}, C_{b3}) = 2.35 \text{ in.}$$



(a)



(b)

Fig. D.8. Potential splitting crack locations: a) Across the plane of rebar; b) side face.

It should be noted that

" $A_{btr}$  = cross – sectional area of an individual transverse bar crossing the potential plane of splitting ( $in.^2$ )."

If #6 ties @ 4½ in. c/c is provided as transverse reinforcement in the non-contact splice zone in the column then,

$$k_{tr} = \frac{40A_{tr}}{sn} = \frac{40 * 4 * 0.44}{4.5 * 22} = 0.71 \text{ in.}$$

$$\lambda_{rc} = \frac{d_b}{c_b + k_{tr}} = \frac{\frac{11}{8}}{2.35 + 0.71} = 0.45$$

$$l_d = l_{db} * \frac{\lambda_{rl} * \lambda_{cf} * \lambda_{rc} * \lambda_{er}}{\lambda} = 104.4 \frac{1.0 * 1.0 * 0.45 * 1.0}{1.0} = 46.9 \text{ in. (much smaller than } l_{db} = 104.4 \text{ in.)}$$

**Considering the splitting cracks occur on the side face as shown in Fig. D.8(b):**

$$k_{tr} = \frac{40A_{tr}}{sn} = \frac{40 * 0.44}{4.5 * 1} = 3.91 \text{ in.}$$

$$\lambda_{rc} = \frac{d_b}{c_b + k_{tr}} = \frac{\frac{11}{8}}{2.35 + 3.91} = 0.22$$

As  $0.4 \leq \lambda_{rc} \leq 1.0$ ,  $\lambda_{rc} = 0.4$

$$l_d = l_{db} * \frac{\lambda_{rl} * \lambda_{cf} * \lambda_{rc} * \lambda_{er}}{\lambda} = 104.4 \frac{1.0 * 1.0 * 0.4 * 1.0}{1.0} = 41.76 \text{ in.}$$

$l_d = 46.9 \text{ in. (governs)}$

Standard required lap splice length,  $l_s = 1.3 * l_d$  for Class B Splice (AASHTO 5.11.5.3.1 – Lap Splices) in Tension = 61.0 in.

$$\therefore l_s = 61.0 \text{ in.}$$

Total lap splice length for non-contact splices (for a non-contact lap splice distance of 6 in.),  $l_{ns} = l_s + s = 61.0 + 6.0 = 67$  in. (**when the reinforcement confinement factor,  $\lambda_{rc}$  is considered**).

